Color formulation algorithms improvement through expert knowledge integration for automotive effect paints

Amélie Périssé

THÈSE DE DOCTORAT

Université de Pau et Pays de l'Adour
École doctorale Sciences Exactes et leurs Applications 211

Spécialité : Chimie

Par Amélie PÉRISSÉ

COLOR FORMULATION ALGORITHMS IMPROVEMENT THROUGH EXPERT KNOWLEDGE INTEGRATION FOR AUTOMOTIVE EFFECT PAINTS

Amélioration des algorithmes de contretypage de teintes via l'intégration de connaissances expertes pour les peintures automobiles à effets

Thèse CIFRE avec BASF France division Coatings

Directrice de thèse
Dominique LAFON-PHAM (IMT Mines Alès)

Encadrant de thèse
Belkacem OTAZAGHINE (IMT Mines Alès)

Tuteur industriel
Marion L'AOT

Version : 29 Novembre 2019

PhD THESIS

Université de Pau et Pays de l'Adour
Doctoral school of exact sciences and their applications 211

Specialization: Chemistry

By Amelie PERISSE

COLOR FORMULATION ALGORITHMS IMPROVEMENT THROUGH EXPERT KNOWLEDGE INTEGRATION FOR AUTOMOTIVE EFFECT PAINTS

Amélioration des algorithmes de contretypage de teintes via l'intégration de connaissances expertes pour les peintures automobiles à effets

CIFRE PhD thesis with BASF France division Coatings

Thesis director
Dominique LAFON-PHAM (IMT Mines Alès)

PhD supervisor
Belkacem OTAZAGHINE (IMT Mines Alès)

Industrial supervisor
Marion L'AOT

Version: November 29, 2019

Contents

List of figures

List of tables

List of abbreviations

CAM	Color appearance model
CCT	Correlated color temperature
CIE	Commission internationale de l'éclairage (International commission on illumination
CPD	Cycle per degree
CT	Color temperature
DOI	Distinctiveness of image
FI	Flop index
HCPC	Hierarchical clustering on principal components
IQR	Interquartile range
IR	Infrared
LED	Light emitting diode
LGN	Lateral geniculate nucleus
MAD	Median absolute deviation
OEM	Original equipment manufacturer
PCA	Principal component analysis
RI	Refractive index
SEM	Scanning electron microscopy
UV	Ultraviolet

Glossary

Basecoat – Colored layer used to provide the aesthetic aspect of a vehicle. Can be solid or effect

Blending – Repair technique used to smoothen color differences between two adjacent elements

Bracketing – Technique used in photography to take several pictures of the same scene by using different camera settings

Clearcoat – Uncolored layer used to protect paint from environmental and chemical stresses. Can be glossy, satiny, matte or textured

Color travel – Color change according to the angle of observation

Colormatching – Process of reproducing original OEM colors

Cornflake aluminum – Aluminum particles with irregular surfaces and rough edges

Edge to edge – Repair technique used when there is no difference in color between two adjacent elements

Effect color – Basecoat formulation with effect particles

Effect particles – Particles used in effect tinting bases to provide texture. Can be aluminum, interference or pearlescent.

Face view – Viewing angle of 45° compared to the normal angle

Flip view – Viewing angle of 15° to 25° compared to the normal angle

Flip-flop effect – Lightness change according to the angle of observation

Flop modifier – Silica microspheres which cause a disorientation of the effect particles in the coating film

Flop view – Viewing angle of 75° to 110° compared to the normal angle

Frost effect – Yellowish-gold impression at face view and bluish color impression at flop view

Glass flakes – Transparent effect particles acting like little mirrors and offering an intense sparkling

Graininess – Uniformity of light-dark areas in an effect color linked to the use of effect particles

Hiding power – Ability to hide the surface of an object

Hue extinction – When mixed with colored pigments, ability for aluminum particles to entirely hide the chroma.

ISO – Settings of the camera used to brighten or darken a picture

Lens aperture – Settings of the camera used to sharpen or blur a picture

Letdown – Mix of tinting bases at different percentages

Midcoat – Optional layer added between the basecoat and the clearcoat to obtain deep and vibrant colors

Mode value – Intensity value with the most occurrences in a picture histogram

Shutter time – Settings of the camera used to control the global brightness of a picture

Silver dollar aluminum – Aluminum particles with plane surfaces and round edges

Solid color – Basecoat formulation without effect particles

Sparkling – Distinction of flakes by the human eye due to a highly intense light reflection

Specular angle – Angle of observation where the maximum of reflection is obtained

Spot repair – Repair technique used to paint a small durst without being able to distinguish a color difference

Texture – Heterogeneity of the optical film behavior linked to the use of effect particles creating local optical effects

Tinting base – Suspension of a single pigment in a matrix used in the basecoat formulation. Can be solid or effect

Chapter 1. Introduction

Contents

In various artistic or industrial sectors such as cosmetics, transports or luxury, the visual aspect of materials holds a special place. It has become a criterion of evaluation and appreciation in purchase decisions. Indeed, when buying a vehicle, the consumer selects first the brand and model of his future vehicle, then its color before selecting the technical and ergonomic characteristics. Color is a major quality factor and manufacturers need to be imaginative and original in the conception of new color trends for automobiles. This market is then governed by appearance and effects. Customers want to distinguish themselves with a good balance between color and gloss. The coatings revolution has started to fit to the customer's needs: deep and vibrant colors with effects. The color has become so important that even the bumper is now painted. The manufacturers have been able to adapt quickly by offering bright colors from the launch of new vehicles such as the Peugeot 208 (Yellow Faro), the Renault Clio (Orange Valencia), the Citroen C4 Cactus (Emerald Crystal) or the Audi RS Q3 Sportback (Green Kyalami) presented in Figure 1-1.

Figure 1-1: Launch colors of the Peugeot 208 (Yellow Faro), the Renault Clio (Orange Valencia), the Citroen C4 Cactus (Emerald Crystal) or the Audi RS Q3 Sportback (Green Kyalami) from (Turbo, 2019)

1.1. Context

This thesis is conducted in the context of automotive paints with a special focus on refinish automotive coatings. Whatever the reason, accident or resale, a vehicle might need a repair which will involve a repainting of a specific element. In the automotive refinish area, a perfect car repair must be undetectable and invisible for the customer. According to the

quality of the color formula, different repair techniques exist. The first one is the spot repair when the quality of the color formula is close to perfection, so the initial color and the matched one look exactly the same. This quality of formula can be used to fix for example a burst of paint on the body linked to a violent door knock. With this quality, the body shop is able to repair only the burst – any difference to the rest of the element is invisible. If the area to be repaired is bigger, the element needs to be changed before being painted. If the quality of the color formula provided is acceptable, the element, for example the aisle, is dismantled, changed, painted and then reinstalled. In the final result, the observer will not be able to distinguish any difference between the aisle, the door and the hood. This type of repair is called edge to edge. Finally, when one can notice a color difference between the original color and the proposed formula without being able to improve the quality, the body shop fixes the element before reinstalling and painting it. To smoothen the color differences, the paint is sprayed also on the adjacent elements. This last technique is called “blending”; it helps to reduce color differences like those presented in Figure 1-2 where the bumper is not properly matched in color with the aisle and the hood.

Figure 1-2: Noticeable color differences between the aisle, the hood and the bumper after repair (Carrosserie-Geneve.Ch, 2015)

Customers might think that it is easy to reproduce the color of a car but in fact it requires a lot of experiments. Many years of training are required to learn how to color match. That is why, beyond the paint itself, paint manufacturers such as BASF supply to their customers color formulations which allow to reproduce each color shade of the automotive fleet namely several hundreds of thousands of colors. For each color, the formula consists of a mixture of different ingredients which, mixed together, provide a paint with a correct or at least a best possible color match. Two automotive paint categories exist: solid and effect colors. Solid colors are based on the mix of several primary colors. For effect colors, metallic or pearlescent, on top of the primary colors mix, effect particles are added to provide certain optical properties. Depending on the angle of view, the interactions between light and matter produce different effects. The particles added in the paint film produce local optical effects depending on the angle of view. These effects could modify the lightness and/or the hue of the color itself. They are responsible for the heterogeneity of the optical film behavior and therefore the effect (texturing).

Color formulas are developed in the lab by using proprietary matching software which integrates statistical and physical optical models. These models are used to estimate the resulting color starting from a formula or reflectance curves coming from spectrophotometer measurements. They are combined into algorithms which minimize the theoretical color difference between a standard and the resulting formula. However, the prediction models have their own limitations – this applies in particular to the color descriptors currently used. The colorimetric description does not allow a complete representation of the visual color perception. The color descriptors commonly used, CIELab coordinates, are quite efficient for solid colors but not efficient enough for effect colors. Indeed, visual texture descriptors are not available today to correctly characterize these effect colors and the global appearance is hence not perfectly described. The result obtained during the formulation process is not precise enough to obtain a good match after the first trial. It must be repeated several times by an experienced colorist who manually adjusts the formula to lead to a satisfying formula. Based on his own experience, the colorist is able to reproduce a color. It is also important to note that the issues of efficiency and repeatability depend on the human factor. The improvement of descriptors by the addition of texture descriptors to color descriptors would allow the enhancement of the color matching process.

The main objective of the present thesis is to qualify and to quantify the visually perceived attributes such as the sparkling effect or the size of the effect particles in the formula. In effect coatings, the sparkling effect is linked to optical manifestations at the microscopic and macroscopic levels. Effect particles are micrometric flakes which provide light interaction. In the case of aluminum particles, when they are lighted, the specular light intensity is much stronger than the incident light. These particles act like tiny mirrors and are responsible for the sparkling effect. Therefore, due to the light spreading triggered by light reflection, the sparkles could appear larger than the physical size of the particles. Besides, it is also important to consider the complexity of what is perceived by a human observer – the visual impression is based on a complex combination of color, effect particles and also the concentration of the different elements in the formula.

1.2. Thesis organization

This thesis results from a collaboration between the Center of Materials Research (C2MA) of the IMT Mines Alès and BASF France division Coatings within the framework of the CIFRE convention (Conventions Industrielles de Formation par la REcherche). The objectives of this PhD thesis are multiple. In a first step, it is necessary to define new descriptors considering the texturing of the optical signal before correlating them to the visual acceptance of a color formulation by experienced colorists. One field of investigation is based on the integration of the human color evaluation through sensorial analysis. The second axis is to adapt the perceived descriptors into physical descriptors extracted from optical data acquisitions.

At first, through the second chapter, the mechanism allowing the transformation of light into color will be presented. Color vision rests on the triplet light-object-observer and the three pillars will be discussed in detail. First, the light radiation as a combination of waves will be explained as well as different light sources. Then, the interaction of light and matter will be analyzed by considering different processes such as reflection, absorption or scattering.

Finally, it will be necessary to understand the color vision mechanism of the human visual system by considering the eye and especially the retina which plays a crucial role in color vision with its two kind of photoreceptors: cones and rods. The visual path will then be analyzed to understand the interactions between the eye and the brain. The adaptation of the human visual system to its environment and in particular to contrast and visual acuity will be explained.

The third chapter will be devoted to color measurement. To this end, first, standardization of light sources with the establishment of illuminants and the photometric methods used will be presented. Then, in order to measure color, the functioning of the human visual system was standardized by quantifying the spectral responses of its photoreceptors. This standardization led to the introduction of the two CIE standard colorimetric observers in 1931 and 1964, respectively. Colorimetry is the science of color measurement. Through the establishment of uniform color spaces such as CIELab or CIECAM02, it is then possible to define color differences to better understand the different types of color shifts. Numerous computational models have been developed to better represent the color differences distinguishable by the human visual system. A non-exhaustive list will be presented such as CIE1976, CMC (l:c), AUDI95 and AUDI2000.

The fourth chapter will focus on refinish automotive coatings. After understanding the behavior of light and matter in Chapter 2, we will herein discuss different types of pigments involved in the formulation of automotive paints such as aluminum, specific effect pigments or traditional pigments. A quick presentation of sample preparation and spraying will be made. In a second part, the state of the art considering various types of evaluations of the color is presented, instrumental as well as visual. Measuring devices such as spectroradiometers and spectrophotometers as well as the importance of the measurement angles will be detailed. For a decade, new portable devices have been introduced into the market. They allow color measurement as well as image acquisition. From the images captured by those devices, texture parameters have been derived: sparkling and graininess. However, neither of them corresponds exactly to visual appearance and perception.

After having defined the constraints and limits of the systems of measurement and the representation of color perception generated by effect colors, the fifth chapter focuses on the definition of new texture parameters. To this end, different constituents involved in the formulation of effect colors will be analyzed to better understand their impact on visual appearance. One of the objectives of the PhD thesis is to make use of expert knowledge in terms of visual expertise. The aim here is to bring these fields of expertise together and to more clearly define their respective content to better understand them and to base the new texture descriptors on what the human eye can discern and not the other way around. The different steps leading to their determination will be detailed.

The identification of texture descriptors was the first step of the expert knowledge mobilization. The aim of this sixth part is to set up sensory analysis sessions in which experienced observers will have to evaluate the different descriptors previously defined. The evaluation protocol will be detailed because it is the key to guarantee consistent ratings

between the different judges. Indeed, by standardizing the observation conditions including inclination angles and type of lighting, it is thus possible to ensure homogeneous conditions from one observer to another. Finally, in order to define the mean observer on each descriptor, different statistical data analysis methods will be presented to choose the best fitting one compared to the results obtained.

Last, but not least, the adaptation of texture descriptors into physical texture descriptors is described. For this, different samples are photographed with a high-resolution camera. At first, it is necessary to select the appropriate settings. As a matter of fact, the sensors of the device are not able to measure a large dynamic range in luminance. It is hence necessary to be able to simplify the settings during the acquisition in order to better reproduce the perception by the human visual system. Indeed, the objective is not just to measure but to measure in the way that would best fit the perception of the human eye. By setting up all the parameters except the exposure time, it will then be possible to establish a link between the luminance of the samples and the exposure time for the picture acquisition. In addition, the challenge of this part is also to reproduce the observation conditions during sensory analysis tests to be able to define a correlation between the visible and the measurable. Finally, once the lighting conditions and the settings are defined, the physical texture descriptors will be determined from the images. Statements given by expert observers will be at the origin of their definition. This should allow a better correlation between measurable and perceptible factors. Indeed, all the core of present thesis rests on the definition of texture descriptors corresponding as much as possible to the evaluations made by experts.

Finally, the results obtained during this thesis are discussed and an outlook for a potential future work in this field is given.

Chapter 2. From light to color

Contents

We live in a world full of light and colors. In our environment (plants, objects …), everything seems to be colored but it is important to really understand what the nature of color is. Indeed, the perception of color is a very specific field which mixes physical laws and very specific physiological and psychological conditions. This chapter will be focused on the understanding of color and its creation.

Human beings tried to understand this complex process for ages, but it is only at the end of the 17th century that they started to solve it. In 1666, Newton discovered the decomposition of sunlight when crossing a prism (Newton, 1671). For different angles, the prism refracts diverse colors, from violet to red with all shades of blue, green, yellow and orange. By this experiment, Newton showed that color is intrinsic to light.

Color perception involves several factors. First, color cannot exist without light. The light source is the first step in color sensation of the observed object. The material which constitutes the observed object reflects or transmits all or a part of the light rays (also called colored stimulus) emitted by the light source. The eyes, altogether, then capture those light rays and convert the multiple received stimulus signals into a color signal which can be transmitted to the brain. The brain will then identify and name the color of the observed object. Color perception is then highly dependent on the light source, the observed object, the eyes and the brain. The first three elements form the triplet “light-object-eye”.

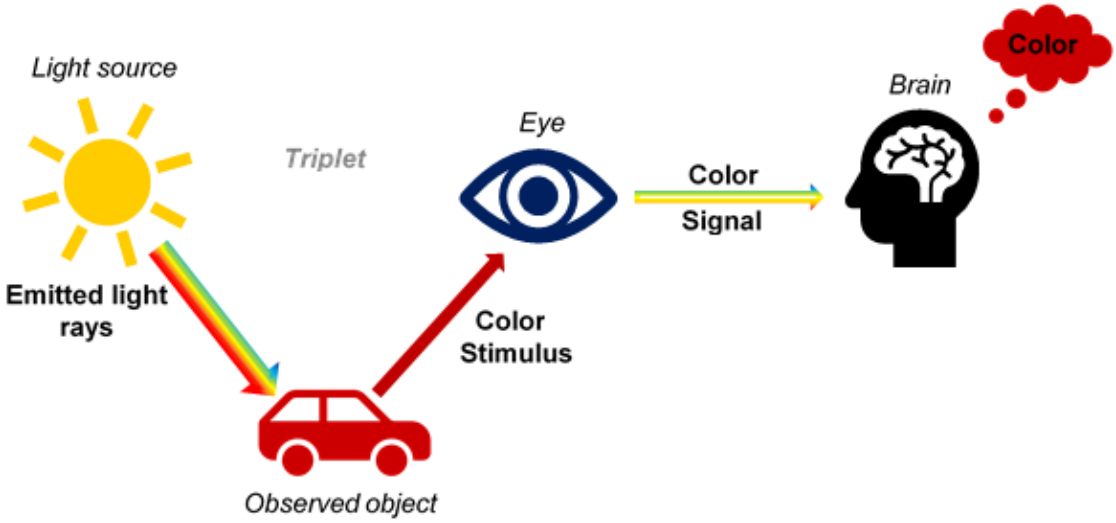

Figure 2-1: Color perception inspired from (Chrisment et al., 1994)

2.1. Light source

2.1.1. Visible spectrum

Light is one of the mandatory elements for color perception. Without light, the human visual system is unable to function and consequently see colors. Light can be defined as a physical phenomenon which transports energy from one place to another in the form of electromagnetic radiation. This can also be described as a stream of photons. Photons are massless particles with a velocity equivalent to speed of light in vacuum, 299 792 458 m/s. An electromagnetic radiation is defined by its wavelength, λ in m. Even if the electromagnetic spectrum covers a wide range of wavelengths, from 10^{-16} m to 10^{6} m, the visible range for the human eye is between 380 nm and 780 nm (see Figure 2-2).

The visible spectrum is continuous with no boundaries or gaps from one color to another one. Six named color ranges can be defined from this spectrum: violet (380 nm – 450 nm), blue (450 nm – 495 nm), green (495 nm – 570 nm), yellow (570 nm – 590 nm), orange (590 nm – 620 nm) and red (620 nm – 780 nm). At the boundaries of a color range, for example

at 495 nm, the color defined can be considered as a green or a blue according to the observer. By moving a little around the boundary, a greenish blue or a bluish green is then obtained, the famous turquoise.

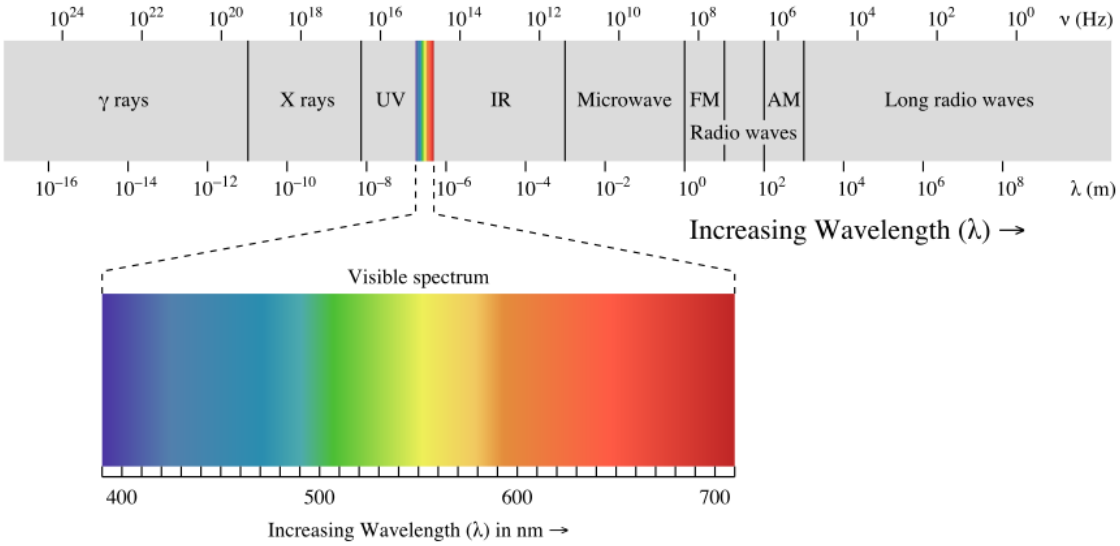

Figure 2-2: Electromagnetic spectrum and visible spectrum from (ChemistryLibreTexts, 2018)

The visible spectrum can also be obtained when a beam of sunlight is crossing a glass prism. Newton discovered this phenomenon in 1666 and reported it in his “New Theory about Light and Colours” to the Royal Society (Newton, 1671). The conclusion drawn is that *“light itself is a heterogeneous mixture of differently refrangible rays”* or in other words, color is an intrinsic property of white light.

2.1.2. Light sources

Sunlight is obviously not the only existing light source. Light can be naturally or artificially produced by for example the sun, stars, fire, incandescent or fluorescent lamps or light emitting diodes (LEDs). Two types of light sources exist: temperature and luminescence radiators. They can be classified into two categories according to the way the light is obtained, naturally or artificially (Klein, 2010a). The visual reference is the sun.

Table 2-1: Several types of light sources adapted from (Klein, 2010a)

Temperature radiators		Luminescence radiators
Natural	**Artificial**	**Artificial**
Sunlight Stars	Blackbody radiator Incandescent lamp	Fluorescent lamp LED

There is no equienergetic light, meaning there is no light having a continuous and flat spectrum, hence the interest of using blackbody radiators as references. To characterize the light sources, their spectral power distributions are compared with the spectral energy distribution of a blackbody radiator. At room temperature, a blackbody appears black. During its heating, a blackbody becomes red, yellow, white and then blue according to the temperature. The Planck law of radiation (2-1) gives the spectral power distribution of a blackbody radiator.

$$S(\lambda,T)d\lambda = \frac{2\pi hc^2}{(\exp\left[\frac{hc}{k\lambda T}\right]-1)\lambda^5}d\lambda \qquad (2\text{-}1)$$

With *S(λ, T), spectral power distribution (unit: W/m^3)*
λ, wavelength (unit: m)
T, temperature (unit: K)
c, speed of light in vacuum (c=299 792 458 m/s)
h, Planck constant (h=6.626 077 x 10^{-34} J.s)
k, Boltzmann constant (k=1.380 648 x 10^{-26} J/K)

The color of the spectrum emitted by a blackbody changes with temperature; Kelvin defined a method to characterize temperature radiators: the correlated color temperature (or CCT) (Wyszecki and Stiles, 1982d). The light emitted by a radiator is compared to the temperature of the blackbody radiator which emits the maximum of light at the same color. According to the CIE[1] (Commission Internationale de l'Éclairage), *"the correlated color temperature is the temperature of the Planckian radiator whose perceived color most closely resembles that of a given stimulus at the same brightness and under specified viewing conditions"* (CIE, 1987).

The main natural light source is the sunlight, which is obviously not constant. The spectrum of sunlight can be associated to a black-body around 5 500 K. Known as artificial light source, lamps are electric lights and depend on the light bulb used. An incandescent light bulb is made from a tungsten wire filament which is heated by an electric current and then glows. Its CCT is around 2 800 K. This system can be compared to a black-body as its emission spectrum is only dependent on its temperature. For a halogen lamp, the filament is surrounded by a small amount of halogen gas (iodine or bromine). This combination improves the lifespan of the source and raises the color temperature to 3 100 K (Klein, 2010a). All light sources are subject to variations for several reasons. For sunlight, latitude, season, air pollution or weather conditions have a considerable impact while lifespan or materials have one for lamps. Besides, a colored sample can produce different colored sensations merely based on lighting conditions (see Figure 2-3).

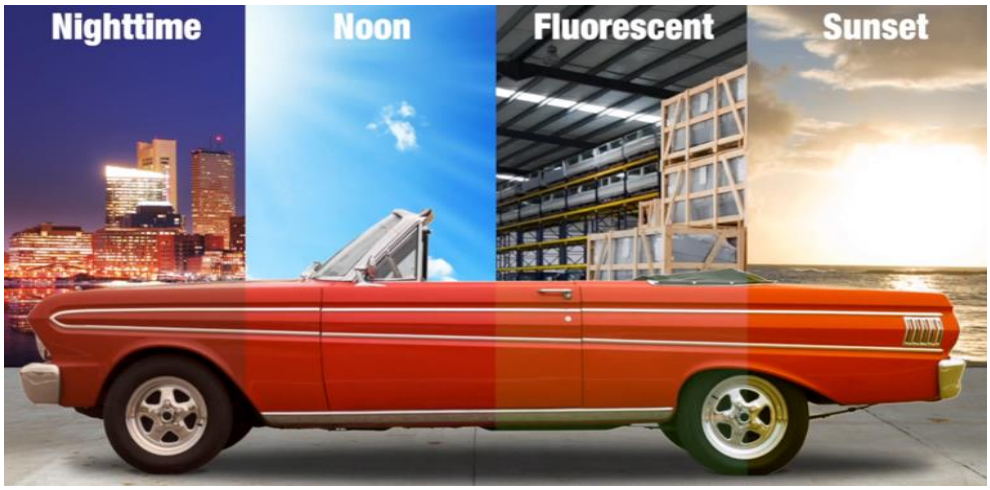

Figure 2-3: Colored sensations according to lighting conditions from (X-Rite, 2018c)

[1] CIE : Commission Internationale de l'Éclairage which oversees normalization and standardization for color quantification or colorimetry

2.1.3. Light: wave-particle duality

Light is an electromagnetic wave, meaning a combination of an electric wave and a magnetic wave. The electromagnetic wave is described by two vectors: $\vec{E}$ for the electric field and $\vec{B}$ for the magnetic field (see Figure 2-4).

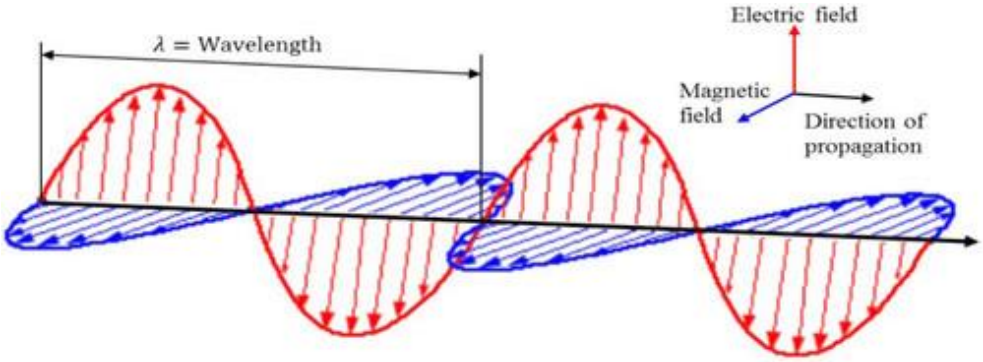

Figure 2-4: Electric and magnetic fields from (Tang, 2015)

2.1.3.1. Quantum approach

Light is both, a wave and a stream of particles (photons, which are massless particles). Their energy E can be described by the Planck-Einstein relation (2-2).

$$E = \frac{hc}{\lambda} \qquad (2\text{-}2)$$

With *E, photon energy (unit: eV[1])*
λ, wavelength (unit: m)
c, speed of light in vacuum (c=299 792 458 m/s)
h, Planck constant (h=6.626 077 x 10^{-34} J.s)

Absorption is a loss of energy explainable by either the wave properties of light or the quantum aspects of photons (Crowell, 2019).

Light absorption of matter (molecule, atom, ion …) occurs when the energy E is equal to the atomic energy difference between two energy levels. In other words, quantum changes in matter lead to photon absorption., Energy is created by electronic, vibrational and rotational transitions in matter and this energy is described by the Born-Oppenheimer approximation (2-3).

$$E_{molecule} = E_{electronic} + E_{vibrational} + E_{rotational} \qquad (2\text{-}3)$$

In the equation (2-3), the electronic transition is defined in the UV or visible area, the vibrational transition in the IR area and the rotational transition in the far IR area. So only the electronic transition is responsible for the color of matter. The electronic transitions are linked to the motion of one valency layer electron from a defined quantum state to another defined quantum state.

[1] 1eV=1.60218 x 10^{-19} J

2.1.3.2. Wave approach

Each electromagnetic radiation in media is governed by Maxwell's equations (2-4), (2-5), (2-6) and (2-7), (Griffiths, 1999).

$$\vec{\nabla} \cdot \vec{B} = 0 \qquad (2\text{-}4)$$

$$\vec{\nabla} \cdot \vec{E} = \frac{\rho}{\varepsilon_0} \qquad (2\text{-}5)$$

$$\vec{\nabla} \times \vec{E} = -\frac{\partial \vec{B}}{\partial t} \qquad (2\text{-}6)$$

$$\vec{\nabla} \times \vec{B} = \mu_0 \vec{j} + \mu_0 \varepsilon_0 \frac{\partial \vec{E}}{\partial t} \qquad (2\text{-}7)$$

With $\vec{E}$*, electric field (unit: V/m²)*
$\vec{B}$*, magnetic field (unit: A/m)*
ρ*, electric charge density (unit: C/m³)*
$\vec{J}$*, electric current density (unit: A/m²)*
ε_0*, permittivity in vacuum (unit: F/m)*
μ_0*, permeability of medium in vacuum (unit: N/A²)*
$\vec{\nabla} \cdot$ *divergence, mathematical operator*
$\vec{\nabla} \times$ *curl, mathematical operator*

The first equation, (2-4), is known as Maxwell-Thomson equation. The magnetic field divergence is equal to 0 because the magnetic transfer moves from one site to another one. The second equation, (2-5), is known as Maxwell-Gauss equation. The electric field divergence is proportional to the charge distribution. The third equation, (2-6), is known as the Maxwell-Faraday equation. The curl of the electric field is inversely proportional to the magnetic field variation overtime. This variation triggers the electric field as it is used for example in the dynamo lamps. Then, for the last one, the Maxwell-Ampère equation, (2-7), the magnetic field triggers a change in electric field overtime. Those last two equations show how these two fields are linked and how a change in the magnetic field triggers a proportional change in the electric field and vice versa.

2.2. Light-matter interactions

After describing the characteristics of a light source, the interaction between the object and the light rays can now be considered. First, two classes of objects can be distinguished: the self-luminous objects which can create light (e.g. sun, fire, fireworks, lightning) and the non-self-luminous objects which are seen because of the light reflected off them (e.g. car, house, moon).

Color perception of non-self-luminous objects is linked to various phenomena of light: reflection, refraction, absorption, scattering, interference or diffraction. Objects and materials are perceived by the eye depending on how they affect the light that lights them. In other words, the light that illuminates an object will be changed by its interactions with matter. For example, if two cars, one blue and one red, are considered, the blue car reflects in the blue area (which means that the rest of the light spectrum is absorbed by the object) while the red one reflects in the red area, see Figure 2-5.

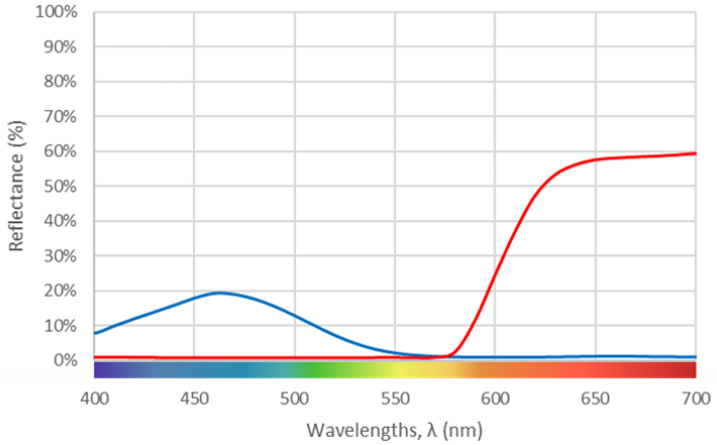

Figure 2-5: Comparison of two colored cars (one blue car - in blue - and one red car - in red) inspired from (Chrisment et al., 1994)

When a light source illuminates an object, it absorbs certain monochromatic wavelengths and reemits others. By considering a red car, all the monochromatic wavelengths will be absorbed except for the red ones, which will be reemitted. The human eye receives reflected light rays which are closely linked to the interaction between light and material.

2.2.1. Light processes

When light strikes an object, its path is changed in many ways according to its optical properties. Various terms are involved to describe the interaction of light with matter.

2.2.1.1. Reflection and reflectance

Reflection occurs when light illuminates an object. According to the reflection law, the angle at which light strikes the matter is equal to the angle at which light leaves the surface with respect to the normal of the reflecting surface, see Figure 2-6. Besides, in this physical process, there is no change in wavelengths. If the surface of the object is matte or textured, the ray will be reflected diffusely according to the roughness of the surface. It is noticeable that, for visual observation of a glossy surface, it is mandatory to avoid observation in the direction of the specular angle (Klein, 2010a).

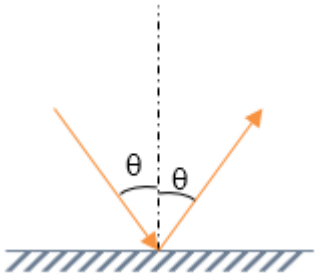

Figure 2-6: Light reflection adapted from (Klein, 2010)

The ratio between the incident light, I, and the reflected light, J, is called the reflectance, R. The reflectance spectrum is the plot of the reflectance as a function of wavelength. The reflectance is dependent on the measurement angle. The reflectance factor is calculated according to the equation (2-8).

$$R_\lambda = \frac{J_x}{I_x} \qquad (2\text{-}8)$$

2.2.1.2. Refraction

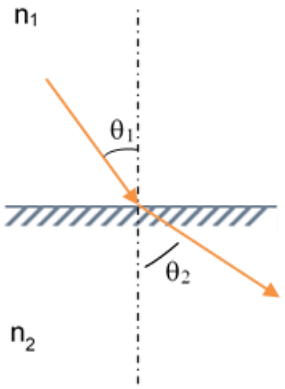

Figure 2-7: Light refraction adapted from (Klein, 2010)

In many cases, only a little part of light is reflected by the surface, the rest goes into the medium by refraction. A change in optical density between the two media triggers a change of the speed of light which leads to a change in direction of the light ray, see Figure 2-7. According to the Snell-Descartes law of refraction (2-9), when light goes from one medium of refractive index (RI) n_1 to another one with a RI of n_2, the light is bent by an angle obtained according to the equation (2-9) (Klein, 2010a).

$$\frac{\sin\theta_2}{\sin\theta_1} = \frac{n_1}{n_2} \qquad (2\text{-}9)$$

2.2.1.3. Absorption and absorbance

Light can be absorbed by objects after it strikes matter and is then converted into energy (Klein, 2010a). Absorption is dependent on the electromagnetic frequency of light and on the chemical structure of the object. When photons of light beams interact with atoms or molecules of an object, the electrons of the object are excited and start vibrating. Many mechanisms can explain light absorption such as atomic vibration and rotation, charge transfer, molecular orbital theory … Since atoms and molecules have their own natural frequency of vibration, they absorb only selected frequencies of visible light. If an object absorbs light of specific wavelengths of the visible spectrum, the observer will not be able to see these colors, but he will see the remaining wavelengths which are reflected and form the color of the object.

The Beer-Lambert law (2-10) is used to express absorption in transparent objects or liquids. Absorbance values span the range between 0, no absorption, through infinity, complete absorption.

$$A = \varepsilon l c \qquad (2\text{-}10)$$

With *A, absorbance*
ε, molar absorptivity
l, path length of the beam of light
c, concentration

2.2.1.4. Interference of light

Most of the pigments used in automotive coatings are based on the light processes previously described (reflection, absorption and refraction). However, it is possible to increase the effects triggered by adding individual traditional light processes together (Klein, 2010a). The impressive color effects of soap bubbles or bird feathers are due to this phenomenon. These specific effects are more and more popular in automotive coatings formulation. To reach those impressive color effects, the individual effects triggered by these traditional pigments are too weak. Pigment particles coated with several layers are used to obtain such appearances by interference of light. The colors of these pigments result from

the superposition of wavelengths. Figure 2-8 shows this phenomenon. The incident wave R1 is refracted in the layer before being reflected by the opaque background. This wave is then reflected at the outer boundary of the layer, R'1. R'2 is the reflected wave of the incident wave R2. On top of the layer, the waves R'1 and R'2 superimpose.

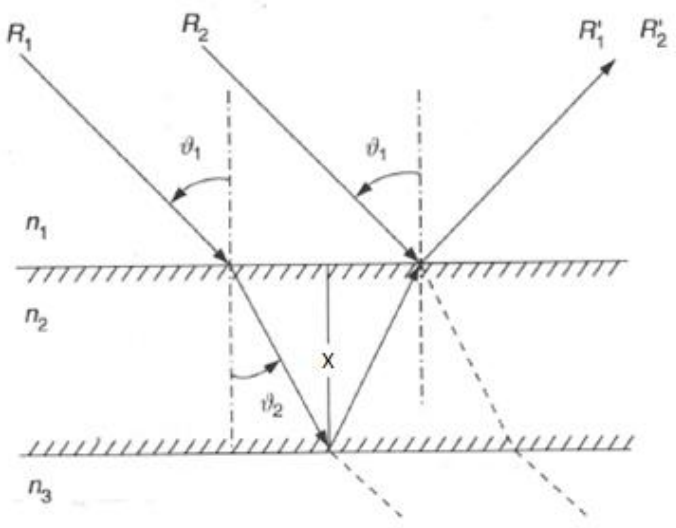

Figure 2-8: Interference of light at a layer of different refractive indices from (Klein, 2010a)

As either the thickness of the film, X, the angle of observation or the wavelength changes, the color produced by constructive interference changes.

2.2.2. Scattering and diffraction

2.2.2.1. Light scattering by a particle

When a particle of one RI is surrounded by a medium of another RI, reflection, refraction and diffraction can occur. The impact of these three phenomena is dependent on the particle size and the wavelength of light (Jarrige, 2013). For macroscopic objects, the interaction between light and object is governed by the equations developed by Newton and is known as lenses. When the particle size is similar or slightly larger (up to ten times) than the wavelength of light, light interacts by using Mie scattering. For smaller particles, light scatters according to a mechanism expressed by Rayleigh.

Particles behave as multipoles which reemit the incident wave. Part of the incident wave is then distributed in the medium according to its own angular law. This phenomenon is called scattering.

It is important to consider that the scattering size of a particle can be larger than the physical size. Moreover, even if incident light rays do not strike the particle but brush past it, they can be scattered.

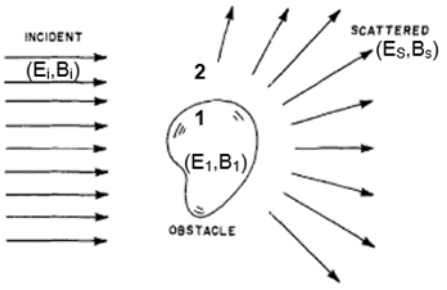

Figure 2-9: Light scattering from (Bohren and Huffman, 2007)

2.2.2.1.1. Mie theory

Based on Maxwell's equations resolution and published in 1908, Mie theory describes the light scattering by a single and spherical particle of one RI embedded by a medium of another RI (Mie, 1908). The strength of the scattering is dependent on four factors: the RI of the particle, the RI of the medium, the diameter of the particle and the wavelength of incident light. The relationship between those four parameters and the scattering strength is explained by Mie theory, which consists of three parameters: the size parameter, κ, (2-11), the relative refractive index, m, (2-12), and the cross section of scattering, $C_{SCA,}$ (2-13). The cross section of scattering, C_{SCA}, is given in units of an area, typically square microns and stands for the area of the particle which interacts with light by scattering.

$$\kappa = kn_{medium} = \frac{2\pi r}{\lambda} n_{medium} \tag{2-11}$$

$$C_{SCA} = \frac{2\pi}{k^2} \sum_{i=1}^{\infty} (2n+1)(|a_i|^2 + |b_i|^2) \tag{2-12}$$

$$m = \frac{n_{particle}}{n_{medium}} \tag{2-13}$$

With C_{SCA}*, cross section of scattering*
a_i *and* b_i*, expansion coefficients of a scattering electromagnetic field*
k, molar attenuation coefficient
κ, size parameter
r, radius of the scattering particle
λ, wavelength of light
m, relative refractive index
$n_{particle}$*, RI of particle*
n_{medium}*, RI of medium*

From these three parameters, the scattering efficiency, $Q_{SCA,}$ (2-14), and the amount of scattering per unit of volume, $S_{MIE,}$ (2-15), are calculated according to the following equations.

$$Q_{SCA} = \frac{C_{SCA}}{\pi r^2} \tag{2-14}$$

$$S_{MIE} = \frac{C_{SCA}}{\frac{4}{3}\pi r^3} = \frac{3Q_{SCA}}{4r} \tag{2-15}$$

However, Mie theory has certain limits. The first limitation is linked to the particle shape. Pigment particles are not perfectly spherical and can be aggregated or cylindrical in some cases. Besides, the particle must be isolated from other particles. In paint films for example, scattering is not created by single particles but by multiple particles which trigger multiple scattering. Besides, the distribution in size and the form of particles make the phenomena more complex.

2.2.2.1.2. Rayleigh theory

When the particle size is below one tenth of the wavelength of light, Rayleigh theory is used to describe the scattering. Due to the very small particle size, it is assumed that the shape of the particle has no influence on light diffraction.

The efficiency parameter, Q_{SCA}, evaluates the scattering of a particle. It is calculated according to equation (2-16).

$$Q_{SCA} = \frac{8}{3}\left(\frac{2\pi r}{\lambda}\right)^4 \left(\frac{n_{particle}^2 - 1}{n_{particle}^2 + 2}\right)^2 \quad (2\text{-}16)$$

With Q_{SCA}, *scattering efficiency parameter*
r, *radius of the scattering particle*
λ, *wavelength of light*
$n_{particle}$, *RI of particle*

Rayleigh theory is especially used to explain the blue color of the sky (Strutt, 2009). The intensity of the light scattered varies due to the inverse of the fourth power of the wavelength. In other words, shorter wavelengths (blue) are scattered more strongly than longer wavelengths (red).

2.2.2.2. Light scattering by a group of particles

In coating films, the distance between particles tends to become smaller and smaller due to the high pigment concentration in formulas. In this case, multiple scattering occurs. In coating industry, TiO_2 particles of approximatively 0.25 µm in size are used to obtain the biggest light-scattering (DuPont™, 2007). Mie theory is very useful to understand light scattering, but it presents some limitations especially for the particle shape. The particles are not perfectly spherical and moreover, are often joined in conglomerates. Besides, when light is scattered by a group of particles, two phenomena not explained by Mie theory occur. The first one is the multiple scattering which creates the opacity of the coating films and the second one is the loss of scattering when two particles scattered are close.

As explained before, even if incident light rays do not strike the particle but brush past it, they can be scattered. The loss of scattering can be easily explained by considering two particles and their light scattering volume. When the gap between two particles is big enough, their light scattering volumes do not overlap (Figure 2-10.a.) but, when it starts to become smaller and smaller, the volumes start to overlap (Figure 2-10.b.) and loss of scattering occurs.

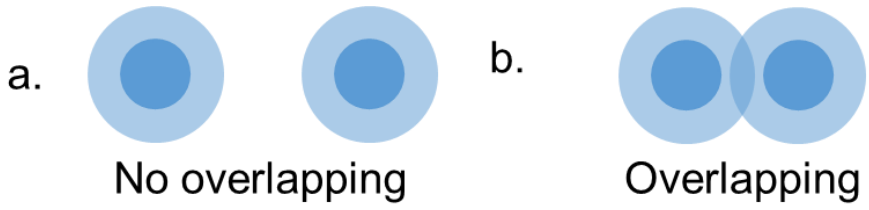

Figure 2-10: Loss of scattering due to particle scattering volumes overlapping

To formulate paints, formulators use solvent, pigments and dispersant polymers among other things. As pigment particles are very diluted in the solvent, they are far enough from each other and can create their own scattering volume without overlapping. When the coating film starts to dry, the solvent molecules are evaporated while pigment particles tend to get closer together until, eventually, their scattering volumes overlap.

Light scattering is close to light absorption. An equation like the Beer-Lambert law describes the amount of scattering (2-17).

$$Amount\ of\ scattering = SX \qquad (2\text{-}17)$$

With *S, amount of light scattered*
X, thickness of the sample

2.2.2.3. The Kubelka-Munk theory

So far, only the scattering phenomenon itself has been considered by either a single particle or a group of particles. In a coating film, billions of particles are involved. In 1931, Kubelka and Munk developed a theory based on the simultaneous absorption and scattering of light from colorant layers (Geniet, 2013). The different layers form a homogeneous material and not a composite of discrete particles in a resin. This consideration frees from limitations of Mie's theory. The Kubelka-Munk theory of reflectance simplifies the light path by assuming its perpendicularity to the surface air-object. It also gives a quantitative description of light-scattering colorant layers as reflectance, transmittance or hiding power.

According to this theory, the coating layer can be divided into several elementary layers with boundaries parallel to those of the complete thickness which have the same properties. The elementary layer is at a distance x of the illuminated surface. Its thickness is defined as dx, whereas X is the total thickness of the colorant layer. The elementary layer is very thin compared to the global layer (dx << X) but it is very wide compared to the pigment particle size. The object is illuminated with incident light of intensity I_0 and after absorption, scattering or transmission, the reemerging light has intensity I. For the elementary layer, two diffuse light fluxes can be distinguished: one going ahead downward through the layer, i, and the other, simultaneous, upward through the layer, j, (Wyszecki and Stiles, 1982a).

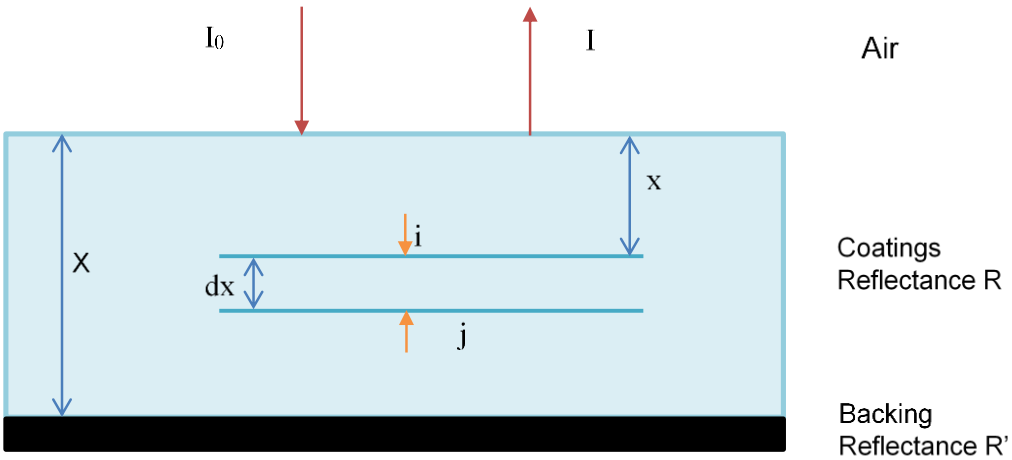

Figure 2-11 : Schematic diagram of light traveling in a colorant layer inspired from (Geniet, 2013)

K is the absorption coefficient which is described as the fraction of absorption of light energy in the elementary layer. S is the scattering coefficient which is described as the fraction lost by having its direction reversed.

During its passage through the elementary layer, the upward-proceeding, j, is reduced by absorption by the amount j(K+S)dx, and increased by scattering in exactly the same way as is the downward-proceeding flux, iSdx (2-18). On the other hand, the downward-proceeding flux, i, is reduced by the amount i(K+S)dx by absorption and increased by scattering by the amount jSdx (2-19). By integrations and mathematical calculations, explicit expressions for reflectance R can be obtained.

$$-di = -(S+K)idx + jSdx \tag{2-18}$$

$$dj = (S+K)jdx + iSdx \tag{2-19}$$

Divide (2-18) by *i* and (2-19) by *j* and add together those equations:

$$\frac{dj}{j} - \frac{di}{i} = d\,ln\frac{j}{i} = -2(K+S)dx + S\left(\frac{i}{j} + \frac{j}{i}\right)dx$$

$$\frac{d\,ln{}^{j}/_{i}}{dx} = -2(K+S) + S\left(\frac{i}{j} + \frac{j}{i}\right) \tag{2-20}$$

Define $R = {}^{I}/_{I_0}$ and $r = {}^{j}/_{i}$ and replace in (2-20)

$$\frac{\mathrm{d}\ln \mathrm{r}}{\mathrm{dx}} = -2(\mathrm{K}+\mathrm{S}) + \mathrm{S}\left(\frac{1}{\mathrm{r}} + \mathrm{r}\right)$$

$$\frac{\mathrm{d}\ln \mathrm{r}}{\mathrm{dx}} = \frac{\frac{\mathrm{dr}}{\mathrm{r}}}{\mathrm{dx}} = \mathrm{S}\left[-2\left(\frac{\mathrm{K}}{\mathrm{S}}+1\right) + \left(\frac{1}{\mathrm{r}} + \mathrm{r}\right)\right]$$

$$\frac{\mathrm{dr}}{\mathrm{r}\left[-2\left(\frac{\mathrm{K}}{\mathrm{S}}+1\right) + \left(\frac{1}{\mathrm{r}} + \mathrm{r}\right)\right]} = \mathrm{Sdx}$$

$$\int_{\mathrm{R}'}^{\mathrm{R}} \frac{\mathrm{dr}}{\mathrm{r}\left[-2\left(\frac{\mathrm{K}}{\mathrm{S}}+1\right) + \left(\frac{1}{\mathrm{r}} + \mathrm{r}\right)\right]} = \mathrm{S}\int_0^{\mathrm{x}} \mathrm{dx}$$

$$\int_{R'}^{R} \frac{dr}{1 + r^2 - 2r\left(\frac{K}{S}+1\right)} = S\int_0^{X} dx \tag{2-21}$$

Define $\mathrm{a} = \frac{\mathrm{K}}{\mathrm{S}} + 1 = \frac{\mathrm{S+K}}{\mathrm{S}}$ and replace in (2-21)

$$\int_{R'}^{R} \frac{dr}{1 + r^2 - 2ar} = S\int_0^{X} dx \tag{2-22}$$

To solve this integral (2-22), it is necessary to define the solutions of the polynomial

$$\Delta = 4a^2 - 4$$

$$r = \frac{2a \pm \sqrt{4a^2+4}}{2} = a \pm \sqrt{a^2-1}$$

$$r^2 + 1 - 2ar = \left(r - a - \sqrt{a^2-1}\right)\left(r - a + \sqrt{a^2-1}\right)$$

$$\frac{1}{r^2+1-2ar} = \frac{A}{r-a-\sqrt{a^2-1}} + \frac{B}{r-a+\sqrt{a^2-1}}$$

$$\frac{1}{r^2+1-2ar} = \frac{A\left(r-a+\sqrt{a^2-1}\right) + B(r-a-\sqrt{a^2-1})}{\left(r-a-\sqrt{a^2-1}\right)\left(r-a+\sqrt{a^2-1}\right)}$$

By comparing coefficients for r and for constants,

$$\begin{cases} A\left(r-a+\sqrt{a^2-1}\right) + B\left(r-a-\sqrt{a^2-1}\right) = 1 \\ A + B = 0 \end{cases}$$

$$\begin{cases} A = \dfrac{1}{2\sqrt{a^2-1}} \\ B = \dfrac{-1}{2\sqrt{a^2-1}} \end{cases}$$

Replace in (2-22)

$$\int_{R'}^{R} \left(\frac{\frac{1}{2\sqrt{a^2-1}}}{\left(r-a-\sqrt{a^2-1}\right)} + \frac{\frac{-1}{2\sqrt{a^2-1}}}{\left(r-a+\sqrt{a^2-1}\right)} \right) dr = S \int_0^X dx$$

$$\int_{R'}^{R} \left(\frac{1}{\left(r-a-\sqrt{a^2-1}\right)} - \frac{1}{\left(r-a+\sqrt{a^2-1}\right)} \right) dr = 2S\sqrt{a^2-1} \cdot \int_0^X dx$$

$$\left[ln \frac{r-a-\sqrt{a^2-1}}{r-a+\sqrt{a^2-1}} \right]_{R'}^{R} = 2S\sqrt{a^2-1}X$$

$$\ln \frac{\mathrm{R}-\mathrm{a}-\sqrt{\mathrm{a}^2-1}}{\mathrm{R}-\mathrm{a}+\sqrt{\mathrm{a}^2-1}} - \ln \frac{\mathrm{R}'-\mathrm{a}-\sqrt{\mathrm{a}^2-1}}{\mathrm{R}'-\mathrm{a}+\sqrt{\mathrm{a}^2-1}} = 2\mathrm{S}\sqrt{\mathrm{a}^2-1} \cdot \mathrm{X}$$

By defining $b = \sqrt{a^2-1}$,

$$ln \frac{R-a-b}{R-a+b} - ln \frac{R'-a-b}{R'-a+b} = 2SbX$$

$$ln \frac{(R-a-b)\cdot(R'-a+b)}{(R-a+b)\cdot(R'-a-b)} = 2SbX \qquad (2\text{-}23)$$

Consider the limiting conditions where the global layer is infinite, then $R=R_\infty$ and the backing reflectance can take any value since the light cannot reach it. To simplify the equation, the backing reflectance R' is set to 0, R'=0

$$R_\infty = \mathrm{a} - \mathrm{b} = \mathrm{a} - \sqrt{\mathrm{a}^2-1} = 1 + \frac{\mathrm{K}}{\mathrm{S}} - \sqrt{\left(\frac{\mathrm{K}}{\mathrm{S}}\right)^2 + 2\frac{\mathrm{K}}{\mathrm{S}}}$$

$$a = \frac{{R_\infty}^2 + 1}{2R_\infty}$$

$$\frac{K}{S} = \frac{(R_\infty - 1)^2}{2R_\infty} \qquad (2\text{-}24)$$

$$b = \frac{1 - {R_\infty}^2}{2R_\infty}$$

Replace a and b in equation (2-23) to get the expression of R

$$R = \frac{\frac{1}{R_\infty}(R' - R_\infty) - R_\infty\left(R' - \frac{1}{R_\infty}\right)exp\left(\left(\frac{1}{R_\infty} - R_\infty\right)SX\right)}{(R' - R_\infty) - \left(R' - \frac{1}{R_\infty}\right)exp\left(\left(\frac{1}{R_\infty} - R_\infty\right)SX\right)}$$

Equation (2-24) is known as the Kubelka-Munk function. The reflectance R_∞ can only be lower than 1 if the absorption coefficient, K, is non-null.

For many years, in various industries (paint, ink, plastic …), it is needed to create specific colors for customers. The customer provides a standard to be color-matched. The “right” color can be matched either by a knowledge-based trial and error approach or by computational color recipe calculation. For the first approach, colorists mix various pigments to obtain the perfect match. For computed color formulation, colorists use a spectrophotometer, a device measuring the reflectance of the reference and the samples. The matching process is helped by an algorithm which selects and adjusts the different proportions of the pigments. This algorithm is based on the Kubelka-Munk theory.

As a start, it is mandatory to characterize each pigment by creating several letdowns (also called primary binary blends), such as the respective pigment in white or the pure pigment for example. These letdowns (at least 2) are measured with a spectrophotometer and the calculation can be made according to the Kubelka-Munk function, (2-24).

$$\left(\frac{K}{S}\right)_p = \frac{\left(1 - R_p\right)^2}{2R_p} = \frac{C_p K_p}{C_p S_p} \qquad (2\text{-}25)$$

$$\left(\frac{K}{S}\right)_{mix} = \frac{(1 - R_{mix})^2}{2R_{mix}} = \frac{C_p K_p + C_{white} K_{white}}{C_p S_p + C_{white} S_{white}} \qquad (2\text{-}26)$$

With *$(K/S)_p$, ratio for pigment,*
R_p, reflectance of the letdown “pigment”
C_p, concentration of pigment
R_{mix}, reflectance of the letdown “pigment+white”
C_{white}, concentration of white
K_{white}, absorbance coefficient of white
S_{white}, scattering coefficient of white

The absorbance and scattering coefficients of the pigment, K_p and S_p, can then be derived from the two previous equations, (2-25) and (2-26).

Once all the pigments from a given set to be used have been characterized, the computed color formulation process can be used. To predict color and according to the Kubelka-Munk theory, the absorption and scattering coefficients, K and S, of a colored mixture can be deducted from the individual coefficients of each pigment. This theory is based on a law of additivity, the law of Duncan. The coefficients of the mixture are calculated by summation of the weighted coefficients of each pigment composing the final color.

$$K = K_0 + c_1k_1 + c_2k_2 + \cdots + c_Nk_N = K_0 + \sum_{i=1}^{N} c_ik_i \qquad (2\text{-}27)$$

$$S = S_0 + c_1s_1 + c_2s_2 + \cdots + c_Ns_N = S_0 + \sum_{i=1}^{N} c_is_i \qquad (2\text{-}28)$$

With *K and S, absorption and scattering coefficients of the mixture*
K_0 and S_0, absorption and scattering coefficients of the substrate
c_i, concentration of individual pigment
k_i, unit absorptivity of individual pigment
s_i, unit scattering of individual pigment

Divide (2-27) by (2-28)

$$\frac{K}{S} = \frac{K_0 + c_1k_1 + c_2k_2 + \cdots + c_Nk_N}{S_0 + c_1s_1 + c_2s_2 + \cdots + c_Ns_N} = \frac{(1 - R_\infty)^2}{2R_\infty} \qquad (2\text{-}29)$$

Equation (2-29) is known as the two-constant Kubelka-Munk theory. In many color-matching problems such as in paint industry, the scattering is mostly provided by the white pigment added in the formulation or by the substrate itself. When the scattering coefficient S_0 is large in comparison to the scattering provided by the pigments, the equation (2-28) can be simplified to $S \approx S_0$. By simplification of the equation (2-29), equation (2-30) is obtained; it is known as the single-constant Kubelka-Munk theory.

$$\frac{K}{S} = \frac{K_0 + c_1k_1 + c_2k_2 + \cdots + c_Nk_N}{S_0} = \frac{K_0}{S_0} + c_1\frac{k_1}{S_0} + c_2\frac{k_2}{S_0} + \cdots + c_N\frac{k_N}{S_0}$$

$$\frac{K}{S} = \frac{(1 - R_\infty)^2}{2R_\infty} \qquad (2\text{-}30)$$

The algorithm, based on linear least-squares techniques, will adjust the different pigment quantities to minimize the spectral difference between the standard to color-match and the theoretical reflectance curve of the mixture of scattering pigments. The Kubelka-Munk theory is mainly suitable for simple mixtures such as solid colors. However, when the mixtures start to become more complex, this theory is not applicable anymore.

2.3. Human color vision

After describing the characteristics of a light source and the interactions between the object and the light rays, human color vision can now be considered. Since Newton discovered the multichromatic composition of light, color vision has been investigated to understand how the human visual system works. Color vision is the ability to distinguish differences in light composition. The field of vision science is very sophisticated, only an overview of the most important topics will be given in this paragraph.

To have the ability to see, an organism must have on one hand a receiving organ to focus the electromagnetic wave on a sensitive surface and on the other hand a processing organ to group and analyze the different signals. For the human visual system, the eye and the brain respectively assume these two functions.

2.3.1. Anatomy of the eye

Both eyes are spherical globes with an average diameter of 25 mm. The distance between those two eyes is about 6 cm. Each eye is in one eyeball and then linked to the brain thanks to the optic nerve. Eyes are composed of several elements which lead to vision. A vertical cross-section through the eye is presented in Figure 2-12.

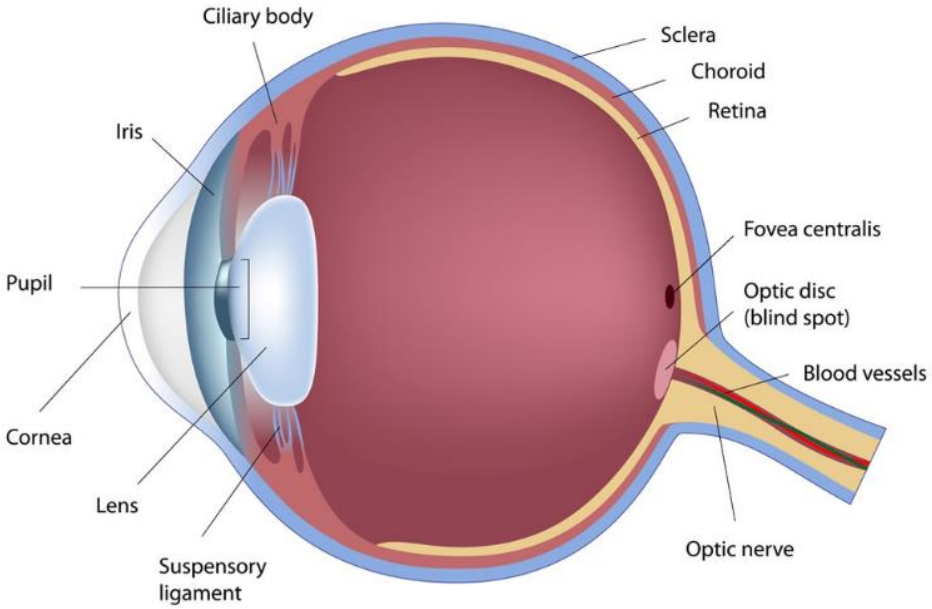

Figure 2-12: Anatomy of the eye from (Iristech, 2018)

For better understanding, the eye can be compared at first sight to a camera (National.Keratoconus.Foundation). In a camera, the front camera lens focuses light on the film and when light hits the film, the picture is taken. The eye functioning is very close. First, the lens allows light to pass through before being focused by the cornea on the retina. When light hits the retina, cells collect the signal to convert it into electric signals which are transmitted to the brain. The color sensation is then created. The following elements are presented according to their position in the light path through the eye.

2.3.1.1. The cornea

The first element crossed by light rays is the cornea (Wyszecki and Stiles, 1982b). The cornea is the transparent front part of the eye through which light rays enter. Its thickness is about 0.5 mm while its RI is around 1.377. According to Snell's law of reflection (see (2-9)), a change of media with two different RIs leads to a change in the light rays' direction. Its main function is then to refract light based on its curved shape. Most of the light entering in the eye is focused by the cornea which handles two-thirds of the eye's total optical power. The cornea must stay perfectly clean and transparent. Regular closing of the eyelids and tear secretion keep the surface of the cornea free of any impurity. The cornea tends to repair minor abrasions by itself but deeper abrasions create scars and the transparency of the cornea is lost.

2.3.1.2. The iris and the pupil

After being refracted, light rays cross the iris and the pupil (Wyszecki and Stiles, 1982b). The iris is a flat and circular structure in the eye with an adjustable opening in the center, the pupil. The iris sphincter muscle contracts or extends the pupil to modulate the amount of light that reaches the retina. If there is too much light the pupil is contracted and if not, extended. This modification linked to the ambient light is involuntary and is also called the pupillary reflex. The color of the iris is related to the genetic code of each individual and is linked to the concentration of melanin. In some cases, the lack of melanin leads to a red color of this structure for people with albinism. As the pupil absorbs most of the light touching the eyes, it appears as a black sphere in the center of our eyes.

2.3.1.3. The lens

After their focusing, the light rays pass through the lens (Wyszecki and Stiles, 1982b). The lens is a transparent and flexible structure pinpointed just behind the iris, which helps to refract light before being focused on the retina. By changing its shape and its focal distance, it focuses the crossing light rays to create clear images of objects at various distances which can be easily seen by accommodation. If one looks at a close object, the lens becomes thicker. On the contrary, for a distant object, it becomes flatter. This change in thickness leads to an increase or a decrease of the optical power, respectively, and eventually our vision of the object is sharpened. With age, the lens tends to become harder so it loses its flexibility and observers cannot focus on close objects anymore – this is called presbyopia. The lens looks like an ellipsoid and a lack of curvature of the lens can lead to vision abnormalities such as myopia (high bending) where far objects seem fuzzy or hyperopia (low bending) where nearby objects seem fuzzy. Other abnormalities come from lens degenerations which can be related to age as e.g. cataract due to opacification of the lens cells.

2.3.1.4. The retina

After all this travel through the eye, light rays finish by reaching the retina, found at the back of the eye and covering 75% of the human eye (Wyszecki and Stiles, 1982b). This thin layer is composed of 150 million of photosensitive cells which are present everywhere in the retina except for the center part, the so-called blind spot (the connection between the eye and the optic nerve). They start the conversion of optical signals to neural signals which are

then transmitted to the brain. Color vision relies on the retinal processing which will be explained in the next parts: 2.3.2. Structure of the retina (page 25) and 2.3.4. The visual pathway (page 30).

2.3.1.5. The optic nerve

The optic nerve is the last structure of the eye before the transmission of the visual information to the brain. It is made of the axons of the ganglion cells (Wyszecki and Stiles, 1982b). The optic nerve is made of one million of fibers while each retina counts around 150 million of photosensitive cells. There is a high compression of the optical signal with loss of information before its transfer to the brain. Since the optic nerve is connected to the retina, there is a small area which would have been covered by photoreceptors where no visual stimulation can occur, the blind spot.

2.3.2. Structure of the retina

The retina is the very first neural structure involved in color vision (Rigaudière, 2013). It has photosensitive cells and cells which send chemical and electrical signals to the brain. 150 million of nervous cells are complexly organized in different layers of the retina to discriminate colors and detect contrast and motion. The light rays entering in the eye hit first the ganglion cells and the other layers before stimulating the photoreceptors and being absorbed by the pigmented cells, the pigment epithelium. Diverse types of nervous cells are in the retina such as horizontal cells or bipolar cells which coordinate the transmission of signals to the brain. These cells are schematically organized in a double structure with a radial structure to preserve the image and a transverse one to detect contrast effects by modulating the direct signal according to the adjacent signals as exemplified in Figure 2-13.

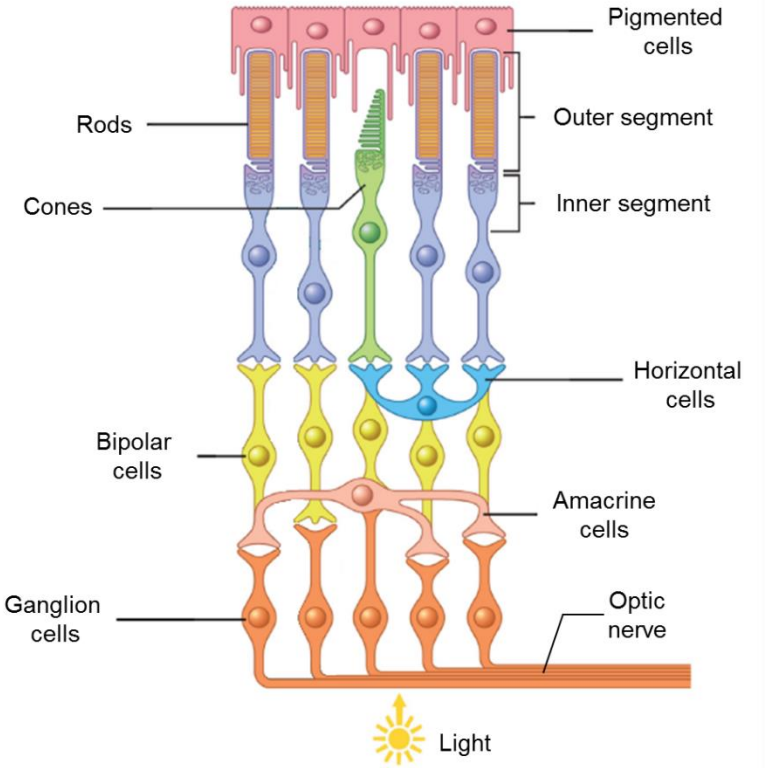

Figure 2-13: Structure of the retina, picture adapted from (Salesse, 2017)

2.3.2.1. Pigmented cells

The pigmented cells form the external layer of the retina. Their high concentration in melanin leads to its very dark color. This layer assumes three roles: a screen role, a place of exchanges and a role in the metabolism of the retinal. It serves as a screen because the pigmented cells absorb scattered light or an excess of light to avoid glare. Besides, this layer is very important in the retina physiology. As a place of exchanges, the pigmented cells are needed to share essential substances (oxygen or water) to photoreceptors and other cells. By its high concentration in melanin, this layer can give vitamin A (retinal) to photoreceptors for rhodopsin regeneration. Rhodopsin is a light-sensitive protein essential in the visual phototransduction (see paragraph 2.3.3).

2.3.2.2. Rods and cones

In each retina, around 150 million of photoreceptors assume the visual phototransduction. The human retina counts about 120 million rods which are extremely sensitive to light and 7 million cones that exhibit sensitivity selectivity as a function of the wavelengths. Rods, rod-shaped photoreceptors, are present everywhere in the retina except for the center part, the so-called fovea. Rods are used for vision under scotopic conditions where the light level is very low (below 10^{-4} cd/m²) and caused by their non selective sensitivity, objects seem greyish. That explains the famous saying “all cats are grey in the dark”. Cones, cone-shaped photoreceptors, are mainly found in the center of the retina. They are less sensitive to light but sensitive to wavelengths. Three types of cones can be found: short-wavelength cones (S), sensitive to blue, middle-wavelength cones (M), sensitive to green and long-wavelength cones (L), sensitive to red, (Fairchild, 2013c). Their spectral sensitivities are illustrated in Figure 2-14. Cones handle our vision under photopic conditions (normal lighting conditions, above 10 cd/m²) and our ability to see the world around us in color. However, there are fewer blue cones than green and red cones with a proportion of 1 for 16 for 32. Actually, this is explained by the absence of blue cones in the very central area of the fovea.

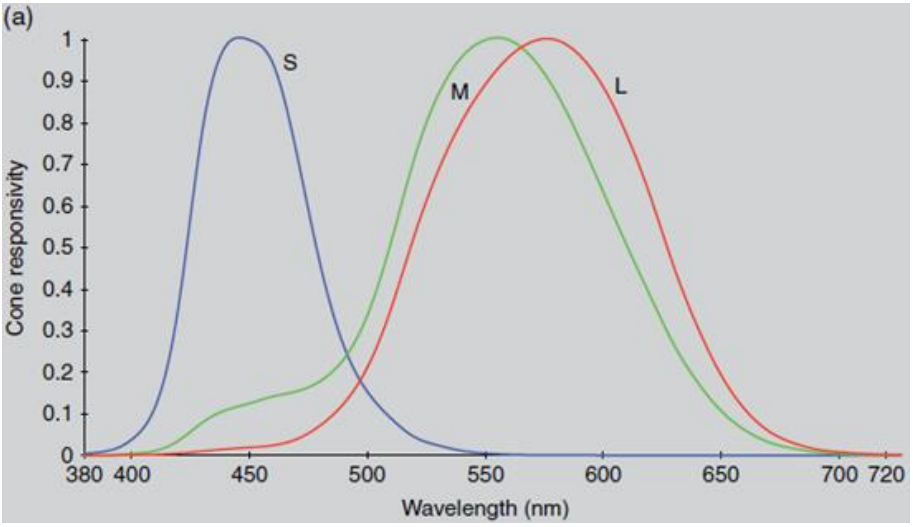

Figure 2-14: Spectral sensitivity of the S, M and L cones from (Fairchild, 2013c)

The photoreceptors are specific neurons with a membrane holding photopigments. These photopigments change their molecular structure after absorbing photons. To detect

light, the photoreceptors rely on the light sensitivity of the rhodopsin for rods and the iodopsin for cones. Three types of iodopsin exist and are present in the cones according to their wavelength sensitivity: the cyanolabe, sensitive to short wavelengths, the chlorolabe, to medium wavelengths, and the erythrolabe, to long wavelengths, (Beaudot, 1994). The two visual pigments, rhodopsin and iodopsin, are similar and consist of the union of retinal and opsin. The only difference noticeable is on the opsin. For rods and S cones, the opsin is made of 348 amino acids while 364 are needed for M and L cones. For example, cone M and cone L have only 4% of difference in their structure while cone S and cone M differ by 40%. Differences in protein structure lead to differences in wavelength sensitivity. The sensitivity of the retinal is conditioned by the structure of the protein around it.

The fovea is found right at the center of the retina. In this area with a width of 2 degrees, the concentration of cones is around 140 000 cones/mm². This small area equivalent to the size of our thumbnail held at arm's length handles color and spatial vision at a very high accuracy. Rods are few in the region near the fovea but increase in number in peripherical regions.

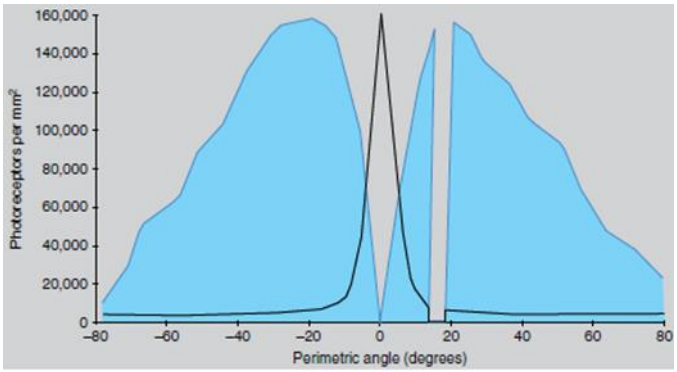

Figure 2-15: Density of photoreceptors (blue for cones and black for rods) in the retina from (Fairchild, 2013c)

A blind spot can also be noticed at 15° degree from the fovea. In this area, the optic nerve is formed and there is no room for photoreceptors (Fairchild, 2013c).

2.3.2.3. Bipolar cells

The bipolar cells are connected to the photoreceptors on one side and to the ganglion cells on the other side and sometimes even to the horizontal cells. The signals transmitted to the ganglion cells are in form of graduated potentials (depolarization or hyperpolarization) depending on the ON or OFF type of the bipolar cells. Two types of pathways exist: direct, one photoreceptor is linked to one bipolar cell, or indirect, several photoreceptors are connected to one horizontal cell which is linked to one bipolar cell. The direct pathway is mainly found in the fovea. The diffusion of the sensorial signal is quicker with this type of connection. It explains the reason why the visual acuity is better in this area. In the peripherical retina, thousands of photoreceptors are linked to one horizontal cell.

2.3.2.4. Horizontal cells

The horizontal cells are sideways connected to several photoreceptors on one side and bipolar cells on the other side. They inhibit the activity of the neighboring cells to increase the acuity of the sensorial signals. When light rays hit the retina, some of the photoreceptors are strongly lighted while others are weakly illuminated. By reducing or cutting off the sensorial signal of the weakly illuminated photoreceptors, only the signal emitted by the strongly illuminated photoreceptors is transmitted to the ganglion cells. The horizontal cells improve the contrast perception.

2.3.2.5. Ganglion cells

The ganglion cells are connected on one side to the amacrine cells and to the bipolar cells and on the other side form the optic nerve. One million of these cells are counted in the retina and their density is low around the fovea (one cone for one ganglion cell) but increase in the peripherical areas due to its high number of connections to photoreceptors. These cells handle the signal transmission from the retina to the brain (Rodieck, 1998). They estimate three types of contrast: luminance, spectral and temporal. The luminance contrast conveys the difference in light spatial distribution over the entire retina. The spectral contrast enables to compare activities resulting from the cones. Finally, the temporal contrast serves to distinguish the speed with which lightening varies in the center and the periphery of the retina (Imbert, 2006).

The ganglion cells are classified into three groups but more than 15 categories exist according to (Wassle, 2004). The parvocellular ganglion cells, P-cells, are small and found in the fovea. They stand for 80% of the ganglion cells. The P-cells are useful for luminance, temporal and spectral contrasts with object discrimination, detail perception and chromatic vision. Some of them offer a high chromatic resolution between green and red. The magnocellular ganglion cells, M-cells, are wide and found in retina peripherical area. They are connected to thousands of photoreceptors thanks to amacrine and bipolar cells. The M cells, 5% of the ganglion cells, help in temporal contrast with motion and form detection. The koniocellular ganglion cells, K-cells, are not very known and the latest studies suppose a role in luminescence coding and motion detection in only one direction.

2.3.3. Visual phototransduction

The processing of visual information starts in the retina thanks to the light detection of photoreceptors. Rods and cones handle light absorption and transduction of the signal. The signal is then transmitted to bipolar, amacrine and ganglion cells before being transmitted to the brain. The conversion of electromagnetic energy of light into a change in electrical potential and then neural activity is a complex process called the visual phototransduction.

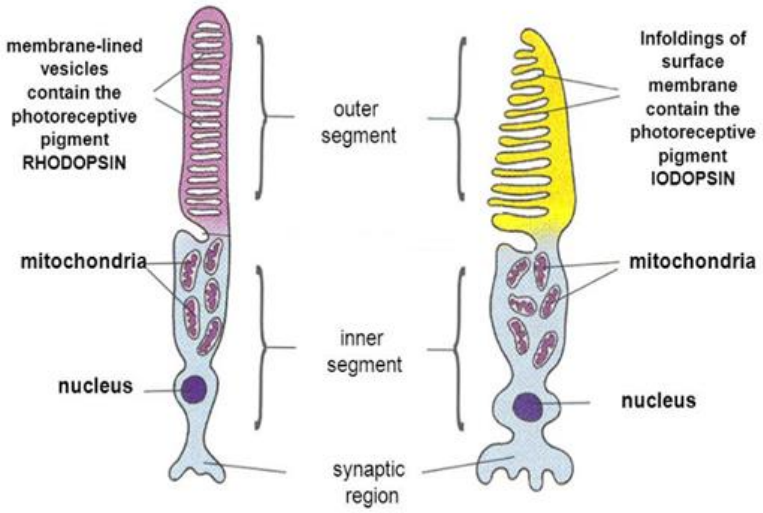

Figure 2-16: Rod (left) and cone (right) structures from (Powell, 2016)

Rods and cones structure are globally similar (see Figure 2-16). They are made of an outer segment, an inner segment, a nucleus and a synaptic termination. The only difference consists in the form of their outer segment, the light sensitive part. A folding of the plasma membrane is seen for cones while rods consists of a stacking of disks surrounded by a plasma membrane. The rod outer segment has a piling of 500 to 2,000 disks and each side of a disk contains in average 26,000 molecules of rhodopsin (Buzhynskyy et al., 2011).

A schematic view of the phototransduction process is presented in Figure 2-17. The phototransduction starts when light strikes the retina (Salesse, 2017). A rhodopsin molecule contained in a photoreceptor captures a photon. This results in a photo-isomerization of the 11-cis-retinal contained in rhodopsin (or iodopsin) into all-trans-retinal. Before its isomerization, the 11-cis retina is bound to the opsin that surrounded it. Once isomerized, the all-trans retinal does not have the proper complementary form anymore. The retinal is dissociated from the opsin. The opsin no longer connected to its chromophore is bleached, the retinal photobleaching. A conformational change from rhodopsin (or iodopsin) to metarhodopsin II (MII) allows the activation of transducin, a G protein. This is the first stage of phototransduction amplification. MII activates 1300 molecules of transducin per second. Transducin (G) in turn activates phosphodiesterase (PDE) in the plasma membrane that hydrolyzes cyclic guanosine monophosphate (cGMP). This hydrolysis is the second amplification step since a PDE molecule hydrolyzes 6,000 to 8,000 cGMP per second. The cGMP molecules accumulate and cause the closing of the cationic channels with an incoming current. This closure causes a membrane hyperpolarization of the photoreceptors and a stop of glutamate release. The hyperpolarization of photoreceptors results in a cascade depolarization of bipolar cells and then ganglion cells before the transmission of the message to the brain.

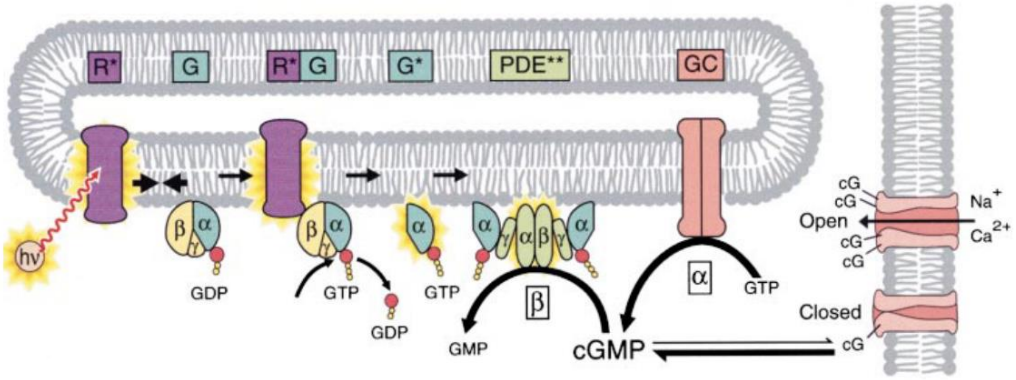

Figure 2-17: Schematic of the visual phototransduction from (Leskov et al., 2000)

The photoisomerization of 11-cis-retinal to all-trans-retinal in photoreceptors is the first step of vision (Kono et al., 2008). As vision is an on-going process, the reconversion of bleached all-trans-retinal to 11-cis-retinal is needed. After a photon being captured by rhodopsin, the 11-cis-retinal isomerized in all-trans-retinal is released in the outer segment of the photoreceptor. In this segment, the all-trans-retinal is reduced to the all-trans-retinol. Interphotoreceptor retinoid-binding proteins (IRPB) present in the photoreceptors help in the transport of all-trans-retinol to the pigmented cells contained in the retinal pigment epithelium (RPE).

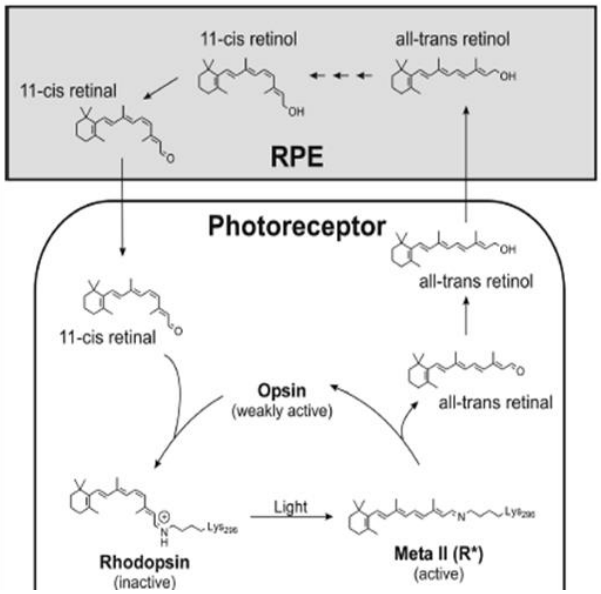

Figure 2-18: Conversion of all-trans-retinal to 11-cis-retinal from (Kono et al., 2008)

In the RPE, three enzymes handle the conversion of all-trans-retinol to 11-cis-retinal: the lecithin retinol acyl transferase (LRAT), the isomerohydrolase (RPE65) and the cellular retinaldehyde binding protein (CRALPB) (Pepperberg and Crouch, 2001). The all-trans-retinol is transformed to all-trans-retinyl ester with LRAT. Catalyzed by RPE65, these esters are isomerized and hydrolyzed in 11-cis-retinol which is then oxidized into 11-cis-retinal. To complete the visual cycle, newly generated 11-cis retinal is transported back to the photoreceptors to regenerate rhodopsin. In some cases of high and sudden glare, it might be difficult to see; this is due to the depletion of 11-cis retinal in rods.

2.3.4. The visual pathway

The visual information is projected in mirror-inverted effect on the retina. After being converted by the retina, the visual information is then transferred to the brain by the optic nerve. This transmission process includes a crossing of axons at the optic chiasma, a continuation in the optic tract before arriving to the lateral geniculate nucleus (LGN). From the LGN, the optic radiations travel to the primary visual cortex. Figure 2-19 describes the visual pathway.

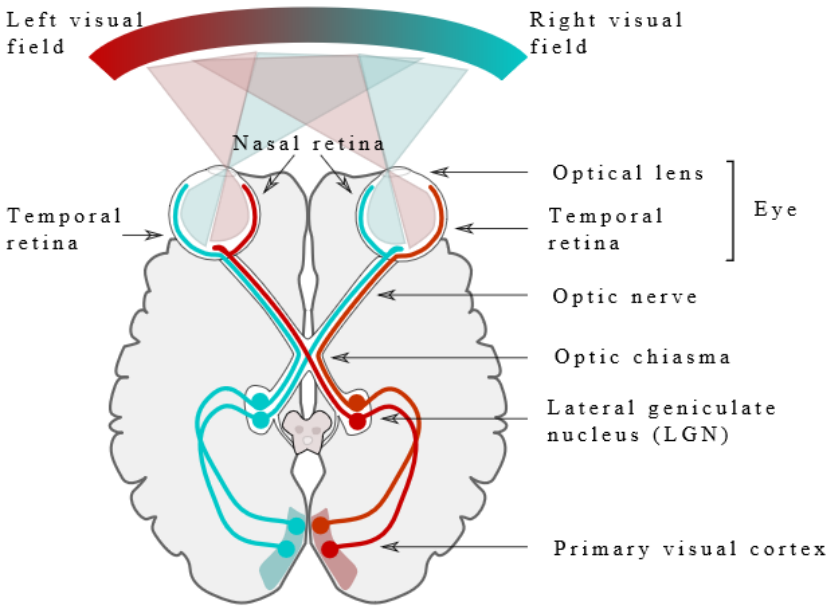

Figure 2-19: Visual pathway from the retina to the primary visual cortex from (Elster, 2018)

2.3.4.1. The optic chiasma

After being projected on the retina, the image can be cut down in two halves with the fovea as the center. For each retina, the first half close to the nose is called the nasal half and the other one, close to the temple, the temporal half. In the left eye, the nasal side sees the left part of the visual scene while the temporal side sees the right part of the visual scene and vice versa for the right eye. Globally, the left nasal side and the right temporal side see the same field of view which is referred to as the left hemifield; the opposite applies to the right hemifield. The optic nerve fibers on the nasal sides of each retina cross over the optic chiasma while the two temporal sides stay on the same side and do not cross. It is therefore the place where the visual information of the same hemifield is connected and then continues its pathway via the LGN. The right hemifield is treated by the left cerebral hemisphere while the left hemifield is treated by the right cerebral hemisphere. Each hemisphere of the brain receives information from the opposite side of the visual scene (Remington, 2012).

2.3.4.2. The lateral geniculate nucleus (LGN)

The axons of the ganglion cells form the optic nerve where the visual information passes before arriving at the LGN. The LGN is the first synaptic relay center for the visual pathway in the brain. This part of the brain, the thalamus, receives visual information from the retina. This is the first connection between the retina and the primary visual cortex (Remington, 2012).

The LGN consists of a stack of six layers which implies that some aspects of the visual information are separately processed in this relay. The left LGN receives the axons of the right temporal half and the left nasal half and vice versa for the right LGN. The axons from the eye on the same side as the LGN (ex: right eye for right LGN) connect to layers 2, 3 and 5 while those from the eye on the other side (ex: left eye for right LGN) connect to 1, 4 and 6. Layers 1 and 2 are called the ventral layers while the layers 3 to 6 are the dorsal layers.

The ventral layers hold larger neurons than the dorsal layers. As for ganglion cells, the terms magnocellular and parvocellular are used to qualify the connections made in the different layers (Tovée, 2008).

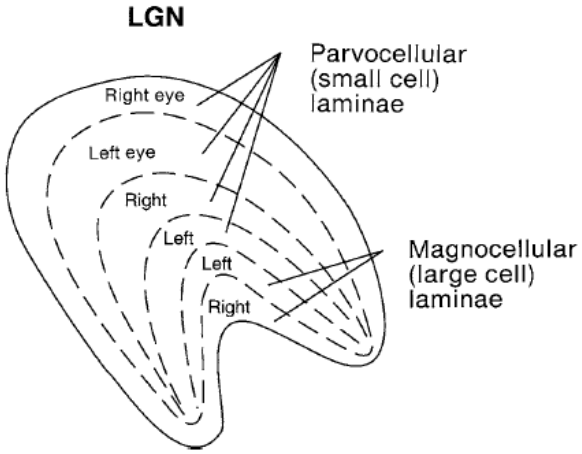

Figure 2-20: Schematic diagram of the left LGN from (Tovée, 2008)

Thus, the magnocellular ganglion cells (M) will connect in the ventral magnocellular layers 1 and 2 while the parvocellular ganglion cells (P) connect in the dorsal layers 3 to 6. The koniocellular ganglion cells (K) are found between each layer. This confirms a parallel processing of distinct information channels.

2.3.4.3. From the LGN to color perception

After the LGN, the transformed signals reach the back of the brain where the center of our visual perception is located, the visual cortex. The color perception is then produced, 100 to 150 ms after photon absorption in the retina. In the theory of human color perception, two theories confront: Young-Helmholtz theory and the Hering theory.

In the 19th century, Young (1802) and Helmholtz (1850) studied color perception. The Young-Helmholtz theory assumes a trichromatic color vision where three types of receptors located on the retina and sensitive to a specific range of wavelengths exist (Fairchild, 2013c). These photoreceptors could be classified into three categories: sensitive to short wavelengths (blue), to medium ones (green) and to long wavelengths (red). This theory assumes then that the color perception relies on a mix of all three photoreceptors, the additive properties of color mixtures. Nowadays, since 1983 and the experiment of Dartnall, Bowmaker and Mollon, these three photoreceptors are known as the cone cells.

Conversely, in 1878, Hering assumed that color perception works as a system based on color opponency in the opponent colors theory (Fairchild, 2013c). He noticed some color combinations are impossible to see such as greenish-red or yellowish-blue even if it should be possible to perceive them according to the Young-Helmholtz theory. Hering suggested a color perception based on the activity of three opponent systems (or receptor pairs): white-black, red-green and yellow-blue. In that theory, yellow-blue receptors cannot send messages about both colors at the same time.

Even if the two theories seem to be contradictory, in the middle of the 20th century, various researches lead to the combination of the trichromatic and the opponent-colors theories such as (Svaetichin and Macnichol, 1959), (De Valois et al., 1958) or (Wiesel and Hubel, 1966). It is now well established that both theories complement one another. The trichromatic theory gives an adequate description of light processing at retinal level while the opponent colors theory explains the transformation of the nerve impulses into an achromatic signal and two opponent chromatic signals (yellow-blue and green-red). Those two are gathered under the naming stage theory where the color perception starts by the trichromatic vision with the photoreceptors and then the color opponency occurs partly in the retina and partly in the visual pathway. (Boynton, 1986) proposed a simplified color vision model diagram as detailed in Figure 2-21.

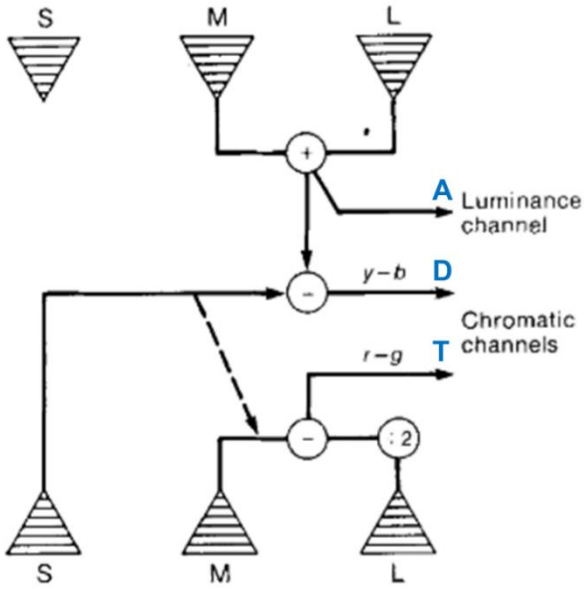

Figure 2-21: Simplified color vision model diagram adapted from (Boynton, 1986)

This color vision model represents the output of the color-opponent process which is converted into three channels: A for Luminance, T for Red-Green and D for Yellow-Blue. As explained in the diagram in Figure 2-21, each new channel is a combination of the input signals from the cones, represented by triangles S, M or L according to their sensitivity to wavelengths. The addition of signals from M and L cones leads to the luminance channel, A. The yellow-blue channel, D, is linked to the sum of the signals from M and L cones minus the input of the S cones. Finally, the red-green channel, T, is obtained by subtracting L signal minus twice the value of the M signal.

2.3.5. Visual adaptation to the environment

The human visual system is not a static one as it must adapt itself to changes such as in lightness or chroma. In order to optimize its response to viewing conditions, the retina adjusts its sensitivity according to lighting conditions thanks to the two types of photoreceptors, the cones for high levels of light (photopic conditions) and the rods for low levels of light (scotopic vision). Various types of mechanisms of adaptation exist such as the luminance adaptation and the chromatic adaptation. The sensitivity of the eye is then

measured by determining the minimum luminance needed to see and thus produce the visual sensation, the intensity threshold.

The luminance adaptation can be divided into two categories: light and dark adaptations. The human visual system can work at different levels of illumination from 0.0003 lx to 100,000 lx according to two mechanisms: a change in the pupil size and an alternative or cumulative function of the photoreceptors.

The dark adaptation occurs when going into a dark area, coming from a very light area. The visual system responds to the lack of light by increasing its sensitivity. The dark adaptation is detailed in Figure 2-22.

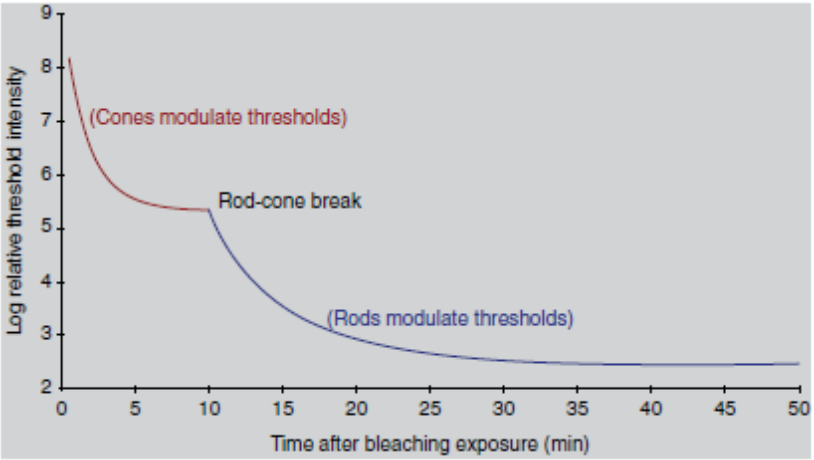

Figure 2-22: Dark adaptation curve from (Fairchild, 2013c) where the rods take the advantage over the cones after 10 minutes before reaching their maximum of efficiency after 30 minutes

At first, the surroundings seem completely dark but after a few minutes, objects can be distinguished. As seen in Chapter 2, paragraph 2.3.2.2, the cones are used under high intensity while rods dominate under low lighting conditions. When going into the dark area, the cones cannot work anymore but the rods are bleached due to the high light intensity. In the dark, the rhodopsin contained in the rods starts to regenerate but this process takes a certain time, around 10 minutes. After 30 minutes, the rods' sensitivity is at its maximum of efficiency. To help this adaptation, a change in pupil' size is noticed.

During dark adaptation and the transition from photopic to scotopic conditions, rods and cones work together until rods take over completely from cones. This stage is known as the mesopic condition. Under photopic conditions, the maximum of sensitivity of cones is around 555 nm (green-yellow) but it decreases at 500 nm (blue-green) under scotopic conditions. The Purkinje shift illustrates this change in sensitivity. Purkinje noticed a change in color appearance of flowers which appeared bright red on a sunny afternoon while at dawn they looked very dark. Conversely, by considering the leaves, they seemed very dark during daylight and brighter at low intensity light conditions. The Purkinje shift is simulated in Figure 2-23. Under photopic conditions, the flower is brighter than the background while, under scotopic conditions, it is darker (Tovee, 2008).

Figure 2-23: Simulation of the Purkinje shift from photopic conditions (left side) to mesopic conditions (middle) and then scotopic conditions (right side) adapted from (Wikipedia, 2019b)

Light adaptation is the reverse process of dark adaptation. It occurs when going into a very light area from a dark area. Compared to dark adaptation, the process is faster, around 1 minute, as only one photon can initiate the reactivation of rhodopsin.

The chromatic adaptation is the ability of the human visual system to adapt itself to changes in illumination conditions while preserving the color appearance of objects. This adaptation is important to ensure the color constancy. A banana will always appear yellow under a sunny sky, a cloudy sky, a fluorescent lamp or when lighted by candles. It is based on a scaling of the cones' sensitivity according to the light.

2.3.6. Human visual acuity

Visual acuity corresponds to the ability of the human visual system to discern details in images. The separating power of the eye is then measured as the ability to visually separate two distinct objects. Logically, the visual acuity is inversely proportional to the distance of observation. In order to check it, the Snellen eye chart is typically used. Developed in 1862 by Hermen Snellen, a Dutch ophthalmologist, this chart consists of different rows of letters of different sizes (see Figure 2-24). The observer should observe the chart at a distance of 6 meters. This test is useful to determine how well letters and shapes can be distinguished.

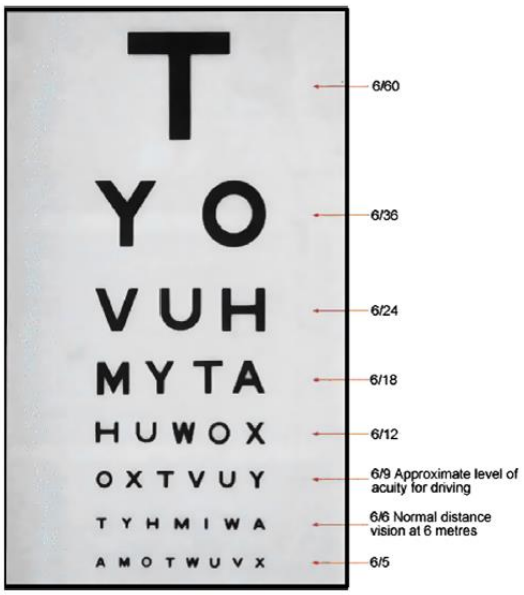

Figure 2-24: Snellen eye chart for visual acuity measurement from (Lindfield and Das-Bhaumik, 2009)

Luminance adaptation and chromatic adaptation are mainly retinal adaptation while contrast adaptation is cortical (Webster and Wilson, 2000). According to (Pelli and Bex, 2013), contrast is the relative difference between a target and the background in terms of luminance. Contrast may be defined as the Weber contrast (2-31) or the Michelson contrast (2-32).

$$\text{Weber constrast} \quad W = \frac{L_{max} - L_{min}}{L_{background}} \qquad (2\text{-}31)$$

$$\text{Michelson contrast} \quad M = \frac{L_{max} - L_{min}}{L_{max} + L_{min}} \qquad (2\text{-}32)$$

With L_{max}, *luminance maximum*
L_{min}, *luminance minimum*
$L_{background}$, *luminance of the background*

The human visual system is sensitive to contrast due to the answer of the ganglion cells. In equations (2-31) and (2-32), by considering the denominators, Weber refers to a background while Michelson does not.

This sensitivity is measured by using the contrast sensitivity function (CSF). This function represents the contrast sensitivity of one individual as a function of the spatial frequency of a stimulus. Figure 2-25 can be used to distinguish the visible contrast from the invisible contrast, where the abscissa represents the spatial frequency, in ordinate, on the left the sensitivity to contrast in scales log or in decibel[1] and on the right the contrast in percentage.

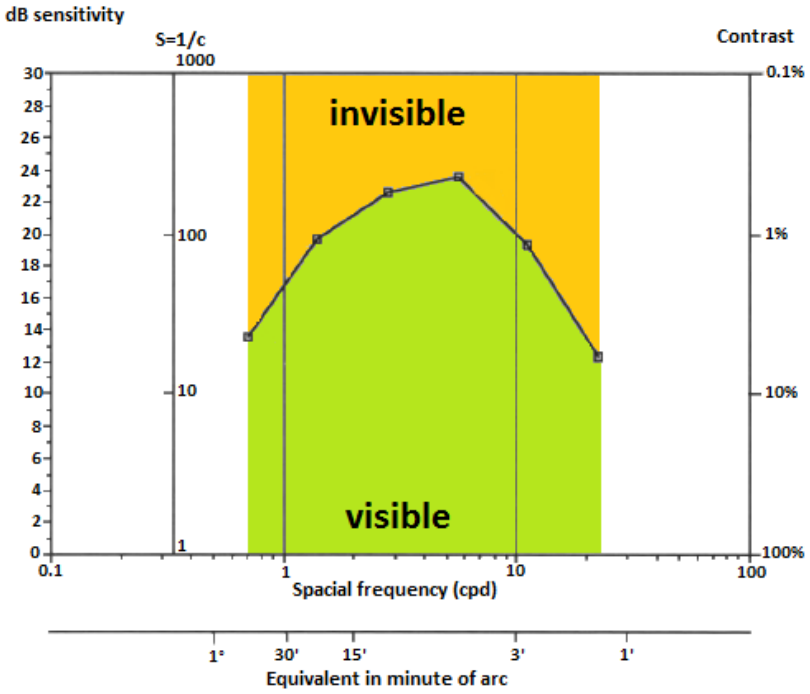

Figure 2-25: Contrast sensitivity function with the invisible part in orange and the visible part in green adapted from (Zanlonghi, 1991)

[1] 1 decibel = 10 log(1/contrast)

In vision science, in a scene, the size of a detail depends on the viewing distance. Traditionally, these sizes are given in values of angle, degree or minutes of arc, with 1'=1/60°. By considering trigonometric relations, an object of size, d, seen at a viewing distance of D is observed under an angle, α, such that tan α = d/D (see Figure 2-26).

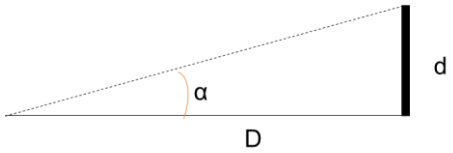

Figure 2-26: Adaptation of the trigonometric relations to determine the size of a detail in a scene

Many optical illusions are based on contrast sensitivity and simultaneous contrast[1]. For example, in Figure 2-27, the internal bar is filled with the same grey level but the background color changes from darker to lighter values. Visually, the inner bar does not appear plain but shaded. Its shading looks inverted compared to the shading of the background.

Figure 2-27: Example of simultaneous contrast from (Carbon, 2014)

The visual perception depends not only on the characteristics of the observed object itself, but also on those of the environment. That is why, during sample observation it is absolutely necessary to control the environment and the conditions of observation in order to not distort the results.

2.4. Conclusion

The ability of the human visual system to see color is based on the triplet: light source, object, observer. Without any one of the three elements, color cannot exist. An important characteristic of the human visual system is its binocularity due to the existence of two eyes, which leads to a better relief perception, the stereopsis. As seen in Chapter 2, paragraph 2.3.1, the average distance between the two eyes of a human is about 6 cm. Each eye observes the same object but from a different angle. The images are then transmitted to the brain with a horizontal offset. By considering effect coatings, the effect particles in the coating formula create a micro texture in the film. In this case, the left and the right eyes do not see the particle in the same orientation. The information sent to the left and the right LGNs are then not identical. We suppose the binocularity coupled with the offset sent to the LGNs would be at the origin of the phenomenon of the perceived flicker or sparkling which is considered in the next chapters.

[1] Simultaneous contrast is a phenomenon where two different colors affect each other

Besides, according to Paul Eluard, *"the earth is blue like an orange"*. This quote seems unrealistic because an orange is orange and not blue. It is possible to sort color according to eleven color classes (e.g. yellow, blue, green or red) that are defined as basis. These color class identifications can be either linked to physiologic faculties of the eye, intrinsic faculties, or specific knowledge acquired by learning processes. How would it be possible to describe a color as raspberry red if one has never seen a raspberry? (Roberson et al., 2000) decided to compare lexicons from English speakers and Berinmo speakers (people from Papua New Guinea) on 160 colors. First, the English speakers sorted the colors into eight color classes while Berinmo speakers sorted them into five classes. Based on the boundaries of the color classes, no common feature was found. The Papuan do not differentiate blue and green colors as the English do. To describe, it is necessary to say and therefore to name, whereas, to compare, it is enough to give appreciation, equivalent or different.

Finally, the human visual system is affected by color vision deficiencies due to the lack of photoreceptors. As seen in Chapter 2, paragraph 2.3.2.2, color perception builds on the presence of three types of cones: S, M or L depending on their sensitivities. However, it is possible to develop a lack of L-cones, protanopia, of M-cones, deuteranopia, or S-cones, tritanopia. Humans affected by protanopia or deuteranopia are able to distinguish red and green while people affected by tritanopia have some difficulties in distinguishing blue and yellow (Fairchild, 2013c). Color blindness is linked to an inherited problem. However, it does not result in a real handicap. Color vision deficiency does not affect men and women in the same way. Males are more affected than females. Indeed, the genes responsible for color blindness are on the X chromosome (NIH, 2019). Males have one X chromosome while females as two. To be affected by color blindness, women need to have defect in their two X chromosomes which is relatively rare. However, in the genetic inheritance transmitted to their children, the gene affection one of the X chromosomes may be part of it. We therefore note the genetic character of color vision deficiencies. The affected persons have their own reference system (see Figure 2-28) where the missing shades are replaced by different shades of grey.

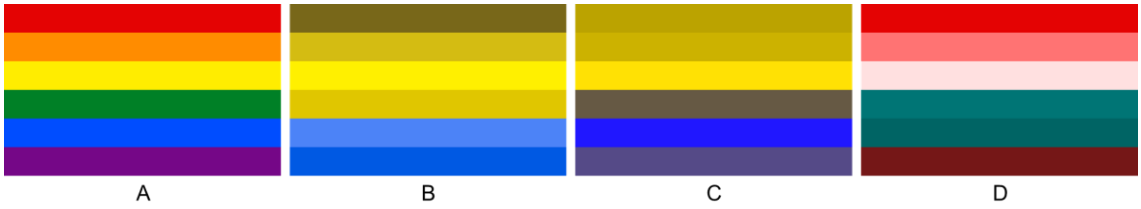

Figure 2-28: Differences in color perception: A, normal trichromatic vision, B protanopia vision, C deuteranopia vision and D tritanopia vision from (Wikipedia, 2019a)

Color is an easily measurable physical phenomenon while color perception is a much more complex phenomenon. This perception is based on an evaluation by our brain of physical phenomena due to the light beams coming from the observed object.

Chapter 3. Color measurement

Contents

In the previous chapter, the nature of color was explained by answering the question "Why is color?". The interaction of light sources, object and the human visual system allows color to exist. Color is then an attribute of visual sensation. Colorimetry is the branch of color science dedicated to the physical description of color. According to (Schanda, 1997), colorimetry is *"the science and technology used to quantify and describe physically the human color perception".* Colorimetry can be divided into two categories: basic (measurement of color), and advanced (color difference measurement). (Wyszecki, 1973) gave a definition of those two categories. Basic colorimetry is "*a tool used to make a prediction on whether two lights (visual stimuli) of different spectral power distributions will match in color for certain given conditions of observation*" while advanced colorimetry represents the "*methods of assessing the appearance of color stimuli presented to the observer in complicated surroundings as they may occur in everyday life*".

The first requirement to perceive color is a light source to start the vision process which is modulated according to the properties of the object once it is caught by the human visual system. Each element of the triplet "light-object-observer" must be either quantified or

standardized, depending on what you want to measure (properties or appearance of a surface, characteristics of lighting systems …). Light sources are quantified by the measurement of their spectral power distributions by photometry: this relates to measurement of radiometric quantities at individual wavelengths.

This chapter will describe first the standardization of the light sources with photometric methods and the CIE illuminants, followed by basic colorimetry with the definition of a standard observer. Eventually, some methods used in advanced colorimetry are described.

3.1. Standardization of light sources

In industry, color perception is crucial, especially for customers. Would you cook pasta if half of the content of the box was browner than the other? Would you buy a greenish tomato sauce? To compare colors, it is necessary to define lighting conditions well and to guarantee same references in terms of spectral power distribution. The main problem in optical measurement is then the quantification of light sources and lighting conditions. As the human eye is not equally sensitive to all wavelengths of visible light, photometry was introduced to weigh the spectral power distribution at each wavelength with a factor representing the eye's sensitivity to light.

3.1.1. Photometry

Photometry is the science of measurement of light in terms of its perceived brightness by the human eye. Photometry is hence the basis to evaluate light sources. The standardization of photometric systems pursued by the CIE led to two standard photometric observers for photopic and scotopic vision and the associated luminous efficiency function, respectively V(λ) and V'(λ) (Wyszecki and Stiles, 1982c). Each function is normalized and set to 1 at λ_m=555 nm for photopic vision and at λ'_m=507 nm for scotopic vision, see Figure 3-1.

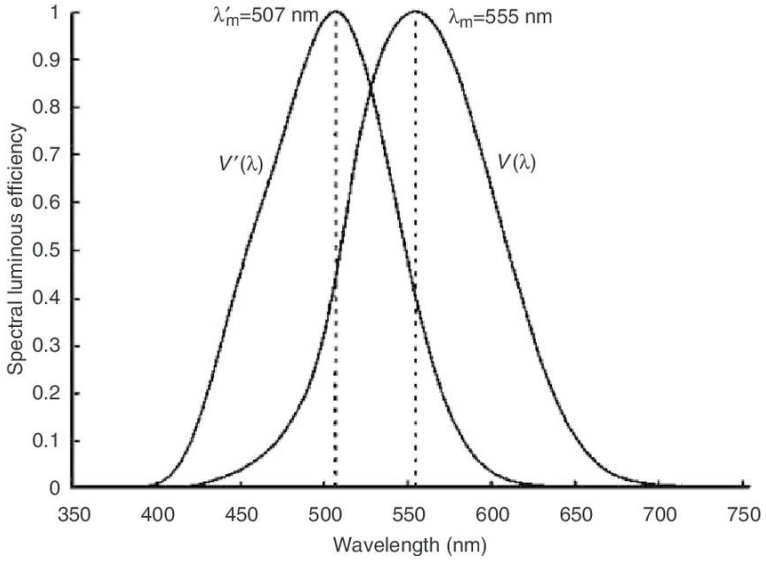

Figure 3-1: Spectral luminous efficiency functions, V(λ) and V'(λ), defining the standard photometric observers for photopic and scotopic vision (Fotios and Goodman, 2012)

The luminance of light, L_v, can be defined as a photopic photometric quantity, (3-1).

$$L_v = K_m \int_\lambda L_{e,\lambda} V(\lambda) \mathrm{d}\lambda \qquad (3\text{-}1)$$

With L_v, *luminance (unit: lm/m²/sr)*
K_m, *maximum photopic luminous efficacy (K_m = 683 lm/W)*
$L_{e,\lambda}$, *radiance (unit: W/m²/sr)*
$V(\lambda)$, *photopic spectral luminous efficiency function*

Photopic photometric quantity can be measured according to three methods: broad-band photometry, spectroradiometric photometry or visual photometry. Only the second method is explained here, the other methods are detailed in (Wyszecki and Stiles, 1982c). In the spectroradiometric photometric method, the photopic photometric quantity is determined by measuring the radiance of light, $L_{e,\lambda}$, and then by calculating the luminance, L_v, (3-1). However, it is important to note that for the following, only relative spectral distribution will be used. For that, a spectral radiance standard is needed such as e.g. tungsten filament lamps.

3.1.2. CIE illuminants

To reproduce light sources with a constant spectral power distribution, technical light sources have been created. They allow a high reproducibility of several spectrums such as cloudy daylight or tungsten filament lamp. It has been decided to standardize several light sources often used, the illuminants. These technical light sources (light source or illuminant) are known with their color temperature but it is not always easy to either model their spectral power distribution or prove their color temperature. The CCT has been introduced to estimate the temperature at which it would be necessary to heat a black body to obtain the visual impression given by a light source.

3.1.2.1. CIE standard illuminants

To reproduce the spectrum of a temperature radiator, the technical light sources are made of a filament in metal which is heated with an electric energy and surrounded by a gas. The thickness of the filament, the applied voltage and the surrounding gas will lead to a specific color temperature. A tungsten filament lamp will be reproduced with a tungsten filament surrounded by bromine or iodine. The tungsten-filament lamp with a color temperature of 2 856 K is named the standard illuminant A by the CIE in 1931. The spectral power distribution of the illuminant A can be calculated by equation (3-2), derived from the Planck law of radiation. For an illuminant, the shape of the spectrum is important and without any notion of intensity due to the normalization. The wavelength dependence is shown in Figure 3-2.

$$S_A(\lambda) = 100 \cdot \left(\frac{560}{\lambda}\right)^5 \cdot \frac{\exp\left[\frac{1.435 \cdot 10^7}{2848 \cdot 560}\right] - 1}{\exp\left[\frac{1.435 \cdot 10^7}{2848\,\lambda}\right] - 1} \qquad (3\text{-}2)$$

For our visual system, our main light source is daylight. In 1963, the CIE decided to create new illuminants. The spectral power distribution must consider the different variations of daylight, from early morning to late evening or from a blue sky to a cloudy sky. The CIE standard illuminant D_{65} has a correlated color temperature at 6 504K. It corresponds to an average daylight at midday on cloudless north sky and its spectral power distribution is defined by a table published by the CIE (CVRL, 2019). The CIE standard illuminant D_{65} corresponds to a UV-filtered, high-pressure xenon lamp.

The two CIE standard illuminants, A and D_{65}, are characterized by their relative spectral power distribution $S(\lambda)$. It corresponds to the standardization of their spectral power distribution to 100 for a wavelength of 560 nm (see Figure 3-2).

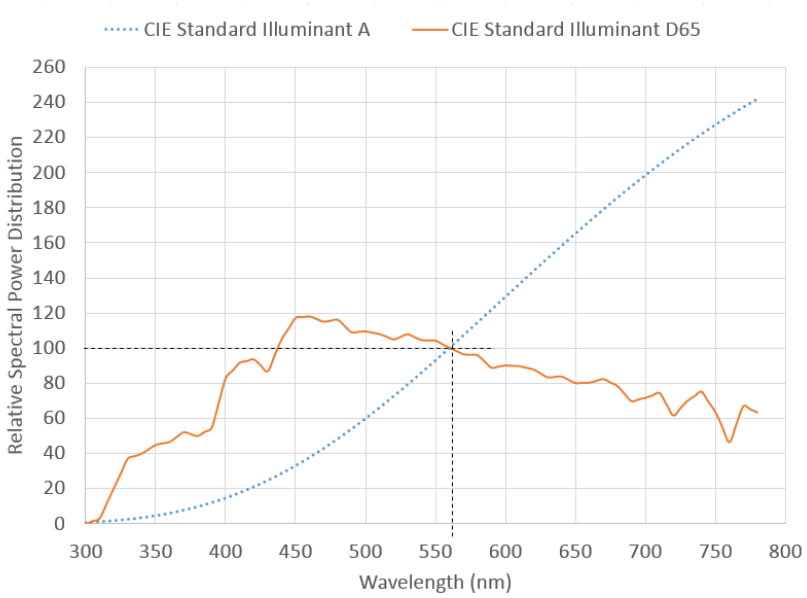

Figure 3-2: Relative spectral power distribution of the CIE standard illuminants A (in blue) and D_{65} (in orange) standardized to 100 at a wavelength of 560nm adapted from (Fairchild, 2013b)

3.1.2.2. CIE illuminants

Only two illuminants are standardized by the CIE, illuminant A and illuminant D65, but many other illuminants exist.

Established in 1931, illuminant B stands for direct noon sunlight with a color temperature (CT) around 4 870K while illuminant C represents average daylight with a CT around 6 770K. Besides D65, three daylight illuminants have been defined: D50 with a CT around 5 000K, D55 with a CT around 5 500K and D75 with a CT around 7 500K. Illuminants D have been created to better represent natural daylight with the “horizon” light, D_{50}, as example. Illuminant E is an equal-energy radiator with a constant spectral power distribution. This illuminant is only used for theoretical approaches. Then, the set of illuminants F stands for several types of fluorescent light sources. Twelve illuminants have been created, from F1 to F12 but only F2 (cold white, line spectra, CT~4 230K), F7 (bluish white, broadband, CT~6 500K) and F11, also called TL84, (white daylight, triband source, CT~4 000K) are used in colorimetry.

3.2. Basic colorimetry

As described in the previous chapter, the visual human system is sophisticated. Visual phototransduction starts in the retina with both two types of photoreceptors: rods and cones. Basic colorimetry focuses on the first level of vision: the absorption of energy by photoreceptors. Photoreceptors are either sensitive to light or to wavelength according to their shape. To quantify human visual response, spectral responsivities of the three types of cones are defined. The foundations of colorimetry are based on the fundamental empirical laws of additive color mixing developed by Grassmann in 1853. He assumed that any color can be matched by a linear combination of three primaries: R, G and B. This law is the foundation of colorimetry (see (3-3)). A color (C) can be matched by a certain amount of red (***r***), a certain amount of green (***g***) and a certain amount of blue (***b***).

$$C = \boldsymbol{r}R + \boldsymbol{g}G + \boldsymbol{b}B \qquad (3\text{-}3)$$

With *C, color to match*
r, g and b, amount of primaries
R, G and B, set of primaries

It was then mandatory to establish the set of primaries, R, G and B, also called tristimulus values. This system was introduced in 1931 by the CIE.

3.2.1. The CIE 1931 2° Standard Colorimetric Observer

Wright (1928) and Guild (1931) worked on color matching stimuli by using trichromatic color theory and Grassmann's laws. The aims of their experiments were to recreate white light from RGB primaries. The experiments were conducted with 17 observers by using a 2° circular split screen. At a viewing distance of 50cm, a 2° field of view is equivalent to a 1.7cm circle (Fairchild, 2013b).

3.2.1.1. RGB system

In 1931, based on two independent experiments performed by Wright and Guild, the CIE adopted a standardized system: the CIE 1931 Standard Colorimetric Observer or 2° Standard Observer. The observation standardization system was needed to be able to repeat additive color matches. The spectral composition and the luminance of each primary had been specified. The spectral composition was based on the use of a single wavelength value: 700 nm for red, 546.1 nm for green and 435.8 nm for blue. For the luminance, it had been decided that for a luminance of 1 cd/m² for red, 4.5907 cd/m² of green and 0.0601 cd/m² of blue were needed. This standardization led to the $\overline{r}(\lambda)$, $\overline{g}(\lambda)$ and $\overline{b}(\lambda)$ color matching functions as seen in Figure 3-3. These color matching functions correspond to the chromatic response of the average human viewing.

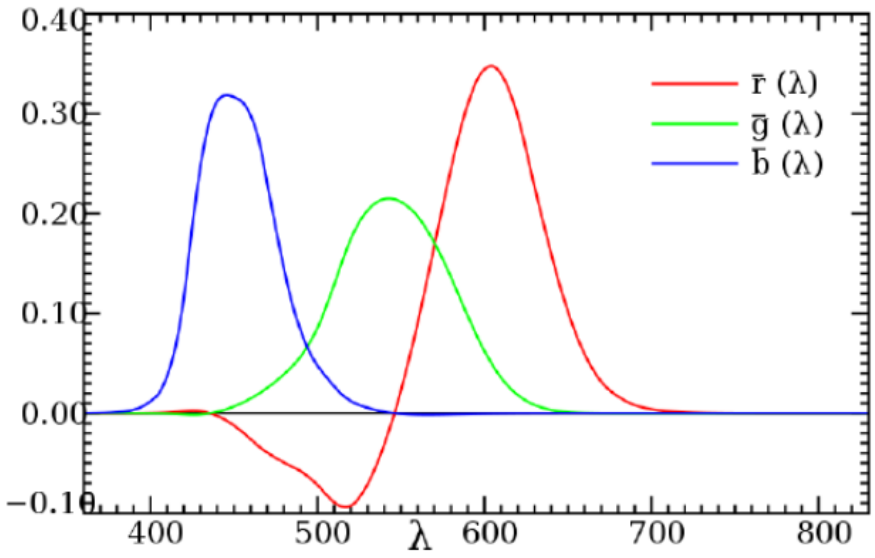

Figure 3-3: Color matching functions for the CIE 1931 RGB system using monochromatic primaries at 700.0, 546.1 and 435.8 nm adapted from (Fairchild, 2013b)

The color matching functions show the amount of RGB primaries needed. The tristimulus values of a stimulus can be obtained by generalized equations, (3-4).

$$R = \int_{\lambda} P(\lambda)\bar{r}(\lambda)d\lambda \qquad G = \int_{\lambda} P(\lambda)\bar{g}(\lambda)d\lambda \qquad B = \int_{\lambda} P(\lambda)\bar{b}(\lambda)d\lambda \tag{3-4}$$

With $\bar{r}(\lambda)$, $\bar{g}(\lambda)$ *and* $\bar{b}(\lambda)$, *color matching functions*
$P(\lambda)$, *spectral power distribution of the stimulus*
R, G and B, tristimulus values

3.2.1.2. XYZ system

However, for a wavelength value included between 435.8 nm and 546.1 nm, this implies a negative amount of light needed to desaturate the stimuli. Adding a negative amount of light is impossible. Therefore, in 1931, the CIE decided to transform the RGB system into the XYZ system. For that, the RGB primaries were replaced by imaginary primaries which were more saturated than the monochromatic lights. Transformation between the CIE1991 RGB and the CIE1931 XYZ tristimulus values is given by the following matrix transformation, (3-5).

$$\begin{vmatrix} X \\ Y \\ Z \end{vmatrix} = \begin{vmatrix} 2.768\,892 & 1.751\,748 & 1.130\,160 \\ 1.000\,000 & 4.590\,700 & 0.060\,100 \\ 0 & 0.056\,508 & 5.594\,292 \end{vmatrix} \times \begin{vmatrix} R \\ G \\ B \end{vmatrix} \tag{3-5}$$

$\bar{r}(\lambda)$, $\bar{g}(\lambda)$ and $\bar{b}(\lambda)$, the color matching functions, can be converted into $\bar{x}(\lambda)$, $\bar{y}(\lambda)$ and $\bar{z}(\lambda)$, the standard color matching functions according to the same matrix transformation. After the conversion, the amounts of XYZ light needed to match the stimuli are either positive or null.

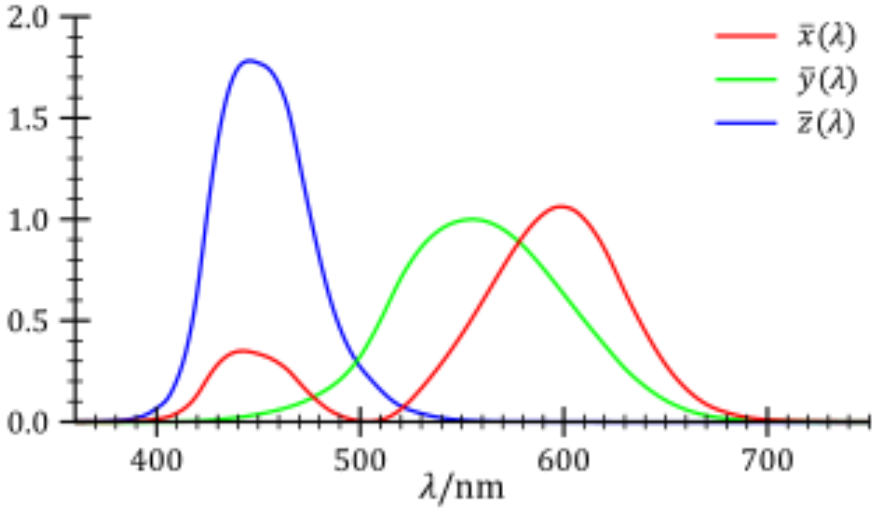

Figure 3-4: Standard color matching functions for the CIE 1931 XYZ system adapted from (Fairchild, 2013b)

In colorimetry, there is a distinction between direct light and transmitted or reflected light: self-luminous or non-self-luminous objects. In the first case, light is directly produced by the source such as the sun, light bulbs or fluorescent materials. In the second case, the material is only able to reflect or transmit a part of the received light. It leads to a change in the spectral distribution of the light because only one part of the light reaches the eye of the observer. To consider this modification, a relative color stimulus function, $\phi(\lambda)$, is added into the tristimulus value calculations, (3-6).

$$\phi(\lambda) = R(\lambda) \times S(\lambda) \tag{3-6}$$

With $\phi(\lambda)$, *relative color stimulus function*
$R(\lambda)$, *spectral reflectance factor*
$S(\lambda)$, *relative spectral power distribution of the light*

The tristimulus values can be obtained by the generalized equations, (3-7).

$$X = k\int_{\lambda} \phi(\lambda)\bar{x}(\lambda)d\lambda \qquad Y = k\int_{\lambda} \phi(\lambda)\bar{y}(\lambda)d\lambda$$

$$Z = k\int_{\lambda} \phi(\lambda)\bar{z}(\lambda)d\lambda \qquad k = \frac{100}{\int_{\lambda} S(\lambda)\bar{y}(\lambda)d\lambda} \tag{3-7}$$

With $\overline{x}(\lambda)$, $\overline{y}(\lambda)$ *and* $\bar{z}(\lambda)$, *standard color matching functions*
$\phi(\lambda)$, *relative color stimulus function*
X, Y and Z, the standard tristimulus values
k, constant
$S(\lambda)$, *relative spectral power distribution of the illuminant*

The constant k represents normalized white light used to light the surface to be measured. In the case of characterization of light sources, this coefficient is equal to 683 (Viénot and Le Rohellec, 2013).

To make understanding easier, the tristimulus values are converted into chromaticity coordinates: x, y, and z, (3-8). It has been decided that in the CIE XYZ color space, Y is the measure of luminance. Chromaticity is then linked to the two chromaticity coordinates: x and y.

$$x = \frac{X}{X+Y+Z} \qquad y = \frac{Y}{X+Y+Z} \qquad z = \frac{Z}{X+Y+Z} = 1 - x - y \qquad (3\text{-}8)$$

Since the human eye is composed of three types of cones, a full plot of all colors would be a 3D diagram but it is easier to represent colors in a 2D diagram than in a 3D diagram. The CIE XYZ color space is transformed into the xyY color space, in which the luminance component, Y, has been removed and the x and y components have been plotted into a 2D diagram: the chromaticity diagram (Figure 3-5). The straight line between λ=380nm and λ=780nm is called the purple straight. The colors located on this line are fully saturated and cannot be represented by spectral colors. The outer curve represents the place of all monochromatic colors.

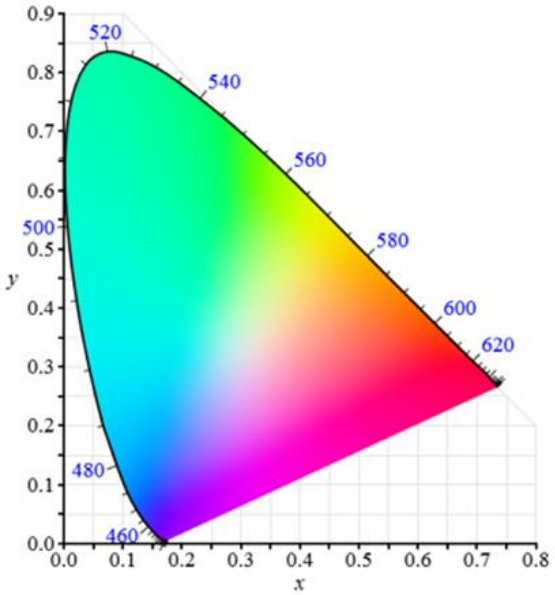

Figure 3-5: The CIE xy chromaticity diagram from (Perz, 2010)

3.2.2. The CIE 1964 Standard Colorimetric Observer

In 1931, the CIE standardized a 2° Colorimetric Observer. As the color sensitivity of the eye changes according to the angle of view, a second standard observer has been introduced in 1964. The CIE defined an additional standard observer based upon a 10° field of view and defined it as the CIE 1964 Observer or the 10° Supplementary Standard Observer. At a viewing distance of 50 cm, a 10° field of view is equivalent to an 8.8 cm circle. An observation angle of 2° is not adequate for a correct color assessment. This configuration only considers the functioning of the cones. However, the stimulus falls on a larger distance and the functioning of the rods must be taken into account.

The 1964 Standard Colorimetric Observer was standardized after Stiles and Burch and Speranskaya experiments (1959). This modification triggered a change in the

monochromatic primaries wavelengths. For an observation angle of 10°, the chosen RGB primaries have the respective wavelengths 645.2 nm, 526.3 nm and 444.4 nm.

The 2° Standard Observer should be used for 1° to 4° viewing angles and the 10° Supplementary Standard Observer for viewing angles larger than 4°. The transformation between the $R_{10}G_{10}B_{10}$ and the $X_{10}Y_{10}Z_{10}$ tristimulus values is given by the following matrix transformation (3-9).

$$\begin{vmatrix} X_{10} \\ Y_{10} \\ Z_{10} \end{vmatrix} = \begin{vmatrix} 0.341\,080 & 0.189\,145 & 0.387\,529 \\ 0.139\,058 & 0.837\,460 & 0.073\,160 \\ 0 & 0.039\,553 & 1.026\,200 \end{vmatrix} \times \begin{vmatrix} R_{10} \\ G_{10} \\ B_{10} \end{vmatrix} \qquad (3\text{-}9)$$

$\overline{r_{10}}\,(\lambda)$, $\overline{g_{10}}\,(\lambda)$ and $\overline{b_{10}}\,(\lambda)$, the $R_{10}G_{10}B_{10}$ color matching functions can be converted into $\overline{x_{10}}\,(\lambda)$, $\overline{y_{10}}\,(\lambda)$ and $\overline{z_{10}}\,(\lambda)$, the $X_{10}Y_{10}Z_{10}$ color matching functions according to the same matrix transformation (Schanda, 2007).

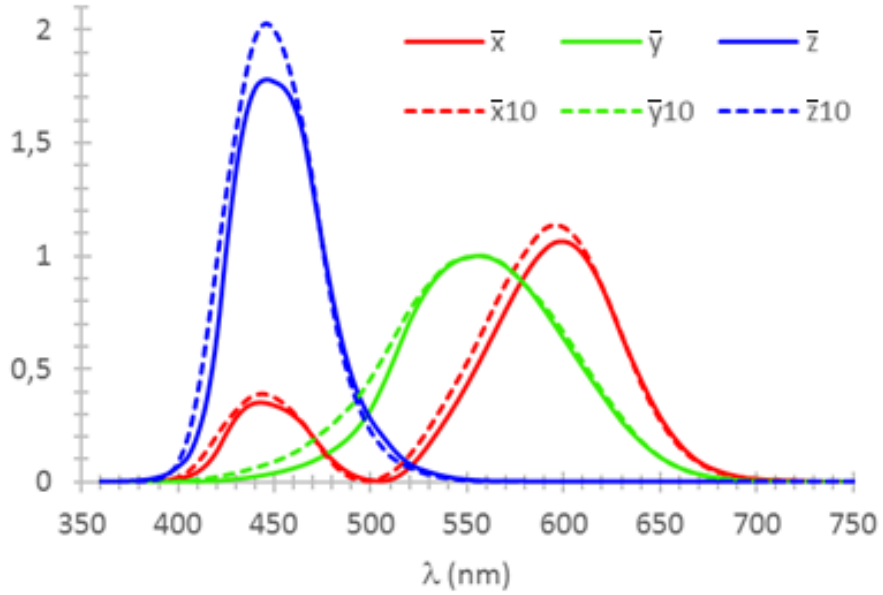

Figure 3-6: Color matching functions for the CIE 1931 XYZ system using monochromatic primaries at 700.0, 546.1 and 435.8 nm (solid lines) and for the CIE 1964 $X_{10}Y_{10}Z_{10}$ system using monochromatic primaries 645.2, 526.3 and 444.4nm at (dotted lines) adapted from (Schanda, 2007)

The tristimulus values can be obtained by the generalized equations below, (3-10).

$$X_{10} = k_{10} \int_{\lambda} \phi(\lambda)\overline{x_{10}}\,(\lambda)d\lambda \qquad Y_{10} = k_{10} \int_{\lambda} \phi(\lambda)\overline{y_{10}}\,(\lambda)d\lambda$$

$$Z_{10} = k_{10} \int_{\lambda} \phi(\lambda)\overline{z_{10}}\,(\lambda)d\lambda \qquad k_{10} = \frac{100}{\int_{\lambda} S(\lambda)\overline{y_{10}}\,(\lambda)d\lambda} \qquad (3\text{-}10)$$

With $\overline{x_{10}}\,(\lambda)$, $\overline{y_{10}}\,(\lambda)$ *and* $\overline{z_{10}}\,(\lambda)$, *color matching functions*
$\phi(\lambda)$, *relative color stimulus function*
X_{10}, Y_{10} *and* Z_{10}, *tristimulus values*
k_{10}, *constant*
$S(\lambda)$, *relative spectral power distribution of the illuminant*

The chromaticity coordinates for the 10° observer can also be defined (3-11). The $x_{10}y_{10}$ chromaticity diagram looks like the xy chromaticity diagram.

$$x_{10} = \frac{X_{10}}{X_{10} + Y_{10} + Z_{10}} \qquad y_{10} = \frac{Y_{10}}{X_{10} + Y_{10} + Z_{10}}$$
$$z_{10} = \frac{Z_{10}}{X_{10} + Y_{10} + Z_{10}} = 1 - x_{10} - y_{10} \qquad (3\text{-}11)$$

3.3. Advanced colorimetry

The CIE 1931 chromaticity diagram is the basis of modern colorimetry but it also stands for the comparison of two colors. The perceived color difference is not proportional to the physical stimulations of the visual system.

To characterize a color stimulus according to the visual assessment, three parameters are used: brightness, saturation and hue (see Figure 3-7). The shade, also called hue, is a visual sensation which leads to color names such as blue, green or red; it is linked to the dominant wavelength. The terms chroma or saturation are linked to the color intensity. Some objects are pure red and others less pure red turning to grey. The brightness or lightness is linked to light reflectance. Some objects are bright red and others are dark red.

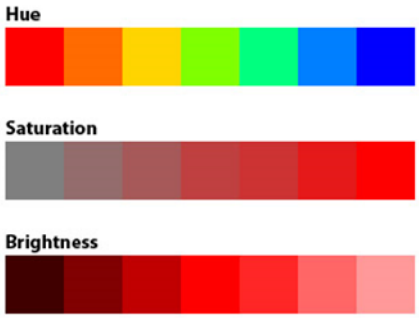

Figure 3-7: Brightness, saturation and hue definitions adapted from (Perz, 2010)

Psychophysical experiments were carried out to measure color differences and to find threshold color difference data. This threshold is the ability for an observer to notice a color difference between two stimuli and it is based on the “just noticeable difference”.

3.3.1. Noticeable color differences

When the observation conditions change, the human visual system can adapt itself to keep a consistency in the appearance of the object. Three noticeable differentiations take place: the luminance differences, the wavelength differences and the chromaticity differences.

3.3.1.1. Luminance differences

The human visual system can adapt itself to the surrounding luminance. It can work from 0.0003 lx to about 100 000 lx thanks to the retina responsivity. This is due to pupil dilatation and photoreceptor sensitivity. To quantify the luminance-differential threshold, Weber developed an experiment based on luminance discrimination (Wyszecki and Stiles, 1982e). If an observer was not able to notice a difference in luminance between a test light (L) and a variable light (L’), the variable light luminance (ΔL) was increased (Figure 3-8, left). This experiment was useful to determine the luminance sensitivity or Weber curve (Figure 3-8, right). The discontinuity between 10^{-3} and 10^{-2} cd/m² is due to the passing from rods to cones.

From 10^{-1} to 10^{4} cd/m², the relative threshold is constant but increases drastically after 10^{4} to show the beginning of dazzling.

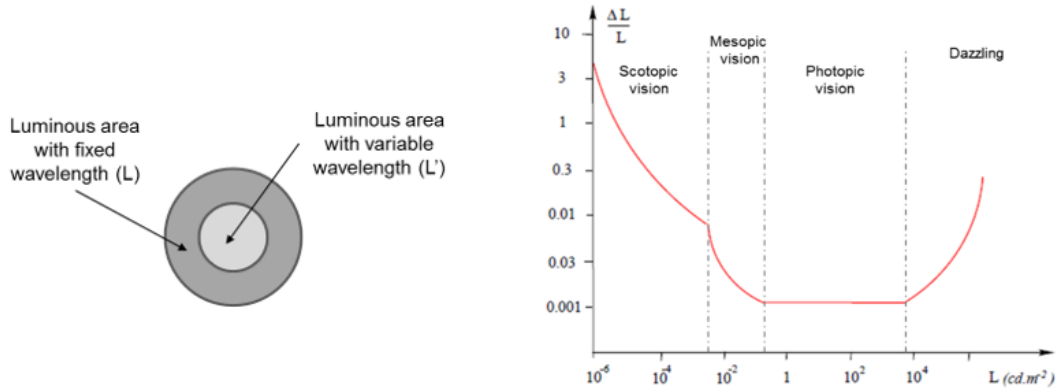

Figure 3-8: Left: Weber experiment on luminance differences; Right: Luminance sensitivity or Weber curve as observed for "white" stimuli adapted from (Wyszecki and Stiles, 1982e)

3.3.1.2. Wavelength differences

To measure human ability to discriminate two colors with adjacent wavelengths, Wright and Pitt studied color-differential thresholds. For these experiments, the luminance was set and the color variation was analyzed for each monochromatic light. The observer was placed in front of two luminous areas: one with a fixed wavelength (λ) and the other one with a variable wavelength. The wavelength was moved until a difference (Δλ) was perceived. The results of the experiment are shown in Figure 3-9.

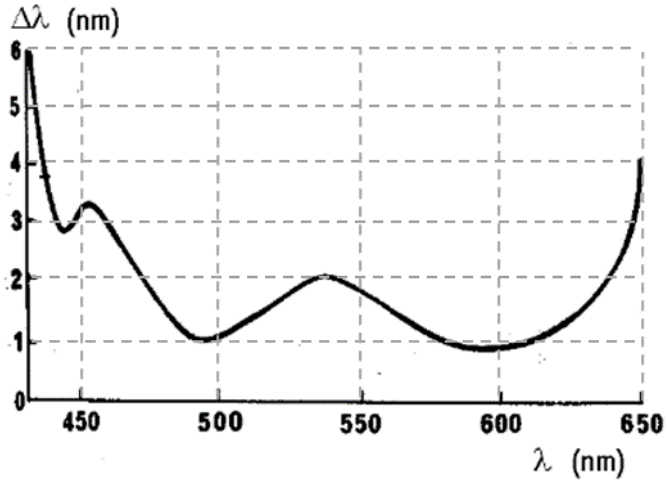

Figure 3-9: Wright and Pitt experiments on wavelength differences adapted from (Wyszecki and Stiles, 1982e)

Between 475 and 625 nm, the variation in wavelength is lower than 2 nm. At 490 nm (greenish-blue) and at 590 nm (yellowish-orange), two minimums are reached. The eye sensitivity is important because a variation of 1 nm in wavelength is detected. Before 450 nm and after 625 nm, variation in wavelength increases a lot. It is more and more difficult to identify a difference between the two luminous areas. After 700 nm, the observer is no longer able to determine this difference.

3.3.1.3. Chromaticity differences

MacAdam based his tests on the experiments carried out by Wright and Pitts. He adopted the same procedure with an observer looking at one fixed color and one color which can be adjusted by the observer. For this experiment, the lightness was fixed to 50. In this case, the observer adjusted the color until the test color was color matched. Twenty-five test colors were selected. MacAdam found that all the matches, once plotted into the CIE 1931 chromaticity diagram, fell into an ellipse, Figure 3-10. The size and orientation of the ellipses are mainly linked to the test color. The center dot of each ellipse represents the test color.

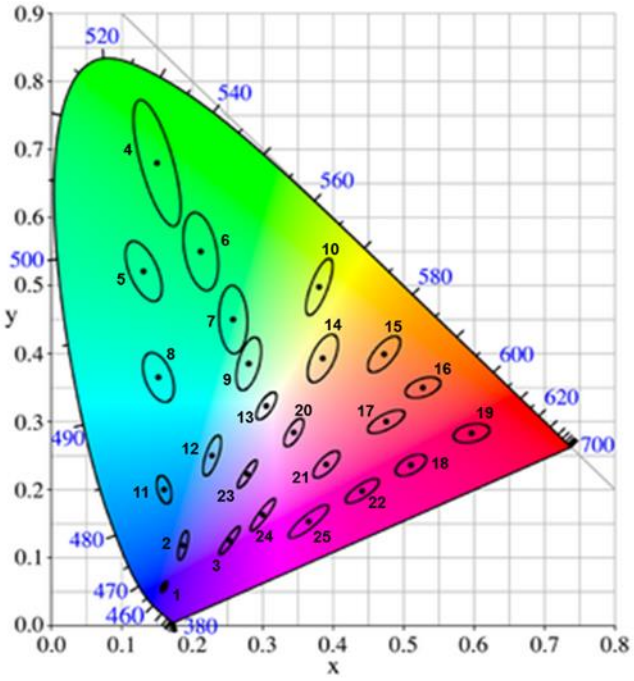

Figure 3-10: MacAdam ellipses plotted in the CIE 1931 xy chromaticity diagram from (Perz, 2010)

The ellipses are very small in the blue area, small in the red area and tend to become bigger in the green area. In other words, the representation space chosen does not allow to quantify the just noticeable differences. This representation is distorted from the perceptual point of view. This observation is not in harmony with the eye sensitivity. The human eye can perceive changes in green based components and the visual system reinforces the degradation effect for blue colors. The CIE 1931 Chromaticity Diagram is not perfect to match the human color perception because it does not consider the lightness value.

3.3.2. Uniform color spaces

According to the CIE 1931 xy chromaticity diagram, the Wright and Pitt experiment and the MacAdam ellipses, two colors close to each other may sometimes be distinguished by the observer and sometimes not. This distinction or absence thereof is highly dependent on their position in the chromaticity diagram. To overcome this disadvantage, lots of experiments were carried out to set up a perceptually uniform color space for which any color deviation would be reduced to a metric distance.

3.3.2.1. CIELab color space

Color stimuli are three dimensional, therefore, the use of the CIE 1931 xy chromaticity diagram is not adequate due to the low impact of luminance. To evaluate color differences between two stimuli, a uniform color space is needed. The CIE worked on the development of a homogenized color space which can correlate the visual appearance. In 1976, the CIE standardized two uniform color spaces: CIELuv and CIELab. The CIELab system is

recommended for non-self-luminous colors and the description herein will be restricted to this system.

3.3.2.1.1. Definition of CIELab coordinates

The CIELab color space is based on three attributes: L* (black to white contribution), a* (red to green contribution) and b* (yellow to blue contribution). These attributes correspond to the Hering theory (see Chapter 2, paragraph 2.3.4.3). First, the X, Y and Z tristimulus values for the color stimuli are converted into "value" functions X*, Y* and Z*, (3-12).

$$X^* = \sqrt[3]{X/X_N} \qquad Y = \sqrt[3]{Y/Y_N} \qquad Z^* = \sqrt[3]{Z/Z_N} \qquad (3\text{-}12)$$

With X_N, Y_N *and* Z_N, *tristimulus values for the illuminant*
X, Y *and* Z, *tristimulus values for the color stimuli*

The tristimulus values for some illuminants are given in Table 3-1.

Table 3-1: Tristimulus values for some illuminants (X_N, Y_N and Z_N) for 1931 CIE 2° standard colorimetric observer or CIE 1964 10° standard colorimetric observer

	1931 CIE standard colorimetric observer (2°)			1964 CIE standard colorimetric observer (10°)		
	X_N	Y_N	Z_N	X_N	Y_N	Z_N
D65	95.04	100.00	108.88	94.81	100.00	107.32
A	109.85	100.00	35.58	111.14	100.00	35.20

To calculate the CIELab Cartesian coordinates, the following equations are used, (3-13).

$$L^* = 116Y^* - 16 \qquad a^* = 500(X^* - Y^*) \qquad b^* = 200(Y^* - Z^*) \qquad (3\text{-}13)$$

It becomes obvious that for $Y/Y_N < (16/116)^3$ (≈0.002624) the lightness value, L*, will be negative and this is not possible. The first recommendation made by the CIE was to restrict the scope of use of the equations to $Y/Y_N > 0.01$.

It became necessary to extend the CIE recommendation down to $Y/Y_N = 0$. Following a linear extrapolation made by Pauli (Pauli, 1976), the formulas can be written as followed.

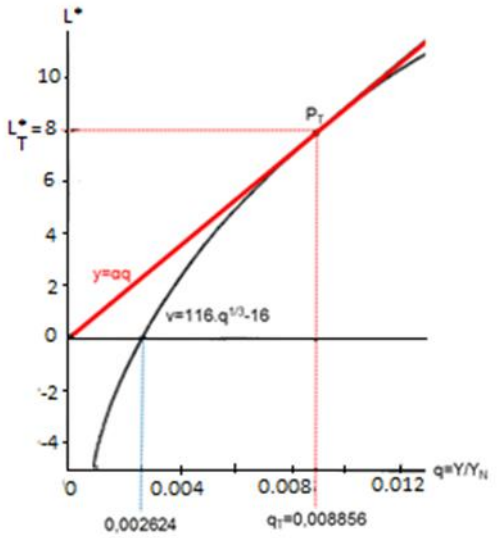

Figure 3-11: Extension of the CIE recommendation for negative lightness values made by Pauli

$$L^* = 116f(Y/Y_N) \qquad a^* = 500\{f(X/X_N) - f(Y/Y_N)\} \qquad b^* = 200\{f(Y/Y_N) - f(Z/Z_N)\}$$

The three functions $f(X/X_N)$, $f(Y/Y_N)$ and $f(Z/Z_N)$ are given by:

$$f(q) = \begin{cases} q^{\frac{1}{3}} - 16/116 & for\ q > \gamma \\ \alpha q & for\ q \leq \gamma \end{cases}$$

Both functions f(q) and their respective derivatives must be continuous over the whole range.

For $q > \gamma$,

$$\begin{cases} L^* = 116q^{1/3} - 16 \\ \dfrac{dL^*}{dq} = \dfrac{116}{3}q^{-2/3} \end{cases}$$

For $q \leq \gamma$

$$\begin{cases} L^* = \alpha q \\ \dfrac{dL^*}{dq} = \propto \end{cases}$$

At the point of tangency, P_T,

$$\begin{cases} L^* = 116q^{1/3} - 16 = \propto q \\ \dfrac{dL^*}{dq} = \dfrac{116}{3}q^{-2/3} = \alpha \end{cases} \Leftrightarrow \begin{cases} q = ({}^{6}/_{29})^3 = (24/116)^3 = 0.008856 \\ \alpha = 116\left({}^{29^2}/_{108}\right) = 903.3 \end{cases}$$

The coordinates of the point of tangency, P_T, with the curve are

$$\begin{cases} q_T = 0.008856 \\ L_T^* = 116(q_T^{1/3} - 16) = 8 \end{cases}$$

The tangency is described by its slope, α.

$$\alpha = \frac{y_T - y_0}{x_T - x_0} = \frac{L_T^*}{q_T} = 903.3$$

Then, the equation of the tangency can be written

$$L^* = \frac{L_T^*}{q_T} \cdot q$$

Yet,

$$L^* = 116Y^* - 16 \Leftrightarrow Y^* = \frac{L^* + 16}{116} \Leftrightarrow Y^* = \frac{\frac{L_T^*}{q_T}q + 16}{116} \Leftrightarrow Y^* = \frac{841}{108}q + \frac{4}{29}$$

After generalization to the whole range, the CIELab coordinates can be written as the equations (3-14).

$$L^* = 116f(Y/Y_N)$$
$$a^* = 500\{f(X/X_N) - f(Y/Y_N)\}$$
$$b^* = 200\{f(Y/Y_N) - f(Z/Z_N)\}$$
$$f(q) = \begin{cases} q^{\frac{1}{3}} - 16/116 & for\ q > (24/116)^3 \\ (841/108)q + 4/29 & for\ q \leq (24/116)^3 \end{cases} \quad (3\text{-}14)$$

From the CIELab cartesian coordinates, it is possible to calculate the polar coordinates, C* and h*, (3-15). C* is the chroma also called the radius vector and h* is the hue angle or polar angle which should be converted to be in the range between 0° and 360°, h_{ab}, (3-16).

$$C^*_{ab} = \sqrt{a^{*2} + b^{*2}} \qquad h_{ab} = \frac{180°}{\pi} arctan(b^*/a^*) \quad (3\text{-}15)$$

The CIELab color space can be divided into 4 quadrants (see Figure 3-12) to facilitate h* conversion.

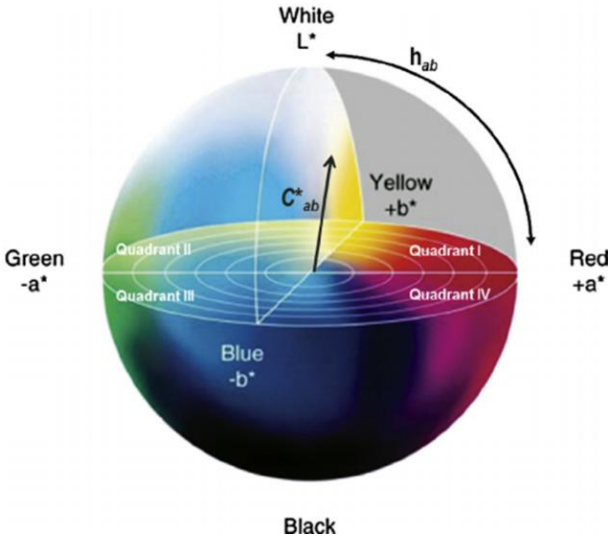

Figure 3-12: CIELab color space

Quadrant I (a*>0 and b*>0)
$$h_{ab} = \left|\frac{180°}{\pi}\arctan(b^*/a^*)\right|$$

Quadrant II (a*<0 and b*>0)
$$h_{ab} = 180 - \left|\frac{180°}{\pi}\arctan(b^*/a^*)\right|$$

Quadrant III (a*<0 and b*<0)
$$h_{ab} = 180 + \left|\frac{180°}{\pi}\arctan(b^*/a^*)\right|$$

Quadrant III (a*>0 and b*<0)
$$h_{ab} = 360 - \left|\frac{180°}{\pi}\arctan(b^*/a^*)\right| \quad (3\text{-}16)$$

3.3.2.1.2. Limitations of the CIELab color space

As seen previously, from tristimulus values, XYZ, and white reference, $X_NY_NZ_N$, it is then possible to define the CIELab coordinates, L*, a*, b*, C* and h*. In order to define the perceptual uniformity of this system, the Munsell Book of Color was used as colors of reference.

The Munsell Book of Color was developed in 1909 by Albert Henry Munsell. It is a perceptual scale where the distances between hues are supposed to be perceptively equal based on visual assessment. The aim of this system was to classify colors according to three parameters: hue, value and chroma. All the colors can be represented in a three-dimensional solid with the value measured at the core (vertical axis) of the solid from 0 (black) to 10 (white), the chroma corresponding to the distance the value axis and the hue corresponding to the direction in the horizontal axis. Even if the description is quite close to the chromatic circle, it is however possible that the purer yellow and the purer blue are not located at the same level due to differences in value. Besides, the variable hue is classified into five principal categories (Red, Yellow, Green, Blue and Purple) along with five intermediate categories (Yellow-Red, Green-Yellow, Green-Blue, Blue-Purple and Purple-Red) (Landa and Fairchild, 2005). A representation of this classification is shown in the Munsell color tree in Figure 3-13. Each branch represents one of the ten hue categories.

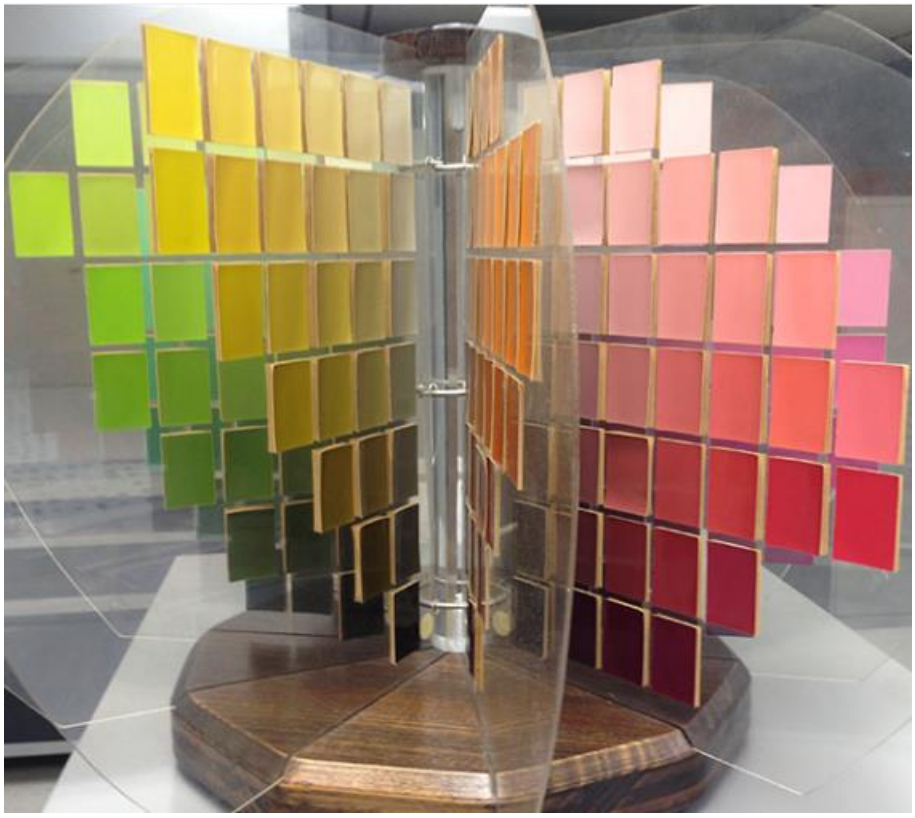

Figure 3-13: Munsell color tree representation with the branches representing each hue category from (Munsell.COLOR, 2019, Larboulette, 2007)

From the Munsell color space and in order to estimate the uniformity of the CIELab color space, the colors of chroma and hue at value 5 were plotted according to the CIELab coordinates, a* and b* (see Figure 3-14).

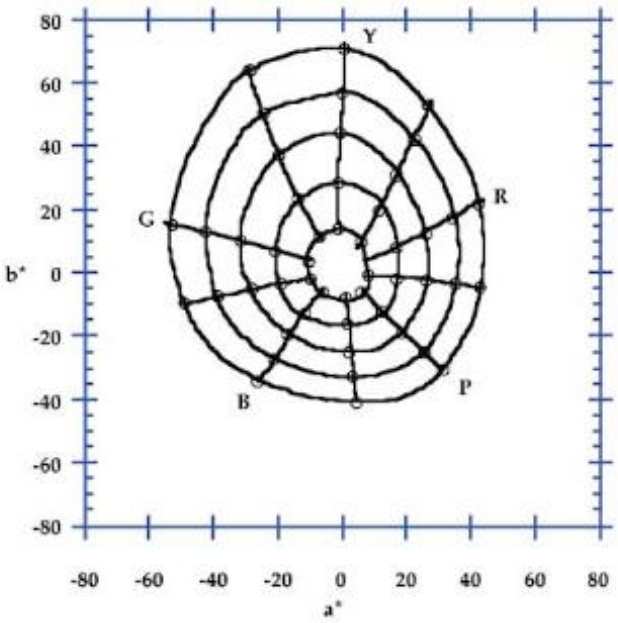

*Figure 3-14: Munsell colors of chroma and hue at value 5 plotted in the CIELab a*b* plane from (Fairchild, 2013a)*

The Munsell system was designed to be perceptually uniform in chroma and hue. Once plotted according to the CIELab a*b* plane, a network of concentric circles and radiating lines should be obtained. As presented in Figure 3-14, the organization of the Munsell colors according to the associated CIELab coordinates, a* and b*, shows an acceptable regularity. However, by comparing yellow and blue colors (see axis B and Y on Figure 3-14), a dissymmetry can be noticed. Thus, for a change of the same perceptible intensity between two colors belonging to a same axis, the changes in the CIELab coordinates will not be identical from one branch to another. Hence, a change in the yellow area will lead to a higher change in the CIELab coordinates than in the blue area.

Another limitation of the CIELab color space is linked to a chromatic adaptation produced by the normalization of the XYZ tristimulus values to those of the light source, $X_N Y_N Z_N$. This chromatic adaptation is called the Von Kries transformation but in the CIELab color space only a simple one is used. It does not correspond to the behavior of the human visual system, in which the cones' responses are first linearized before being normalized. The adaptation can create some discrepancies between visual color evaluation and measured color evaluation. This false Von Kries transformation in the CIELab color space was studied by (Liu et al., 1995). In their study, they compared the perceived hue shift in color of the gemstone tanzanite to the hue change calculated from CIELab coordinates under two illuminants, D65 and A. The calculated hue change, from blue to blue-green, is contrary to the perceived hue change, from blue to purple. However, by adapting a correct Von Kries transformation based on the cones' responses, the correct hue change is predicted.

Finally, it is also important to note that the CIELab color space was developed in order to compare colored objects of same size and shape that are observed in white and light grey surroundings. Besides, CIELab cannot be easily adapted to different viewing environments.

3.3.2.2. CIECAM02 based color space

Although certain limitations exist with the CIELab color space as discussed previously, it is quite useful for most situations. However, in order to overcome the limitations mentioned above, new Color Appearance Models (CAM) were created: CIECAM97 and CIECAM02. CAMs are used to extend traditional colorimetry with XYZ tristimulus values and the CIELab color space by predicting color stimuli under a wide range of conditions. As an input, the tristimulus values of the stimuli, the illuminant, the level of luminance and also the conditions of observations were necessary. CAMs are then able to provide perceptual attributes such as chroma, saturation or hue. All CAMs are characterized by three points: the chromatic adaptation transformation, a uniform representation space and appearance attributes (Luo and Li, 2007). As explained previously, the CIELab color space does not allow the prediction of luminance effects and the changes of perception depending on the background and the surroundings. The main objectives of these two CAMs were to match the color appearance on a display or a hard copy where traditional colorimetry was not efficient enough to this end.

Many researches were carried out by the CIE TC1-34 working group to define first the CIECAM97. The CIECAM02 model developed and standardized later by the CIE (TC8-01) improves the considerations of the different luminance levels and the chromatic adaptation (Luo and Li, 2007). Models CIECAM97 and CIECAM02 are only developed for a single input color and a certain illumination environment. They break down the illumination environment and the color stimulus into three components: the stimulus, the background and the surroundings as in Figure 3-15.

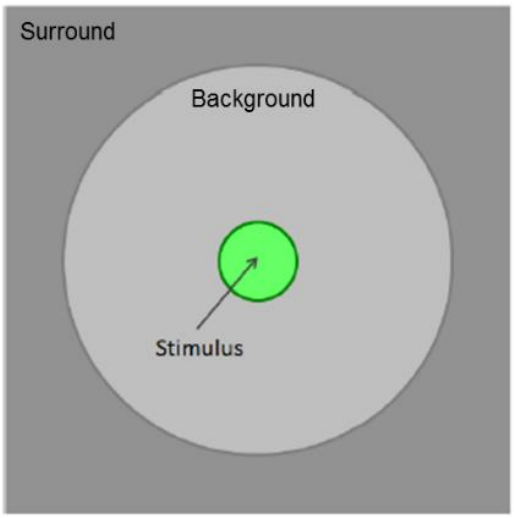

Figure 3-15: Modeling of the conditions of observations and the different components of the viewing field adapted from (Mornet, 2011, Luo and Li, 2007)

The color stimulus corresponds to the observed color. It is defined to cover a uniform patch of about 2° of visual angle. The background is the area surrounding the stimulus extended from the edges of the stimulus to around 100° of visual angle in all directions. Then, the surroundings extend to the limits of the viewing field.

A schematic diagram of the CIECAM02 model is given in Figure 3-16. It illustrates the input data, the parameters and the output data.

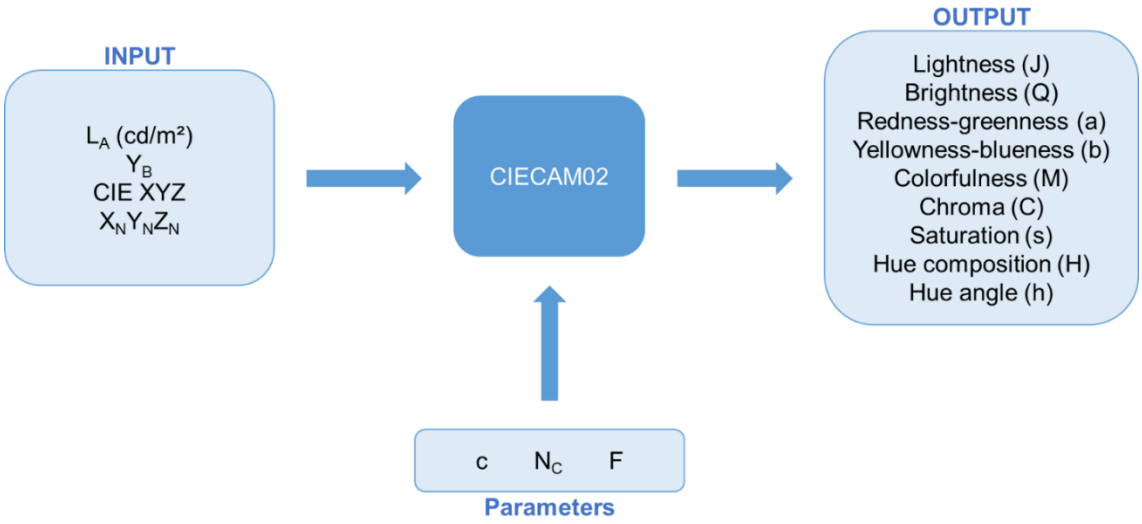

Figure 3-16: Schematic diagram of the CIECAM02 model adapted from (Luo and Li, 2007)

The input data of this model are the tristimulus values of the stimulus, XYZ, the tristimulus values of the white of reference, $X_N Y_N Z_N$, the luminance of the adaptive field (cd/m²), L_A, and the luminance factor of the background, Y_B. On top of these data, parameters of viewing state are added: the impact of the surroundings, c, the chromatic induction factor, N_C, and the incomplete adaptation factor, F. These three parameters are selected from Table 3-2 according to the viewing conditions.

Table 3-2: Parameters of viewing state of CIECAM02 from (Luo and Li, 2007)

Viewing conditions	c	NC	F
Average	0.69	1.0	1.0
Dim	0.59	0.9	0.9
Dark	0.535	0.8	0.8

Then, many output data are coming from the model: the lightness, J, the brightness, Q, the redness-greenness, a, the yellowness-blueness, b, the colorfulness, M, the chroma, C, the saturation, s, the hue composition, H, and the hue angle, h.

In order to determine the output data, intermediate factors must be calculated. Dependent on viewing conditions and surroundings, they include a luminance level adaptation factor, F_L, a background induction factor, n, a brightness-chromatic induction factor, N_{CB}, a brightness-background induction factor, N_{BB}, and an exponential non-linearity factor, z. These factors are calculated according to the following equations (3-17).

$$k = \frac{1}{5L_A + 1} \qquad F_L = 0.2k^4(5L_A) + 0.1(1 - k^4)^2(5L_A)^{1/3}$$
$$n = \frac{Y_B}{Y_N} \qquad N_{BB} = N_{CB} = 0.725(1/n)^{0.2} \qquad z = 1.48 + \sqrt{n} \qquad (3\text{-}17)$$

The degree of adaptation D is then calculated as a function of the environment. In theory, it can take values from 0, for non-adaptation, to 1, for complete adaptation. In practice, the

minimum value is 0.65 for dark viewing conditions and converges exponentially towards 1 for average viewing conditions. It is calculated according to equation (3-18).

$$D = F\left(1 - \frac{1}{3.6}exp\left(\frac{-L_A - 42}{92}\right)\right) \tag{3-18}$$

With all these factors, the chromatic adaptation transformation is determined, (3-19).

$$\begin{bmatrix} R \\ G \\ B \end{bmatrix} = M_{CAT02} \times \begin{bmatrix} X \\ Y \\ Z \end{bmatrix} \qquad M_{CAT02} = \begin{bmatrix} 0.7328 & 0.4296 & -0.1624 \\ -0.7036 & 1.6975 & 0.0061 \\ 0.0030 & 0.0136 & 0.9834 \end{bmatrix} \tag{3-19}$$

The coordinates $R_CG_CB_C$ representing the colors corresponding to an illuminant of same energy are calculated based on equations (3-20).

$$\begin{aligned} R_C &= \left(\frac{Y_N}{R_N}D + (1 - D)\right)R \\ G_C &= \left(\frac{Y_N}{G_N}D + (1 - D)\right)G \\ B_C &= \left(\frac{Y_N}{B_N}D + (1 - D)\right)B \end{aligned} \tag{3-20}$$

The post-adaptation signals of the sample $R_CG_CB_C$ are then transformed using the cones' response formula of Hunt-Poirier-Estevez, M_H, (3-21).

$$\begin{bmatrix} R' \\ G' \\ B' \end{bmatrix} = M_H M_{CAT02}^{-1} \times \begin{bmatrix} R_C \\ G_C \\ B_C \end{bmatrix}$$

$$M_H = \begin{bmatrix} 0.38971 & 0.68898 & -0.07868 \\ -0.22981 & 1.18340 & 0.04641 \\ 0.00000 & 0.0000 & 1.0000 \end{bmatrix} \tag{3-21}$$

The final coordinates for CIECAM02 are then calculated before the calculation of the appearance attributes, shown in Figure 3-16, according to equations (3-22).

$$\begin{aligned} R_a &= \frac{400\left(\frac{F_L R'}{100}\right)^{0.42}}{\left(\frac{F_L R'}{100}\right)^{0.42} + 27.13} + 0.1 \\ G_a &= \frac{400\left(\frac{F_L G'}{100}\right)^{0.42}}{\left(\frac{F_L G'}{100}\right)^{0.42} + 27.13} + 0.1 \\ B_a &= \frac{400\left(\frac{F_L B'}{100}\right)^{0.42}}{\left(\frac{F_L B'}{100}\right)^{0.42} + 27.13} + 0.1 \end{aligned} \tag{3-22}$$

The succession of the different equations detailed above are used either for the sample or the white reference.

The yellowness-blueness and redness-greenness dimensions are first calculated (3-23).

$$a = R_a - \frac{12}{11}G_a + \frac{1}{11}B_a \qquad b = \frac{1}{9}(R_a + G_a - 2B_a) \tag{3-23}$$

The achromatic answer for the sample, A, is also computed (3-24). The achromatic answer for the white, A_N, is obtained from the same equation.

$$A = \left(2R_a + G_a + \frac{1}{20}B_a - 0.305\right) \cdot N_{BB} \tag{3-24}$$

It is now possible to define all remaining color appearance attributes for CIECAM02. The different equations are gathered in Table 3-3.

Table 3-3: Calculation of the color appearance attributes for CIECAM02

Hue angle, h	$h = \arctan\left(\frac{b}{a}\right)$
Lightness, J	$J = 100\left(\frac{A}{A_N}\right)^{c \cdot z}$
Brightness, Q	$Q = \frac{4J}{100c}(A_N + 4)F_L^{0.25}$
Chromaticity, C	$C = t^{0.9}\sqrt{\frac{J}{100}}(1.64 - 0.29^n)^{0.73}$ With $t = \frac{\frac{5000}{13}N_C N_{CB} e_t \sqrt{a^2 + b^2}}{R_a + G_a + \frac{21}{20}B_a}$ $e_t = \frac{1}{4}\left(\cos\left(\frac{\pi h}{180} + 2\right) + 3.8\right)$
Colorfulness, M	$M = CF_L^{0.25}$
Saturation, s	$s = 100\sqrt{\frac{M}{Q}}$

The advantage of CIECAM02 is based on the consideration of surroundings and viewing conditions. This system is able to predict color appearance accurately under a wide range of conditions. This model is also reversible. However, by considering the cones' response formula of Hunt-Poirier-Estevez in the calculation, this model is not suitable for highly illuminated scenes where the cones could be saturated or mesopic or scotopic conditions, under which rods strongly contribute in the vision mechanism. Besides, this model is quite complex.

3.3.3. Color differences

In color industries, the distance between two perceived colors is the metric of interest to evaluate the color matching quality. This metric is needed to convert differences which can only be described with adjectives such as “darker” or “redder” into distances. The distance between two colors is given as ΔE*. This metric is helpful to describe how far a sample is away in terms of color from the reference to be color-matched. Different studies have triggered different ΔE* calculations with the intention to get closer to representing the human perception of color differences. It is important to note that the concept of difference is justified only for colors relatively similar. It becomes very complex to compare colors that are too far apart.

3.3.3.1. CIE 1976 color difference formulas

The aim of color differences is to describe differences between colors that are really perceptible to the human eye. To calculate the color metric, it is first needed to calculate the difference coordinates between a color of reference (R) and a sample (S) (Figure 3-17). Once calculated, they can be converted into coloristic terms, (3-25).

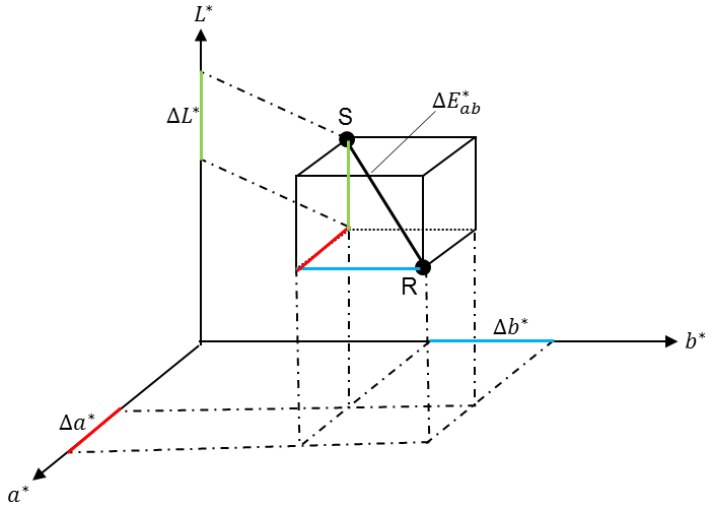

Figure 3-17: Representation of the cartesian coordinate differences between a reference (R) and a sample (S) adapted from (Chrisment et al., 1994)

$$\Delta L^* = L^*_S - L^*_R \qquad \Delta a^* = a^*_S - a^*_R \qquad \Delta b^* = b^*_S - b^*_R$$
$$\Delta L^* \begin{cases} < 0: darker \\ > 0: lighter \end{cases} \qquad \Delta a^* \begin{cases} < 0: greener \\ > 0: redder \end{cases} \qquad \Delta b^* \begin{cases} < 0: bluer \\ > 0: yellower \end{cases} \qquad (3\text{-}25)$$

Based on the three-dimensional Pythagorean theorem, the color difference ΔE^*_{ab} is defined, (3-26).

$$\Delta E^*_{ab} = \sqrt{\Delta L^{*2} + \Delta a^{*2} + \Delta b^{*2}} \qquad (3\text{-}26)$$

The CIELab coordinates can be broken down into brightness, chroma and hue as seen before. The color difference ΔE^*_{ab} can also be described by the lightness difference ΔL^*, the chroma difference ΔC^*_{ab} and the hue difference ΔH^*_{ab} (see Figure 3-18 and equations (3-27)). For the hue contribution, it is needed to convert the hue angle deviation (Δh_{ab}) into a hue metric difference ΔH^*_{ab}.

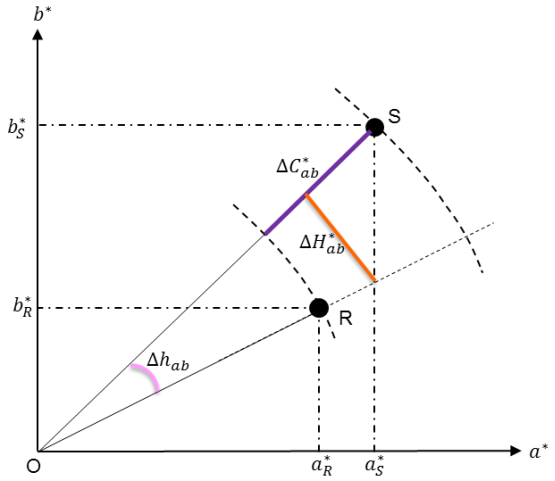

Figure 3-18: Representation of the polar coordinate differences between a reference (R) and a sample (S) adapted from (Chrisment et al., 1994)

$$\Delta C_{ab}^* = C_{ab,S}^* - C_{ab,R}^* \qquad \Delta h_{ab} = h_{ab,S} - h_{ab,R}$$
$$\Delta H_{ab}^* = 2\sqrt{C_{ab,S}^* C_{ab,R}^*} \cdot \sin(\Delta h_{ab}/2) \qquad (3\text{-}27)$$

From these differences, the color difference ΔE_{ab}^* can also be defined, (3-28).

$$\Delta E_{ab}^* = \sqrt{(\Delta L^*)^2 + (\Delta C_{ab}^*)^2 + (\Delta H_{ab}^*)^2} \qquad (3\text{-}28)$$

3.3.3.2. CMC (l:c)

The CIELab formulas showed some inconsistencies especially for use in the textile industry. In 1984, the Color Measurement Committee normalized a new color difference formula, CMC (l:c). CIE 1976 color difference formulas are based on tolerances which can be assimilated to spheres of equal size, but the British textile industry showed that the tolerance limits are represented by ellipsoids of different size. The two weighting factors, l and c, are linear parametric factors which are needed to control the sensitivities to lightness and chroma. In the textile industry, these factors are set to 2:1. The CMC (l:c) formula brings into play several weighting factors which can be calculated as explained in equation (3-29).

$$\Delta E_{CMC(l:c)} = \sqrt{\left(\frac{\Delta L^*}{l S_L}\right)^2 + \left(\frac{\Delta C_{ab}^*}{c S_C}\right)^2 + \left(\frac{\Delta H_{ab}^*}{S_H}\right)^2}$$

$$S_L = \frac{0.040975\, C_{ab,S}^*}{(1 + 0.01765\, L_S^*)} \qquad S_C = \frac{0.0638\, C_{ab,S}^*}{1 + 0.0131\, C_{ab,S}^*} + 0.638$$

Unless $L_S^* < 16$, then $S_L = 0.511$

$$S_H = S_C(fT + 1 - f) \qquad f = \sqrt{\frac{(C_{ab,S}^*)^4}{(C_{ab,S}^*)^4 + 1900}} \qquad (3\text{-}29)$$

or $T = 0.38 + |0.4\cos(35° + h_{ab,S})|$ $\quad if\ h_{ab,S} < 164\ or\ h_{ab,S} > 345$

$T = 0.56 + |0.2\cos(168° + h_{ab,S})|$ $\quad if\ 164 \le h_{ab,S} \le 345$

3.3.3.3. AUDI95

Audi developed a new tolerance model called AUDI95, which is better adapted to the field of automotive paint (Dauser, 2012). This formula is particularly suitable for effect paints with strong flop effects. With AUDI95, there is a distinction between chromatic and achromatic colors based on CIELab coordinates. In the following equations, γ_i indicates the angle of measurement[1] (see Chapter 4, Figure 4-14).

For achromatic colors, i.e. C*≤10 or C*≤18 and L*≥27, the CIELab cartesian coordinates (L*a*b*) are used with several weighting factors, (3-30).

$$\Delta E' = \sqrt{\left(\frac{\Delta L^*}{S_{dL}}\right)^2 + \left(\frac{\Delta a^*}{S_{da}}\right)^2 + \left(\frac{\Delta b^*}{S_{db}}\right)^2}$$

$$S_{da_{\gamma_i}} = 0.50 \qquad S_{db_{\gamma_i}} = 0.50 \qquad \textit{(3-30)}$$

$$S_{dL_{\gamma_i}} = 0.11\sqrt{L^*_{\gamma_i}} + \frac{22.5}{|\gamma_i|} \qquad L^*_{\gamma_i} = \sqrt{L^*_{reference}\, L^*_{Sample}}$$

For chromatic colors, i.e. C*>10 except C*≤18 and L*≥27, the CIELab polar coordinates (L*C*h*) are used with several weighting factors, (3-31).

$$\Delta E' = \sqrt{\left(\frac{\Delta L^*}{S_{dL}}\right)^2 + \left(\frac{\Delta C^*_{ab}}{S_{dC}}\right)^2 + \left(\frac{\Delta H_{ab}}{S_{dh}}\right)^2}$$

$$S_{dL_{\gamma_i}} = 0.11\sqrt{L^*_{\gamma_i}} + \frac{22.5}{|\gamma_i|} \qquad L^*_{\gamma_i} = \sqrt{L^*_{reference}\, L^*_{Sample}}$$

(3-31)

$$S_{dC_{\gamma_i}} = 0.34\sqrt{C^*_{\gamma_i}} - 0.25\sqrt{L^*_{\gamma_i}} + \frac{30.0}{|\gamma_i|} \qquad C^*_{\gamma_i} = \sqrt{C^*_{reference}\, C^*_{sample}}$$

$$S_{dh_{\gamma_i}} = 0.10\sqrt{C^*_{\gamma_i}} - 0.14\sqrt{L^*_{\gamma_i}} + \frac{15.0}{|\gamma_i|} + 0.50$$

3.3.3.4. AUDI2000 or DIN6175

Around the year 2000, car manufacturers started to propose to their customers effect colors containing very small mica pigments. With this kind of pigment, there is almost no dependency of the viewing angle and it is difficult to differentiate effect colors from solid colors. Audi improved its AUDI95 tolerance model to AUDI2000 by changing the weighting factors, (3-32).

[1] for $\gamma = \{\gamma_1, \ldots, \gamma_N\}$ with $\gamma_i \in \{15°, \ldots, 110°\}$ and $i = \{1, \ldots, N-1\}$

$$S_{da_{\gamma_i}} = 1 \qquad S_{dL_{\gamma_i}} = \left(\frac{\left|L^*_{\gamma_i} - L^*_{\gamma_{i+1}}\right|}{\gamma_{i+1} - \gamma_i}\right)^{2/3} + 0.002C^*_{45} + 0.33$$

$$S_{db_{\gamma_i}} = 1 \qquad S_{dC_{\gamma_i}} = 1.478\left(\frac{\left|C^*_{\gamma_i} - C^*_{\gamma_{i+1}}\right|}{\gamma_{i+1} - \gamma_i}\right) + 0.014C^*_{45} + 0.27 \qquad (3\text{-}32)$$

$$S_{dh_{\gamma_i}} = 0.800\left(\frac{\left|C^*_{\gamma_i} - C^*_{\gamma_{i+1}}\right|}{\gamma_{i+1} - \gamma_i}\right) + 0.004C^*_{45} + 0.30$$

For the minima angle, -15°, the weighting factors are calculated according to equations (3-33).

$$S_{dL_{-15}} = 1.2\left(\frac{\left|L^*_{15^\circ} - L^*_{25^\circ}\right|}{25 - 15}\right)^{2/3} + 0.002\ C^*_{45} + 0.33$$

$$S_{dC_{-15}} = 1.2 \cdot 1.478\left(\frac{\left|C^*_{15^\circ} - C^*_{25^\circ}\right|}{25 - 15}\right) + 0.014\ C^*_{45} + 0.27 \qquad (3\text{-}33)$$

$$S_{dh_{-15}} = 1.2 \cdot 0.800\left(\frac{\left|C^*_{15^\circ} - C^*_{25^\circ}\right|}{25 - 15}\right) + 0.004\ C^*_{45} + 0.30$$

For the maxima angle, 110°, the weighting factors are calculated according to equations (3-34).

$$S_{dL_{110}} = 0.5\left(\frac{\left|L^*_{75^\circ} - L^*_{110^\circ}\right|}{110 - 75}\right)^{2/3} + 0.002\ C^*_{45} + 0.33$$

$$S_{dC_{110}} = 0.5 \cdot 1.478\left(\frac{\left|C^*_{75^\circ} - C^*_{110^\circ}\right|}{110 - 75}\right) + 0.014\ C^*_{45} + 0.27 \qquad (3\text{-}34)$$

$$S_{dh_{110}} = 0.5 \cdot 0.800\left(\frac{\left|C^*_{75^\circ} - C^*_{110^\circ}\right|}{110 - 75}\right) + 0.004\ C^*_{45} + 0.30$$

3.4. Conclusion

Standardization of the lighting conditions allows for color comparison under a specific illuminant such as D65 with a known spectral power distribution. Wherever and whenever the measurement is made, the lighting conditions are repeatable. Moreover, the CIE also worked on the standardization of two observers to better correlate what we see to what we measure. Based on CIELab coordinates, color differences were developed following the rule to always be as sensitive as the human visual system.

The established color differences (CIELab, CMC, AUDI) allow for a better correlation of perceptible color differences. A trained observer is thus able to compare two colors and to attribute the perceived differences to existing measurable descriptors (light/dark, yellow/blue or green/red). The physical descriptors are based on the trichromatic vision of human beings (see Chapter 2). In the field of automotive coatings, however, Audi has developed its own color differences: Audi95 or Audi2000. Both of them are weighted according to the color class of the measured color: chromatic or achromatic. Besides of these weighting factors, for Audi2000, new weighting factors have been added according to the measurement angles used in control processes.

Nevertheless, even if an observer is able to compare colors, the color differences are only efficient for plain colors (called solid colors in automotive coatings). Onlooking at the cars in a parking lot, one can notice a high percentage of effect colors. To qualify these specific colors is not easy because no apparent texture descriptors exist. Hence, it is necessary to create and introduce texture descriptors for automotive coatings to be able to qualify texture differences such as the color or quantity of the perceived effect, following similar logics as for existing color descriptors. Besides, texture evaluation works based on contrast and not based on a point by point evaluation. In the case of automotive effect coatings, we do not look at a solid paint in an environment but at a texture with existing contrasts in luminance and chromaticity.

Chapter 4. Automotive coatings

Contents

Coatings for the automotive industry meet many requirements. The aesthetic aspect is one of the main requirements for customers but coatings must also fulfill specifications in terms of functionality. These requirements are important for customers. Vehicles will be exposed to rain and UV radiation, gravel from the road, corrosion and scratches inherent to brushes used in the car wash process. To ensure the durability of the paint over years, different layers are successively sprayed to combine strength and aesthetics (BASF Coatings GmbH, 2012). All the layers together are just a tenth of a millimeter thick (see Figure 4-1).

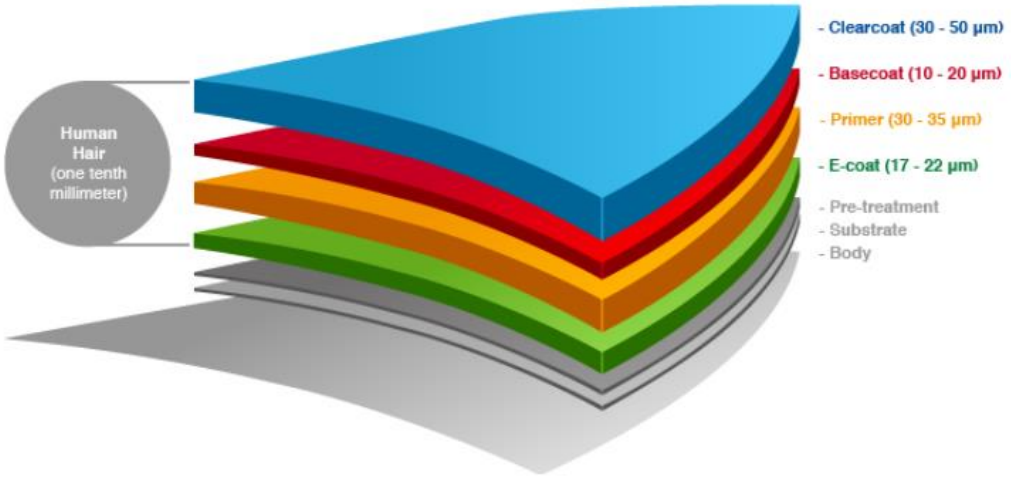

Figure 4-1: Arrangement of the different layers in automotive coatings (BASF Coatings GmbH, 2012)

The car body in galvanized steel is washed and then degreased before being successively sprayed by a series of layers that give anti-corrosion protection, color and gloss to the paint. Each layer fulfills a specific function. First, the body is dipped in a chemical phosphating bath. This process will improve the roughness of the surface and then promote the adhesion of the following layer. As second layer, E-coat or cataphoresis is applied as first full coat. Cataphoretic treatment is an organic coating method using an electrolytic deposition process. It protects the car body from atmospheric agents and then prevent it from corrosion of the body that cannot be achieved easily by spraying. Besides, as the body is fully dipped into the electrolytic coating bath, all cavities are coated which would not have been the case if a spray-painting technique would have been used. The third coat is the primer, which consists of organic polymeric material and brings a protective function. It protects the underlying structure against stone-chipping. The dry primer layer can be easily sanded to offer a smooth surface before application of the basecoat. The basecoat, the fourth coat, is the colored one; it offers unique characteristics to the car while serving current trends. Basecoat color can be either solid or effect. Then, the last layer is the clearcoat - this layer is also thicker and is used to protect paint from environmental and chemical stresses such as UV radiation, scratches, or weather conditions. The clearcoat layer can be glossy, satiny, matte or textured.

This arrangement in 5 layers is only valid for automotive OEM[1] coatings, thus referring to brand-new cars produced in the car plants of all car manufacturers such as Renault-Nissan, PSA or Volkswagen group. The present thesis work was carried out in the automotive refinish coatings division of BASF Coatings France. In the car refinish process, whether you need to fix the entire bumper or a tiny scratch, usually three coats (primer, basecoat and clearcoat) are sprayed at the car body shop, see Figure 4-2.

Figure 4-2: Arrangement of the different layers in refinish coatings

4.1. Refinish coatings

In the field of refinish coatings, two types of repair exist: the edge-to-edge method and the blending method. The type of technique used depends on the quality of the proposed color formula. An edge-to-edge repair process will be preferred when the quality of the color formula is considered as very good. The element in question (a car door for example) is dismantled from the entire car, fixed and repainted. Once reassembled, one is not able to distinguish a color difference between the element repaired and the rest of the car. For a color formula of good quality but having a slight deviation with the initial shade, the blending method is used. The element is fixed and then repainted by blending the color into the adjacent elements. This approach helps to lessen the differences between the element fixed and the rest of the car. However, an experienced sprayer can even do an edge-to-edge repair with an only reasonable mixing formula just by adapting the application technique. A satisfactory repair must be invisible to the customer. That is why, beyond the paint itself,

[1] OEM: original equipment manufacturer

paint manufacturers provide their customers with a database containing color formulas. This database allows them to reproduce all the colors of a car fleet, i.e. hundreds of thousands of references. The process of reproducing the original OEM color in the chosen refinish coating technology is also called colormatching.

The color formulas correspond to a mixture of different pigmented bases (see Chapter 4, paragraph 4.1.1.2) and binders or thinners. Color formulas are developed in the lab by using a proprietary matching software which integrates statistical and physical optical models. These predictive models are combined with algorithms to minimize the theoretical difference between a target color (a car for example) and the color of a calculated formula.

4.1.1. Composition of the basecoat

For this PhD thesis, the focus was put on the basecoat formulation and the influence of the different components on the global and visible aspects of the effect particles. The basecoat is a mixture of different components suspended in a polymer matrix. For refinish coatings, pigmented bases are supplied to body shops: the tinting bases. Each tinting base consists of ideally a single pigment, solid or effect, in a suspended system made of binder, fillers, additives and solvents. To colormatch the original shade, the body shop technician prepares a mixture of several tinting bases in a binder according to the mixing formula, then dilutes the formulation thus obtained before application.

4.1.1.1. Formulation of the basecoat

The basecoat hence consists of different constituents: the binder, the pigments, the fillers, the additives, the solvents and the thinner. A typical proportional distribution of the components is specified in Figure 4-3.

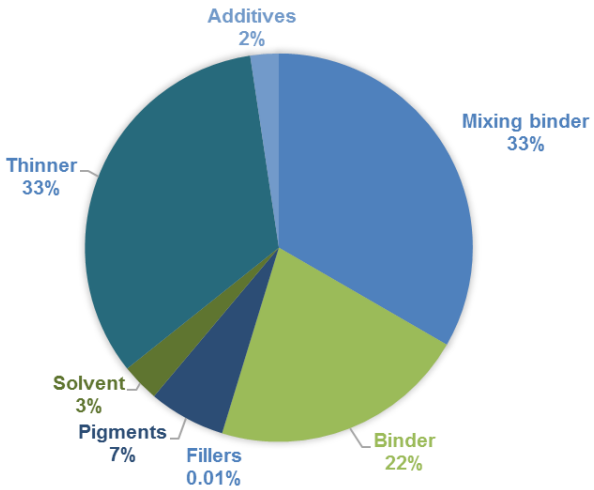

Figure 4-3: Proportions of the different components in the basecoat formula

The binder is the main constituent of the basecoat. It guarantees the physicochemical characteristics of the paint and allows the correct wetting of the pigments. Two types of binder are used in the basecoat: one in the tinting base for the pigment wetting and one in the mixing component to allow a crosslink of the paint film during drying and its adhesion to the substrate

(Stoye and Freitag, 1998). Pigments are insoluble suspended particles. They bring hue and opacity to the basecoat according to their size, their microstructural arrangement and their chemical composition. The pigments can be organic (examples: phthalocyanines or quinacridones) or inorganic (examples: carbon black or iron oxides) (Klein, 2010a). The fillers are white powders such as carbonates or silicates which are used to improve the hiding power of the basecoat while giving specific characteristics such as resistance to abrasion or to climatic conditions. The additives, present in small quantities, reinforce the basic properties of the painting by avoiding the appearance of bubbles during the application or by improving the tension of the film. Drying or coalescing agents are also used. Solvents reduce the viscosity of the paint to improve its application. Solvents used in formulation are light solvents, they evaporate quickly and have no impact on pigment and filler placement. The thinner is also a solvent which is heavier than the other ones and which allows to reduce the viscosity while keeping an adequate evaporation rate for optimal placement of the particles after evaporation of the light solvents. Thinner is added just before application.

In order to reduce the emissions of volatile organic compounds (VOC) due to solvents use and thus the environmental impact, the main solvent used in the thinner and in the mixing binder is water. However, a heavy solvent is needed in the formulation to play the role of coalescing agent and to allow the film formation after water evaporation. According to Directive 2004/42 / EC of 21 April 2004, the VOC content of the basecoat and the clearcoat must be less than 420 g/L for waterborne paints.

4.1.1.2. Tinting bases

A tinting base is a mixture of ideally a single type of pigment, a binder, fillers, additives and solvents. Depending on the type of pigment used, the tinting base may be a so-called solid, metallic or pearlescent base. The solid basecoat (basecoat without effect) is obtained by a mixture of several shades of solid tinting bases. It should be noted that solid colors do not show a color change depending on the viewing angle (flip-flop effect). On the other hand, by mixing effect tinting bases with solid tinting bases, an effect color (color with effects) will be obtained. Unlike solid colors, effect colors have a flip-flop effect, a change in lightness and/or hue, depending on the viewing angle.

4.1.1.2.1. Solid tinting bases

Each solid tinting base represents a basic color: white, black, yellow, red, purple, blue or green. It consists of ideally a single pigment such as red iron oxide or blue phthalocyanine suspended in a resin. Solvents and additives are also added to ensure equivalent viscosity for all solid tinting bases, dispersibility and wettability of pigment particles and stability of the pigment suspension. From one solid tinting base to the other, only the type of pigment and the pigment load change. The pigment load is calculated to assure satisfactory hiding power and an optimum pigment to binder ratio. The solid tinting bases are divided into three types according to the type of pigment used: colored, white and black pigments.

The perceived color is the result of energetic interactions of electromagnetic waves with the pigment particles based on light absorption and scattering processes. Light scattering

occurs if particle size and the wavelengths of the light used for irradiation are in the same range and if the chemical composition of the pigments leads to multipoles – separated electric charge distributions. Those wavelengths of the visible light that are not absorbed by pigment particles lead to the complementary color, the perceived color, see Table 4-1.

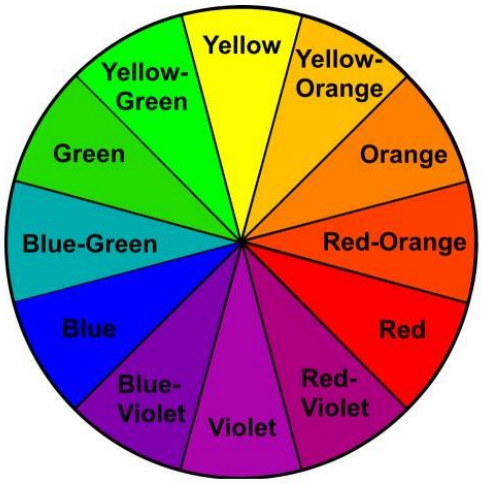

Figure 4-4: Color wheel from (Hoelscher, 2018)

Table 4-1: Spectral range of absorption, light color and complementary color

Spectral range of absorption (nm)	Light color	Complementary color
380-440	Violet	Yellow
440-490	Blue	Orange
490-570	Green	Red
570-595	Yellow	Violet
595-605	Orange	Blue
605-750	Red	Green

Colored pigments are typically based on selective wavelength absorption. There are two classes of pigments: organic and inorganic pigments. Inorganic pigments, such as red or yellow iron oxides, provide dull colors with a high hiding power while organic ones, such as blue or green phtalocyanines are colorful with a high color strength (Klein, 2010a). The use of those pigments is essential to match commercial colors. They bring about a change in color (chromaticity, lightness or hue).

White pigments assume a special role in coatings industry due to their excellent light scattering. Titanium dioxide, TiO_2, in its rutile or anatase crystal structure, is preferred due to its high opacity and brightness. Due to better scattering properties, stability and durability, the rutile structure is preferred. Optimal sizing of TiO_2 particles is needed to reach those properties. The particle size should be slightly less half the wavelength of light. If we consider an average wavelength of 550 nm, the maximum of scattering is reached when particle size is around 0.2-0.3 µm in diameter as shown in Figure 4-5. For a particle size of 0.2 µm, the maximum of light scattering is reached.

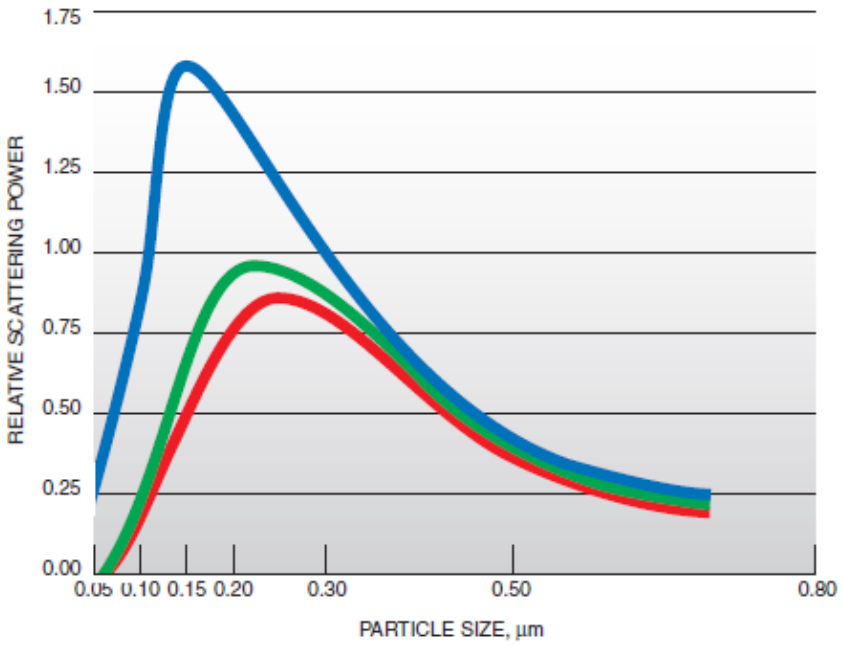

Figure 4-5: Relative light scattering power of rutile TiO_2 for blue, red and green light as function of TiO_2 particle size from (DuPont™, 2007)

For titanium dioxide particles of 0.15 µm in diameter, light scattering in the red and green zones is significantly lower than light scattering in the blue zone. A TiO_2 pigment of 0.15 µm in diameter is then bluer than the one of 0.2 µm; this phenomenon is called undertone. When considering a translucent film, pigment particle size will affect either, reflected and transmitted colors. When colored pigments are used in combination with aluminum particles, a color flop is seen: the frost effect (Klein, 2010a). Such letdowns[1] or colors have a yellowish-gold impression at face view[2] and a bluish color impression at flop view[3]. A sizable part of the blue light is reflected while more yellow light, yellow being the complementary color to blue, is transmitted.

The main feature of black pigments is their dominant light absorption. They are used for black colors or for darkening other types of colors. Black pigments may have a yellowish or bluish undertone. They can also be very dark and very intense (referred to as “deep”).

4.1.1.2.2. Effect tinting bases

Automotive manufacturers offer more and more effect colors to their customers. Those specific colors show a change in lightness and/or chroma according to the observation angle. The angle dependency is linked to single or multiple reflection, interference or diffraction of light by metallic, pearlescent or interference pigments (see Chapter 2, paragraph 2.2). These types of visual effects cannot be reached with traditional absorbing pigments. Moreover, the visual sensation triggered by those pigments on color vision is not simple because our human visual system is made to perceive only absorbed colors. Two families of effect tinting bases can be distinguished: metallic tinting bases and special tinting bases according to the type of

[1] Letdowns: mix of tinting bases at different percentages
[2] Face view: it corresponds to a viewing angle of 45° (more details on pages 81-82)
[3] Flop view: it corresponds to a viewing angle of 75° to 110° (more details on pages 81-82)

pigment used. It is important to note that effect pigments cannot be thicker than 500 nm. This limit in size is essential to guarantee a correct particle organization in the coating film, a smooth surface once varnished and also to avoid particles shattering during the spraying process.

4.1.1.2.2.1. Metallic pigments

Metallic pigments are made from metal flakes which act like small mirrors and give metallic reflection (Klein, 2010a). The incident light is mostly reflected and the remaining part is absorbed by the surface. Light reflection and absorption modulate the typical metallic brilliance and its greyish color. The metallic behavior is influenced by the particle size, the chemical nature of the pigment, the aspect of the particle edges and surface, the thickness and the particle orientation in the basecoat film. The particle orientation in the coating film is itself influenced by the spraying process. The maximum of reflection, visible near specular angle, is achieved by metallic flakes that are perfectly parallel to the substrate – the so-called mirror effect.

A new type of metallic pigments starts to become popular in the market: colored metallic flakes. These colored flakes are metallic pigments which are coated by a colored component such as copper or red iron oxide or cobalt (Klein, 2010a).

Classic metallic pigments are divided into two categories according to their morphology: cornflakes and silver dollars. Cornflake particles display irregular surfaces and rough edges due to the fracture from other flakes in the manufacturing process. Silver dollar particles, on the contrary, are produced by elaborate grinding techniques with polishing paste to ensure plane surfaces and round edges. Those two types of aluminum particles are presented in Figure 4-6.

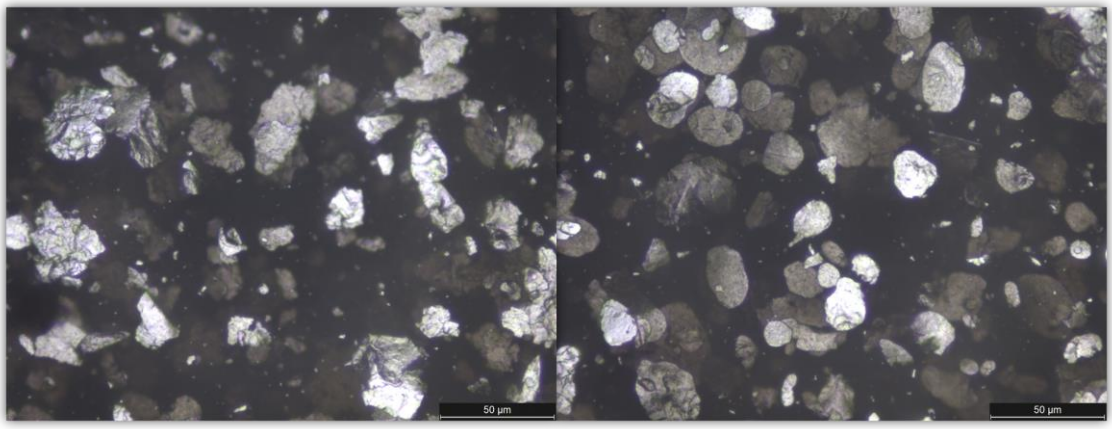

Figure 4-6: Light microscopy images of two letdowns, scale indicating 50 µm. Left: cornflake aluminum tinting base mixed with black tinting base. Right: silver dollar aluminum tinting base mixed with black tinting base

The structural specificities of the two types of aluminum lead to different optical behaviors or characteristics. The main parameters are summarized in Table 4-2 from (Klein, 2010a).

Table 4-2: Comparison of optical properties between cornflake and silver dollar aluminums, from (Klein, 2010a)

Characteristic	Cornflakes	Silver dollars
Sparkling	Minor – low	Visually noticeable
Graininess	Low	Visible
Flip-flop	Light swing	Dark swing
Hiding power	High	Low
Hue extinction	High	Low

The optical characteristics are defined by:

- Sparkling (or glittering, optical roughness): distinction of flakes by the human eye due to a highly intense light reflection;
- Graininess (or coarseness, texture or salt and pepper effect): uniformity of light-dark areas;
- Flip-flop (or flop effect, light to dark effect or travel): metallic coloration between face and flop;
- Hiding power (or covering capacity): ability to hide the surface of an object;
- Hue extinction: when mixed with colored pigments, ability for aluminum particles to entirely hide the chroma.

4.1.1.2.2.2. Special effect pigments

The last group of effect pigments used in automotive coatings industry are special effect pigments. They imitate the nacre luster of natural pearls, butterfly wings or peacock feathers with their iridescent colors (Klein, 2010a). This group comprises two types of pigments: pearlescent and interference pigments. One can distinguish the monochromatic particles which do not lead to a color change according to the angle of observation (see also: color travel) as opposed to the polychromatic particles with color travel. The first type of particles is characterized by multiple reflections while the second type is based on constructive interference. The effects resulting from the use of these kinds of pigments are the pearl effect, the iridescent effect, the metallic effect, two-tone colors or color travel effects. The produced colors depend on the different refractive indices, the thickness of the pigment, the angle of observation and the global basecoat color, also called the mass tone color. The flake thickness is between 30 nm and 1 µm. Specific effect pigments can show a sparkling effect if they are coarse enough.

Special effect pigments are mainly symmetrically coated substrates of at least one layer. The substrate is made of mica, natural or synthetic, aluminum oxide, chromium oxide, iron oxide, silica or borosilicate (Klein, 2010a). The coating consists of one or several layers of metal oxide (iron oxide, titanium dioxide or chromium oxide). Natural effect pigments are duller than the synthetic ones. The substrate of these particles should have a significant difference in RI compared to the other coated layers. Pigments split light into two complementary colors according to their thickness. The reflected color is dominant in regular reflection (face view) while the transmitted one dominates at other viewing angles.

Mica-based effect pigments can be coated by either a single layer of titanium dioxide, a combination of titanium dioxide – metal oxide or a single layer of iron-III-oxide. With a single layer of titanium dioxide, the resulting colors can be silver, yellow, red, blue or green, depending on the thickness of the layer (Klein, 2010a). The cross-section in Figure 4-7 shows the mica substrate in the middle surrounded by a single layer of titanium dioxide.

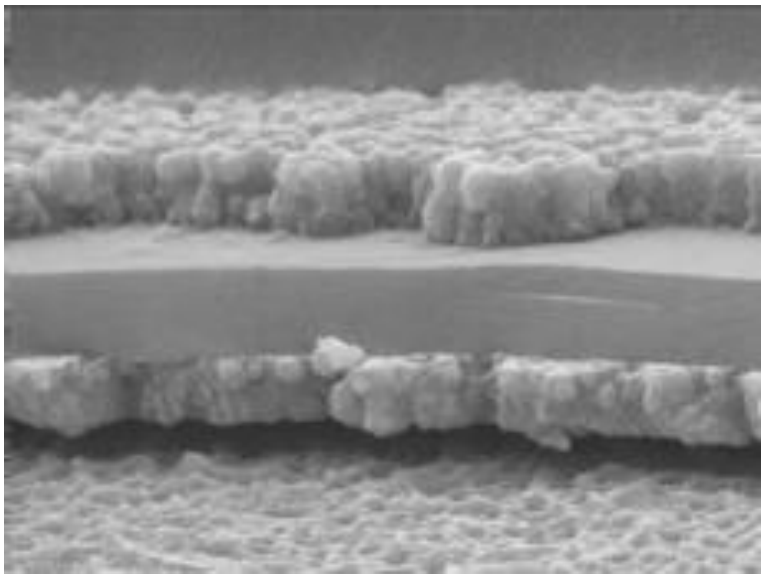

Figure 4-7: SEM[1] picture of a cross-section through a mica-based particle with a single layer of titanium dioxide from (Pfaff, 2009)

By superimposing a layer of iron-III-oxide on top of the titanium dioxide layer, the color obtained is gold, for titanium iron oxide, silver, iron blue, blue and for chromium-III-oxide, green. The pigments obtained show a color travel. Another possibility is to directly coat a layer of iron-III-oxide on the mica substrate to obtain either bronze, copper or red effects depending on the thickness of the layer.

It is also possible to use a silica substrate. Silica-based pigments offer several advantages compared to pigments based on mica substrates. The substrate preparation guarantees a uniform thickness of the flakes as illustrated in Figure 4-8. The resulting interference color is more chromatic than for mica-based pigments because the thickness irregularities of the substrate reduce light travel. Besides, silica has a lower RI, 1.46, compared to mica, 1.58. By controlling the thickness of the substrate, the RI can be reduced by making very thin flakes, around 50 nm, which are then transparent. This provides strong interference effects with new color travel behavior and a strong chromatic strength.

[1] SEM: scanning electron microscopy

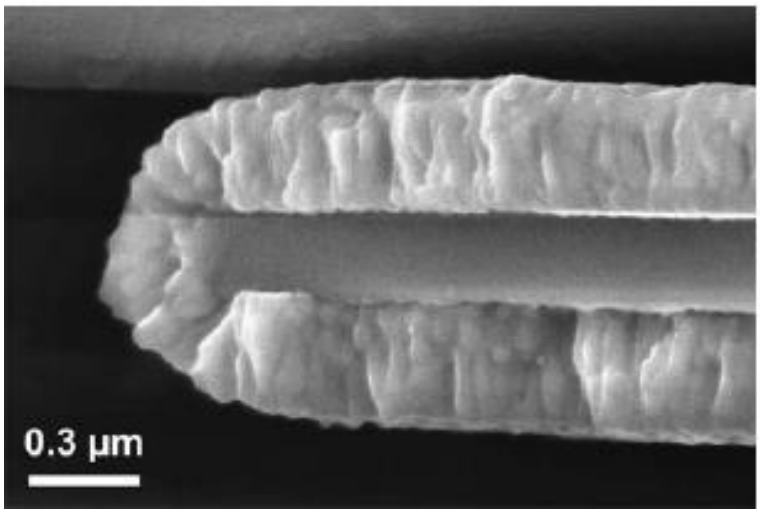

Figure 4-8: SEM picture of a cross-section through a silica-based particle coated with α-Fe_2O_3 (Eivazi, 2010)

Sparkling properties can be improved by using borosilicate as substrate (Klein, 2010a). These pigments are totally transparent and have a smooth and plane surface – they are called glass flakes and their sparkling properties are very intense.

A new type of special effect pigment starts to be introduced in the automotive coatings market, the so-called diffractive pigments (Klein, 2010a). The effect of these pigments is based on light diffraction. The specific surface of the substrate with grooves allows the reflection and the transmission of light rays. SpectraFlair®, developed by Viavi Solutions Inc, is a perfect example of these pigments; it is a three-dimensional aluminum substrate coated with magnesium fluoride. In direct light, SpectraFlair® shows a multi-rainbow effect.

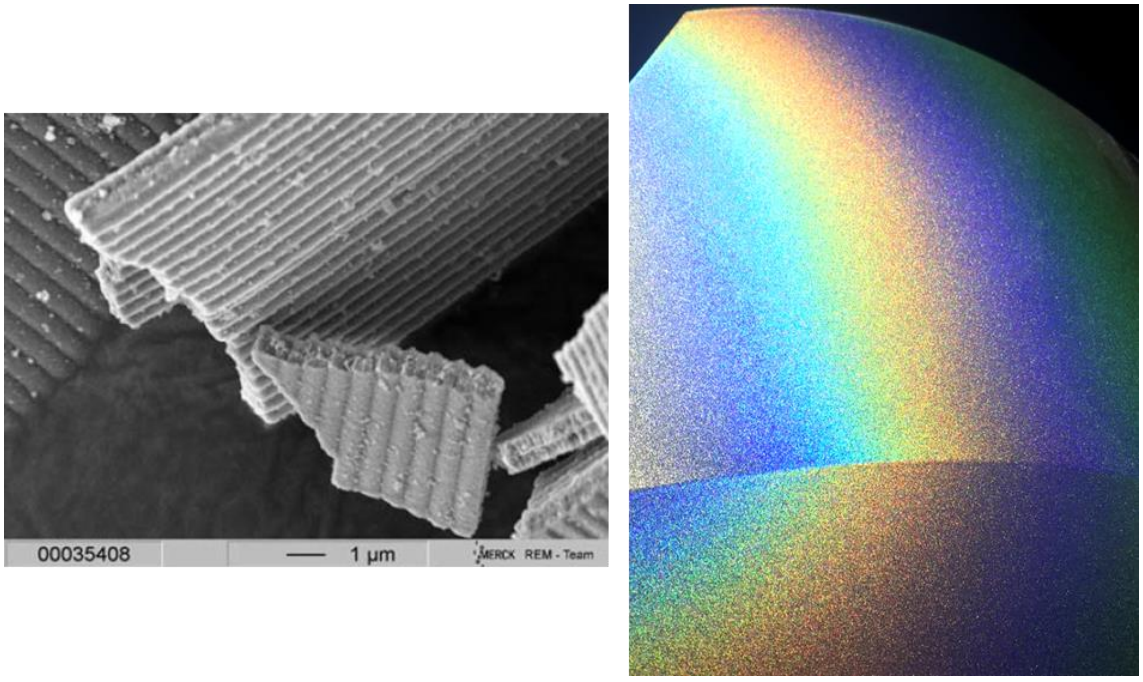

Figure 4-9: Left: SEM picture of a diffractive pigment (Pfaff, 2009); Right: SpectraFlair® multi-rainbow effects

4.1.1.2.3. Flop modifier

The microstructural organization of the effect particles in the coating film is very important. A perfect application leads to particles that are aligned with the metallic panel. So-called flop modifiers, that are also available for color matching, are made of silica microspheres suspended in a polymer matrix. These spheres cause a disorientation of the effect particles in the coating film. This disorientation is confirmed by the SEM pictures in Figure 4-10 from (Maile et al., 2005).

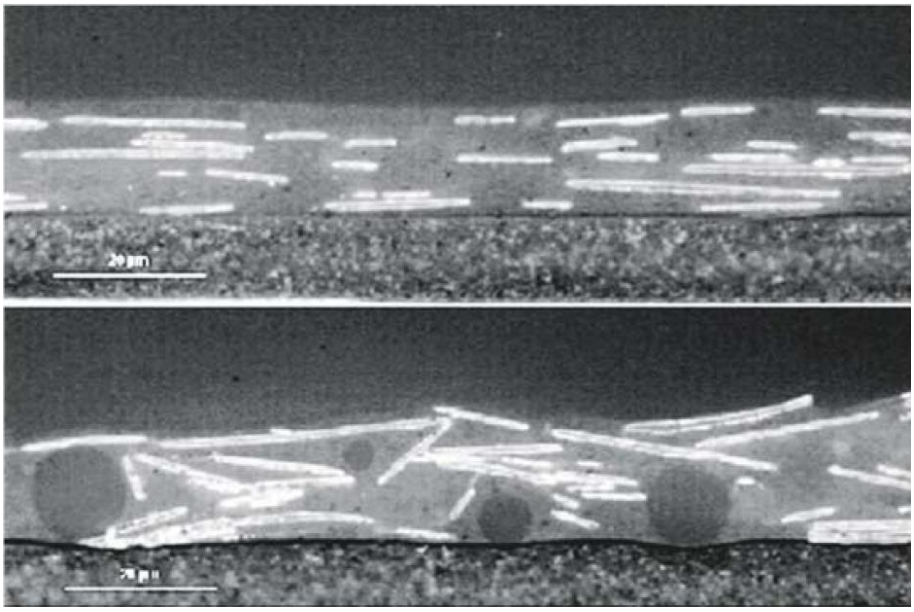

Figure 4-10 : Orientation behavior of effect pigments in a solventborne car refinish basecoat with (top) and without (bottom) flop modifier, the scale indicates 20µm from (Maile et al., 2005)

Regarding those two SEM cross-sections, a change in the orientation of effect pigments is clearly noticeable. Solvent evaporation during the drying of the basecoat tends to orient the particles more parallel to the substrate. When flop modifier is added to the basecoat formula, the orientation of the flakes is less organized and more random. By changing the orientation angle of the effect particles, they will appear more sparkling and larger. In some cases, the flop modifier produces a change in lightness by reversing the flop effect from light to dark to dark to light. It is important to note that this special tinting base can only be used for effect colors.

4.1.2. Sample preparation

Once the paint formula is selected, several tinting bases, solid and/or effect, are mixed together with the mixing binder to obtain the desired shade.

Let’s consider the example of a famous color from PSA group, aluminum grey. The color formula is given in Table 4-3. To colormatch this shade, it is needed to mix together the mixing binder, two aluminums (M99/01 and M99/02), a white (A032), a black (A926), a blue (A503), a red (A359) tinting bases and the flop modifier. They are stirred before being diluted with the thinner.

Table 4-3: Color formula of aluminum grey from PSA

Tinting base	Amount (g)
Mixing binder	69.86
M99/01	18.19
M99/02	5.10
A032	2.55
A926	0.99
A503	0.55
A359	0.22
Flop modifier	2.55
Thinner	50.00
Total	150.00

The color formula is sprayed using a Sata HVLP (high volume low pressure) gravity-feed spray gun on a precoated metal panel to assure paint adhesion. Spraying is done in a dry on dry process. A first layer of an average thickness of 4 µm is sprayed on the panel and then dried for five minutes of venturi ventilation. A second layer of an average thickness of 10 µm is applied. In the case of an effect paint, a third layer is needed. It is sprayed after a drying break of five minutes and its thickness is around 1 µm. This last layer is needed to ensure a correct placement of the effect particles. The thickness of the film, once it has dried, is 10-15 µm. The painted panel must dry at least fifteen minutes at room temperature before applying the clearcoat. The clearcoat application consists of two successive layers of an average thickness of 20 µm with a flash-off phase without venturi ventilation. A waiting time of ten minutes is needed to avoid an orange peel effect. The panel is finally heated at 70°C for 30 minutes to let the clearcoat crosslink.

In the field of automotive coatings, car manufacturers often propose new color trends. They want to differentiate themselves on the aesthetic part by proposing very chromatic and transparent colors. This is for example the case with Renault's now famous "Flame Red", launched in 2011. To color match a color as chromatic and as transparent as the color proposed, the spraying process needs to be adapted by utilizing a tricoat technology. This technology is based on the addition of a new layer between the basecoat layer and the clearcoat layer: the so-called midcoat. The midcoat is a transparent binder with only a small quantity of tinting bases, either solid and/or effect.

4.2. Color and texture evaluations

To confirm the good quality of a formula, it is necessary to control the potential color shift and also to compare the initial texture to the texture of the color-matched sample. Several devices are available on the market to evaluate the overall quality of color. Besides, a visual control is also carried out to confirm the same color, texture and behavior of the color travel between sample and reference.

4.2.1. Color evaluation

As explained in Chapter 2, color perception is based on the triplet “light-object-observer”. Since the 1960’s, color measuring instruments have been available on the market. These devices are suitable for numerical quantifications of color impressions. Even if measurements in principle should correlate to visual impressions, a combination of color measurement and visual evaluation can be quite valuable. The observer is then replaced by a device measuring color and a computer connected to it, see Figure 4-11.

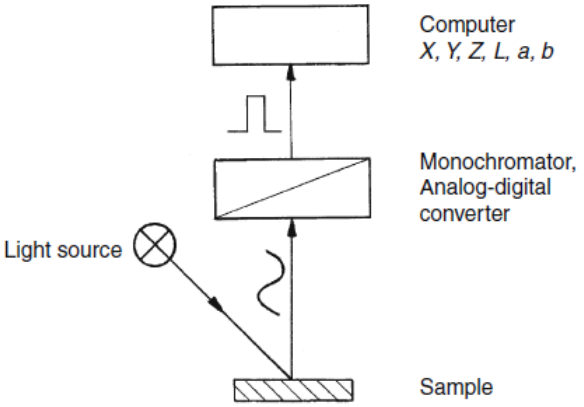

Figure 4-11: Schematic principle of a color measuring device from (Klein, 2010b)

4.2.1.1. Instruments measuring color

The instrument measuring color is made from optical components and photodiodes, which can convert the trichromatic stimulus into a computer signal. Three types of devices are available to provide the tristimulus values without using the human eye: spectroradiometers, spectrophotometers and tristimulus-filter colorimeters (Wyszecki and Stiles, 1982a).

4.2.1.1.1. Spectroradiometers

Spectroradiometers are the most comprehensive devices to quantify color impressions. They measure the spectral power distribution of the radiance emitted by a surface or in other words, the radiometric quantities as a function of the wavelength. According to (Grant, 2011), the radiance is “*an elemental quantity of radiometry, expressing the power per unit area and per unit projected solid angle from a source*” (units: W/m².sr). The test source measured may be either an active emitter, or a passive reflector. The measurement of colorimetric quantities involves the comparison of the test source with a known spectral radiant power distribution.

The radiation emitted by the test source enters through the device to the monochromator which disperses the incoming power and transmits it in narrow wavelength bands to the computer. The outputs of spectroradiometers are, for example, the spectral power distribution, the correlated color temperature, the tristimulus and chromaticity values according to the CIE1931 or the CIE1964 system.

For radiant power measurements, during the present PhD thesis, a Konika-Minolta non-contact spectroradiometer that measures contrasts of 100 000:1 and low luminance levels, down to 0.003 cd/m² was used.

4.2.1.1.2. Spectrophotometers

Spectrophotometers are used to measure the spectral transmittance or reflectance factors of objects. They can also be configured to measure under different illuminations or viewing conditions. Inversely to a spectroradiometer, a spectrophotometer works on a comparison of the radiant power of the reflected light with the radiant power of the incident light. To quantify the radiant power of the incident light, a standard of reflectance factor is used. The CIE recommendation is to use a perfect reflecting diffuser, an ideal uniform diffuser with a reflectance equal to unity. That kind of material is not physically possible, no material offers this property. However, it is possible to use a white standard as an ideal uniform diffuser which can be made of MgO or $BaSO_4$ (Wyszecki and Stiles, 1982a). Another white standard is spectralon, a fluoropolymer, developed by Labsphere.

Spectrophotometers are made of an integrated lighting system and various components such as monochromator or optical couplers. The reflected light is caught by a detector and transmitted to measuring equipment. Modern spectrophotometers have 31 filters to measure the full color spectrum (Mouw, 2017).

Spectrophotometers of different shapes and sizes such as small handheld devices for labs or in-line devices for manufacturing lines are commercially available. Since they can evaluate color under different light sources, spectrophotometers are helpful for metamerism identification. Two objects which have the same spectral power distribution and seem identical under one type of light source, can have a different spectrum under another source. In color industry, metamerism is checked under two illuminants, D65 and TL84 (or F11). Sometimes, illuminant A is used.

4.2.1.1.3. Tristimulus-filter colorimeters

Tristimulus-filter colorimeters work almost the same way as spectrophotometer. The only difference comes from the filters. Tristimulus-filter colorimeters only have 3 filters: red, green and blue. The three filters should match the human visual system with the three color matching functions.

4.2.1.2. Measurement geometries

Spectrophotometers have fundamentally changed color evaluation. They are essential for physical color characterization of absorption pigments. The first recommendation of the CIE concerned the measurement of solid material only (CIE, 1998). Two types of geometries are presented: directional (45:0 or 0:45) and spherical geometries (d:0 or 0:d). It is important to note that the inverse geometries have no impact on the results.

With a 0:45 geometry (respectively 45:0), the sample is illuminated at an angle of 0° (respectively 45°) while the reflected light is detected at 45° (respectively 0°), see Figure 4-12 (Klein, 2010b).

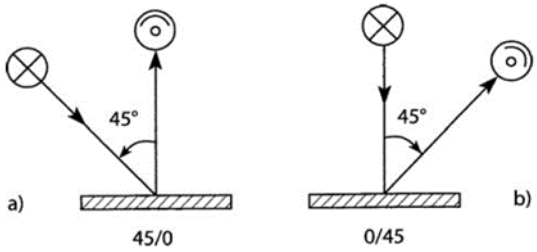

Figure 4-12: Directional measuring geometries: a) 45:0 and b) 0:45 from (Klein, 2010b)

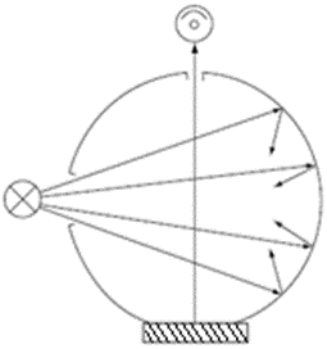

Figure 4-13: Diffuse geometry d:0 adapted from (Klein, 2010b)

The sphere geometry d:0 means diffuse illumination and a detector at 0° (Klein, 2010b). Diffuse illumination is obtained by using a suitable material, Teflon (polytetrafluoroethylene) or barium sulfate, $BaSO_4$, to coat the interior of the sphere. This setup is also called the Ulbricht sphere.

However, in automotive industry, effect colors are more and more popular. These specific colors provide a change in lightness and/or color according to the observation angle. A large number of geometries is needed to better quantify global color travel (KonicaMinolta, 2019). To measure these angle-dependent colors, gonio spectrophotometers with variable directional geometries are used. Gonio spectrophotometers propose either a fixed illumination system and detectors at variable angles or a fixed detector and variable illumination systems. Nowadays, multi-angle spectrophotometers are available on the market. Usually, the detector (or illumination system) is fixed at 45° to the normal and, as recommended by (DIN, 2001), four measurement angles with illumination systems (or detectors) at 25°, 45°, 75° and 110° are available, see Figure 4-14. Two other standardized angles were also implemented in such devices: -15° and 15°.

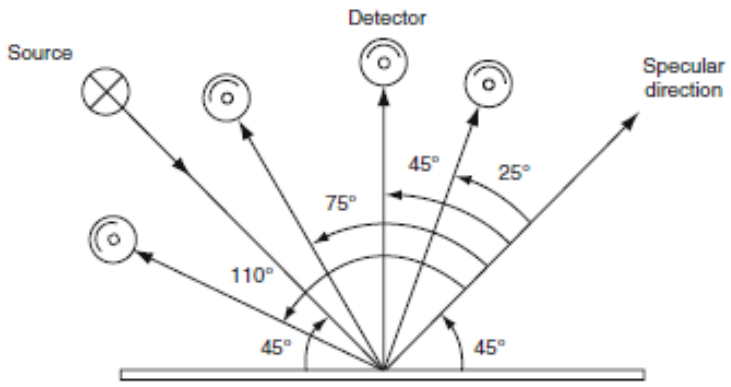

Figure 4-14: Principle of a multi-angle spectrophotometer from (Klein, 2010b)

The angles -15° and 15° are also known as near specular angles, 45° as mid specular angle and 75° and 110° as far specular angles.

4.2.2. Texture evaluation

Multi-angle spectrophotometers are useful to characterize the global color travel of effect colors. However, the effect pigments in coatings formulation need a different physical characterization for optical properties. Some optical characteristics have been developed to quantify the texture: the metallic value, the flop index and the distinctiveness of image (DOI). These three parameters are based on reflectance, R, or lightness, L*, values.

The metallic value was developed to measure the metallic brilliance of a sample or, in other words, the degree of light reflection caused by metallic particles. It is then a comparison of mid specular angle with near specular angle, (4-1). High metallic values stand for high metallic effects (MV up to 5,000) while low metallic values represent low metallic effects (MV ~ 150) according to (Klein, 2010c).

$$MV = \frac{R_{7^\circ}}{R_{45^\circ}} \cdot 100 \qquad (4\text{-}1)$$

The DOI, distinctiveness of image, is used to estimate the uniformity of the metallic effect. It is calculated by either one of the two equations (4-2). As the DOI is linked to the hiding power of metallic particles and then to the low contrast, a high DOI is obtained for fine particles and a low one for coarse ones (Klein, 2010c).

$$a)\ DOI = \left[1 - \frac{R_{14.7^\circ}}{R_{15^\circ}}\right] \cdot 100$$
$$b)\ DOI = \left[1 - \frac{R_{15.3^\circ}}{R_{15^\circ}}\right] \cdot 100 \qquad (4\text{-}2)$$

The flop index is used to describe the lightness travel or flop effect by comparing the near specular and the far specular angles, (4-3). An effect color with a low lightness travel, with fine cornflake aluminum particles, has a low flop index value (FI ~ 20) while a high flop index (FI ~ 60) stands for metallic colors with dark flop, when coarse silver dollar particles are used (Klein, 2010c).

$$FI = 2.69 \frac{(L^*_{15^\circ} - L^*_{110^\circ})^{1.11}}{(L^*_{45^\circ})^{0.85}} \qquad (4\text{-}3)$$

The flop index is a good indication for lightness travel. Let's compare two colors: one is Metallic Grey from Peugeot and the other is Vogue Silver from Honda, see Figure 4-15. These two commercially available colors are two silver greys. Their lightness values at 15°, 45° and 110° are summarized in Table 4-4 with the FI values.

Figure 4-15: Picture of Peugeot Metallic Grey (left) and Honda Vogue Silver (right)

Table 4-4: Lightness and FI values for Peugeot Metallic Grey and Honda Vogue Silver

	Peugeot _ Metallic Grey	Honda _ Vogue Silver
L*(15°)	142.13	133.66
L*(45°)	60.47	62.74
L*(110°)	32.55	31.15
FI	15.12	13.61

The FI values for these two colors are close to each other with a pretty low value but when looking at the pictures, a high difference in texture can be noticed. The aluminum particles in Peugeot Metallic Grey are coarser than the ones in Honda Vogue Silver. Besides, the color from Peugeot seems sparkler than the one from Honda. As a result of light microscopy investigations of these two colors (see Figure 4-16), the metallic effect in Peugeot Metallic Grey (in Figure 4-16, A) can be attributed to cornflake aluminums, while for Honda Vogue Silver (in Figure 4-16, B), the effect is linked to a mixture of cornflake and silver dollar aluminums.

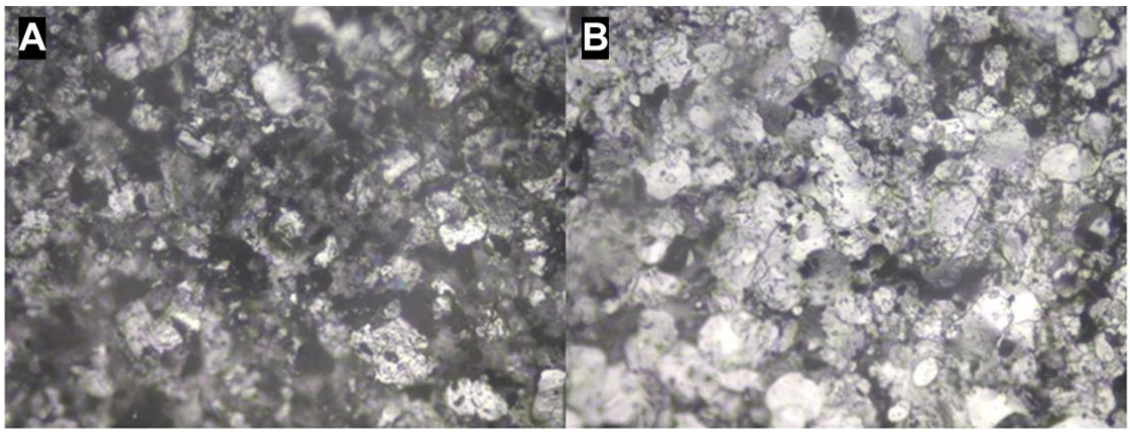

Figure 4-16: Light microscopy observations of two commercial colors, scale indicating 50µm. Left (A): Peugeot Metallic Grey. Right (B): Honda Vogue Silver

As previously explained in Table 4-2, each category of aluminum leads to specific optical properties in terms of sparkling or graininess. Hence, even if the flop index values of the two

colors are close, the formula and especially the aluminum tinting bases used have an important impact on texture evaluation when compared to visual evaluation.

The three parameters are useful to characterize the metallic effect. However, multi-angle spectrophotometers available on the market do not offer directional geometries at 7°, 14.7° and 15.3°. In industries, hence, it is not possible to determine neither the metallic value nor the DOI.

4.2.3. Visual evaluation

For visual assessment, a standardized lighting system must be used. The comparison is then performed in a light booth equipped with the standard illuminant D65. Besides, to avoid metamerism between the formula and the standard, the illuminant TL84 (also called F11) is also used. Visual evaluation is carried out by trained colorists. Indeed, at BASF, every colorist must succeed at the Farnsworth-Munsell 100 test[1] every three years to validate their visual ability to detect small chromatic differences.

The visual evaluation consists of a comparison of the color to be matched (the standard) with the test panel, the sample sprayed in the lab. The two references are observed in the same plane with a spacing of one millimeter between them. Solid colors are mainly observed at 45°. For effect colors, the references are checked at different angles to evaluate the color travel between face and flop. Indeed, as previously explained, effect particles are mainly parallel to the substrate, except when flop modifier is used to disturb the organization (see Chapter 4 paragraph 4.1.1.2.3). As the physical properties are angle-dependent, it is important to tilt the panel to better evaluate the color and the effects at different viewing angles. The main angles are presented in Figure 4-17.

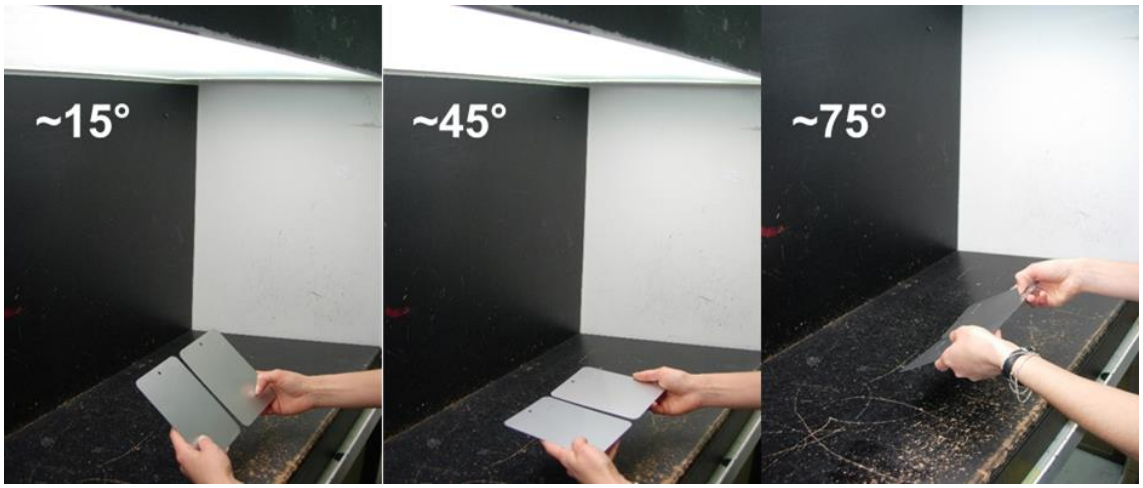

Figure 4-17: Panel orientation under different viewing angles

In the following, the terms “flip view”, “face view”, “flop view”, “flop”, “flip-flop effect” are frequently used. It is important here to explain this wording. Flip view corresponds to a

[1] The Farnsworth-Munsell 100 test is a color vision test made of one hundred color disks which need to be sorted in the correct order.

viewing angle of 15° to 25°, face view of 45° and flop view of 75° to 110°. The lightness flop characterizes a decrease in lightness triggered by metallic coatings when viewed at extreme angles: from 15° to 110°. In the same way, the use of pearlescent materials leads to a change in color according to the viewing angles, the color flop. Normally, lightness flop should be use for metallic coatings and color flop for pearlescent coatings. However, due to the high complexity of automotive coatings with different types of effect pigments in the formula and also due to misuse of language, flop and flip-flop effects are used to express either color and lightness flops.

With visual evaluation, the two references are compared in terms of lightness (brighter or darker), chromaticity (purer or dirtier) or hue (bluer, yellower, greener or redder). For effect colors, each of these criteria is observed at all viewing angles. The color travel of the standard should be replicated in the best way possible. Besides, effect particles are also observed under a directional spot to estimate the sparkling, their size, their quantities and their colors.

4.2.4. Color and texture evaluation

The three texture parameters previously explained in Chapter 4 paragraph 4.2.2 are not efficient for texture evaluation. First, they only consider reflectance values at angles unmeasurable by commercially available multi-angle spectrophotometers. Then, even if the flop index can rate the level of the lightness travel, some limits exist as shown in Table 4-4. Besides, these parameters were developed for metallic effects but interference and pearlescent materials are trendy in automotive coatings formulations.

Beginning of the 21st century, BYK-Gardner, AkzoNobel and Merck associated their knowledge and competencies in the project TARBAM to improve texture evaluation. They came out with a multi-angle spectrophotometer equipped with a camera, the Byk Mac (BYK.Gardner.GMBH, 2009). For the BYK Mac color geometries, an illumination system is located at 45° compared to the normal and 6 detectors are set at -15°, 15°, 25°, 45°, 75° and 110°, see Figure 4-18.

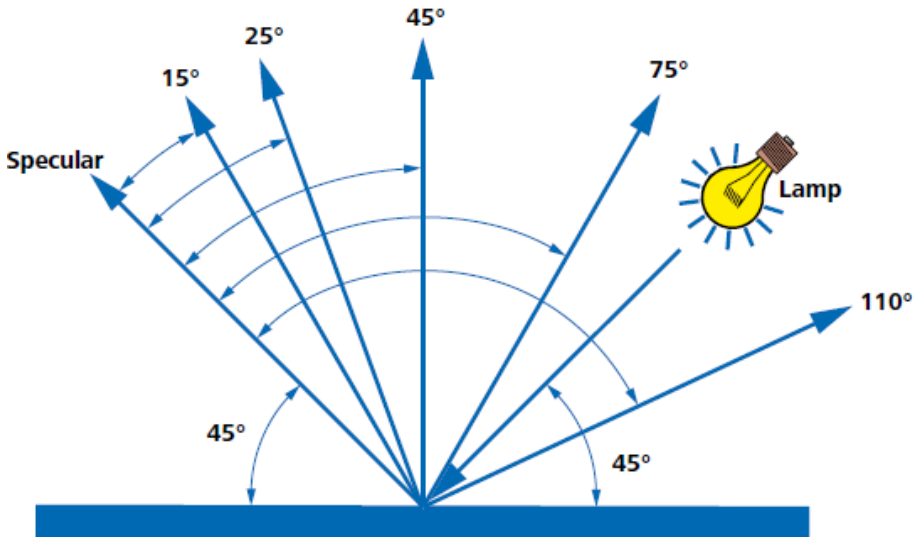

Figure 4-18: Color measurement geometries for the BYK Mac (-15° is not drawn) from (BYK.Gardner.GMBH, 2009)

On top of the color evaluation, the BYK Mac was also designed for texture evaluation by using a black-and-white camera. The camera is set at the normal angle (90° to the sample) and four illumination systems are installed: three directional lights at 15°, 45° and 75° and one diffuse light.

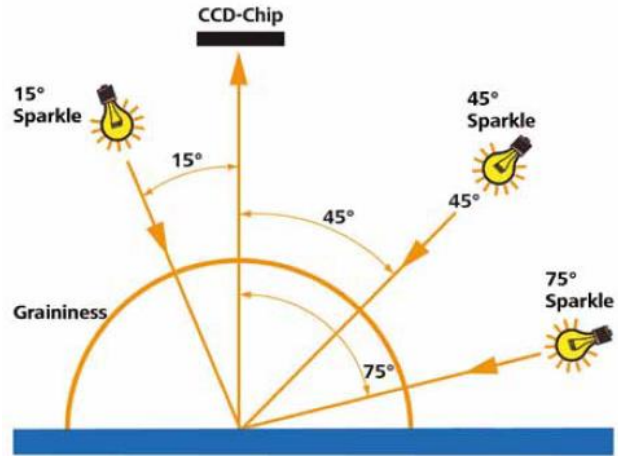

Figure 4-19: Texture measurement geometries for the BYK Mac from (BYK.Gardner.GMBH, 2009)

According to (Sperling and Schwarz, 2011), the directional illumination systems are ensured by LEDs while the diffuse conditions are obtained by lighting a white coated sphere with LEDs. The effects triggered by effect coatings change according to the lighting conditions, see Figure 4-20. Diffuse light stands for a cloudy sky while direct light represents direct sunlight.

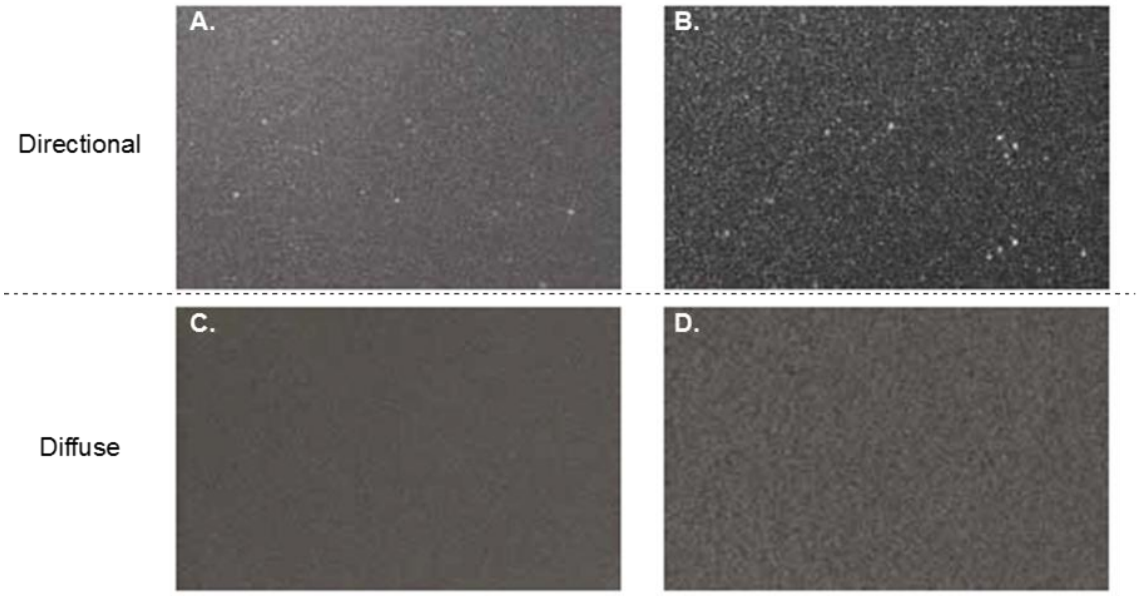

Figure 4-20: Images from BYK Mac under directional conditions (A – low sparkle & B – high sparkle) and diffuse (C – low graininess & D – high graininess) conditions from (BYK.Gardner.GMBH, 2009)

From these black-and-white pictures, based on lightness values, two texture parameters are calculated: sparkling and graininess.

For the sparkling evaluation, direct pictures (15°, 45° and 75°) are used to determine two quantities: sparkling area, S_A, and sparkling intensity, S_I. The sparkling area represents the total sparkly area and the sparkling intensity, the global intensity of all the “sparkle” particles. The “sparkle” particles on pictures are the ones that are lighter than the average lightness level of the picture, (Klein, 2010c). From these two quantities, the sparkle grade, S_G, is calculated according to equation (4-4). As the effect particles are supposed to be parallel to the surface, except in case of flop modifier use, higher values are obtained for the 15° geometry.

$$S_G = \sqrt{S_A \times S_I} \qquad (4\text{-}4)$$

With S_G, *sparkle grade*
S_A, *sparkle area*
S_I, *sparkle intensity*

For the graininess, G, the diffuse picture is used. Also called the “salt and pepper effect” or diffuse coarseness, it stands for the non-uniformity of the effect evaluated on the light and dark fields of the picture. The more uniform the picture is, the smaller the value of graininess and vice versa.

The BYK Mac developed by BYK-Gardner GmbH is the reference for texture evaluation. However, X-Rite commercialized its own multi-angle spectrophotometers with camera since 2018, the MA-T6 and MA-T12 as a response to the BYK Mac. The MA-T6 is made of a detector at 45° compared to the normal and 6 illumination systems at -15°, 15°, 25°, 45°, 75° and 110°. The MA-T12 offers an additional detector. The lighting system is based on several polychromatic white LEDs with blue enhancement (Ehbets et al., 2012). The blue enhancement is needed to compensate for the weakness of the traditional white LEDs in the blue area. The configuration of the MA-T6 is presented in Figure 4-21 in orange.

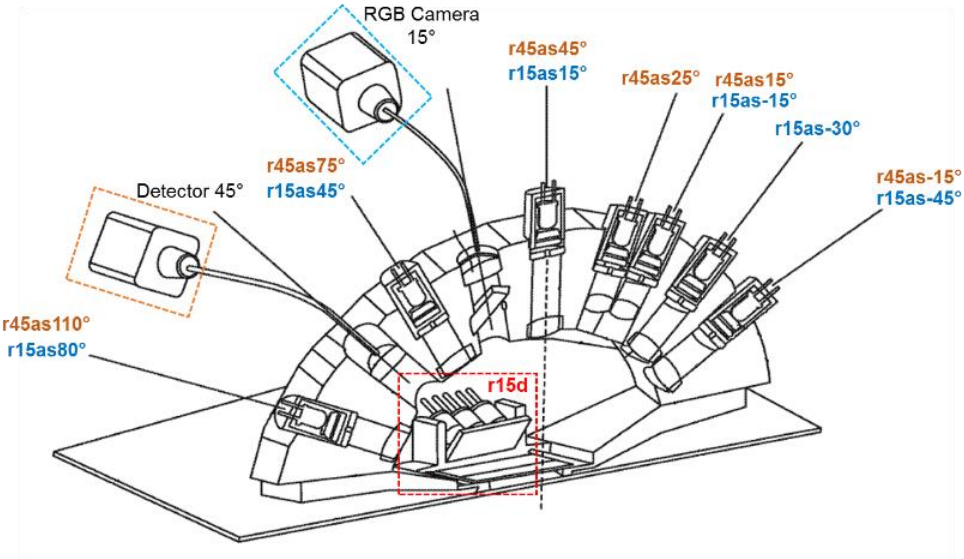

Figure 4-21: Color measurement geometries for the MA-T6 (in orange), directional texture measurement geometries (in blue) and diffuse texture measurement geometry (in red) adapted from (Ehbets et al., 2012)

In addition to the color detector, X-Rite also added a camera for texture evaluation. Contrary to the black-and-white camera in the BYK-Mac, X-Rite uses an RGB camera. The

camera is set at 15° for the MA-T6. The illumination systems used for color measurement are the same that are also used for texture measurement. Six directional geometries are available: -15°, 15°, -30°, -45°, 45° and 80°, see Figure 4-21 in blue. The lighting system used for 25° color measurement (r45as25° in Figure 4-21) cannot be used for texture measurement as the camera is located in the specular. On top of the directional geometries, a diffuse one (r15d) is also set, see Figure 4-21 in red. The diffuse geometry is ensured by 2 sets of 3 white LEDs behind an inclined diffusor film.

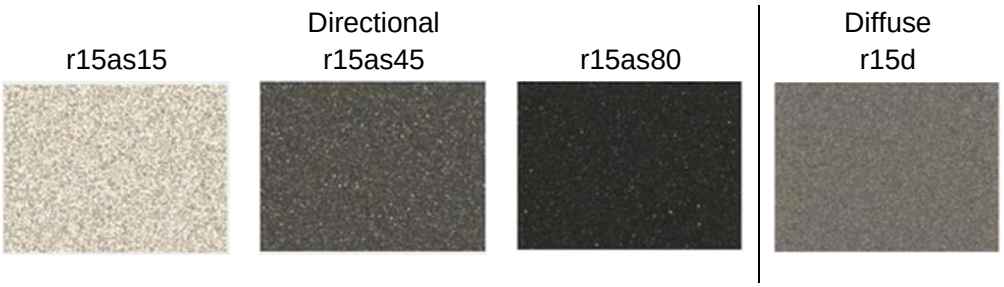

Figure 4-22: Images from MA-T6 under directional (left) and diffuse (right) conditions from (X-Rite, 2018b)

From the colored pictures, see Figure 4-22, the sparkle grade, SG, the coarseness, equivalent to graininess, G, and the color variation are extracted. According to (Gottenbos, 2018), the sparkle grade and the coarseness values have been improved compared to BYK Mac values to better match visual assessment. Due to the RGB camera, it is now possible to determine particle colors and better identify effect particles in color formulas.

Color particle identification has been studied by (Beymore and Krawciw, 2014). A multi-angle spectrophotometer with an RGB camera, such as the X-Rite MA-T6, was used in order to help effect particle determination in coating formulations. Based on several pictures at different viewing angles, the sparkle color distribution is calculated for each directional geometry. The distributions obtained are then an additional input in the database to look for effect pigments which provide the same effect and/or at each angle. By this method, the colormatching should be easier with an automatic selection of effect pigments. However, using an RGB camera does not mean color measurement and clarifications are required regarding the calculation of the sparkle color distribution.

Nowadays, even if device manufacturers such as BYK-Gardner GmbH or X-Rite developed multi-angle spectrophotometers with camera, none of the texture values developed really match the visual appearance. A visual evaluation is needed to validate the formula proposed to colormatch a standard.

4.3. Context and problematic

Based on BASF data extractions for the last three years on new color formulations developed by OEMs, 95% are effect colors and only 5% solid colors. Colormatching of effect coatings is more complex than the one for solid colors. Indeed, the fillers offering optical properties such as aluminum or pearl particles (see Chapter 4 paragraph 4.1.1.2.2) produce an appearance heterogeneity for the coating film. According to the observation angle, the modalities light/matter create various effects: changes in lightness or chroma. In fact, the

effect pigments added in the coating microstructure lead to optical and local gonio-dependent effects. These effects cause the texture effect which is perceived.

The prediction models used in the colormatching process have their own limitations, in particular the color descriptors currently used. They are based on reflectance curves and CIELab coordinates coming from spectrophotometer measurements. The colorimetric theoretical description does not allow a complete representation of the colored sensation. The color descriptors are sufficient for solid colors but only partially for effect coatings. Even if some texture descriptors have been introduced in the new multi-angle spectrophotometers (see Chapter 4 paragraph 4.2.2), they do not correlate to the visual appearance. It is needed to define visual texture descriptors which better or perfectly characterize effect coatings. The objective is to qualify and quantify the perceived attributes such as the apparent particle size or the sparkling effect. Another limitation comes from the fact that several color formulas could lead to the same minimization of the theoretical color distance. However, the type of effect pigments used in the formulation could lead to huge differences in visual appearance.

The effect colormatching process provides a result that is generally not precise enough to achieve the right formula on the first trial. It must be repeated several times and an experienced colorist must manually adjust the formulas by selecting the right effect tinting bases to get a satisfactory formula. This means that only expert colorists can actually produce effect color formulas based on their experience. The improvement of color descriptors as well as the integration into the algorithm of their know-how would thus make it possible to develop an effective system of color formulation for labs.

The objectives of this PhD thesis were to work on color formulation algorithm improvement by defining new texture descriptors considering the textured optical signals and by correlating them to visual appearance. So, one of the most important aspects of this project is the elucidation and integration of human color evaluation through sensorial analysis.

In present PhD thesis, only effect coatings with a glossy clearcoat have been considered. Changes of the system concerned only the basecoat. Different basecoat formulations have been produced by mixing effect and solid tinting bases.

By analyzing effect coatings, the impacts of aluminum or pearl particles are available at different scales. At the macroscopic scale, the overall effect of the particles is visible. The flakes are easily discernible and are causing the sparkling effect and the global change in lightness or hue. At the microscopic scale, the sparkling effect is due to the interaction between the incident light and the effect particles which act like tiny mirrors. At nanoscale, the surface finishes of the particles in the film can be analyzed. For the PhD thesis, the macroscopic scale has been mainly studied to correlate the measurements to visual appearance. A colorist will always try to relate the appearance to a given formula or effect components. Insofar, as the appearance results from interaction in a complex system, the colorist sometimes cannot identify them easily.

Chapter 5. Definition of new texture descriptors

Contents

As explained in the previous chapters, a colorimetric approach based on reflectance curves and then CIELab coordinates is not enough to comprehensively describe the complete visual perception of an effect color by the observer. A new approach based on the combination of colorimetric and texture values has evolved about ten years ago with the launch of a new multi-angle spectrophotometer, the BYK-Mac. Two texture parameters, sparkling and graininess, were developed by BYK-Gardner, Merck and AkzoNobel to better define the optical behavior of effect colors. However, they do not really match the visual impression of texture and hence, the two mentioned parameters may not be enough to describe the human visual perception.

In present PhD thesis, the objective was to find new texture descriptors based on visual appearance of effect colors. To that end, it was necessary to first identify the visible impact of coating components such as aluminum or white tinting bases on the overall visual perception. After the mentioned determination, the objective was to then develop new visual texture descriptors. The determination of these descriptors was based on the input of several experienced observers in order to gather their expert knowledge for the definition of those new texture descriptors. The new texture descriptors should be based on explainable perceptible characteristics; hence, human perception needed to be the unique input for their definition. The different stages which led to the development of the new texture descriptors are explained in the following. The aim of the new descriptors is to avoid false diagnoses based on preconceptions such as a supposed formula.

5.1. Identification of components with a visible influence on basecoat perception

All the samples analyzed during this present thesis work were sprayed on an iron panel coated with a titanium dioxide-based primer on which the basecoat followed by the clearcoat is applied. The only modified element of this system was the formulation of the basecoat. Basecoat formulations of different colors were prepared by mixing solid tinting bases with aluminum tinting bases. For the identification of new descriptors, only aluminum tinting bases were used, since pearl tinting bases would lead to multiple visible effects on basecoat perception linked to this type of pigments (pearlescent and interference). To target the behavior of each tinting base, five categories of components can be defined: aluminum, black, white, colored tinting bases and flop modifier. Although the silica microspheres, used in some formulations to modify the aluminum particle arrangement (flop modifiers – see Chapter 4, paragraph 4.1.1.2.3), are not considered as pigments, they have no effect on color perception but have quite some effects on texture perception.

5.1.1. Tinting bases used and their associated effects

All formulations were prepared using a waterborne paintline: Line 90 from Glasurit®, a premium paintline developed by BASF.

Seven aluminum tinting bases are available in Line 90. The aluminum particles are different in terms of size and/or shape. These two characteristics for the different aluminum particles studied are detailed in Table 5-1. The size, D_{50}[1], is given by the suppliers.

Table 5-1: Characteristics of the aluminum tinting bases of Line 90

Type of pigment	Size, D_{50} (µm)	Name of the tinting base
Cornflakes	10	**M99/00**
	19	**M99/02**
	28	**M99/03**
Silver dollar	16	**M99/01**
	18	**M99/22**
	19	**M99/04**
	24	**M99/21**

For this study, only the yellowish black available in Line 90, **A926**, was used. Indeed, this tinting base is the most used in all commercial formulas because it is a neutral black, neither too blue nor too yellow. Besides, at BASF historically each aluminum tinting base is mixed with **A926** at different ratios to study its optical behavior and the associated color path without any chromatic interferences.

[1] D_{50}: median value of particle size distribution

Three white tinting bases are available in Line 90: A032, A035 and A097. As explained before, the white tinting bases contain titanium dioxide. The grinding process of the pigments leads to different properties. A035 is used as a standard white tinting base with an average particle size D_{50} for titanium dioxide particles of 180 nm. The tinting base A032 is the diluted version of A035 (addition of binder). It is used to improve the accuracy of the paint formulation in the case of very dark colors when only a small quantity of A035 is necessary. Use of the diluted version makes it possible to use a larger quantity of tinting base and thus to improve the precision of the weighing of the formula (and consequently the repeatability) in car body shops. A097 has an average particle size around 80 nm. Its use leads to the frost effect defined previously with the yellowish-gold impression at face view and a bluish color impression at flop view. The characteristics of the three white tinting bases are compared in Table 5-2.

Table 5-2: Characteristics of the three white tinting bases of Line 90

Name of the tinting base	Type of grinding	Size D50 (nm)	Concentration of TiO2 (%)	Visible effect
A035	Classical	180	50%	Masking effect
A032	Classical	180	10%	Masking effect
A097	Micro	80	30%	Frost effect

Colored tinting bases are essential to colormatch OEM colors. Around fifty colored tinting bases exist in Line 90 but only nine of them were used for the creation of the samples during this PhD thesis: two yellows (A115 & A136), three reds (A306, A329 & A372), one violet (A430), one blue (A563) and two greens (A640 & A695).

The associated behaviors of all tinting bases used are summarized in Figure 5-1.

Figure 5-1: Associated effects of the five categories of tinting bases

5.1.2. Creation of ranges

The five categories as listed in Figure 5-1 have an influence on the visual perception of the basecoat. For the first phase, only four of these categories were considered: aluminum, black, white and color. To better understand the impact of the parameters on visual appearance and on texture, several ranges were created and sprayed to be studied for each one:

- The effects of aluminum tinting bases in a black tinting base (called Range 1);
- The effects of one aluminum tinting base in one green tinting base (called Range 2);
- The effects of white and/or colored tinting bases on some aluminum tinting bases (called Range 3).

In the following, it is important to note that the percentages indicated do not correspond to the pigment load in the formula. This percentage refers to the percentage of tinting base involved in the formula. Thus, it does not consider the quantities of mixing binder or thinner needed to prepare the formula for spraying as explained in Chapter 4, paragraph 4.1.2. Besides, the formulas sprayed do not correspond to commercial OEM colors but the formulations tested will help us to evaluate the influence of each constituent alone or combined with the others on the final visual appearance.

For the Range 1 (i.e. Effects of aluminum tinting bases in black tinting base), the tinting base **M99/00**[1] was mixed with **A926**[2] at different ratios. Twenty-four formulations (also called letdowns) were sprayed by gradually increasing the percentage of aluminum tinting base by steps of 2.5% from 0% to 10% and steps of 5% from 10% to 100%. Besides, for the other six aluminum tinting bases, six letdowns were sprayed at 2.5%, 5%, 10%, 25%, 50% and 100% of aluminum tinting base with black. In the end, sixty panels were sprayed in order to study the behavior of aluminum in combination with the black tinting base. The objective of this range was therefore to analyze the impact of the quantity of aluminum tinting base on the lightness, L*.

After studying the optical behavior of aluminum particles in black, the second step was to analyze its effects in a colored tinting base with Range 2. A green tinting base was selected the others because the human visual system is able to discern smaller differences in this area of the chromatic circle (see Chapter 3, Figure 3-9). This high discernibility is linked to the central position of the color green in the spectrum surrounded by blue and red but also the relative lightness of this color (Feisner, 2006). For this purpose, only the aluminum tinting base **M99/00** was mixed at 100%, 95%, 90%, 50% and 5% with **A640**[3]. The objective of this range was to investigate the impact of the quantity of aluminum on chromaticity, C*.

The aim of Range 3 was to estimate the impact of the masstone color with or without titanium dioxide on visual appearance of the letdowns.

[1] **M99/00**: extra fine cornflake aluminum tinting base
[2] **A926**: black tinting base
[3] **A640**: green tinting base

Four aluminum tinting bases were selected for their respective aluminum particles: two cornflakes (M99/00[1] & M99/03[2]) and two silver dollar morphologies (M99/04[3] & M99/21[4]). This choice made it possible to compare the associated effects of size and type (surface state) for each type of aluminum particle and especially those used in M99/03 and M99/21 which are the coarsest aluminums available in Line 90 with a respective D_{50} of 28µm and 24µm. To study the impact of titanium dioxide on texture, two white tinting bases, A035[5] and A097[6], were used. In addition, to observe only the impact of the masstone color on visual appearance, eight solid tinting bases (A115, A136, A306, A329, A372, A430, A563 & A695) were selected. Finally, to test the impact of titanium dioxide and masstone color on visual perception, A035 and A032[7] were used. Indeed, the use of A097 would have brought the frost effect in addition to the changes generated by the masstone color, aluminum or titanium dioxide. This is why this tinting base was not used in this experiment.

The different letdowns sprayed for Range 3 are summarized in Table 5-3, where A_i is the concentration used for the aluminum tinting base and **Ci** is the concentration for solid tinting bases.

Table 5-3: Summary of the different formulations sprayed for Range 3

	Ai	Ci	A097	A035	A032
#1	70%	-	30%	-	-
#2	70%	-	-	30%	-
#3	70%	30%	-	-	-
#4	70%	25%	-	5%	-
#5	70%	20%	-	10%	-
#6	70%	5%	-	25%	-
#7	70%	30%	-	-	10%

During this phase, 234 letdowns were sprayed to study variations related to type, size and percentage of aluminum tinting bases in the formula (i.e. Range 1), the hue extinction (i.e. Range 2) and the impact of masstone color and/or titanium dioxide on visual appearance (i.e. Range 3).

5.1.3. Analysis of the influence of four categories of tinting bases on visual appearance

As previously discussed, a large number of samples were sprayed to evaluate the influence of the different paint constituents. Different analyses were performed on all the panels such as spectral measurements, visual analysis or light microscopy investigations.

[1] M99/00: extra fine cornflake aluminum tinting base
[2] M99/03: coarse cornflake aluminum tinting base
[3] M99/04: medium silver dollar aluminum tinting base
[4] M99/21: coarse silver dollar aluminum tinting base
[5] A035: classical white tinting base
[6] A097: micro milled white tinting base
[7] A032: classical white tinting base (diluted version)

All samples were visually checked in a light booth under the illuminant D65 and with a spotlight for direct light. The objective of this analysis was to be able to detect if a threshold effect in texture was visually noticeable and what was the impact of the amount of aluminum on lightness. Panels with **M99/00**[1] (i.e. Range 1) were visually controlled. Between 10% and 100% of aluminum, few changes are visually detectable for the human eye. However, between 0% and 10%, significantly more changes are noticeable. Moreover, to construct a logical sequence of these panels according to the percentage of **M99/00** is relatively obvious due to the strong change in lightness, see Figure 5-2.

Figure 5-2: Letdowns of M99/00 with A926, from 100% to 0% of aluminum tinting base content

For the second part of Range 1, it was to be checked if, by visual assessment, several observers would classify the letdowns in the same order and regardless of the percentage of aluminum used. Five observers reclassified two series of seven letdowns according to the strength of the effect: the first series comprises the letdowns with 100% of aluminum tinting base (see Figure 5-3) and the second one the letdowns with 10% (see Figure 5-4). For the ease of reading, only the mean observer is shown in the two following charts.

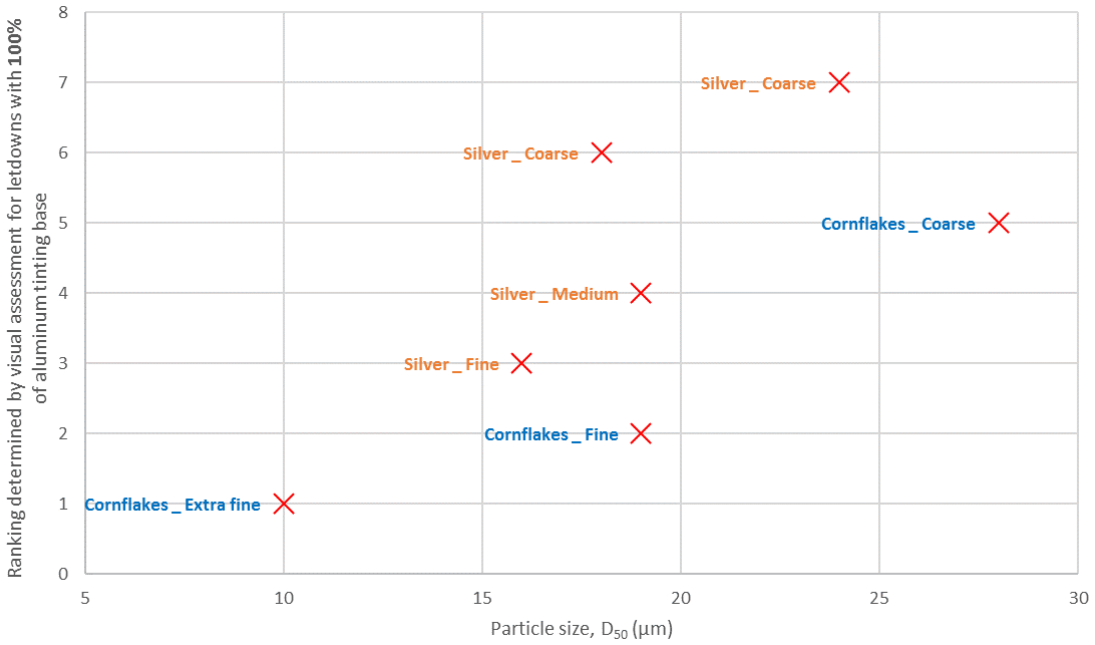

Figure 5-3: Sorting of letdowns with 100% of aluminum tinting base from Range 1 according to the strength of the effect by 5 observers

[1] **M99/00**: extra fine cornflake aluminum tinting base

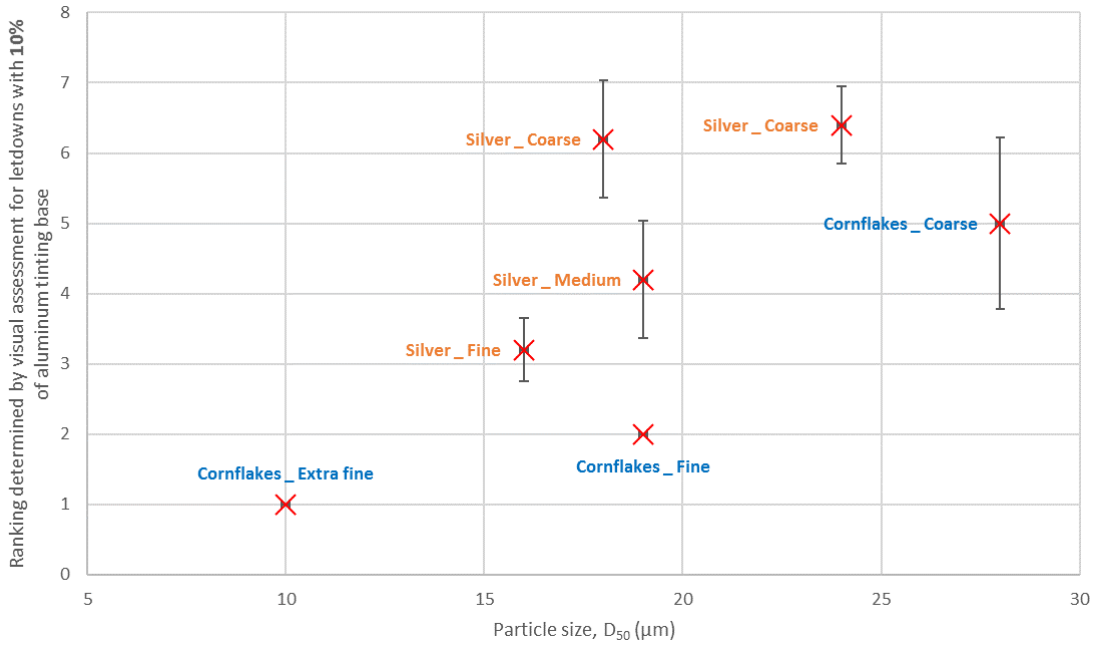

Figure 5-4: Sorting of letdowns with 10% of aluminum tinting base from Range 1 according to the strength of the effect by 5 observers

The type, the size and the amount of aluminum tinting base have a strong influence on the lightness values, L*, but also on visual appearance. The sorting of the two series of letdowns (100% and 10%) by visual assessment by experts was more obvious for 100% of aluminum content than for 10%. Below a certain amount of aluminum, the human eye is no longer able to differentiate the aluminum tinting bases despite large variations in particle size (see Figure 5-4). From the charts (Figure 5-3 and Figure 5-4), it is easily recognizable that, for the same particle size (Silver _ Medium and Cornflakes _ Fine), silver dollar aluminum particles provide more effect than cornflake aluminum particles.

To analyze the samples, spectral measurements were performed using a spectroradiometer (Konica Minolta CS-2000). This device measures the energetic luminance in W/sr/m^2. The lighting system is provided by several Solux lamps (50W, 36°, 4 700 K) that reproduce the full spectrum of daylight while maintaining a color rendering index of 99%. The energetic luminance measurements are converted into reflectance values. Range 2 was analyzed by spectral measurements to confirm the visible hue extinction. The reflectance curves thus obtained are presented in Figure 5-5. It is important to note that the colors of the curves in Figure 5-5 do not correspond to the perceived colors of the letdowns.

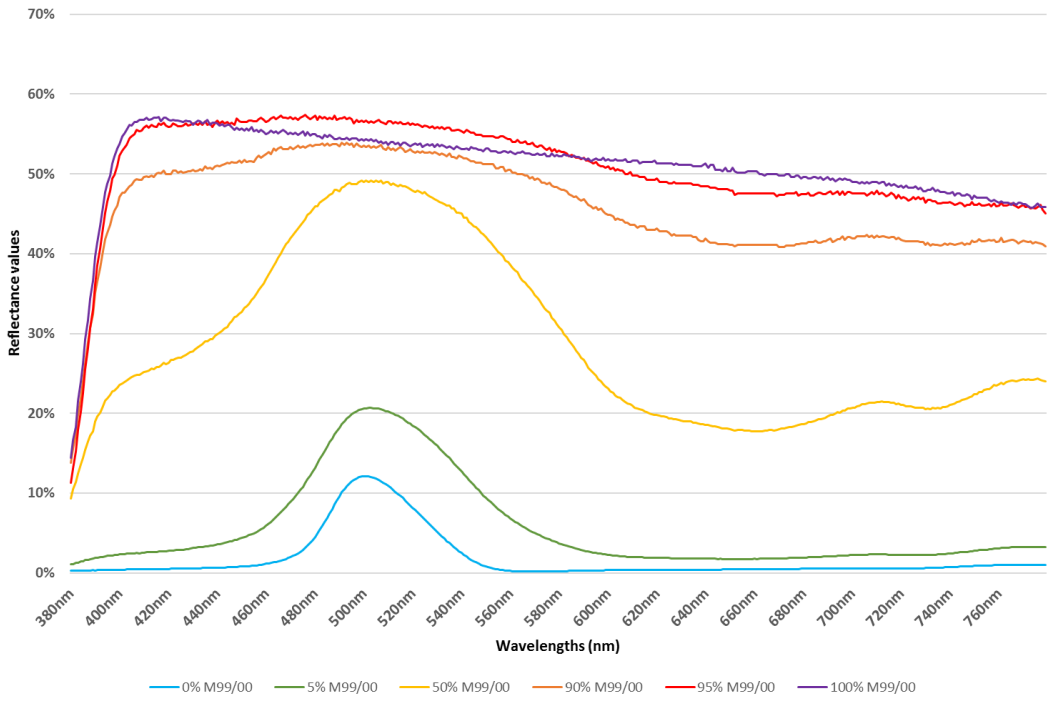

Figure 5-5: Reflectance curves of the panels from Range 2 with 0% of M99/00 (in blue), 5% of M99/00 (in green), 50% of M99/00 (in yellow), 90% of M99/00 (in orange), 95% of M99/00 (in red) and 100% of M99/00 (in purple)

At 0%, 5% and 50% of **M99/00**[1], a peak in the green area (480 – 540 nm) can be observed. However, a flattening in the signal can be noticed between 90% and 95% of **M99/00** in the formulation. Visually, this observation corresponds to a loss in chromaticity also called hue extinction, see Figure 5-6.

Figure 5-6: Panels from Range 2 with different percentages of aluminum tinting base, M99/00, in green tinting base

This effect results from the low concentration of green tinting base but also from the high density of aluminum particles in the sample. Regardless of the colored tinting base used, in presence of a high percentage of **M99/00** (around 95%), the sample will appear achromatic. However, it is important to note here that **M99/00** is an extra fine cornflakes aluminum. Its hiding power is dominant due to its shape and its size. The flakes tend to cover the entire surface and to overlap with each other, leading to hue extinction.

[1] **M99/00**: extra fine cornflake aluminum tinting base

When considering a coarse silver dollar aluminum such as **M99/21**[1], its hiding power is critical. The coarse particles interfere and cannot be positioned perfectly in parallel to the panel surface. For **M99/21,** more than 95% of aluminum tinting base is needed to reach hue extinction as illustrated in Figure 5-7. Indeed, at 95% of aluminum tinting base, the green shade is still noticeable.

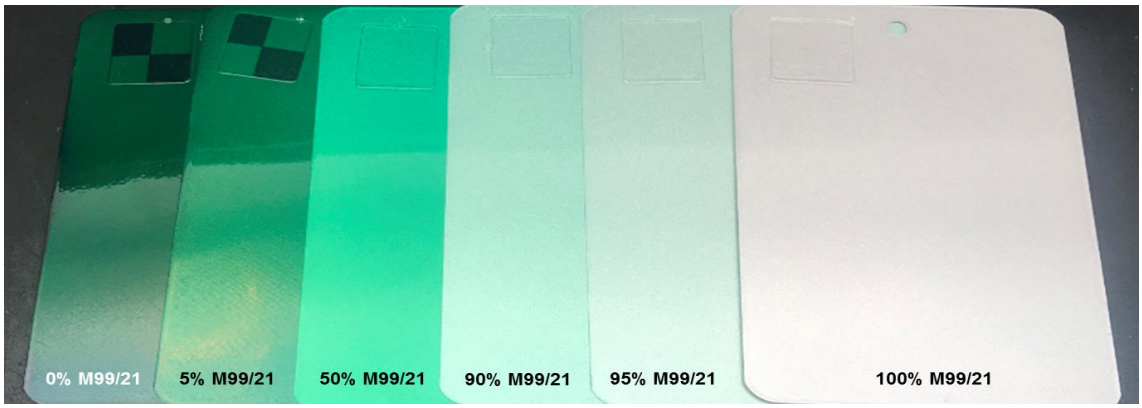

Figure 5-7: Panels from Range 2 with different percentages of aluminum tinting base, M99/21, in green tinting base

The concept behind Range 3 was to consider the impact of masstone color and/or titanium dioxide on visual appearance. The use of titanium dioxide has an impact on the perceptibility of the aluminum particles. Particles are buried or hidden in the coating film. In order to check if this kind of effects can be easily characterized, the samples were also analyzed using a binocular microscope equipped with a camera. The objective was then to confirm the aforementioned hypothesis and its potential link to the concentration of titanium dioxide in the formula but also to compare the two types of titanium dioxide, classic and micro milled.

First, the effects of the two white tinting bases, **A035**[2] (D_{50}=180 nm) and **A097**[3] (D_{50}=80 nm), were analyzed. The pictures obtained by microscope analysis with a magnification x20 are shown in Figure 5-8.

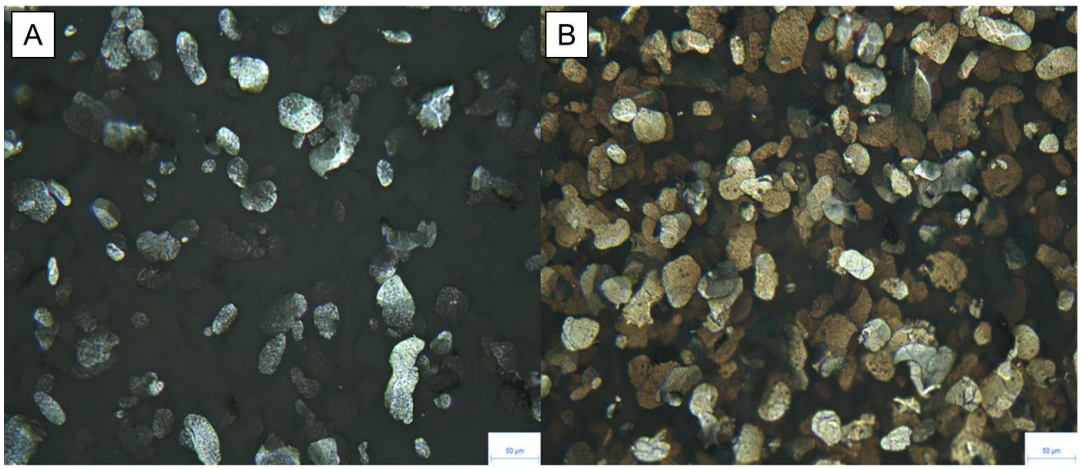

Figure 5-8: Light microscopy images of two letdowns: 70% M99/04 + 30% A035 (A) and 70% M99/04 + 30% A097 (B), scale indicating 50 µm

[1] **M99/21**: coarse silver dollar aluminum tinting base
[2] **A035**: classical white tinting base
[3] **A097**: micro milled white tinting base

The letdown represented in Figure 5-8.A, 70% of M99/04[1] with 30% of A035[2] presents the “masking effect”. Indeed, even if the amount of aluminum particles is high, only the particles on top of the coating film are visible, the others seem to be buried in the depth of the film. On the other hand, for the letdown containing 70% of M99/04 with 30% of A097[3] (Figure 5-8.B) the aluminum particles at different depths can be observed. In addition, the yellowish gold impression of the frost effect is also noticeable. The frost effect is confirmed in the image of Figure 5-9 where the letdown containing 70% of M99/04 with 30% of A097 (B) is blueish except for in the center, where a gold effect is present.

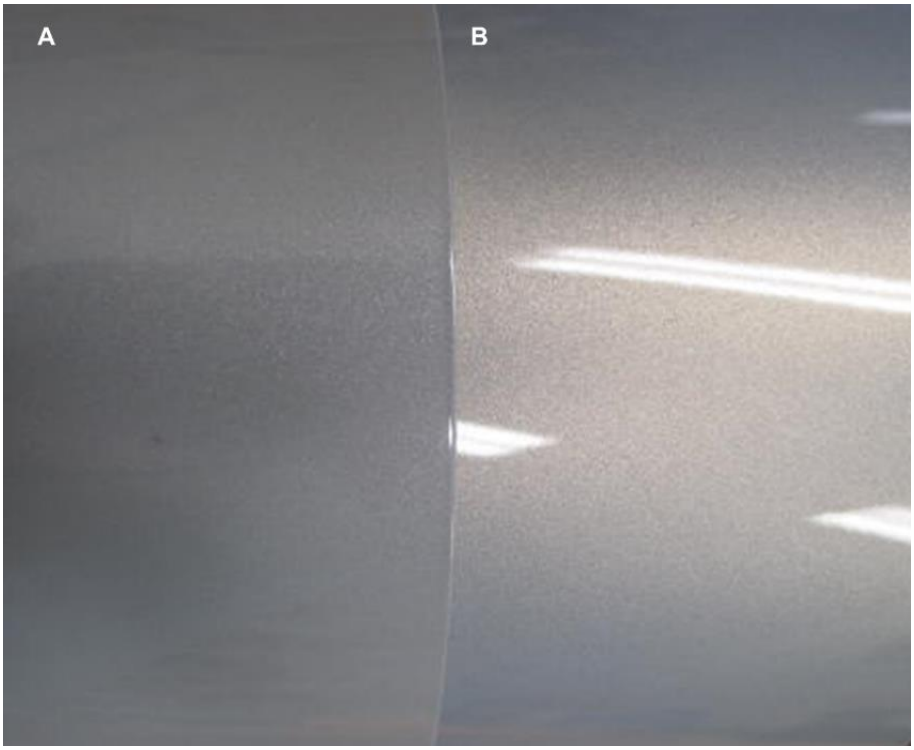

Figure 5-9: Pictures of two letdowns 70% M99/04 + 30% A035 (A) and 70% M99/04 + 30% A097 (B)

The combined impact of the masstone color and the titanium dioxide was also checked with the help of light microscopy. Figure 5-10 shows light microscopy observations of four letdowns obtained from a combination of A115[4], M99/21[5] and A035.

[1] M99/04: medium silver dollar aluminum tinting base
[2] A035: classical white tinting base
[3] A097: micro milled white tinting base
[4] A115: yellow tinting base
[5] M99/21: coarse silver dollar aluminum tinting base

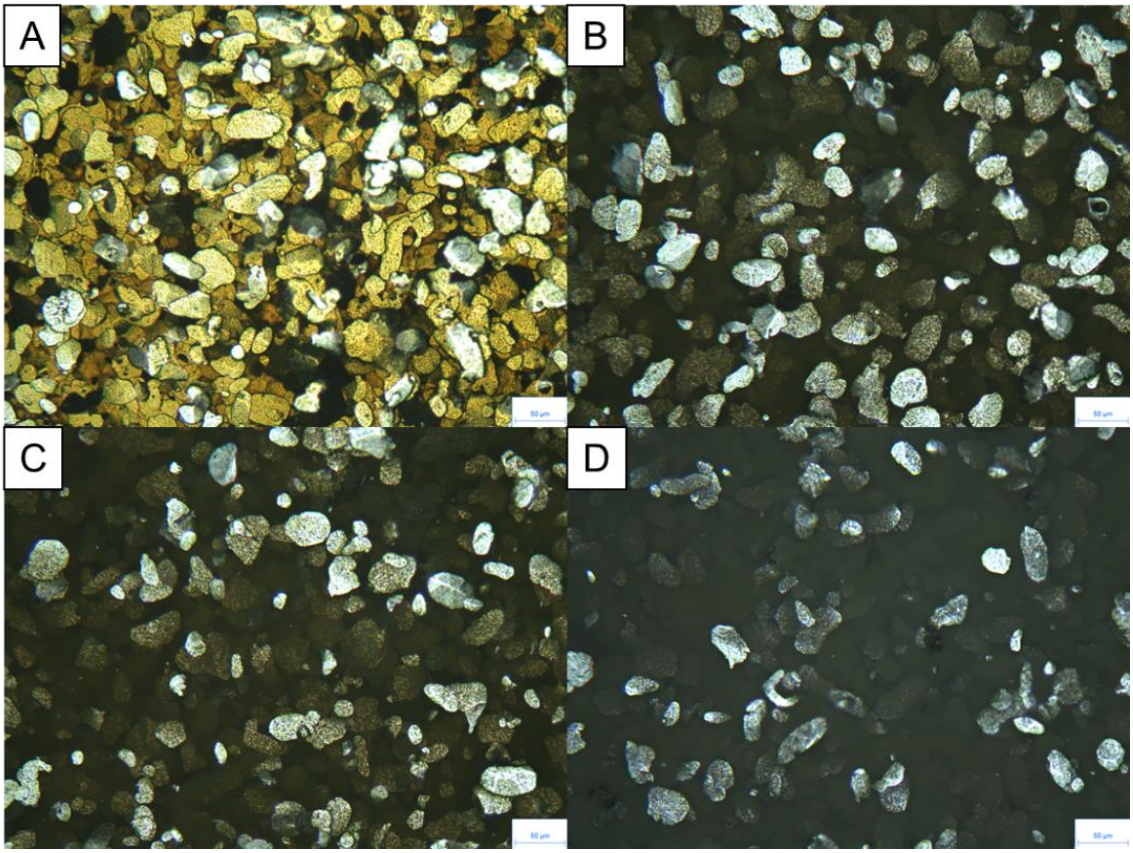

Figure 5-10: Light microscopy images of four letdowns: 70% M99/21 + 30% A115 (A), 70% M99/21 + 25% A115 + 5% A035 (B), 70% M99/21 + 20% A115 + 10% A035 (C) and 70% M99/21 + 5% A115 + 25% A035 (D), scale indicating 50µm

According to these images, it can be assumed, that the higher the concentration of **A035**[1], the stronger the masking effect. The images also confirm the loss of depth perception for the aluminum particles in the coating film when this white tinting base is used.

The masking effect is also discernible in Figure 5-11 for which the four letdowns obtained with a combination of **A115**[2], **M99/21**[3] and **A035** were photographed. These four letdowns contain the same percentage of aluminum tinting base, **M99/21**. Only the quantities of yellow and white tinting bases, **A115** and **A035** respectively, were adjusted in order to highlight the masking effect. The loss of depth perception depending on the organization of the aluminum is confirmed by these four pictures. In Figure 5-11-A, the sparkling dots corresponding to the aluminum particles are easily visible while they tend to become hidden when the percentage of white tinting base increases.

[1] **A035**: classical white tinting base
[2] **A115**: yellow tinting base
[3] **M99/21**: coarse silver dollar aluminum tinting base

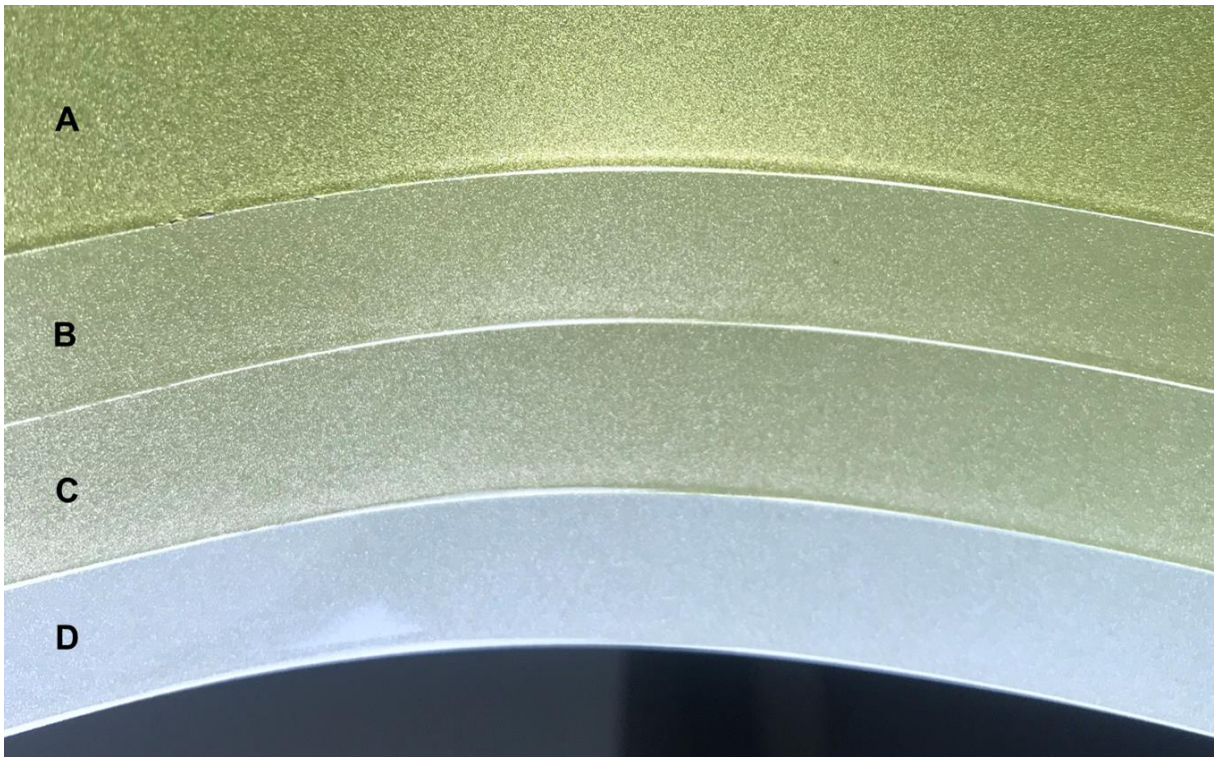

Figure 5-11: Photographs of four letdowns: 70% M99/21 + 30% A115 (A), 70% M99/21 + 25% A115 + 5% A035 (B), 70% M99/21 + 20% A115 + 10% A035 (C) and 70% M99/21 + 5% A115 + 25% A035 (D)

5.1.4. Assessment of the different ranges

By spraying different samples to constitute three ranges, it was possible to study the impacts of different components: aluminum, black, white and colored tinting bases.

The first range highlighted the impact of aluminum on visual perception. The samples were created by mixing an aluminum tinting base with a black tinting base. The visual sorting of the samples according to the perceptible amount of aluminum particles by experts is facilitated by the change in lightness L*. However, by considering letdowns of the same ratio with only a change in the aluminum tinting base, it was more difficult to sort them according to the global effect of aluminum particles and especially at low concentration of aluminum.

The second range was created to estimate the impact of the aluminum tinting base concentration on the chromaticity of the samples. With a very high concentration of aluminum tinting base, the colored appearance is completely hidden in favor of the greyish appearance due to the aluminum particles. This phenomenon corresponds to hue extinction.

Finally, for the third range, the objective was to compare the impact of titanium dioxide on the visual appearance. Depending on the size of the TiO_2 particles, either the masking

effect for **A035**[1] or the frost effect for **A097**[2] can be noticed. As a consequence of the masking effect, the sparkling effect of letdowns with a high amount of **A035** is destroyed.

5.2. Categorization test in order to determine new texture descriptors

The associated effects of the different categories of tinting bases were studied by the creation of different ranges. It is now known that some specific effects are inherent to the type of pigments used in the formula. However, even if the effects are for example called sparkling, frost effect or hue extinction by several authors (see Chapter 4, paragraph 4.1.1.2.2), it is not obvious that observers, even experienced ones, are able to classify visual appearance of texture according to the same criteria. To simplify the evaluation step, a categorization test was organized. Indeed, the purpose of this test was to highlight common characteristics to certain samples in order to define the associated texture descriptors. For the range creation phase, almost 250 letdowns were sprayed. Looking at all samples would be redundant and would have led to significant visual fatigue for the observers. 49 letdowns were randomly selected for this test without any selection criteria.

The conditions of these visualization tests have been standardized in order to ensure the consistency of the results obtained between the different industrial sites where the tests were carried out (IMT Mines Alès, BASF Clermont and BASF Münster). The lighting conditions were controlled to ensure optimal lighting. First, the free sorting method was favored at the expense of other sorting methods (hierarchical sorting, directed sorting or Napping® method).

5.2.1. Presentation of the different sorting methods

The sorting task is a simple method used for collecting similarity data which is established on categorization, a cognitive process routine (Chollet et al., 2014). The main objective is to obtain information about sensory differences among objects. This task can be either performed by novice or trained panelists. Assessors are asked to group together stimuli based on the similarities they perceive. Two objects sorted together are close and two objects rarely grouped together are far apart. The sorting task is a non-descriptive method, but the assessors can also be asked to describe the criteria applied. This procedure is called labeled sorting by (Becue-Bertaut and Lê, 2011).

The sorting task can be free, hierarchical or directed. For the free sorting task, the number of groups and objects per group is determined by the assessor himself or herself. However, he/she can neither group all objects together nor isolate each object in a group of its own. For the directed sorting task, the number of groups and objects per group is determined by the experimenter. The hierarchical sorting task can be either ascendant or descendant. In the first case, the assessor must perform a free sorting task and then successively merge the two groups with the most similarities up to get a single group. In the

[1] **A035**: classical white tinting base
[2] **A097**: micro milled white tinting base

second case, the assessor starts with a free sorting task and then he/she must subdivide each group further to isolate all objects.

Developed by Daniel Katz and Wilbur Hulin in 1933, the sorting task was initially created for a psychological study on facial expressions. The objective of this study was to associate an emotional expression to a picture (Hulin and Katz, 1935). After many years of use in psychology, Lawless adapted this method to the field of sensory evaluation in 1989. The first sensory assessment was based on the sense of smell of several assessors divided into two groups. The assessors had to sort several fragrance materials made from wood, citrus or a mix between wood and citrus. For one group, a free sorting task was proposed and for the second group, it was a directed sorting task of two groups (Lawless, 1989). Due to promising results after its first use in sensory evaluation, the sorting task was used several times in food industries with studies on cheese (Lawless et al., 1995), jam (Blancher et al., 2008) or beer (Chollet and Valentin, 2001), in cosmetic industries with studies on fragrances (Cadoret, 2010) and also in other industries such as the automotive industry with the evaluation of tactile perception of leathers (Faye et al., 2006).

The sorting results of trained and untrained panelists were studied several times to evaluate the consistency of product sensory mapping. A comparison between expert and non-expert panelists was made on visual description of plastic pieces (Faye et al., 2004). A free sorting task followed by a descriptive task was proposed to untrained assessors while experts set up a sensory profile. The results of these two methods were quite similar; the visual characteristics given by experts and non-experts were equivalent. These two methods were also adapted to leather samples (Faye et al., 2006). As seen previously, the conclusions reached on visual and tactile characteristics are similar for untrained and trained assessors. However, these studies involved non-food products and the authors suggested their products were easily differentiable. In food industry, the comparison between novice and expert panelists was for example carried out on breakfast cereals (Cartier et al., 2006). After a descriptive free sorting task on 14 commercially available breakfast cereals, the groups created by untrained and trained assessors were quite similar. For some studies, untrained and trained assessors generated similar product maps (Chollet et al., 2011); other studies also reported differences between those two groups of assessors. According to a study on wine categorization (Ballester et al., 2008), untrained assessors seemed to cluster the products on basic sensory features when trained assessors were more precise and could sort by grape variety.

In order to define texture descriptors, a free sorting method was used on automotive paint samples. As the sorting method is a non-descriptive one, it was decided to add a description phase at the end of the test to describe the groups created by the assessors according to the criteria used.

5.2.2. Procedures for the free sorting task

To be able to notice any texturing of the optical signal, it is important to standardize the lighting conditions. Daylight seems appropriate since vehicles are mainly observed under daylight. For quality control, artificial lighting is used. To analyze the overall visual effect, the

samples were simultaneously placed in a light booth under D65 light. In addition to the diffuse light provided by the light booth, direct light is necessary to better consider the sparkling effect. To this end, a spot was set up with an incandescent bulb of the Solux brand. This bulb reproduces daylight at 4 700K in its full spectrum. The chosen lighting angle is 17°, which represents a 7.5 cm disc radius when the sample is placed 50 cm from the lamp.

A single session per assessor is needed to proceed to the free sorting task. All forty-nine panels were randomly arranged on a table and shown to the assessor simultaneously. Based on his/her own criteria, he/she had to sort the panels into different groups. The instructions given to each assessor were identical and the following text was read to each of them. “You can see 50 panels on the table coated by a metallic coating. You will have to sort all the panels into different piles. Once finished, you will have to give the criteria used for sorting them. You can use the spot light, the diffuse light and you can create as many piles as you want”.

The conditions of observation were free. The only constraint was on the number of groups, between 2 and 48 groups. Besides, the number of panels per piles was free. The assessor had as much time as needed to gather the samples. Once the panels were gathered into piles, he/she had to describe the common features used for the sorting.

As described before, 49 samples were selected by using a software without human choice that could unknowingly falsify the selection. The list of samples selected is detailed in Table 5-4 and photographs of some of them are shown in Figure 5-12.

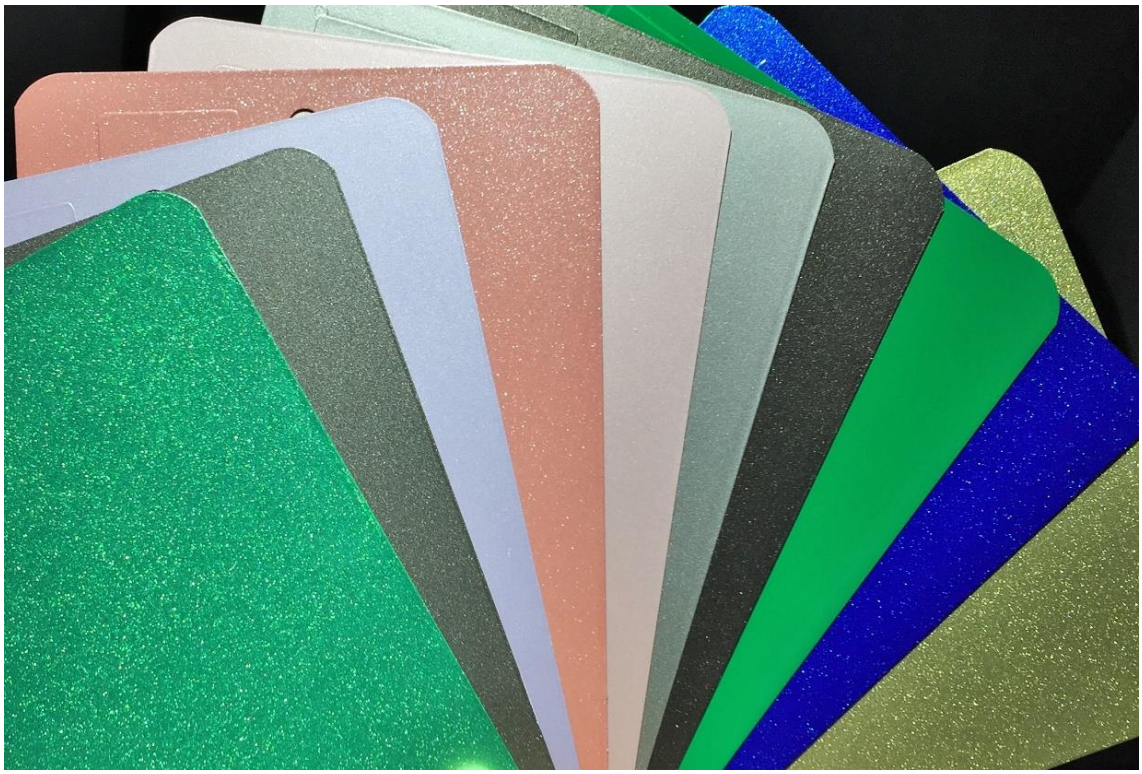

Figure 5-12: Example of letdowns randomly selected for the free sorting task

Table 5-4: List of the 49 letdowns randomly selected for the free sorting task

Formulas	Formulas
30% A115 + 70% M99/04	30% A136 + 70% M99/00
25% A115 + 70% M99/04 + 5% A035	25% A136 + 70% M99/03 + 5% A035
5% A115 + 70% M99/00 + 25% A035	20% A136 + 70% M99/04 + 10% A035
5% A115 + 70% M99/22 + 25% A035	20% A136 + 70% M99/04 + 10% A032
20% A306 + 70% M99/04 + 10% A032	5% A136 + 70% M99/00 + 25% A035
5% A306 + 70% M99/04 + 25% A035	25% A329 + 70% M99/22 + 5% A035
30% A035 + 70% M99/04	20% A329 + 70% M99/00 + 10% A032
30% A097 + 70% M99/04	5% A329 + 70% M99/03 + 25% A035
25% A372 + 70% M99/03 + 5% A035	5% A329 + 70% M99/04 + 25% A035
20% A372 + 70% M99/04 + 10% A035	30% A430 + 70% M99/00
20% A372 + 70% M99/22 + 10% A032	30% A430 + 70% M99/03
5% A372 + 70% M99/04 + 25% A035	25% A430 + 70% M99/00 + 5% A035
5% A372 + 70% M99/22 + 25% A035	25% A430 + 70% M99/04 + 5% A035
25% A563 + 70% M99/03 + 5% A035	20% A430 + 70% M99/22 + 10% A035
25% A563 + 70% M99/04 + 5% A035	5% A430 + 70% M99/04 + 25% A035
25% A563 + 70% M99/22 + 5% A035	95% A926 + 5% M99/00
20% A563 + 70% M99/00 + 10% A035	95% A926 + 5% M99/04
20% A563 + 70% M99/03 + 10% A035	95% A926 + 5% M99/21
20% A563 + 70% M99/03 + 10% A032	95% A926 + 5% M99/22
5% A563 + 70% M99/22 + 25% A035	90% A926 + 10% M99/04
69,5% A695 + 30,5% M99/22	80% A926 + 20% M99/00
59,5% A695 + 30,5% M99/22 + 10% A035	70% A926 + 30% M99/00
30% A695 + 70% M99/03	45% A926 + 55% M99/00
25% A695 + 70% M99/04 + 5% A035	100% M99/02
20% A695 + 70% M99/00 + 10% A035	

A115 & A136: yellow tinting bases
A430: violet tinting base
A695: green tinting base
A035: classical white tinting base
A097: micro milled white tinting base
M99/02: medium cornflake aluminum
M99/04: medium silver dollar aluminum

A306, A329 & A372: red tinting bases
A563: blue tinting base
A926: black tinting base
A032: classical white tinting base (diluted)
M99/00: extra fine cornflake aluminum
M99/03: coarse cornflake aluminum
M99/21: coarse silver dollar aluminum

5.2.3. Results on the free sorting task

The test was carried out by seventeen assessors: 8 novices (4 from IMT Mines Alès and 4 from BASF Clermont site) and 9 experts (7 from BASF Clermont site and 2 from BASF Münster site).

After data analysis of the results from the 17 observers, 7 persons sorted by texture or effect (see histograms in blue in Figure 5-13), 8 by color and the associated color changes (see histograms in yellow in Figure 5-13) and 2 observers by texture + color (see histograms in green in Figure 5-13). This classification into three categories was defined after analysis of the criteria used (see examples on Table 5-5). The number of groups created by the assessors is compared in Figure 5-13.

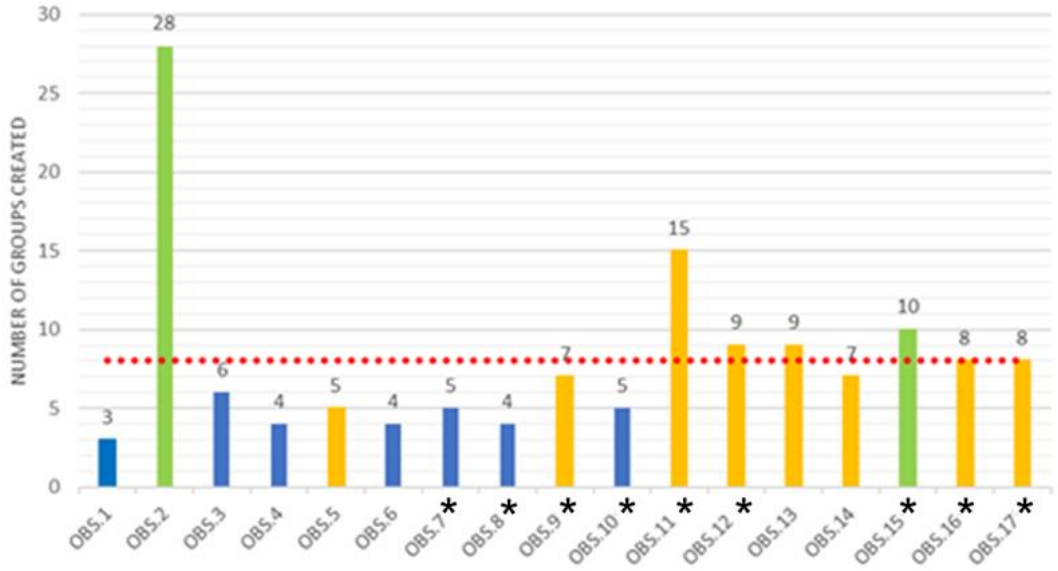

Figure 5-13: Number of groups created by observers during the free sorting task, in blue for a sorting based on texture, in yellow based on color and in green based on texture + color. The expert observers are indicated by an asterisk.

On average, 8.06 groups were created to sort the 49 panels during this free sorting test. However, observers who sorted by texture created less groups (average: 4.42 groups) than those who favored a sorting by color (average: 8.50 groups).

From Figure 5-13, it is deducible that the novice observers preferred a sorting by texture to a sorting by color (4 observers for 1 observer). On the other hand, experienced assessors preferred a sorting by color to a sorting by texture (7 assessors for 3 observers).

After the free sorting task, the observers were asked to name the common features used for the gathering. These definitions were analyzed and are listed in Table 5-5. It is important to note that the lists of features, especially for the sorting based on texture + color, are incomplete.

Table 5-5: List of features used to gather the forty-nine panels during the free sorting task

Criteria used for sorting	Based on Color	Blue / Green / Violet / Yellow
		Orange / Pink / Red / Rust
		Gold / Silver / Champain
		Chromatic / Achromatic
		Dull / Intense
	Based on Texture + Color	Black metallic with coarse aluminum
		Dark achromatic with fine aluminum
		Visible particles at flop (110°)
		Grey side at flop
		Colored travel (flip-flop)
	Based on Texture	Matte / Glossy
		Sparkling
		Glittering
		Graininess
		Quantity / Density

All the observers who decided to sort by texture grouped the samples on a scale of intensity. For example, the criteria used by Observer 3 and Observer 4 is sparkling. For the first observer, six levels were needed (very low, low, low to medium, medium, medium to strong, strong) while, for the second one, four levels were enough (low, low to moderate, moderate to intense, intense). Then, when a deeper analysis was carried out on the word “sparkling”, for Observer 3, it described the quantity of bright spot under direct light while for Observer 4, it defined the amount of light coming from the glitters. The definitions of the wording used for texture classification vary from observer to observer. The word "matte" can describe a very small amount of effect particles in the sample and therefore the lack of very bright spots related to the specular reflection of the particles but also the use of a matting agent in the clearcoat.

The descriptive phase after the categorization step is a crucial step to define new texture descriptors. Observers who described the texture explicitly mentioned only one parameter when sorting. It seemed that a single parameter was not efficient enough to describe the phenomenon of texture signals, since the words size and sparkling do not seem, at first sight, to be linked. In addition, the confrontation of the neophyte and expert vocabulary showed inconsistencies in the wording used.

5.3. Standardization of the wording used by brainstorming Metaplan®

To overcome these linguistic differences, the decision was taken to organize brainstorming sessions on texture to obtain a lexicon approved by experts and neophytes. Those sessions were carried out with the American, the French and the German BASF teams. These three teams are decision makers for any changes in processes or practices within the refinish color organization in BASF Coatings. The objective was to get a list of words describing the apparent texture and also their definition. The lexicons thus obtained were compiled and translated into German, English and French.

These brainstorming sessions are inspired by brainstorming techniques which consist in the search for original ideas by all participants (Delengaigne et al., 2016). The decision was to opt for the Metaplan® technique or Post-It® meeting. This technique, inspired by brainstorming, allows to quickly and easily get all the ideas of a group in a short time, about 15 minutes. Each participant's ideas are written on Post-It®. The sessions were scheduled for 90 minutes; between six and eight persons participated. The overall 70 participants were either neophytes or experts. The two classes of participants were mixed to confront the two types of wording detected during the descriptive phase at the end of the free sorting task. Each session was structured in five phases as given in Figure 5-14.

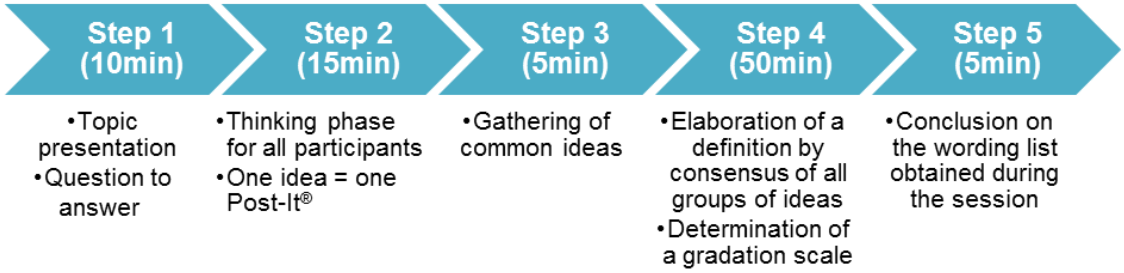

Figure 5-14: Structure of the brainstorming sessions in five phases

The first step was an introduction to the topic and especially to the visual appearance of effect coatings. The question to answer was “Which words can we use to define or characterize effects or texture on effect coatings?”. Then, for the second step, each participant had to think on his/her own and write down all of his/her ideas on Post-It® notes. To help the participants with their reflection, sixteen samples were sprayed. Those samples were selected from a range of OEM colors based on their specificities and sprayed. The selection of samples was based on the effect particles used in the formulation (aluminum, pearl or a mixture), the amount of flop modifier, the use of micro-milled titanium dioxide for the frost effect or a high concentration in titanium dioxide for the masking effect. Indeed, these elements were identified (see Chapter 5, paragraph 5.1.1) as tinting bases having a proven impact on visual appearance of the colors. The third step was needed to gather all the ideas into piles sharing the same idea as for example size, medium, fine and coarse. The fourth stage was the crucial one. The objectives were to find a definition for all groups of ideas by consensus and to then determine a gradation scale. The last step was just a conclusion on the session by showing the participants the wording list they created.

The “word cloud” representation in Figure 5-15 shows the different words obtained during step 2. 633 words were mentioned by the participants. The font size is linked to the number of repetitions. To clarify the word cloud, only the words given at least three times are kept for its conception.

Figure 5-15: Word cloud of the ideas obtained during all brainstorming sessions

The larger the font size, the more often the word was given, so the word “Sparkling” was the most popular word during the sessions, mentioned 48 times. However, by taking a more detailed look at the wording obtained, for example, the words “gleaming”, “mirror”, “intensity”, “sparkling”, “glittering”, “sparkly”, “starry” and “reflective” were used to describe the same idea of light reflection by the effect particles, but the distinction between them is at the discretion of each observer. All the words given during the brainstorming sessions which expressed the same idea were gathered together under a unique term in order to reduce the word cloud, see Figure 5-16.

Figure 5-16: Reduced word cloud of the ideas obtained during all the brainstorming sessions after gathering

The words “Size” and “Light Intensity” were the most popular with 115 and 156 occurrences, respectively. Once combined, the 20 ideas coming from the brainstorming sessions allowed the development of a more detailed lexicon about texture with 17 classes. The results (parameter, gradation scale and definition) are presented in Table 5-6.

Table 5-6: Global lexicon with parameter, scale and definition obtained after the brainstorming sessions with overall 70 participants

Parameters	Gradation	Definition
Particle size	Fine / Medium / Coarse	Apparent particle size
Light spots intensity *(Sparkling, reflection, glittering, gleaming, starry)*	Weak / Medium / Strong	Quantity of light reflected by particles
Spread of particles *(Modality)*	Homogeneous Heterogeneous	Mixture (or not) of different particle sizes
Quantity of bright spots *(Density, particle spacing)*	Few / Medium / A lot	Number of particles on a specific area
Effect color	e.g. Grey, Blue, Yellow	Color of the particles
Effect type	Metallic / Pearl	Type of effect particles used in formulation
Multi effect	Metallic + Pearl	Combination of pearls and aluminum in formulation
Metallic effect	-	Greyish appearance, achromatic effect particles and lightness change between face and flop
Pearl effect	-	Visible colored effect particles and color change between face and flop
Interferential effect	e.g. Green to Red Gold to Violet	Strong color change between face and flop
Flop intensity	-	Strong difference in lightness between face and flop
Iridescent effect		Under the same angle, different colors are emitted by the particles (mainly used for white pearls)
Chrome effect	-	Extra fine aluminum, mirror effect, high intensity of the reflected light, high flop index, very bright at face and very dark at flop
Gold effect	Gold at face Bluish at flop	Specific effect linked to the use of micro-milled titanium dioxide with a gold effect at face and a bluish side at flop
Intensity face-flop	to be determined	Lightness and /or chroma difference between face and flop
Contrast	Weak / Medium / Strong	Difference between particles and masstone color
Particle structure	Flat/Buried/Masking effect Deep	Particle structure in the bulk film

Brainstorming sessions allowed the development of a more detailed vocabulary on texture. However, some definitions are very close such as “flop intensity” and “intensity face-flop”. In order to reduce the list of texture parameters, it is also possible to gather ideas under one descriptor. One descriptor can be used to define either the particle size or the spread of particles. In the same way, another descriptor can define either the contrast or the particle structure.

At the end of the brainstorming sessions, six visual texture descriptors were established: size, intensity, quantity, color, contrast and face-flop. From those six descriptors, the seventeen terms of the global lexicon can be extracted as detailed in Figure 5-17. Some parameters are then associated with several descriptors.

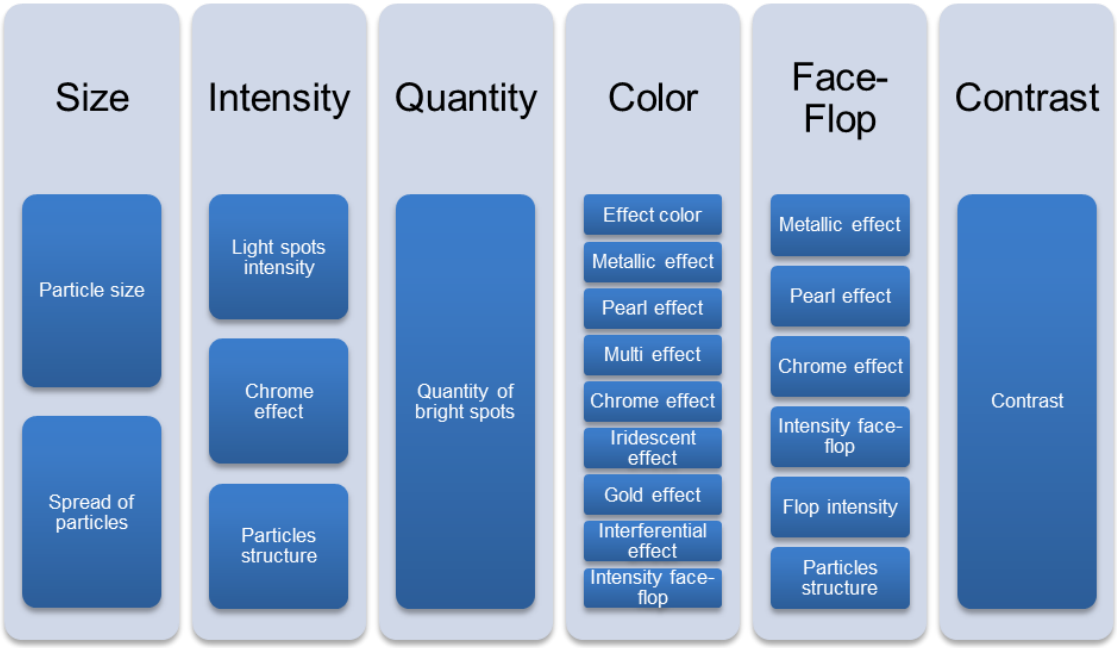

Figure 5-17: Sorting of 17 terms defined during brainstorming sessions into six categories of descriptors

5.4. Preliminary tests on new texture descriptors by three expert observers

As a result of the brainstorming sessions, six visual texture descriptors were defined. However, it was necessary to carry out preliminary studies on them. Three expert observers tested the new descriptors, with several objective to the tests. First, it was necessary to ensure the correct understanding of these parameters by the assessors. Then, the conditions of observation, meaning angle and type of light sources, needed to be standardized and the behavior of the three experts was a good starting point for that standardization. Finally, the overall performances were analyzed by checking the notation of the experts with a reproducibility and repeatability study. The repeatability was tested with the addition of a duplicate sample in the ranges observed and the reproducibility by comparing the notes of the three experts. The three experts had participated in one of the brainstorming sessions held previously.

For these preliminary tests, eight new ranges of letdowns were sprayed. The aluminum tinting bases (7 in total) and the two white tinting bases (conventional, **A035**[1], or micro-milled, **A097**[2]) were diluted with binder to guarantee the same pigment content in the two families of tinting bases. Besides, a ready to use tinting base of the flop modifier (given as FM in Table 5-7) was prepared. It contained the tinting base, the mixing binder and the thinner. The tinting bases prepared for this test were mixed with black tinting base, **A926**[3]. On top of the seven aluminum tinting bases used, it was also decided to consider two mixtures of aluminum tinting bases, **M99/01**[4]+**M99/22**[5] and **M99/03**[6]+**M99/21**[7] at three ratios: 1:1, 1:3 and 3:1. The different formulas sprayed for this study are listed in Table 5-7. The naming “Alu” stands for all aluminum tinting bases. The thirteen panels from Range A are displayed in Figure 5-18.

Table 5-7: Formulas prepared for the preliminary tests on new texture descriptors

Range	Formula
Range A	60% Alu + 40% **A926**
Range B	60% Alu + 40% **A926** + 12g FM
Range C	60% Alu + 27% **A926** + 13% **A035**
Range D	60% Alu + 27% **A926** + 13% **A035** + 8g FM
Range E	60% Alu + 27% **A926** + 13% **A097**
Range F	60% Alu + 27% **A926** + 13% **A097** + 8g FM
Range G	60% Alu + 27% **A926** + 4% **A035** + 9% **A097**
Range H	60% Alu + 27% **A926** + 4% **A035** + 9% **A097** + 8g FM

Figure 5-18: Image of the thirteen panels from Range A, 60% Alu + 40% A926

[1] **A035**: classical white tinting base
[2] **A097**: micro milled white tinting base
[3] **A926**: black tinting base
[4] **M99/01**: fine silver dollar aluminum tinting base
[5] **M99/22**: coarse silver dollar aluminum tinting base
[6] **M99/03**: coarse cornflake aluminum tinting base
[7] **M99/21**: coarse silver dollar aluminum tinting base

Assessors had to evaluate the eight ranges with two types of lighting: diffuse and direct light. The diffuse light was provided by natural sunlight and direct light by a halogen spot corrected in blue (Solux, 4 700K, 17°, 50W). Each evaluator was asked to categorize the letdowns of each range into different groups according to the six visual texture descriptors. To limit visual fatigue, three sessions per observer were organized.

For each range, except for Range E, a duplicate of one of the panels was added. The evaluators identified this panel on all the criteria without knowing the trap. This approach made it possible to evaluate the repeatability of the ratings on the different criteria. For all the ranges, all the criteria and all the observers, the twins were gathered in the same group in 97% of the cases (123/126). Three mistakes were made on two criteria, two for face-flop and one for contrast.

In order to evaluate the reproducibility of the notation, the number of groups formed by criteria are summarized in Table 5-8. The results are then detailed, descriptor by descriptor, and plotted in Figure 5-19. Even if the number of groups created varies from one observer to the other, it is important to note that the arrangement of the samples is equivalent for all observers, only the categorization differs.

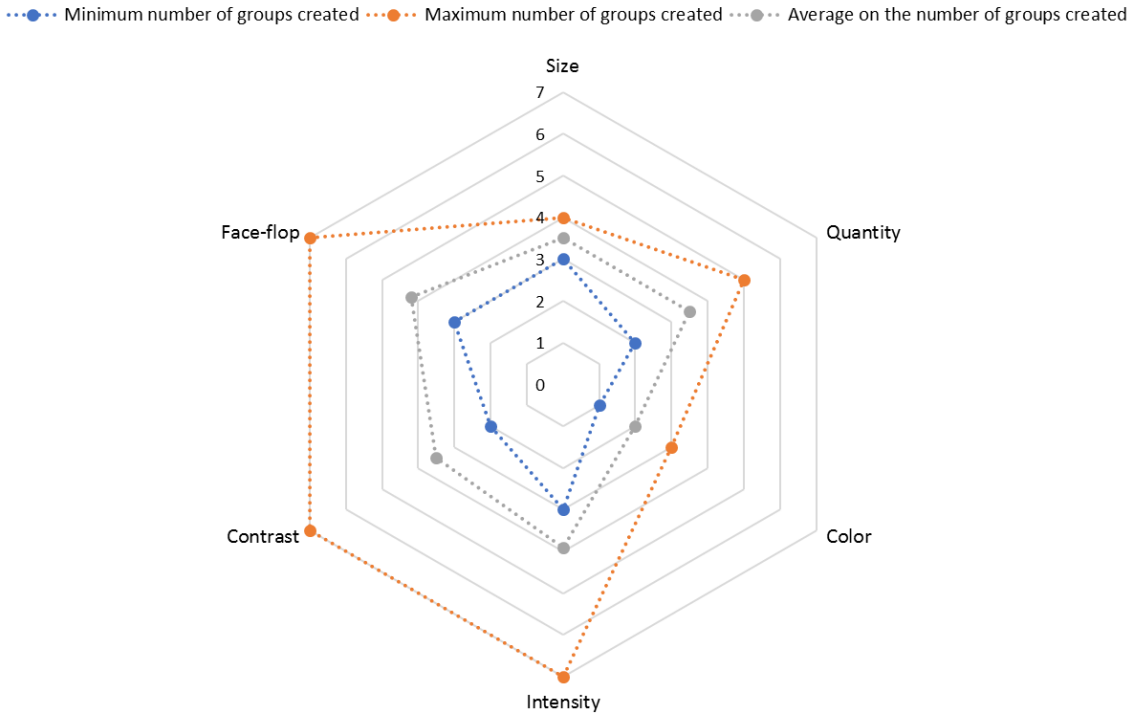

Figure 5-19: Analysis of the number of groups created (min, max and mean) during the stage of assessment by three experts on texture descriptors

Table 5-8: Results of the assessment of the three experts on texture descriptors

	Size	Quantity	Color	Intensity	Contrast	Face-flop
Minimum number of groups created	3	2	1	3	2	3
Maximum number of groups created	4	5	3	7	7	7
Average number of groups created	3.5	3.5	2	3.9	3.5	4.2
Variance	0.3	0.7	0.5	1	1.9	1

For the texture descriptor “Size”, expert observers split the panels in 3 or 4 groups with a mean of 3.5. The categories identified are fine, medium, large and an extra-fine class is added when four groups were created. The variance, or dispersion of the values compared to the mean value, is low at 0.3. Hence, this descriptor seems to be understood by assessors.

For the descriptor “Quantity”, 2 to 5 groups were formed with an average of 3.5 groups. When two groups were set up, the classes according to which the sorting occurred were “not many” or “many” while the formation of five groups allowed to qualify the categories: not many, low, medium, intermediate, a lot. The large differences in the ratings related to the number of groups created a limit for the reproducibility of this descriptor. Besides, sometimes it got mixed up with the descriptors “Contrast” or “Intensity”.

For the descriptor “Color”, assessors qualified their scoring by forming 1 to 3 groups, with 2 groups on average. In some cases, the observers assumed an achromatic color particle while, in other cases, they found a strong difference on the same range with 3 categories: achromatic, slightly gold, gold. However, the letdowns studied were only made of aluminum tinting bases, hence achromatic particles. The gold effect is linked either to the interaction between the yellowish black tinting base; **A926**[1], and the aluminum particles or to the use of micro-milled titanium dioxide, **A097**[2], responsible for the frost effect. The large differences in the ratings related to the number of groups created limit the reproducibility of this descriptor even if the variance is at 0.5. Besides, the visual assessment of this descriptor required a high luminous intensity.

For the descriptor “Intensity”, expert observers gathered the panels in 3 or 7 groups with a mean at 3.9. The segmentation into 3 categories was limited to weak, medium and strong while the one in 7 included the classes: non-existent, very weak, weak, low, medium, strong and very strong. Although this descriptor seems to be pretty well understood by the assessors, again, the large differences in the rating lead to low reproducibility and a variance at 1.

[1] **A926**: black tinting base
[2] **A097**: micro milled white tinting base

For the descriptor “Contrast”, 2 to 7 groups were created with an average of 3.5 groups. The binary answer, yes/no for some observers with the formation of two categories, was nuanced with the creation of seven classes: no, very weak, weak, medium, medium/strong, strong, very strong. This descriptor was hardly understood by the assessors which explains the variance of 1.9. Moreover, it got often mixed up with the descriptors Intensity and Quantity. To improve the evaluation, the standardization of the conditions of observation seems to be needed for a correct interpretation of this descriptor.

For the descriptor “Face-Flop”, the evaluators formed between 3 and 7 groups with an average of 4.2 groups. The division into 3 groups was differentiated according to the categories: light, moderate and strong while a split into 7 classes includes neutral, light, strong, dark flop, light flop, dark yellow-flop and moderate face. This descriptor is very difficult to evaluate and the results are difficult to interpret due to the large disparity of the groups created.

In Figure 5-20, an example is given for which the assessment of two identical samples on each descriptor are plotted. Globally each observer is repeatable to his own assessment. However, comparing the ratings of the three observers on each criterion, the ratings do not conform. Thus, for observer 1 (OBS1), on the criterion Quantity the standardized notation is 1 whereas it is worth 0.5 for observer 2 (OBS2) and 0.67 for observer 3 (OBS3).

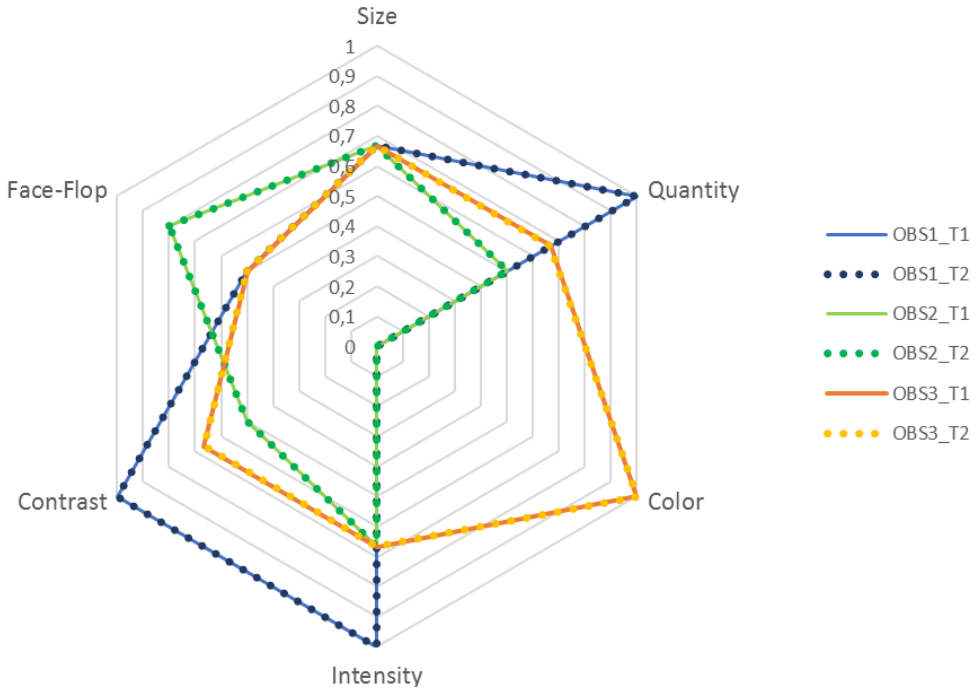

Figure 5-20: Comparison of the ratings of the twins from Range G on each visual descriptor by three observers (OBS1, OBS2 & OBS3), T1 and T2 indicated respectively Twin1 or Twin2

After the preliminary tests on the new texture descriptors created after brainstorming sessions, the repeatability of the confirmed observers is proven, except for three cases where discrepancies in the ratings of Face-Flop and Contrast were found. However, the free categorization of the samples on each perceptual descriptor is not reproducible. Indeed, the differences obtained from one observer to another remain too high to be compared even if

the order established for the range remains the same. In addition, some perceptual descriptors, mainly Contrast and Face-Flop, were difficult to understand for the experienced assessors.

These tests also made it possible to standardize the conditions of observation for each visual descriptor according to the behavior of the three assessors. They are summarized in Table 5-9.

Table 5-9: Standardization of the conditions of observation (light source and angle) for visual assessment

Texture descriptor	Light source	Angle of observation
Size	Diffuse light	~ 45°
Quantity	Diffuse light	~ 45°
Color	Direct light	Close to specular angle, ~15°
Intensity	Direct light	Close to specular angle, ~15°
Contrast	Diffuse light	~ 45°
Face-Flop	Diffuse & direct light	Moving observation from 0° to 100°

To allow for a better understanding of each perceptual descriptor as well as a homogenized scale of ratings, a reference range for each of them was created inspired by the Sensotact® reference scale developed by Renault[1]. Indeed, this referential for tactile perception makes it possible to evaluate and quantify tactile sensations like the hardness or the stickiness of a surface based on a pre-established metric.

5.5. Texture scale creation

During the first phase of preliminary tests on the new texture descriptors, some parameters such as Contrast or Face-Flop were misinterpreted by experienced assessors. In order to limit these problems of misunderstanding, the decision was taken to create a rating scale. Thus, like the Sensotact®, each descriptor is explained by a reference range to better enable its evaluation.

The results of the preliminary tests on the new texture descriptors (see Table 5-8) were the basis to establish the number of references for each range. For each reference, a formulation was created based on expert knowledge for the effect tinting bases. The quantities of effect pigments were visually adjusted to get a sufficient amount to be perceptible without being predominant. At the end of the creation of all the standards, they were submitted to expert assessors for approval. Only the formulations of the final standards are explained below. For all the standards, the masstone is black to avoid all combined effects with colored tinting bases. However, the black tinting base of reference, **A926**[2], used

[1] The Sensotact® is a reference frame used to assess haptic quality perception with 10 descriptors. The descriptors summarize the complete human touch sensation. They are divided into three clusters: orthogonal (hardness, nervousness, memory of shape, stickiness), tangential (fibrous, depth, roughness, braking, slippery) and thermal. For each descriptor, five to six references compose the range. The samples to evaluate are compared to the ranges according to the intensity.

[2] **A926**: black tinting base

for the creation of the ranges (see Chapter 5, paragraph 5.1.2) was not used. A deep black, **A924**[1], was preferred to avoid the yellowish undertone of the **A926**[2].

For the texture descriptor Size, between three and four groups were needed according to the assessors. It was decided to create four standards to match the levels: extra-fine, fine, medium and coarse. Letdowns with aluminum and black were sprayed in order to create those four references. The formulas are gathered in Table 5-10.

Table 5-10: Description of the four references developed for the descriptor Size

Descriptor	Naming	Level	Formula
Size	S_1	Extra-fine	92.5% **A924** + 7.5% **M99/00**[3]
	S_2	Fine	92.5% **A924** + 7.5% **M99/01**[4]
	S_3	Medium	90% **A924** + 10% **M99/03**[5]
	S_4	Coarse	90% **A924** + 10% **M99/21**[6]

Pictures of the different standards were taken with the spectrophotometer MA-T6 (see Chapter 4, paragraph 4.2.4). The four pictures obtained under diffuse geometry (see r15d in red in Chapter 4 Figure 4-21) are gathered in Figure 5-21.

Figure 5-21: Pictures of the four references created for the descriptor Size

[1] **A924**: deep black tinting base
[2] **A926**: black tinting base
[3] **M99/00**: extra fine cornflake aluminum tinting base
[4] **M99/01**: fine silver dollar aluminum tinting base
[5] **M99/03**: coarse cornflakes aluminum tinting base
[6] **M99/21**: coarse silver dollar aluminum tinting base

For the range Color, the objective was to formulate standards which could be either used for aluminum or pearl colors. Pearls or colored aluminum were then added in the formulation in order to define the main families for color particle evaluation. Eight effect tinting bases were selected to guarantee a correct representation of the color space. The quantities of effect tinting bases were visually adjusted to maintain the same visual amount in all the formulations. The sparkling effect of white pearl is typically due to the simultaneous blue, red and green sparkling, see Figure 5-22.

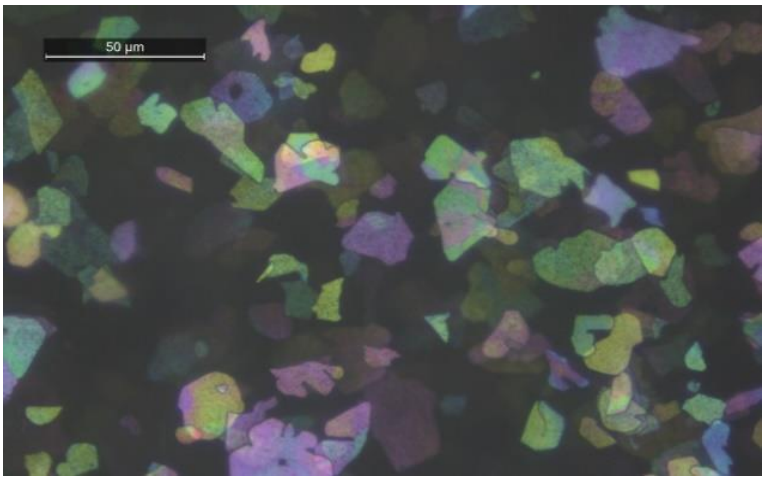

Figure 5-22: Light microscopy image of white pearl tinting base mixed with black tinting base, scale indicating 50µm

The formulas sprayed for the eight references of the range are summarized in Table 5-11.

Table 5-11: Description of the eight references developed for the descriptor Color

Descriptor	Naming	Level	Formula
Color	C_1	Gold	90% **A924**[1] + 10% **E920**[2]
	C_2	Orange	90% **A924** + 10% **E280**[3]
	C_3	Red	90% **A924** + 10% **LAB3505**[4]
	C_4	White	90% **A924** + 10% ***M919***[5]
	C_5	Green	90% **A924** + 10% **E630**[6]
	C_6	Blue	85% **A924** + 15% **LE555**[7]
	C_7	Violet	80% **A924** + 20% **LE405**[8]
	C_8	Aluminum	95% **A924** + 5% **M99/01**[9]

[1] **A924**: deep black tinting base
[2] **E920**: gold aluminum tinting base
[3] **E280**: orange aluminum tinting base
[4] **LAB3505**: red aluminum tinting base
[5] ***M919***: white pearl tinting base
[6] **E630**: green pearl tinting base
[7] **LE555**: blue pearl tinting base
[8] **LE405**: violet pearl tinting base
[9] **M99/01**: fine silver dollar aluminum tinting base

The pictures of the eight references obtained with the spectrophotometer MA-T6 under direct geometry 15° (see r15as15° in blue in Chapter 4 Figure 4-21) are presented in Figure 5-23.

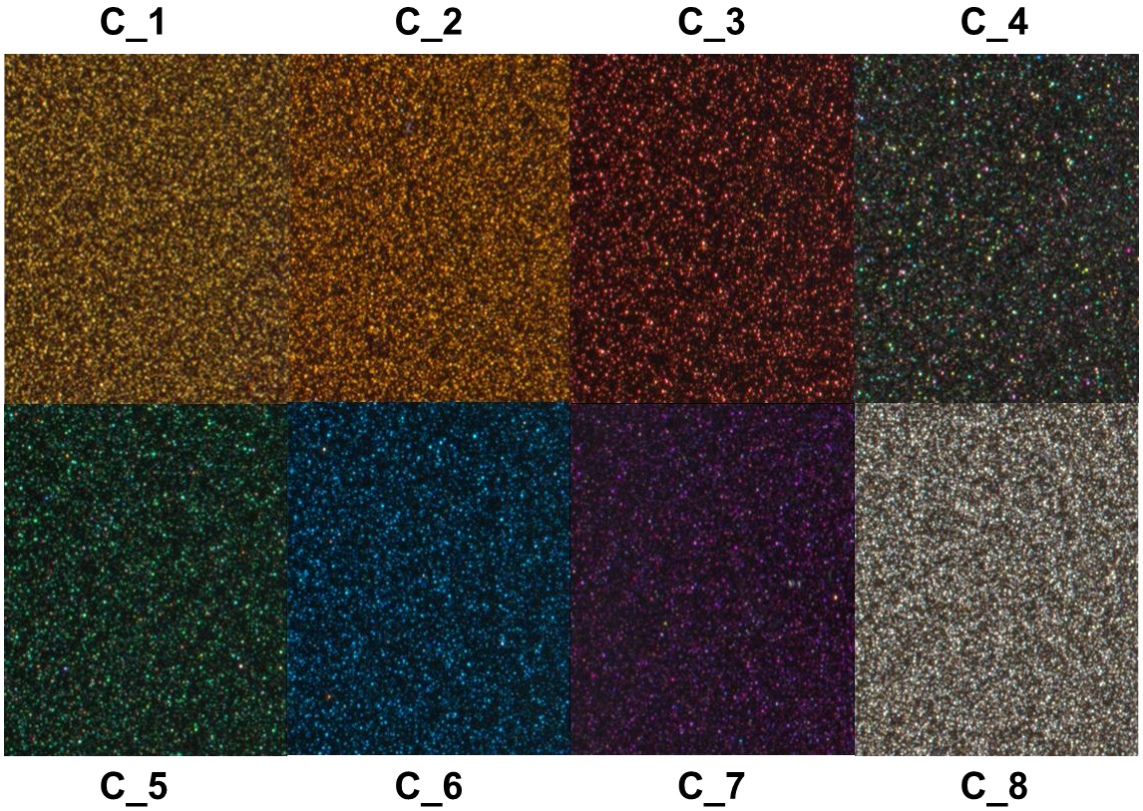

Figure 5-23: Pictures of the eight references created for the descriptor Color

The descriptor Contrast was the most misunderstood by the observers during the first test. To better explain this descriptor a quantity of equivalent of pigment effects for all references was maintained by changing the masstone color according to a grey scale.

In order to maintain the same global effect on the apparent particle content and effect, a new application technique was selected, which is called the tricoat technology based on the addition of a colored transparent layer, or midcoat, (given as MD) between the basecoat (BC) and the glossy clearcoat layers (see Chapter 4, paragraph 4.1.2). The midcoat consists of a neutral binder in which effect and/or colored tinting bases can be mixed. The application process of this layer is based on the spraying of two coats with a drying span between them.

Changes in visual contrast stem from the basecoat color. Different shades of grey allowed to modifiy the visible contrast between the particles compared to the masstone color. The midcoat remains the same. The formulas of the standards are gathered in Table 5-12. For the standard Contrast_Very strong (K_6), the midcoat formulation was changed by using a coarser aluminum and flop modifier to increase the global impression of contrast by playing with the apparent particle size.

Table 5-12: Description of the six references developed for the descriptor Contrast

Descriptor	Naming	Level	Formula
Contrast	K_1	Inexistent	100% **A035**[1]
	K_2	Very low	BC 93.61% **A035** + 6.39% **A927**[2] MD 99.5% Binder + 0.5% **M99/04**[3]
	K_3	Low	BC 91.33% **A035** + 8.67% **A926**[4] MD 99.5% Binder + 0.5% **M99/04**
	K_4	Intermediate	BC 45.15% **A035** + 54.85% **A926** MD 99.5% Binder + 0.5% **M99/04**
	K_5	Strong	BC 5.41% **A035** + 94.59% **A926** MD 99.5% Binder + 0.5% **M99/04**
	K_6	Very strong	BC 85.25% **A924**[5] + 9.38% **A695**[6] + 5.36% **A032**[7] MD 87.35% Binder + 0.35% **M99/21**[8] + 12.29% Flop Modifier

Pictures of the different standards were taken with the spectrophotometer MA-T6 under diffuse geometry (see r15d in red in Chapter 4, Figure 4-21) and are gathered in Figure 5-24.

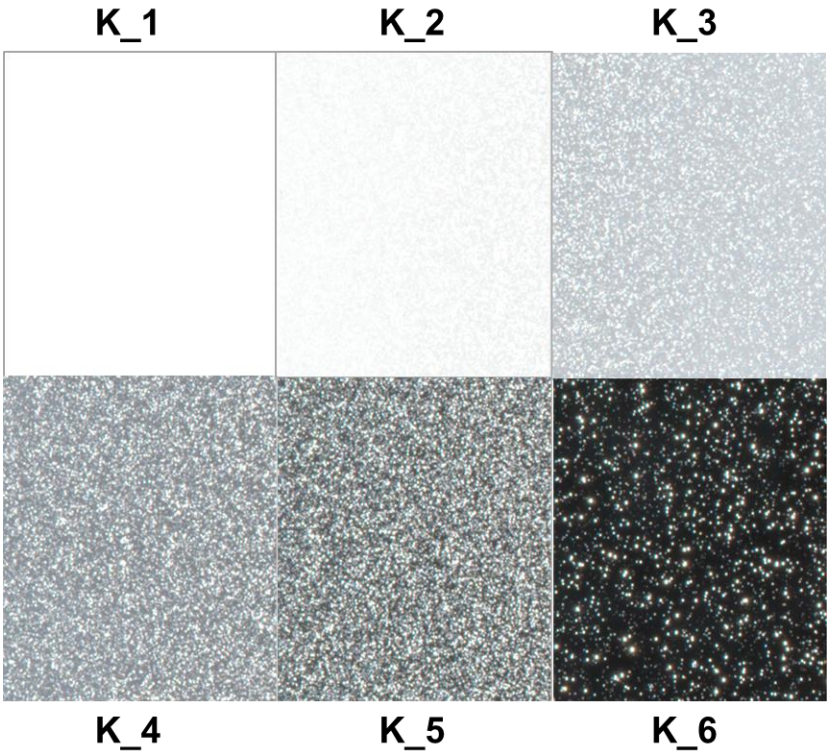

Figure 5-24: Pictures of the six references for the descriptor Contrast

[1] **A035**: classical white tinting base
[2] **A927**: black tinting base (diluted)
[3] **M99/04**: medium silver dollar aluminum tinting base
[4] **A926**: black tinting base
[5] **A924**: deep black tinting base
[6] **A695**: green tinting base
[7] **A032**: classical white tinting base (diluted)
[8] **M99/21**: coarse silver dollar aluminum tinting base

For the descriptor Intensity, the assessors sorted the ranges into four categories on average. This clustering was kept for the intensity scale with the levels: low, moderate, intense and very intense. In order to obtain a high intensity in light reflection, glass flakes were selected from the effect tinting bases available. Indeed, these particles act like little mirrors in coating formulation. To enhance their effect, they were added in the midcoat to leave the particles on top of the coating film and then improve their influence on lighting. The formulations are listed in Table 5-13.

Table 5-13: Description of the four references developed for the descriptor Intensity

Descriptor	Naming	Level	Formula
Intensity	I_1	Low	95% **A924**[1] + 5% **M99/00**[2]
	I_2	Moderate	95% **A924** + 5% **M99/04**[3]
	I_3	Intense	90% **A924** + 10% **M99/21**[4]
	I_4	Very intense	BC 100% **A924** MD 99.7% Binder + 0.3% E025 (glass flakes)

The pictures of the four references obtained with the spectrophotometer MA-T6 under direct geometry 15° (see r15as15° in blue in Chapter 4, Figure 4-21) for the descriptor Intensity are presented in Figure 5-25.

Figure 5-25: Pictures of the four references used for the range Intensity

[1] **A924**: deep black tinting base
[2] **M99/00**: extra fine cornflake aluminum tinting base
[3] **M99/04**: medium silver dollar aluminum tinting base
[4] **M99/21**: coarse silver dollar aluminum tinting base

For the range Quantity, two to five groups were created during the first phase. However, the panels rated during this test contained a maximum of 40% of aluminum tinting bases. In order to assess all types of colors, meaning even silver colors with a high amount of aluminum pigments in formulas, a wide scale was created, while the number of standards was reduced with six expert observers. Changes in quantity of effect pigments were made via the concentration of effect pigments in the midcoat while the basecoat remains black. The formulas of the twelve different standards are gathered in Table 5-14 and the corresponding pictures are displayed in Figure 5-26, using diffuse geometry.

Table 5-14: Description of the twelve propositions of references for the descriptor Quantity

Descriptor	Naming	Level	Formula
Quantity	Q_1	0%	BC 100% **A924**[1]
	Q_2	0.025%	BC 100% **A924** MD 99.975% Binder + 0.025% **M99/04**[2]
	Q_3	0.05%	BC 100% **A924** MD 99.95% Binder + 0.05% **M99/04**
	Q_4	0.1%	BC 100% **A924** MD 99.9% Binder + 0.1% **M99/04**
	Q_5	0.5%	BC 100% **A924** MD 99.5% Binder + 0.5% **M99/04**
	Q_6	1%	BC 100% **A924** MD 99% Binder + 1% **M99/04**
	Q_7	2%	BC 100% **A924** MD 98% Binder + 2% **M99/04**
	Q_8	4%	BC 100% **A924** MD 96% Binder + 4% **M99/04**
	Q_9	6%	BC 100% **A924** MD 94% Binder + 6% **M99/04**
	Q_10	8%	BC 100% **A924** MD 92% Binder + 8% **M99/04**
	Q_11	10%	BC 100% **A924** MD 90% Binder + 10% **M99/04**
	Q_12	100%	BC 100% **M99/04**

[1] **A924**: deep black tinting base
[2] **M99/04**: medium silver dollar aluminum tinting base

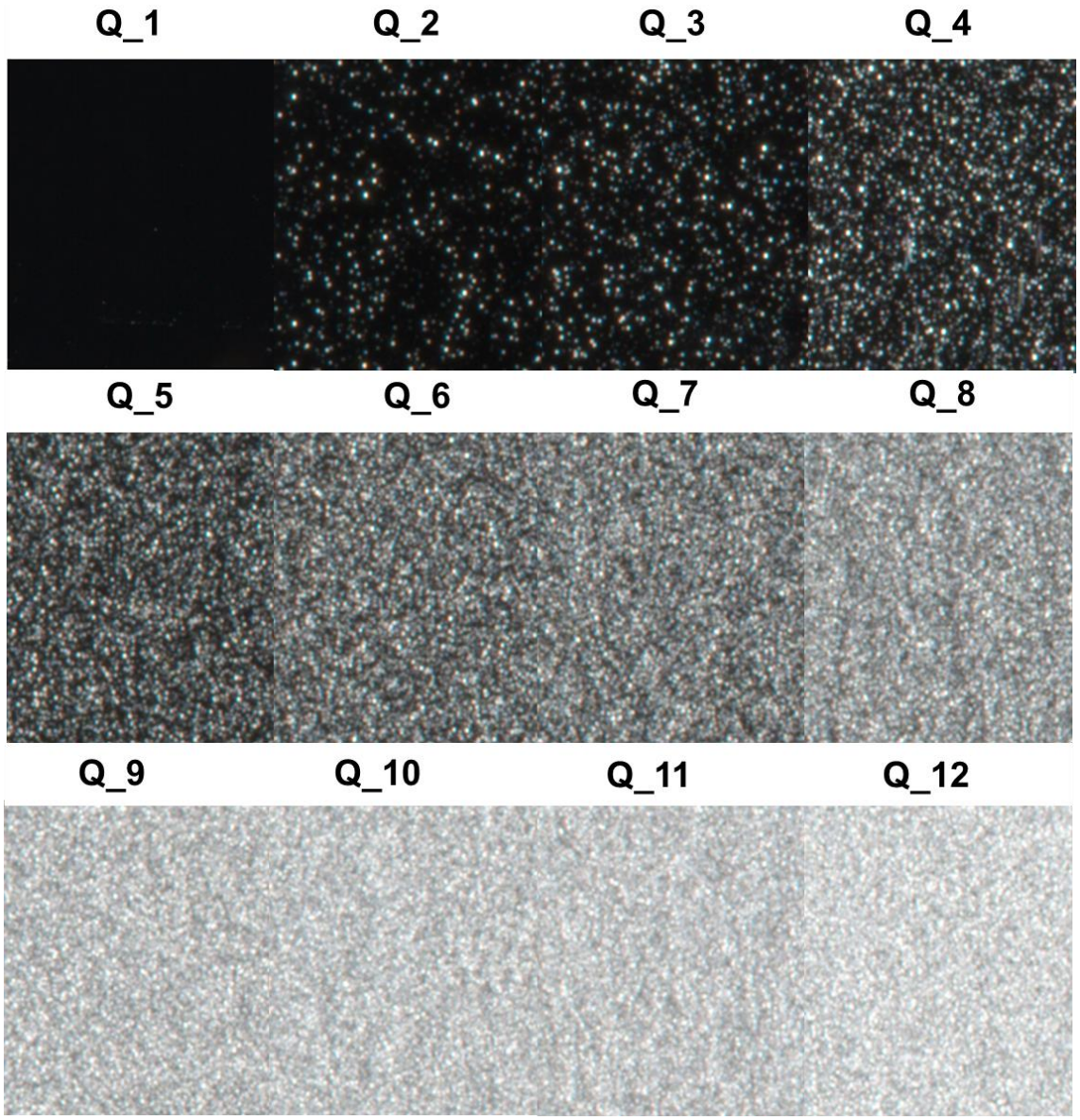

Figure 5-26: Pictures of the twelve references created for the range Quantity

The twelve samples were proposed to six expert observers to reduce their number. They had to select the references needed for the evaluation of the quantity according to their expertise. Four observers decided to reduce the number of standards to 6, one to 5 and one to 4. The popularity of each standard was analyzed and is plotted in Figure 5-27.

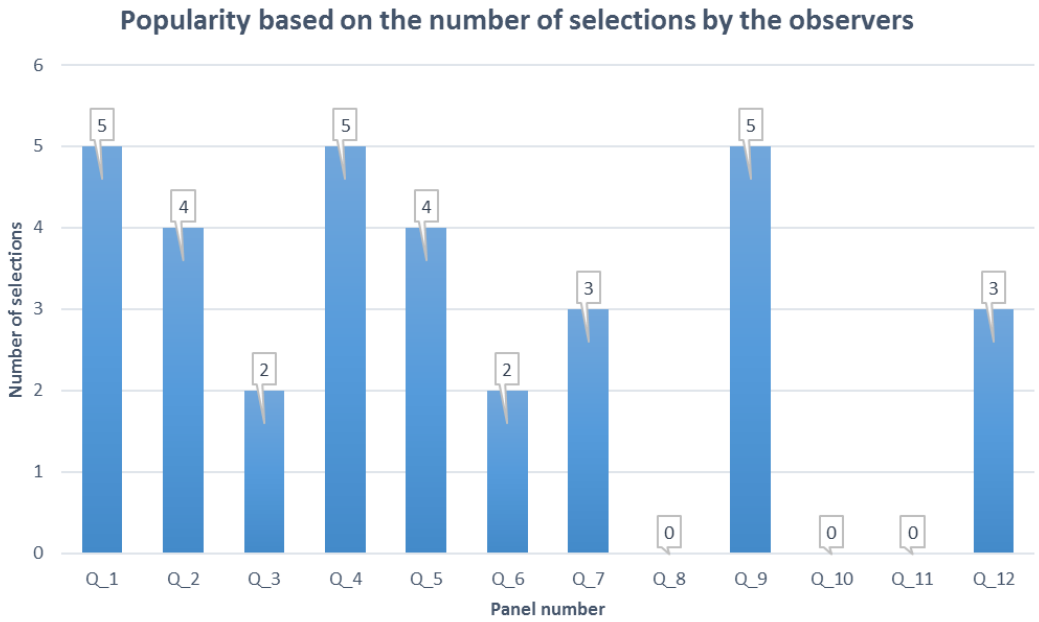

Figure 5-27: Analysis of the popularity of the twelve propositions of references developed for the descriptor Quantity according to the selection done by the observers

First, the decision was taken to keep the extremum panels so Quantity_0% (Q_1) and Quantity_100% (Q_12). Then, according to the number of selections, the panels with 0.025%, 0.1%, 0.5% and 6% of aluminum tinting base (respectively Q_2, Q_4, Q_5 and Q_9) were kept. However, due to an important jump in the perceptive texture, it was decided to add another new standard, Quantity_2% (Q_7). The final scale for quantity evaluation is thus made of seven standards.

The last range to create was the Face-Flop range. During the brainstorming sessions, the difference between face and flop was denoted as flop intensity, interferential effect and intensity face-flop. To estimate the color travel between front view and side view, specific pearls offering strong interference effects were used: ChromaFlair® pigments produced by Viavi. Two of them were selected: the ChromaFlair® Red/Gold 000 and ChromaFlair® Silver/Green 060. The first one offers shifts from red through orange and yellow into green while the second shows a travel from silver through green to purplish blue. Light microscopy images of these two pigments are presented in Figure 5-28.

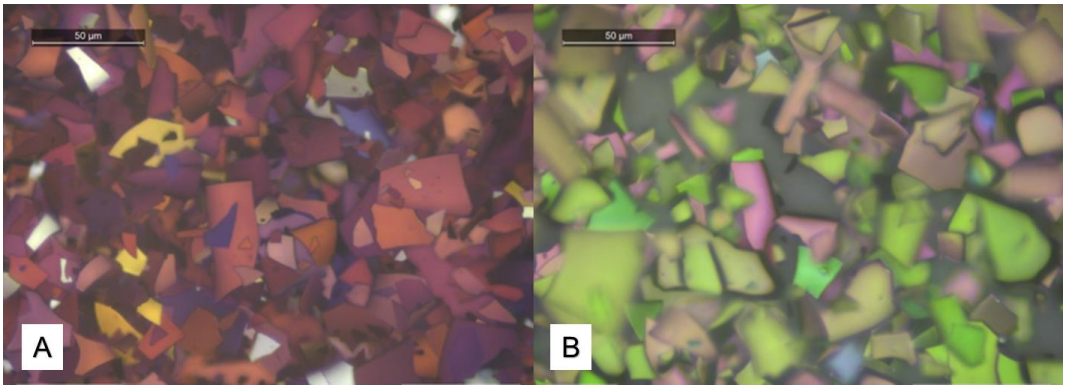

Figure 5-28: Light microscopy observations of the ChromaFlair® Red/Gold 000 (left side, picture A) and Silver/Green 060 (right side, picture B), scale indicated 50 µm

For the lightness change between face and flop, it was necessary to establish a gradation scale. In addition to the traditional aluminum tinting bases, it was decided to use a special aluminum tinting base, **90-905**. The special feature is the extra-fine thickness of the aluminum particles obtained by physical vapor deposition. The particles reflect light like tiny mirrors and are used to reproduce chrome effect like e.g. in aluminum rims.

The formulas of the six references created for the descriptor Face-Flop are gathered in Table 5-15 and the associated pictures, obtained using direct geometry -15° (see r15as-15° in blue in Chapter 4, Figure 4-21), are given in Figure 5-29.

Table 5-15: Description of the six references developed for the descriptor Face-Flop

Descriptor	Naming	Level	Formula
Face-Flop	F_1	Very low	30% **A924**[1] + 60% **M99/00**[2] + 10% **A035**[3]
	F_2	Low	33% **A924** + 67% **M99/00**
	F_3	Moderate	30% **A924** + 70% **M99/04**[4]
	F_4	High	70% **A924** + 30% **90-905**
	F_5	Chromatic	30% **A924** + 70% ChromaFlair® Red/Gold
	F_6	Chromatic	30% **A924** + 70% ChromaFlair® Silver/Green

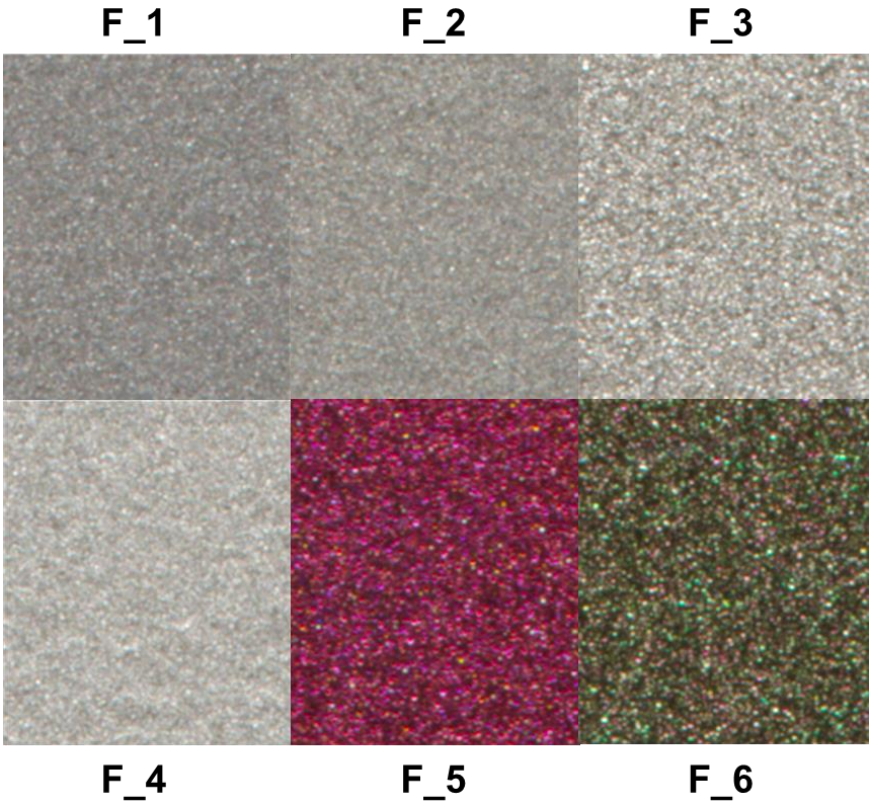

Figure 5-29: Pictures of the six references proposed for the descriptor Face-Flop

[1] **A924**: deep black tinting base
[2] **M99/00**: extra fine cornflakes aluminum tinting base
[3] **A035**: classical white tinting base
[4] **M99/04**: medium silver dollar aluminum tinting base

The descriptor Face-Flop is quite difficult to assess due to the definition itself. The travel between face view and flop view can be either fully chromatic, fully achromatic but also a mix between chromatic and achromatic. Besides, the particles can be visible or not at flop angle (≈ 100°). All of these criteria make the evaluation even more complex. It was decided to not consider this descriptor for the next steps.

Once all the scales were created and sprayed, a special panel holder was designed. The objectives were first to protect the references from damages or scratches due to the frequent contact with metal panels, then to simplify the visual assessment of the six descriptors for the observers and finally to guarantee the alignment of the sample and the references in the same plane of observation and thus same angle.

The panel holder is made of an aluminum sheet which is coated with a matte dark grey color to avoid all interferences, such as light reflection from the panel holder, which could then disturb the observer during the visual assessment. In Figure 5-30, a panel holder is depicted.

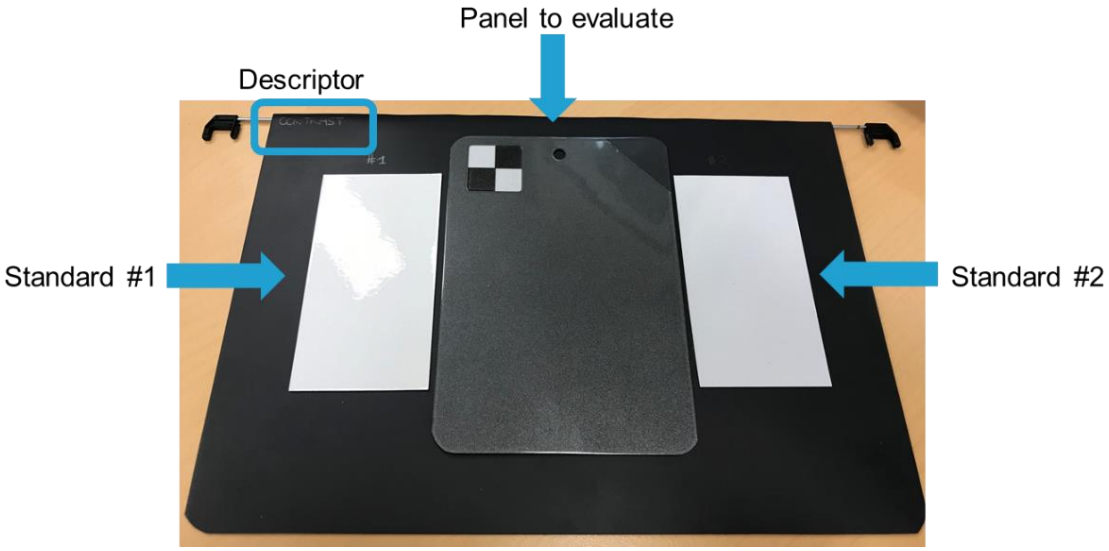

Figure 5-30: Example of a panel holder for the visual evaluation of contrast with standards #1 and #2 also called Contrast_Inexistent (K_1) and Contrast_Very Low (K_2)

To better understand the functioning of the visual assessment using a procedure based on reference samples, let's consider an example. A sample has to be evaluated in terms of Contrast (written down "Panel to evaluate" in Figure 5-30). The question to answer is "Am I able to discern the particles from the masstone color?" or "Is the difference between the masstone color and the particle color big enough to perfectly see them or is it quite difficult to identify particles in the panel to evaluate?". The observer takes the panel to evaluate and has to compare it with the different standards. In a first step he takes the panel holder number 1 made of the standards #1 (K_1 – Contrast_Inexistent) and #2 (K_2 – Contrast_Very Low) and places the panel to be evaluated in the middle of the two. If no visual match is found, he takes the next panel holder made of the standards #2 (K_2 – Contrast_Very Low) and #3 (K_3 – Contrast_Low), places his sample in the middle and compares it to the standards. This process is repeated until a correct visual match with the standards is found.

For the descriptors Size, Contrast, Intensity and Quantity, the number of panel holders is linked to the number of standards. For the descriptor Contrast, five panel holders are available: K_1-K_2, K_2-K_3, K_3-K_4, K_4-K_5 and K_5-K_6. For the descriptor Size, there are 3 panel holders (S_1-S_2, S_2-S_3 and S_3-S_4), same as for the descriptor Intensity (I_1-I_2, I_2-I_3 and I_3-I_4). For the descriptor Quantity, six panels holders are proposed: Q_1-Q_2, Q_2-Q_4, Q_4-Q_5, Q_5-Q_7, Q_7-Q_9 and Q_9-Q_12. However, for the descriptor Color, only one panel holder is available, made of the eight standards, see Figure 5-31. Indeed, as one sample to test can be a mix of several effect pigments of different colors, it was necessary to have the standards on the same panel holder.

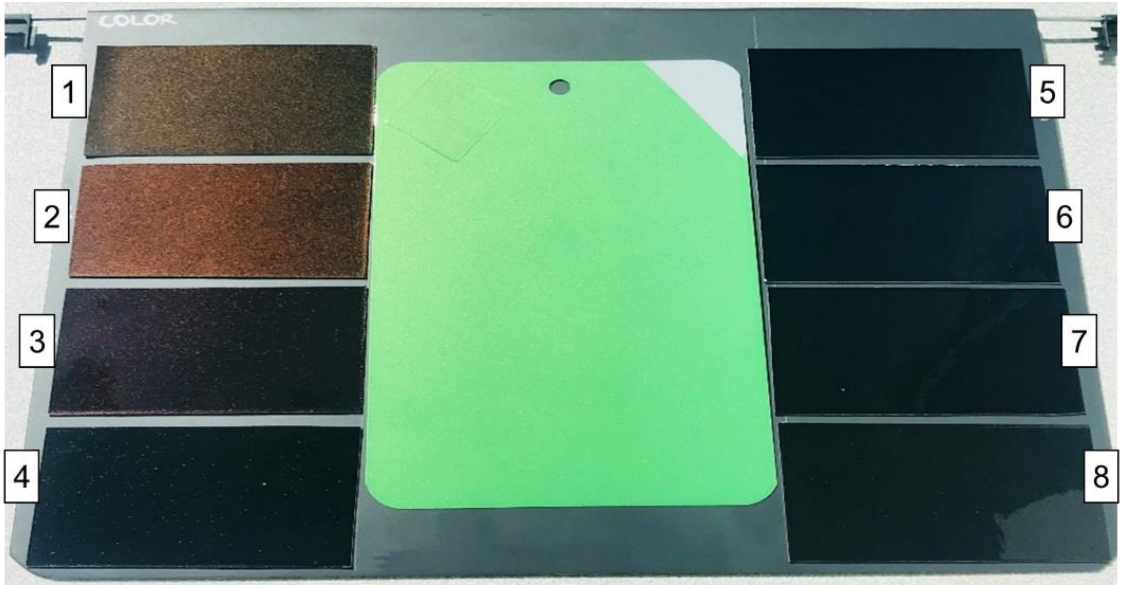

Figure 5-31: Panel holder used for Color evaluation with the eight standards (where #1 = C_1 - Color_Gold, #2 = C_2 – Color_Orange , #3 = C_3 – Color_Red, #4 = C_4 – Color_White, #5 = C_5 – Color_Green, #6 = C_6 – Color_Blue, #7 = C_7 – Color_Violet and #8 = C_8 – Color_Aluminum)

Finally, to guarantee the same conditions of evaluation for all observers (see Table 5-9), a rotating system was used with predefined angles (15°, 25°, 45°, 75° and 110°). The evaluations can be either conducted under a diffuse light source (light booth with illuminant D65) or direct light source (spot light).

5.6. Assessment on the definition of new texture descriptors

The definition of new texture descriptors was an important step in present PhD thesis. The principal objective was to focus on visual appearance. This has been possible by setting up a new approach to move away from the two parameters initially developed by BYK Gardner, sparkling and graininess, and ensure a definition of texture appearance based on six perceptive descriptors.

The identification of the components having a visible influence on visual appearance allowed a clustering into five groups: aluminum, black, white, colored tinting bases and flop modifier. Initially, the pearl tinting bases were set aside to avoid multiple interferences on visual appearance. The huge number of panels sprayed (338) was then used in the free sorting tests. This was the first-time neophyte and expert observers were involved in the

same test session. Besides, when the sorting was made according to texture, it was mainly on one criterion such as sparkling or quantity. Even if the results obtained were not the ones wished-for, they highlighted inconsistencies between the two types of wording. Participants at the free sorting test did not use the same words to describe the same things. It was then necessary to set up a specific wording. Thanks to brainstorming sessions in three BASF Coatings sites (US, France and Germany) with overall seventy participants, experts or neophytes, a wording list was obtained. This is a more detailed list with a definition and also a gradation scale of the lexicon. The number of parameters found during those sessions was quite important; in the following, it was then possible to reduce the list to six descriptors: Size, Color, Contrast, Intensity, Quantity and Face-Flop.

The six texture descriptors coming from the brainstorming sessions were then tested with three expert observers to evaluate first correct understanding but also the repeatability and reproducibility of the ratings done on a free scale. Even if the observers were repeatable to themselves, the reproducibility was not ensured due to the high heterogeneity in the number of groups per descriptor. Moreover, the tests shed light on the misunderstanding of two descriptors, Contrast or Face-flop. In addition to the descriptors found and the associated wording list, it was then necessary to find a method to train the observers to evaluate the descriptors. The solution for this training was the creation of a texture scale in order to better define the characteristics to assess by observation. A graduated texture scale was defined for each descriptor based on really perceptive recommendations. With the standards, it is now easier to rate a panel to evaluate. Besides, the panel holders also created the possibility to guarantee the right angle of observation for both standards and the panel to rate.

The visual texture descriptors are now defined. The objective for the next step was to evaluate the performances of the texture scales in the elaboration of sensorial profiles of test samples.

Chapter 6. Elaboration of sensorial profiles

Contents

Characterizing sensorial perceptions is a matter more complicated than it may seem. The tasks involve a number of parameters that cannot be comprehensively considered and correlated to physical measurements. The definition of new texture parameters explained in the previous chapter coupled to the creation of texture scales is supposed to ensure consistency of the visual assessments. Indeed, the observers share the same wording and also a pre-established metric to simplify the evaluation with the texture scales. Moreover, a sensation always combines two very different notions: a subjective evaluation and an objective evaluation. The implementation of scales makes it possible to master the subjectivity of the assessor and to reduce the variability of his/her results.

Sensorial profiles are obtained by the evaluation of a complex system based only on visual appearance. The resulting descriptions of panels are consequently obtained by the quantification of the descriptors with only the human eye. The sensorial profiles are based on only five descriptors. As explained before, the Face-Flop evaluation is not the simplest one, hence the decision was taken to not consider this descriptor for the next steps.

In a first part, the evaluation protocol will be presented describing the selection of the observers, the samples observed and the conditions of observation. Then, after a brief discussion of statistical methods used for the average observer determination, the results obtained on the five descriptors will be reviewed.

6.1. Protocol of evaluation

The purpose of the characterization of sensorial perceptions is to provide a real sensory identification map, the sensorial profile. In order to obtain coherent results, it is important to respect the protocol of evaluation for all visual assessment sessions and for all participants. A set of conditions must be met for the perception to operate normally and to allow a good evaluation.

All participants of the visual assessment sessions were involved in one session of brainstorming for the creation of a wording list (Thomas, 2016), see Chapter 5, paragraph 5.3. The assessors are considered as experts in their field. The observers were selected from the color labs either in France or in Germany or from the color development team. Six observers are from the French color lab, four from the German lab and two from the color development team. Each participant of the lab is used to evaluate color differences. The visual acuity of the participants is controlled every three years with the Farnsworth test in the light booth.

To avoid visual fatigue of the observers, one session per descriptor with a limited duration of 30 minutes was organized. The first descriptor assessed was Color, then Contrast, Size, Intensity, followed by Quantity. If possible, the sessions were scheduled in the morning and there were no consecutive sessions. A briefing was held at the beginning of each session to really in depth explain its objectives and to present the standards. As determined in Chapter 5, Table 5-9, each descriptor has to be evaluated according to one type of illumination system and one specific geometry. Although the participants are used to making a dynamic evaluation in their daily routine by changing the angle of observation, they were forced here to observe only at one specific fixed angle to be able then to convert the observation conditions to future picture acquisition.

To avoid a bias in assessment from observer to observer, sample presentation followed a specific procedure. The composition of each sample is anonymized. The observers did not know the type of effect pigments in the formulas hence they could only make assumptions based on their know-how. Furthermore, a coding was randomly assigned to each sample. The painted panels were then arranged in ascending order and presented one after the other to the participant. If needed, a cloth was at their disposal to remove dust or finger prints from the panels. 34 panels were selected for this test. They represent all standards created for the different texture scales with the exception of the six standards of the scale for the descriptor Face-Flop.

For the evaluation, an intensity measurement scale was created. For the size, the texture scale consists of four standards. The intensity measurement scale available for the rating is shown in Figure 6-1. The number of the panel to evaluate was written at the beginning of the scale and each standard was represented by a digit which was also indicated on the panel holders. There is a multitude of possibilities in the notation which makes it possible to qualify the perceived intensities compared to the standards (Abbas, 2014). The observer just had to make a cross at the corresponding area. If it was located on one standard (see rating for panel #20 in Figure 6-1), the intensity of the panel to assess was equivalent to one of the standards. The marks were easily converted into numerical values which were used later in the statistical analysis.

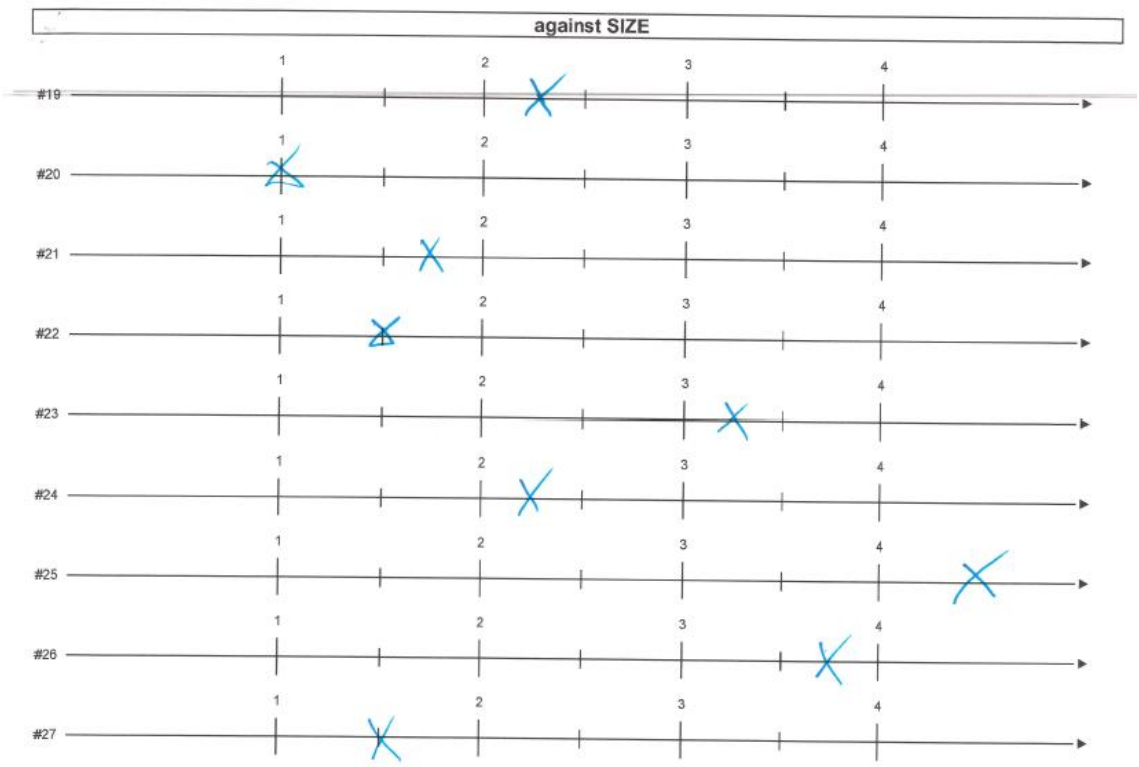

Figure 6-1: Answer sheet of one observer for the evaluation of the descriptor Size

The visual assessment was performed either in a dark room or at least isolated from any light disturbance by a blackout curtain. The tests were performed in a light booth under the illuminant D65 for diffuse illumination or under a spotlight for directional illumination. The spotlights used are LED spots for light intensity evaluation or a Solux incandescent light bulb (36°, 12V, 50W and 4 700K) for color evaluation. The LED spot was preferred to the Solux lamp because it delivers a more powerful light and it is then easier to estimate the intensity of light coming from the particles (Descriptor Intensity). On the other side, the Solux bulb simulates the solar daylight without any weakness in the blue area that would be present for LEDs so it was chosen for the evaluation of the descriptor Color.

For all evaluations, the angle selected was close to the specular angle. At this geometry, the panel receives an incident light ray and returns a refracted light ray. The observer is placed in the trajectory of the refracted light ray. He is therefore blinded by the surface of the panel. This blinding angle allows to define the angle where the maximum of light is reemerged by the panel. The assessor has to be close to the specular without being blinded.

6.2. Elaboration of sensorial profiles

For the elaboration of sensorial profiles, the different observers had to evaluate the thirty-four standards created for the texture scales and for each descriptor, respectively. All the evaluations started with a quick briefing and explanations of the descriptor to assess. Besides, the observers had to select the right angle of observation close to the specular angle but not in the dazzling. The different panel holders were shown to the observers. Figure 6-2 is an illustration of the organization of the elements in the light booth at the beginning of

the test. In that case, the descriptor studied is Size with four standards and three panel holders. The evaluation sheet is placed close to the light booth.

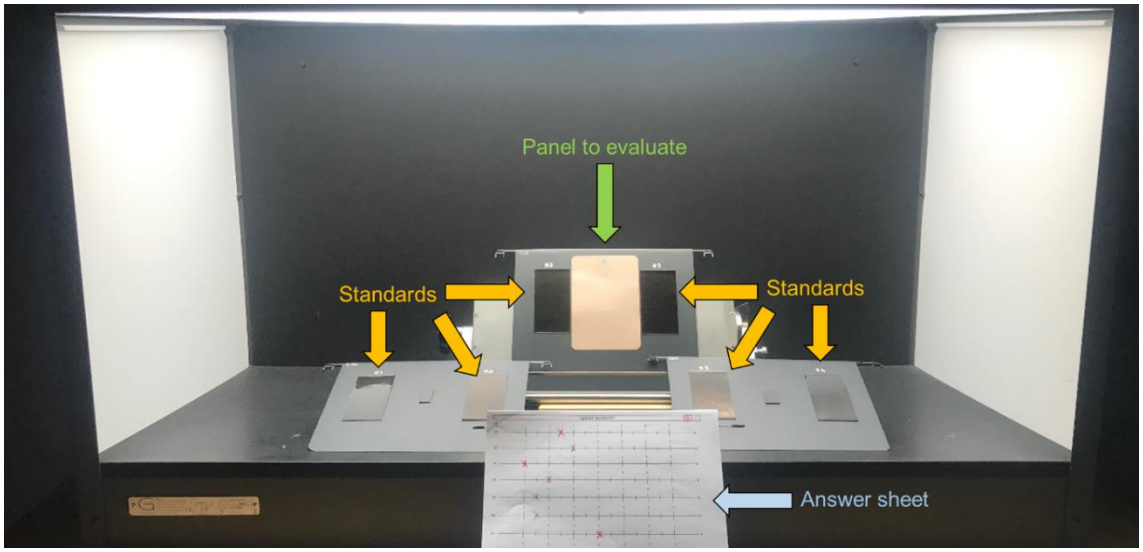

Figure 6-2: Organization of the elements in the light booth for the evaluation of the size where three panel holders are installed, one of which being placed on the rotating system

6.2.1. Ratings on the descriptor Color

The first session was only performed in the French color lab. The descriptor studied was Color. The evaluation was performed under directional lighting created by a Solux lamp close to the maximum of reflection. For this first assessment, only thirteen panels were studied. Eight panels constituted the texture scale Color (from C_1 to C_8) and five other panels were chosen from the other ranges. Only a restricted set of panels was considered, as the standards are mainly formulated with aluminum particles. The results obtained for the six observers are gathered in Table 6-1 where 0 indicates a solid color.

Table 6-1: Evaluations made by the 6 observers from the French color lab on the descriptor Color for 13 panels under directional lighting conditions

Coding	Panel name	OBS1	OBS2	OBS3	OBS4	OBS5	OBS6
C_1	Color_Gold	**1 + 2**	1	1	1	1	1
C_2	Color_Orange	2	2	2	2	2	2
C_3	Color_Red	3	3	3	3	3	3
C_4	Color_White	4	4	4	4	4	4
C_5	Color_Green	5	5	5	5	5	5
C_6	Color_Blue	6	6	6	6	6	6
C_7	Color_Violet	7	7	7	7	7	7
C_8	Color_Aluminum	8	8	8	8	8	8
K_2	Contrast_Very low	8	8	**4**	8	8	8
S_4	Size_Coarse	8	8	8	**4**	8	8
K_6	Contrast_Very strong	8	8	**4 + 8**	8	8	8
I_4	Intensity_Very intense	8	8	**4**	8	8	8
Q_1	Quantity_0%	0	0	0	**6**	0	0

All the assessors evaluated the same panels. In 54% of the case (7 panels), all assigned the same rating. For 4 panels (31%), one observer did not assign the same score as the rest

of the group, twice for OBS3 and for OBS4. For 2 panels (15%), one observer assumed a mix of effect particles in the formula.

For the evaluation of the panels K_2 (Contrast_Very low), I_4 (Intensity_Very intense) and S_4 (Size_Coarse), the experts' assumption based on their know-how seemed to be misleading. Their erroneous assumptions did thus favour precedence over perception. For the example of panel K_2, colorists based on their expertise could assume at first sight a white tricoat due to the important lightness level of the panel. These colors are usually formulated by using a white pearl and the tricoat technology but in that specific case, even if the lightness level is important, the panel K_2 was formulated with aluminum tinting base only (see Chapter 4, Table 4-12). Panel Q_1 (Quantity_0%) is a solid color and thus does not contain any effect particles (see Chapter 5, Table 5-14). The blue effect particles found by the OBS4 in this panel are due to the scratches on the clearcoat.

However, a problem could be identified following this assessment. For two observers, OBS1 and OBS3, a mix of colored effect pigments in the formulation was assumed. In that specific case, however, such a mixture was not used because the formulations selected for the texture range creation are the simplest ones, containing only one type of effect pigment. OEM effect colors available on the market, however, are made by mixing several effect pigments of different colors. The evaluation today is not adapted for the mix of effect pigments. After this ascertainment, the test was not proposed to the German team and will not be considered for the definition of physical texture descriptor in the next chapter.

6.2.2. Assessments of the descriptor Contrast

The second evaluation was focused on the Contrast evaluation. The assessment was done under diffuse lighting with five panel holders, meaning six standards (K_1 to K_6). The thirty-four standards were rated by twelve observers from the two sites. The contrast can be explained as the difference in lightness between the background and the particles. The observers had to rate the panels according to their ability to see or distinguish easily or not the effect particles from 1 (equal to K_1, Contrast_Inexistent) for solid colors to 6 (equivalent to K_6, Contrast_Very Strong) for a maximum of contrast. The results of the different observers are plotted in Figure 6-3 and are summarized in appendix A.1

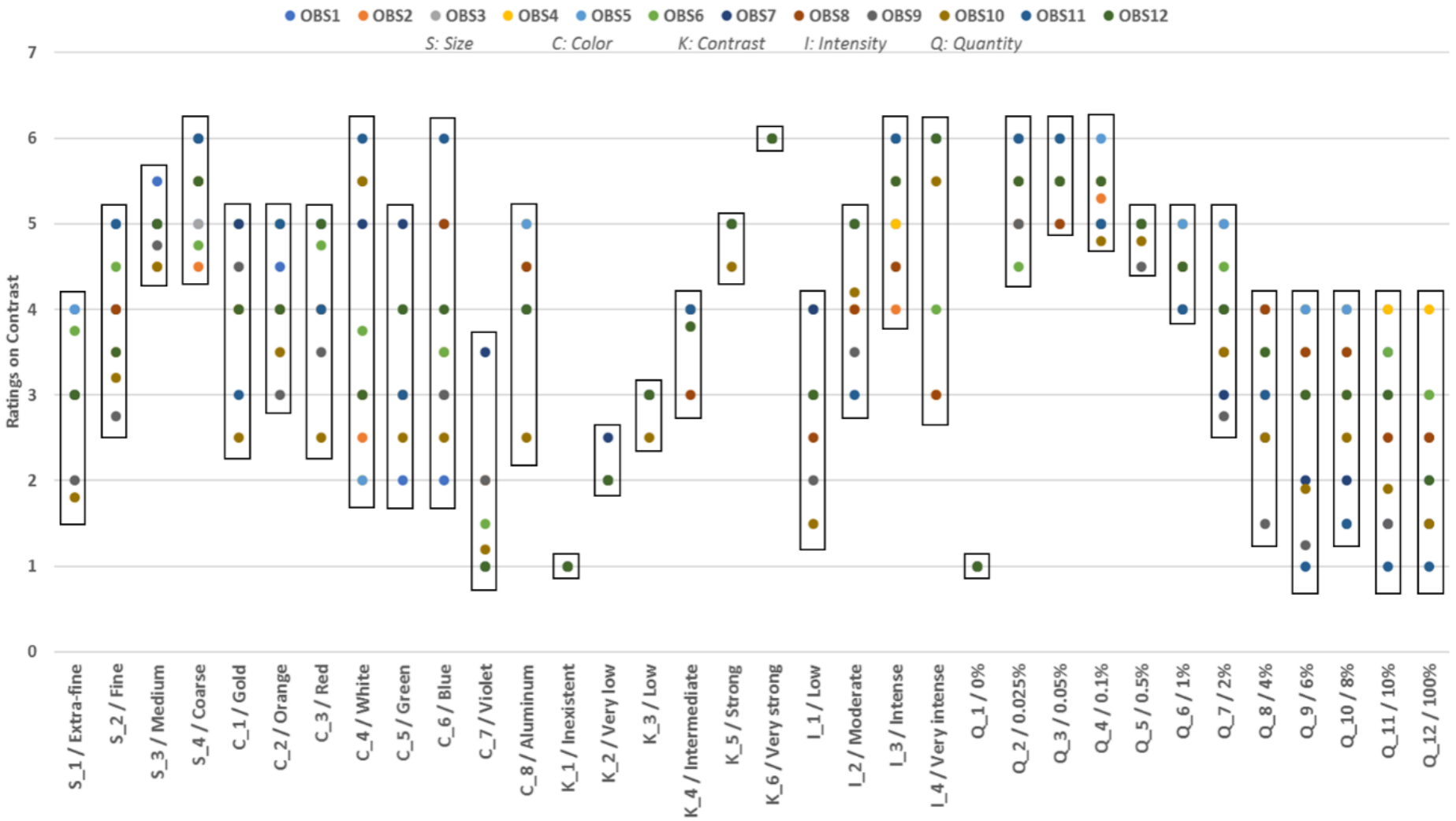

Figure 6-3: Evaluation made by 12 observers under diffuse lighting conditions on the descriptor Contrast for 34 panels, where panels K_1 to K_6 are the standards of the range Contrast

For the descriptor Contrast, the evaluations of the observers follow the same trend, see Figure 6-4. The panels K_1 to K_6 were rated according to their corresponding standards of the range.

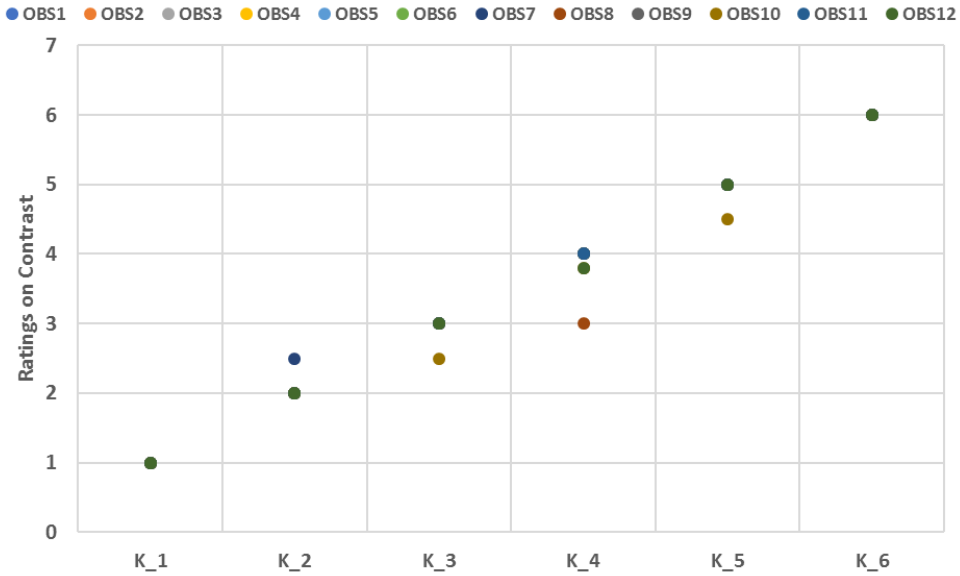

Figure 6-4: Evaluation made by 12 observers under diffuse lighting conditions on the descriptor Contrast for the panels of the range Contrast

By considering the panels Q_1 to Q_12 corresponding to the range Quantity, the observers easily assigned the same rating for the panels with low quantity of effect pigments (Q_2 to Q_6). However, based on Figure 6-5, the evaluation of panels Q_7 to Q_12 was more difficult and the results obtained show a high variation. For example, on the twelve ratings of Q_12 – Quantity_100%, the variance is equal to 0.7 with ratings from 1 to 4. Due to the high concentration of aluminum particles in the coating, the metallic particles cannot be distinguished easily from the background. In fact, isolating these aluminum particles from the background is quite difficult as they overlap.

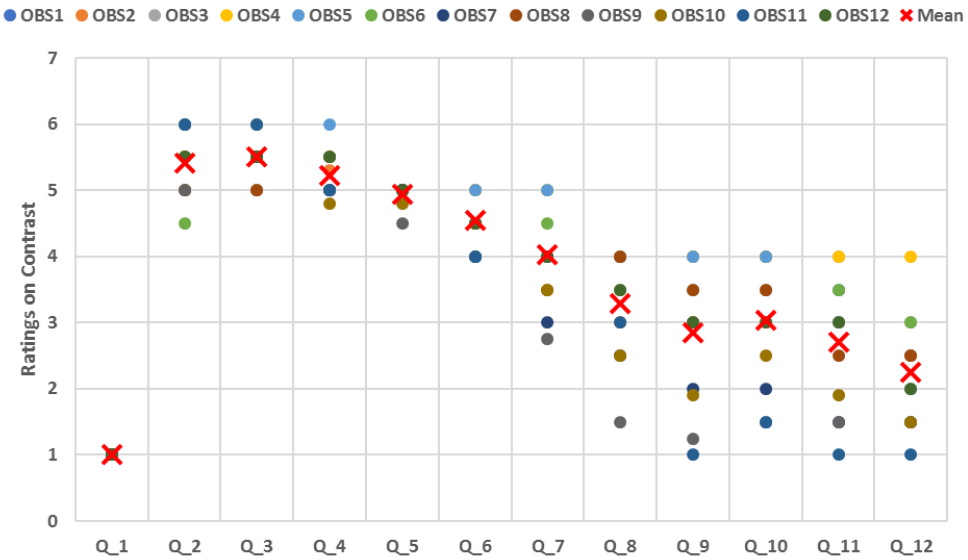

Figure 6-5: Evaluation made by 12 observers under diffuse lighting conditions on the descriptor Contrast for the panels of the range Quantity

However, for panels C_1 to C_8, standards of the range Color, the opinions were rather mixed, see Figure 6-6. One of the reasons is probably linked to the apparent particle size. As explained in Chapter 5, Table 5-11, pearlescent materials are used in the formulas of these standards. These effect particles are finer than the aluminum particles. Moreover, as they are colored, the contrast between the dark background and the effect particles could be difficult to estimate.

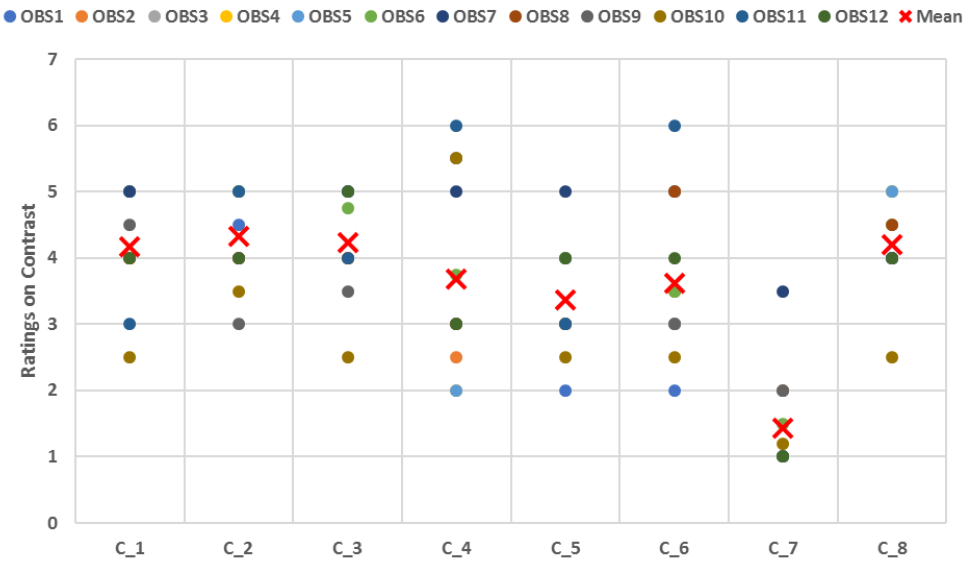

Figure 6-6: Evaluation made by 12 observers under diffuse lighting conditions on the descriptor Contrast for the panels of the range Color

Only the contrast in luminance has been evaluated but in the case of colored references, the chromaticity changes. Possibly, the unassessed chromaticity contrast interferes with the visual evaluations. Also, the human visual system is based on receptor fields of different sizes that collect contrast in luminance. The human eye is not sensitive to contrasts in the same way, but may differ, depending on the size of the object being observed. Nevertheless, with some exceptions, the global tendency in the evaluation is apparent.

6.2.3. Evaluation of the descriptor Size

The third session of visual assessment was dedicated to the evaluation of Size. It was performed by all observers in the light booth. The descriptor Size is linked to the apparent size of the optical effect of one particle. This range is made of four standards (S_1 to S_4) and the ratings are made on the intensity measurement scale and can reach 0 for a solid color or be greater than 4 if the participant thought the size of the size standard #4 (S_4, Size_Coarse) was smaller than the panel to rate. The results are presented in Figure 6-7 and are gathered in appendix A.2.

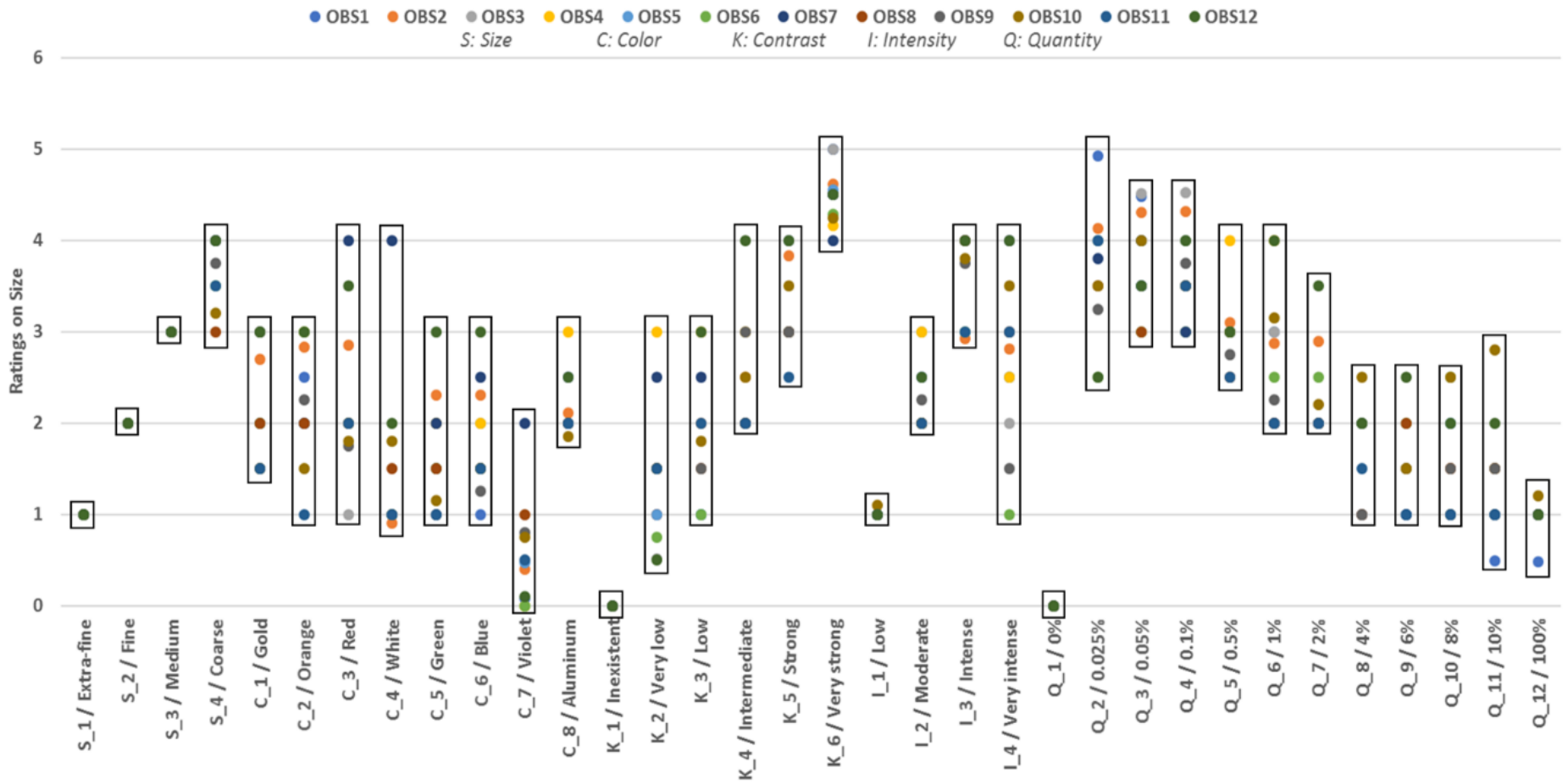

Figure 6-7: Evaluation made by 12 observers under diffuse lighting conditions on the descriptor Size for 34 panels, where panels S_1 to S_4 are the standards of the range Size

For the descriptor Size, the ratings assigned by the observers are in the same range. The observers were able to rate the panels S_1 to S_4 at the same level as the standards of the range with however a little more varied results for the panel S_4, Size_Coarse, see Figure 6-8.

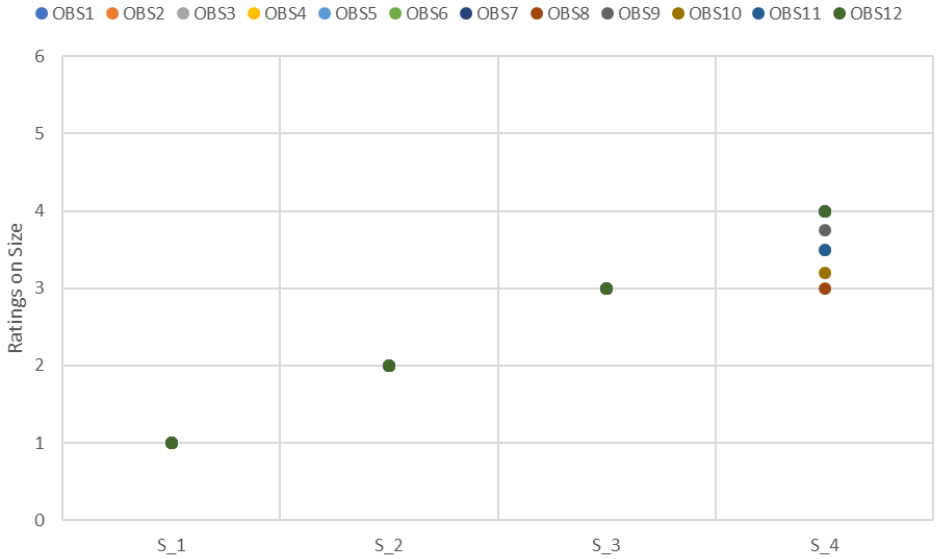

Figure 6-8: Evaluation made by 12 observers under diffuse lighting conditions on the descriptor Size for the panels of the range Size

For the panels from the range Intensity (I_1 to I_4), the assessors agreed on the ratings awarded, with the exception of panel I_4, Very intense, see Figure 6-9. This deviation can be linked to the low amount of effect particles in the formulation (see Chapter 5, Table 5-13).

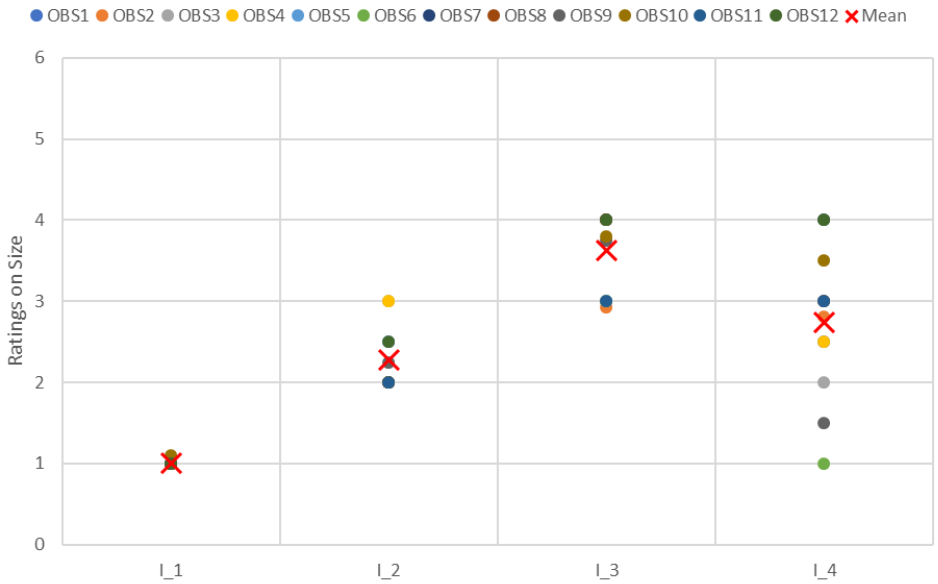

Figure 6-9: Evaluation made by 12 observers under diffuse lighting conditions on the descriptor Size for the panels of the range Intensity

For the range Quantity (Q_1 to Q_12), the assessors in general agreed on the ratings awarded, see Figure 6-10. It is interesting to note here that the references are made of the same aluminum pigment but at different percentages in the formulation. Therefore, when the quantity of aluminum increases, the apparent particle size decreases. This can also be explained by the difficulty to distinguish particles from the background and thus may be perceived as a lower contrast.

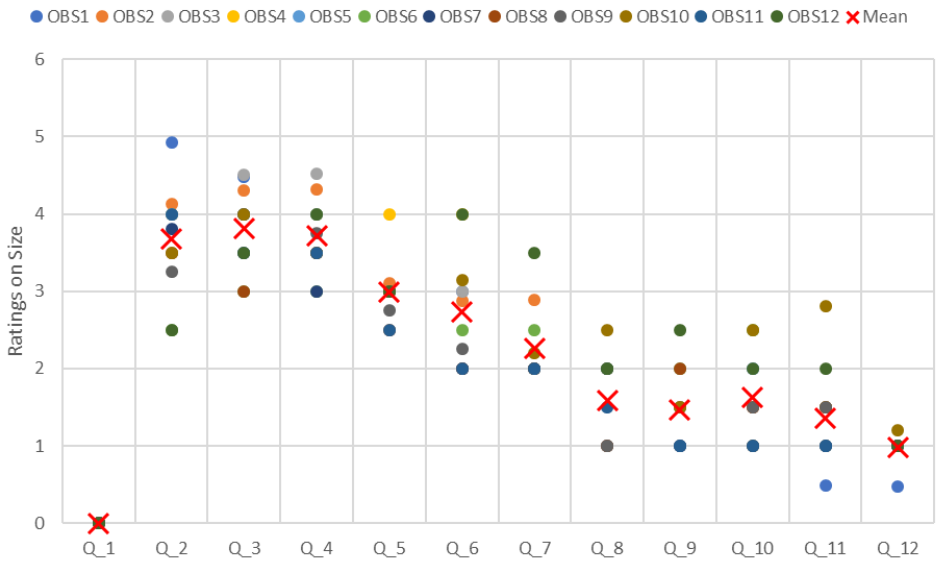

Figure 6-10: Evaluation made by 12 observers under diffuse lighting conditions on the descriptor Size for the panels of the range Quantity

As for the Contrast evaluation previously explained, the same problem with the range Color became obvious, see Figure 6-11. This observation is due to the fine particles in the formula and to the low contrast between the background and the particles on these panels (C_1 to C_8).

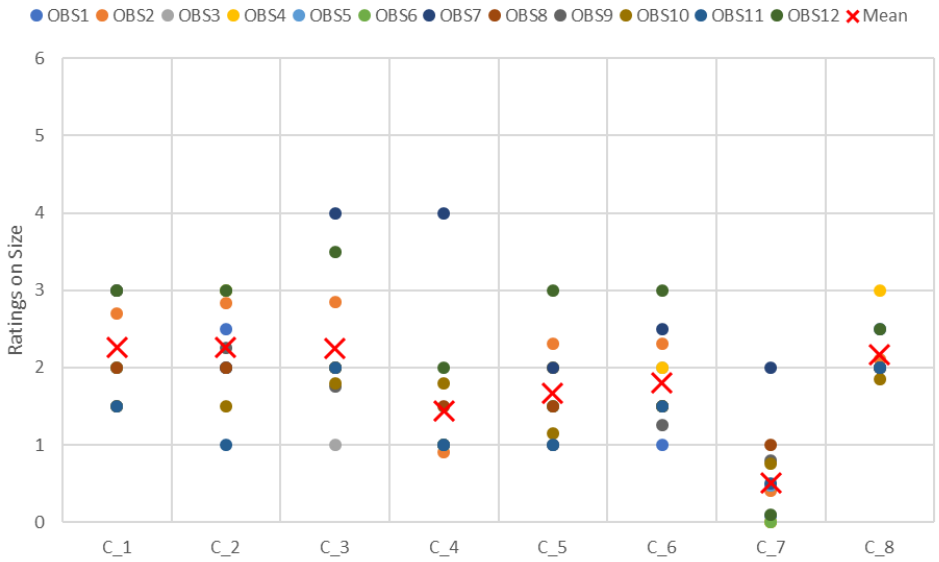

Figure 6-11: Evaluation made by 12 observers under diffuse lighting conditions on the descriptor Size for the panels of the range Color

For the panels K_2 and K_3 (Contrast_Very Low and Contrast_Low respectively) from the range Contrast, the color of the background is quite similar to the one of the particles. To isolate particles can be tricky so the size evaluation is not easy, hence the diverse assessments, see Figure 6-12.

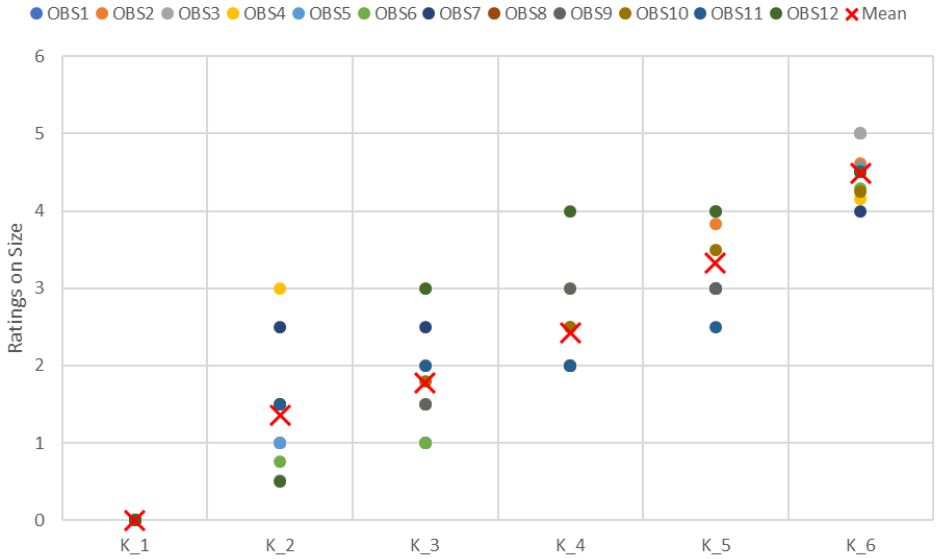

Figure 6-12: Evaluation made by 12 observers under diffuse lighting conditions on the descriptor Size for the panels of the range Contrast

6.2.4. Elaboration of sensorial profile for the descriptor Intensity

The penultimate evaluation concerned the descriptor Intensity. The respective assessment was performed under direct lighting conditions to maximize the reflected light coming from the particles. The objective of this evaluation was to estimate the amount of light reflected by the effect particles. This range is made of four standards: I_1 to I_4. All twelve observers participated in this assessment. As for the size, the rating can be equal to 0 for a solid color or be greater than 4 if the participant estimated the intensity of the panel greater than the one of the intensity standard #4 (I_4, Intensity_Very Intense). The results are plotted in Figure 6-13 and detailed in appendix A.3. The ratings of the thirty-four panels for the descriptor Intensity follow mainly the same trend.

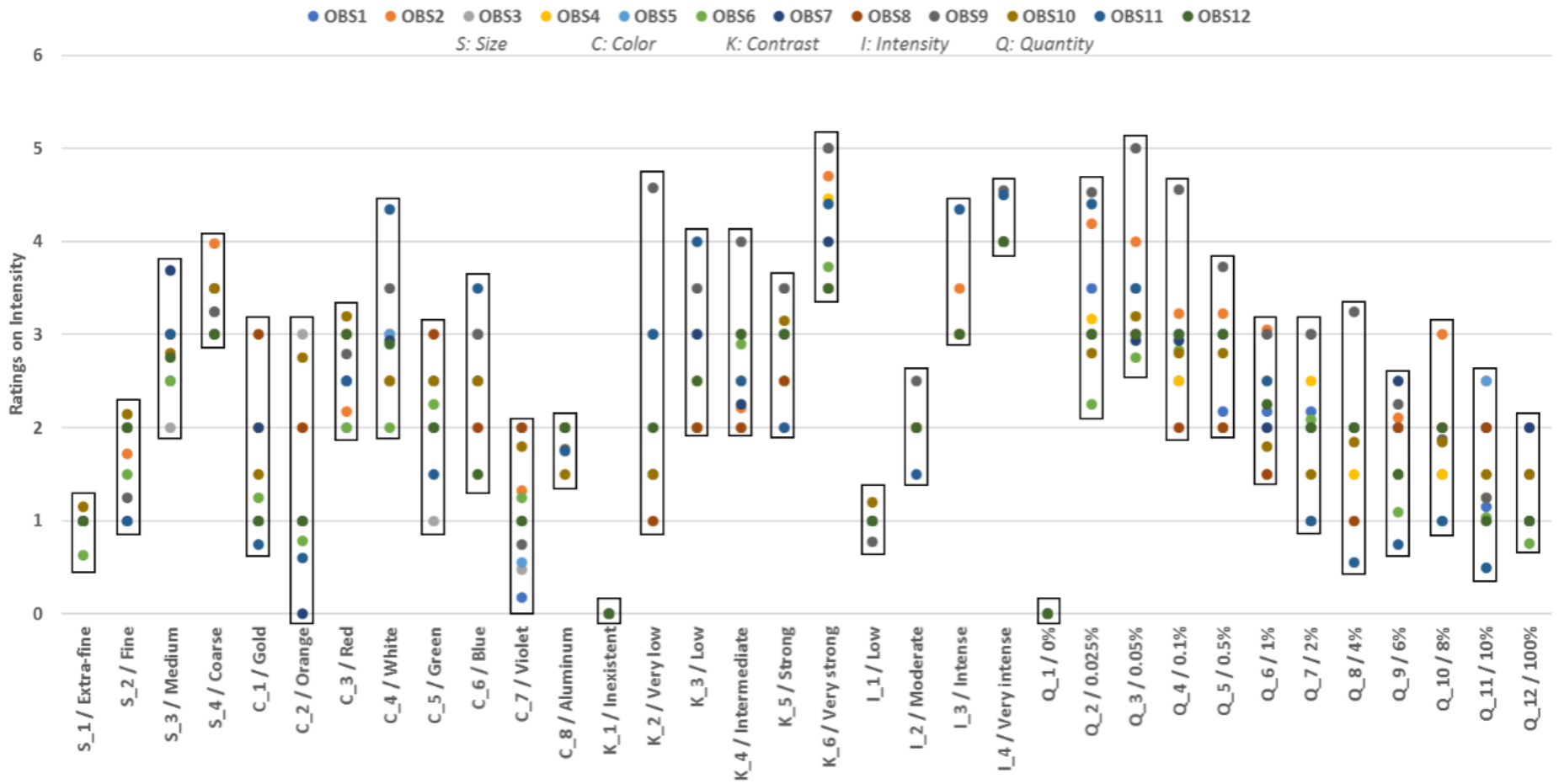

Figure 6-13: Evaluation made by 12 observers under directional lighting conditions on the descriptor Intensity for 34 panels where panels I_1 to I_4 are the standards of the range Intensity

The assessors rated the panels I_1 to I_4 according to the corresponding standards, see Figure 6-14.

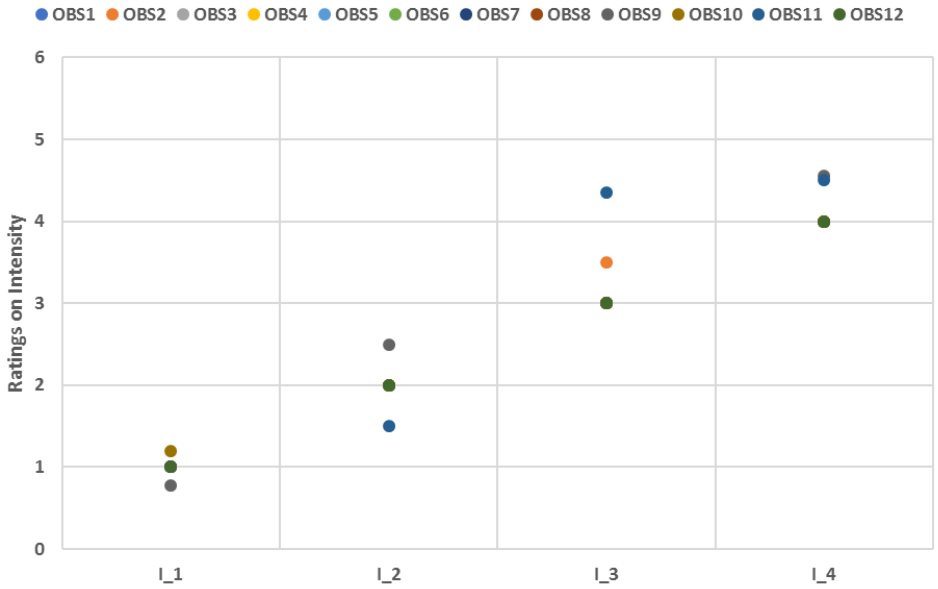

Figure 6-14: Evaluation made by 12 observers under directional lighting conditions on the descriptor Intensity for the panels of the range Intensity

The panels from the range Size (S_1 to S_4) show cohesion in the ratings, see Figure 6-15.

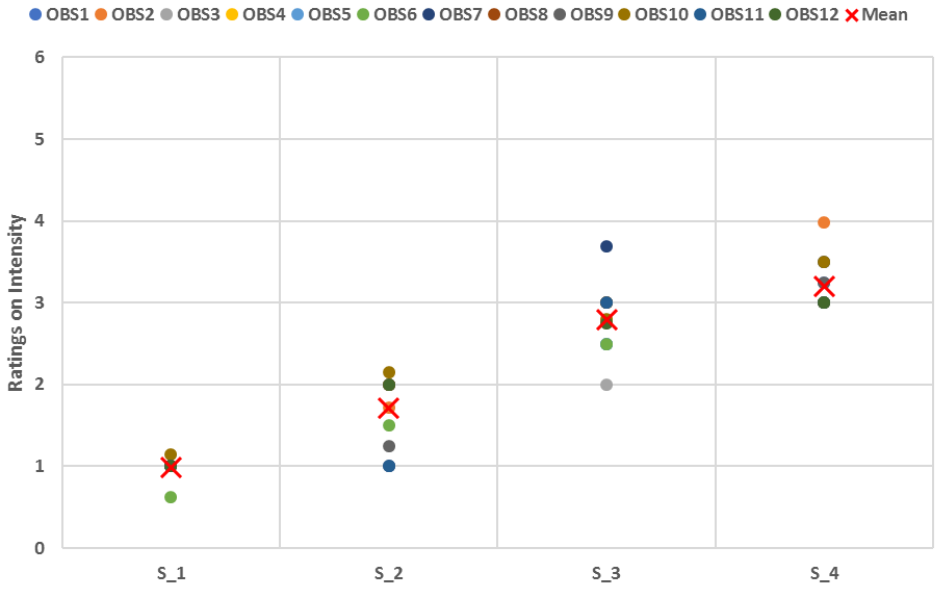

Figure 6-15: Evaluation made by 12 observers under directional lighting conditions on the descriptor Intensity for the panels of the range Size

Larger differences in the evaluation of the panels K_2 and K_3 from the range Contrast (Contrast_Very Low and Contrast_Low respectively) become obvious, supposedly linked to the weak contrast, see Figure 6-16.

Figure 6-16: Evaluation made by 12 observers under directional lighting conditions on the descriptor Intensity for the panels of the range Contrast

As for the evaluation of the previous descriptors, the panels C_1 to C_8 from the range Color were difficult to rate due to the low contrast and the size of the particles used (Figure 6-17).

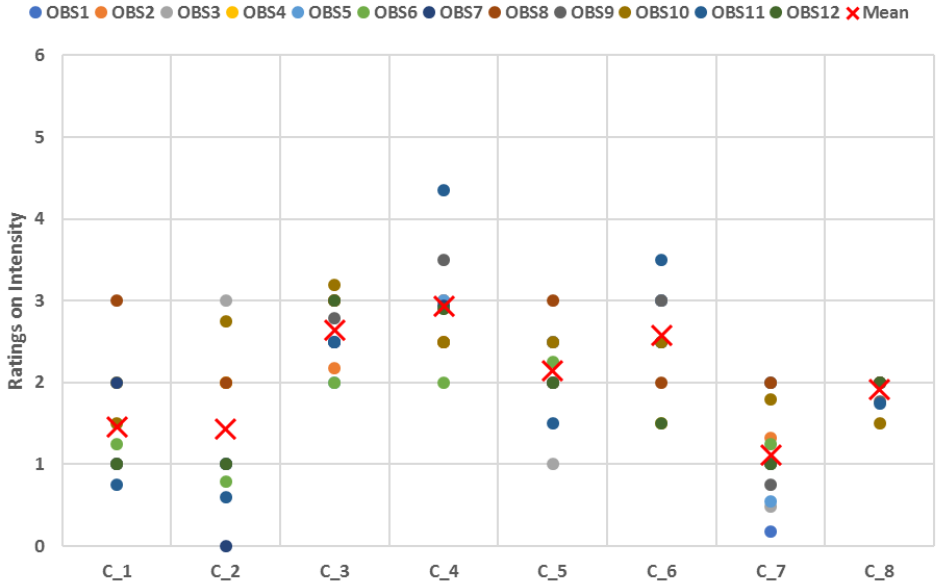

Figure 6-17: Evaluation made by 12 observers under directional lighting conditions on the descriptor Intensity for the panels of the range Color

Then, for the panels of the range Quantity (Q_1 to Q_12), the evaluation globally follows the same trend nevertheless it shows some disparities (Figure 6-18). It is interesting to note here that these eleven panels are made of the same aluminum pigment but at different percentages in the formula. And so, when the quantity of aluminum increases, the relative intensity coming from the particles and perceived by the human visual system decreases. This can be explained anew by the difficulty to distinguish particles from the background and also by a local adaptation in a situation of low contrast (see Figure 6-3 and Figure 6-5).

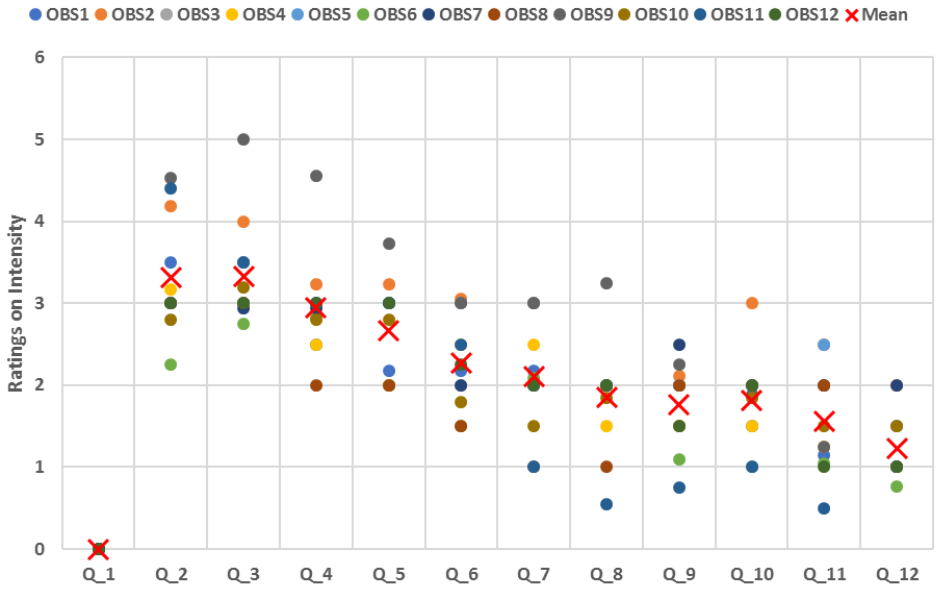

Figure 6-18: Evaluation made by 12 observers under directional lighting conditions on the descriptor Intensity for the panels of the range Quantity

6.2.5. Estimation of the descriptor Quantity

The last evaluation under diffuse lighting conditions was the one for the descriptor Quantity. For the first trial after the conception phase, the range comprised twelve standards. Finding differences between these standards, mainly at high percentage of aluminum particles was quite difficult. Thanks to the comments from the observers, some of the panels were eliminated and the final number of standards kept for the same range is equal to seven (Q_1, Q_2, Q_4, Q_5, Q_7, Q_9 and Q_12). For this assessment, only ten observers participated and their evaluations are gathered in Figure 6-19 and in appendix A.4.

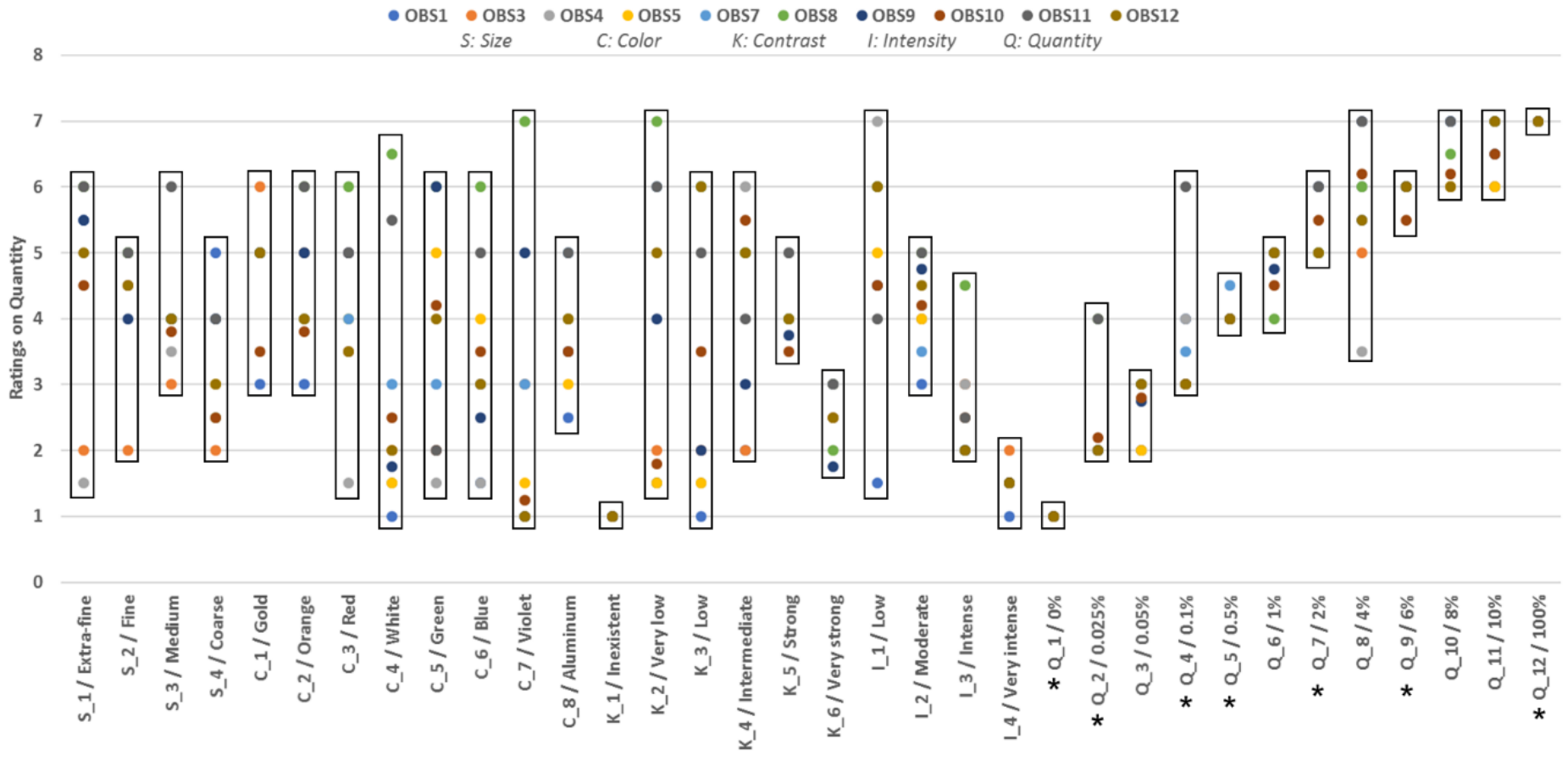

Figure 6-19: Evaluation made by 10 observers under diffuse lighting conditions on the descriptor Quantity for 34 panels where panels from Q_1 to Q_12 are the propositions of the range Quantity and the references are indicated with asterisk

This range was maybe the most difficult to assess for the observers. Firstly, it contains many standards compared to the other ranges. Secondly, it is also a kind of circular range as the difference between the quantity standard #1 (Q_1, solid color) and the quantity standard #7 (Q_12, aluminum color) is reduced. In this specific case, the contrast of the panel Q_12 is low. Indeed, under diffuse lighting conditions it can be considered as a solid color as particles are not easily isolated from the background. Based on their knowledge, participants understood at first sight the formula corresponding to Q_12. Globally, the observers rated the panels of the range Quantity according to their corresponding standards, see Figure 6-20.

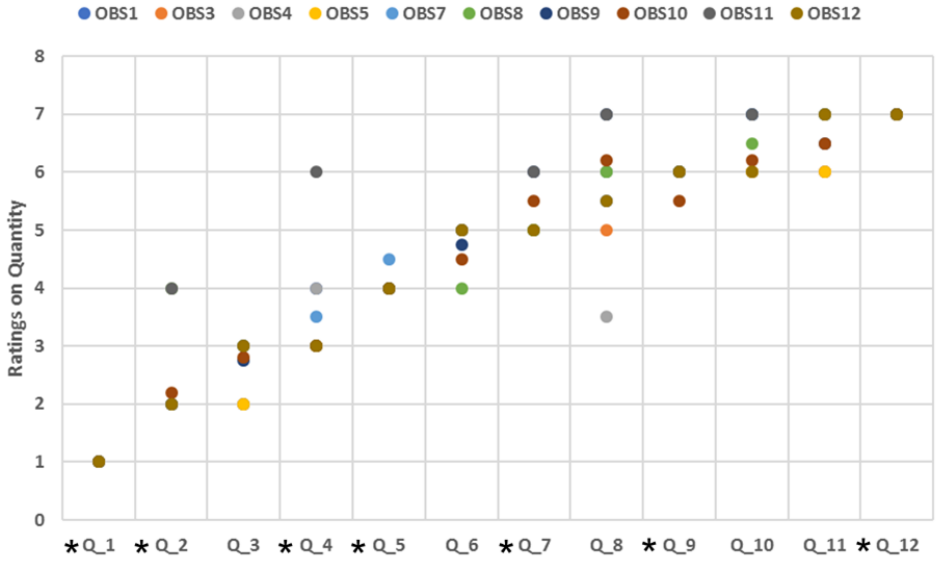

Figure 6-20: Evaluation made by 10 observers under diffuse lighting conditions on the descriptor Quantity for the panels of the range Quantity

However, huge differences in ratings can be noticed for the panels of the range Color (C_1 to C_8), see Figure 6-21. Indeed, the effect particles in formulas are so fine that estimating their quantity is complicated.

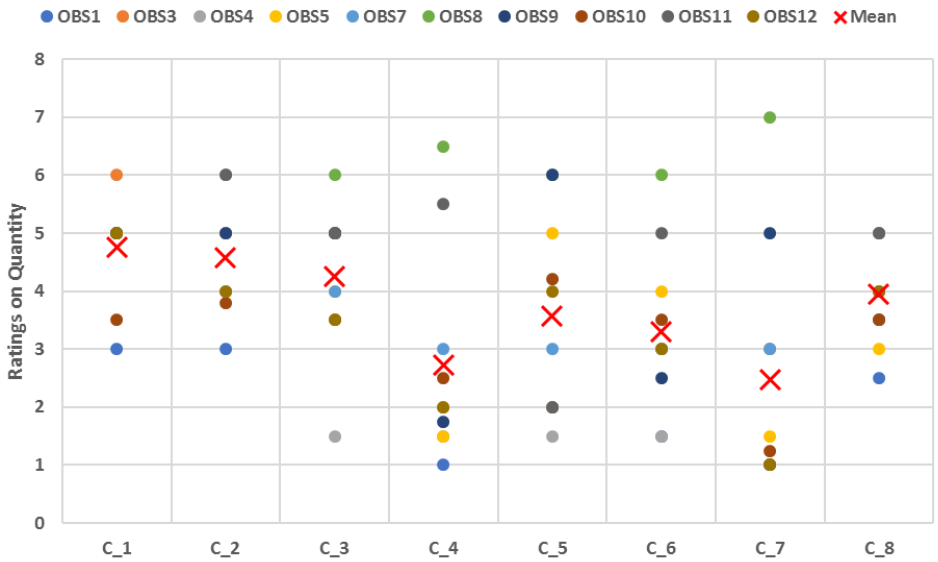

Figure 6-21: Evaluation made by 10 observers under diffuse lighting conditions on the descriptor Quantity for the panels of the range Color

For the panels of the range Contrast and mainly K_2 to K_5, the quantity of effect pigments in the formula is equivalent and only the background color changes with the tricoat technology (see Chapter 50, Table 5-12). For the majority of observers, the perceived quantity of particles decreases along with the global lightness value, see Figure 6-22.

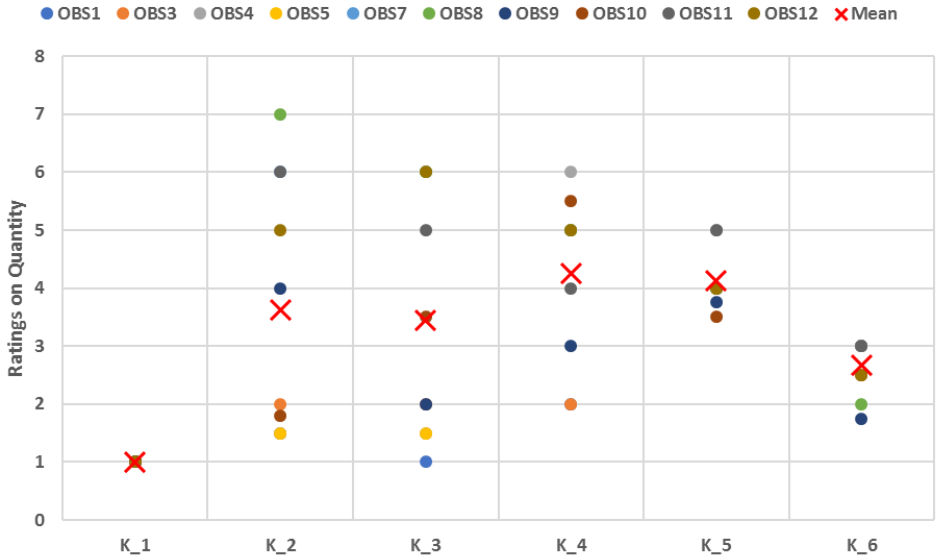

Figure 6-22: Evaluation made by 10 observers under diffuse lighting conditions on the descriptor Quantity for the panels of the range Contrast

The results obtained on the elaboration of sensorial profiles show that, depending on the formula, the defined texture descriptors are more or less important. This means that at the level of the physical signal, the prominent elements can be of several types and can compete with one another.

6.3. Statistical analysis performed on visual assessment data for the definition of the mean observer

After the establishment of sensorial profiles by twelve experienced observers, the objective was then to define a mean observer based on their ratings. The use of a texture scale should have ensured the consistency of the evaluations. However, even if the ratings follow a trend as presented in paragraph 6.2, some observations deviate too much from the others, and are considered as outliers. The deviations are observed mainly for the panels of the range Color (C_1 to C_8) for all the descriptors or the rating obtained for the descriptor Quantity. According to Hawkins, "*an outlier is an observation which deviates so much from the other observations as to arouse suspicions that it was generated by a different mechanism*" (Hawkins, 1980). The detection of outliers is of major importance for the determination of the mean observer. Indeed, for each descriptor, a mean observer should be calculated from the evaluations of all observers. The presence of deviant values could jeopardize the accuracy and the reliability of the mean observer thus obtained. Different methods exist for the evaluation of values of a given system and determination of outliers; these are presented in the following before defining the mean observer.

6.3.1. Outlier labelling

This paragraph is dedicated to a brief description of the techniques which are used for outlier labelling. For a better understanding, some methods cited in literature are presented in the following. The detection of outliers is important because they have an influence on the statistical values such as the mean or the variance.

The Grubbs' outlier test, (Grubbs, 1969), is used to detect outliers for normally distributed data for a set containing a minimum of six values. It detects one outlier at a time and iterates up to the absence of outliers. This test is based on two hypotheses, H_0 and H_1, where H_0 assumes the absence of outliers and H_1 the presence of one outlier. The Grubbs test checks the values which deviate the most from the mean according to equation (6-1).

$$G = \frac{\max(X_i - \bar{X})}{\sigma} \qquad (6\text{-}1)$$

With $\bar{X}$, *mean of the sample*
σ, *standard deviation*

To detect the outliers, the G value obtained should be compared to the critical value, G_{crit}, defined for a significance level α=0.05% or 0.10% and for a number of elements in a set, see Table 6-2. The critical value must be adapted when an outlier is removed from the list.

Table 6-2: Critical value for the Grubbs test with a significance level of 0.05% or 0.10%

n	G_{crit} (α=0.05%)	G_{crit} (α=0.10%)	n	G_{crit} (α=0.05%)	G_{crit} (α=0.10%)
3	1.1531	1.1547	8	2.1266	2.2744
4	1.4812	1.4962	9	2.2150	2.3868
5	1.7150	1.7637	10	2.2900	2.4821
6	1.8871	1.9728	11	2.3547	2.5641
7	2.0200	2.1391	12	2.4116	2.6357

The standard deviation method or SD method is a simple approach which uses the mean and the standard deviation. Two adaptations exist: the 2 SD or the 3 SD as detailed in equation (6-2).

$$2SD\ Method = \bar{X} \pm 2\sigma \quad or \quad 3SD\ Method = \bar{X} \pm 3\sigma \qquad (6\text{-}2)$$

With $\bar{X}$, *mean of the sample*
σ, *standard deviation*

However, it is important to note that the mean and the standard deviation used in the SD method are mainly impacted by outliers (Olewuezi, 2011). The MADe method was then developed to avoid this strong impact of outliers on statistical measurements (Hampel, 1971). This method is based on the definition of an estimator, MAD for median absolute deviation, which corresponds to the median value of the difference between a value and its median,

see equation (6-3). The median or the second quartile (Q2) represents the value under which 50% of the other values lie below.

$$\begin{gathered} 2MADe\ Method = Median \pm 2MADe \\ or \\ 3MADe\ Method = Median \pm 3MADe \\ with \\ MADe = 1.483MAD \\ MAD = Median(|X_i - Median(x)|) \end{gathered} \quad (6\text{-}3)$$

Small sets of samples can be adapted as proposed in equation (6-4) by (Iglewicz and Hoaglin, 1991). The authors' recommendation on the outlier detection is based on a threshold value of 3.5. To be considered as an outlier, the M_i value must be below 3.5.

$$M_i = \frac{0.6745(X_i - \bar{X})}{MAD} \quad (6\text{-}4)$$

The Tukey fences or IQR (interquartile range) method (Tukey, 1977) identifies two boundaries for outlier detection based on the interquartile range, see equation (6-5). The first and the third quartiles, Q1 and Q3, represent 25% of the ratings or 75% which lie below this value, respectively. A value which does not bellow to the outer fences is considered as an outlier, and a value between the inner and outer fences is a potential outlier.

$$\begin{gathered} IQR = Q_3 - Q_1 \\ Inner\ fences: [Q_1 - 1.5\ IQR; Q_3 + 1.5\ IQR] \\ Outer\ fences: [Q_1 - 3\ IQR; Q_3 + 3\ IQR] \end{gathered} \quad (6\text{-}5)$$

With *IQR, interquartile range*
Q_1, first quartile
Q_3, third quartile

Also based on interquartile range, the median rule is the last method presented here. The values must be in the range presented in equation (6-6) to not be considered as outlier.

$$[K_1; K_2] = Q_2 \pm 2.3 \times IQR \quad (6\text{-}6)$$

With *IQR, interquartile range*
Q_2, second quartile or median value

After detailing different methods to identify outliers, it is necessary to determine which one is the most suitable for the definition of the mean observer. The identification methods are tested on the ratings in the next paragraph.

6.3.2. Definition of the mean observer

For the definition of the mean observer, the selection of the appropriate outlier detection method is mandatory. The statistical measurements for the ratings obtained from the ten observers for the panel K_2 for the descriptor Quantity [respectively for OBS1 to OBS10: 1.5; 2; 1.5; 1.5; 6; 7; 4; 1.8; 6; 5]. are gathered in Table 6-3.

Table 6-3: Statistical measurements for panel K_2 obtained for the descriptor Quantity

Mean	Standard Deviation	Median	Q_1	Q_3	IQR
3.63	2.21	3	1.575	5.75	4.175

As explained in Chapter 6 paragraph 6.3.1, the Grubbs outlier test is used for normally distributed data. First, it is necessary to check if the ratings obtained for panel K_2 for the descriptor Quantity follow this prerequisite.

The normality test available in the software Minitab was used (Minitab, 2019). This normality test is based on two hypotheses: H_0, data follow a normal distribution and H_1, data do not follow a normal distribution. If the p-value[1] obtained by this test is less than or equal to the significance level (α=0.05), the hypothesis H_0 is rejected and the data do not follow a normal distribution.

The probability plot obtained after the normality test is presented in Figure 6-23. It represents the estimated cumulative distribution function by plotting the value of each rating against the estimated cumulative probability. In that case, the p-value is equal to 0.042 which is less than the significance level of 0.052. Hence, the data do not follow a normal distribution and the Grubbs outlier test cannot be used.

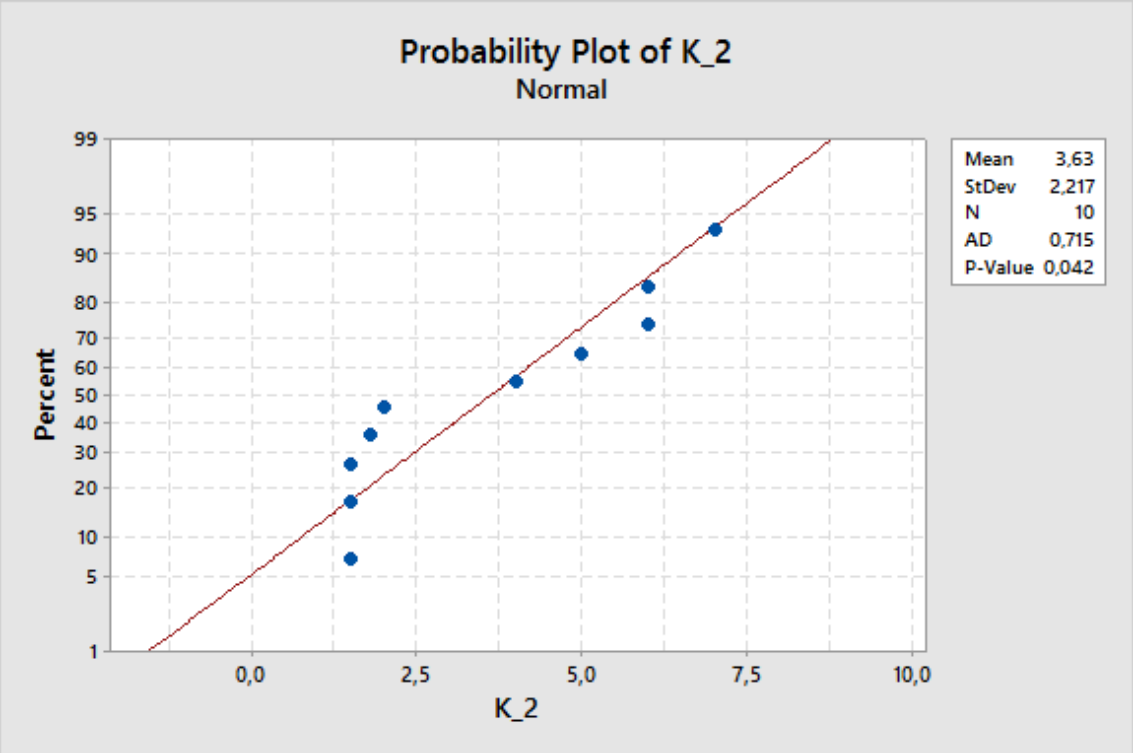

Figure 6-23: Probability plot obtained after normality test in Minitab for the ratings of panel K_2

[1] The p-value or probability value represents the statistical significance in a hypothesis test.

The different methods presented in Chapter 6, paragraph 6.3.1, were applied to the data set of K_2, the results are gathered in Table 6-4.

Table 6-4: Comparison of different methods for outlier detection in the ratings obtained for panel K_2 for the descriptor Quantity based on the observations of 10 participants

Method	Range	Outliers?
Grubbs	Not adapted	Not adapted
2-SD	[-0.80;8.06]	None
3-SD	[-3.02;10.28]	None
2-MADe	[0;3]	5
3-MADe	[0;3]	5
MAD	Not adapted, MAD=0	None
Tukey fences	Inner: [-4.69;12.01] Outer: [-10.95;18.28]	None
Median rule	[-6.60;12.60]	None

Based on the results of the different methods for outlier detection, the Grubbs test, the SD method, the MAD method for small sets of samples, the Tukey fences and the median rule are not applied. Potentially, the 2-MADe and the 3-MADe method seem to be applicable for this case, but they removed 5 outliers so 42% of the set considered. Moreover, the MAD value is equal to 0 so these two tests are maybe not that efficient on the data obtained.

To label the outliers, the decision was taken to use the Kruskal Wallis test in XLStats. This test is non-parametric; it does not assume a normal distribution of the data. It determines if the medians of two or more groups differ and also if all the elements belong to the same group or if one element of the group does not belong to it, the potential outlier. Box plots were then used to highlight the potential outliers. An example of the box plot obtained for the evaluation of the descriptor Contrast is presented in Figure 6-24. The box plots of the panels Q_1 to Q_12 are not shown in Figure 6-24 for the ease of reading.

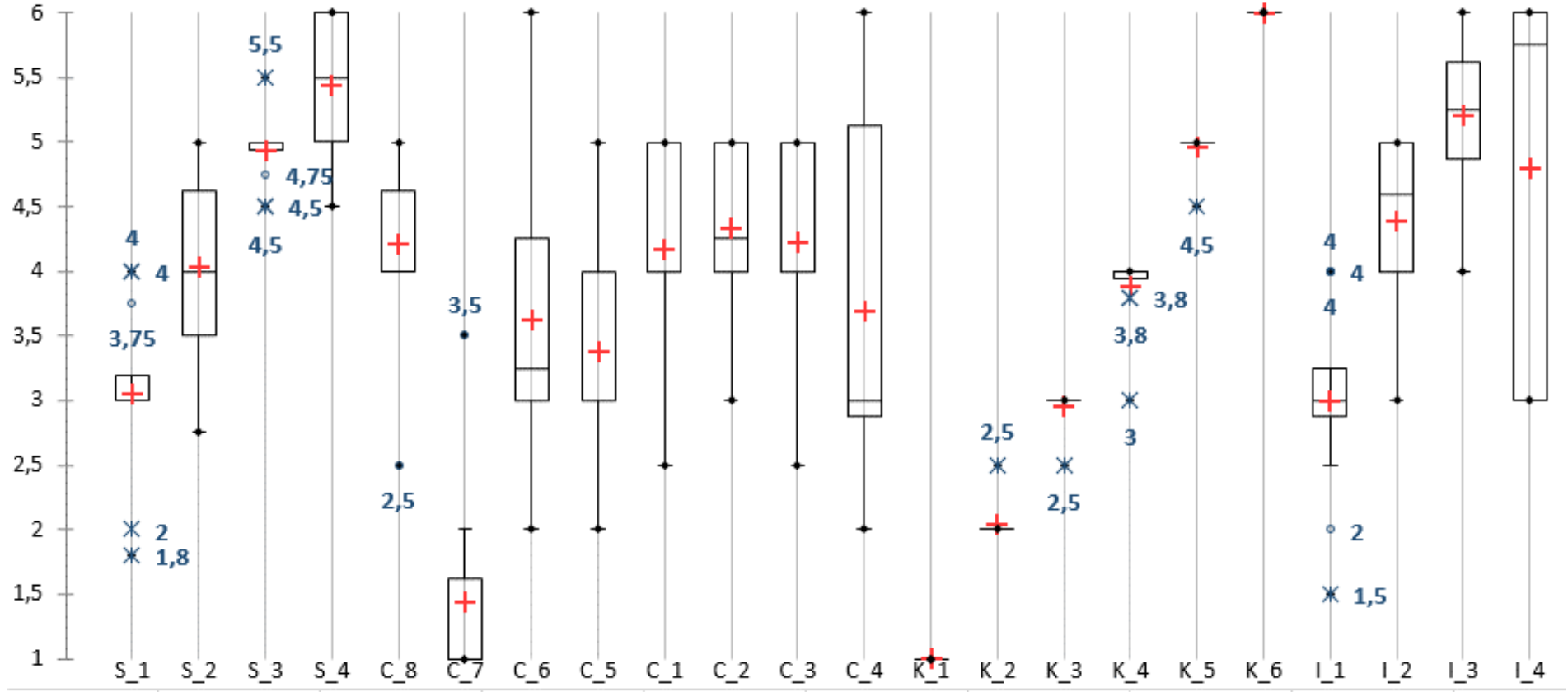

Figure 6-24: Box plot obtained after the use of the Kruskal Wallis test for the evaluation of the descriptor Contrast where the red cross indicates the mean and the blue cross or point the outliers

In a box plot, the upper and lower boundaries of the box represent the first and the third quartiles under which 25% of the ratings or 75%, respectively, lie below. The smaller the interquartile range, the higher the possibility of getting outliers. However, this test can be quite strict. By considering the panel S_3 in Figure 6-24, four outliers are identified at 4.5, 4.5, 4.75 and 5.5. By looking into the results in more detail, the mean value is equal to 4.93, the first quartile to 4.93 too and the third quartile to 5. In that case, the interquartile range is equal to 0.07. Even if the four outliers are relatively close to the other ratings, the very low IQR value leads to a high number of outliers.

The Kruskal Wallis test was performed for the evaluation of all descriptors. 23 outliers were identified for the descriptor Intensity (5.6% of the ratings), 24 for the descriptor Contrast (5.9%), 25 for the descriptor Size (6.1%) and 30 for the descriptor Quantity (8.8%). As expected, the descriptor Quantity presents more outliers than the other descriptors. This descriptor was the most difficult to assess by the observers. However, the number of outliers stays relatively low. It was also possible to analyze the number of outliers by observers to check if one observer is more out of step than others. The number of outliers per descriptor and per observer is plotted in Figure 6-25.

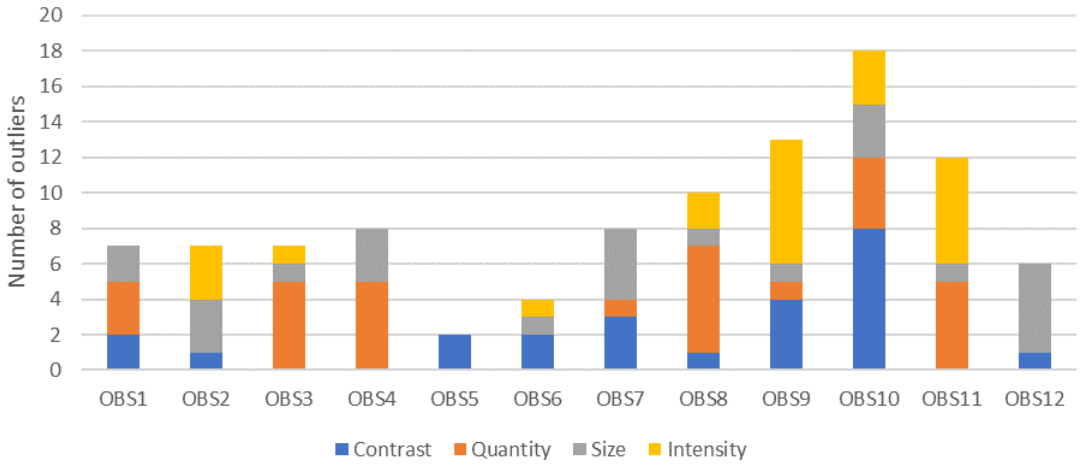

Figure 6-25: Number of outliers per descriptor and per observer

According to Figure 6-25, observer 5 is the one that comes closest to the mean observer as only two of his/her ratings are considered as outliers. Inversely, the observer 10 contributed the most to the number of outliers with a total amount of eighteen. However, based on the 102 outliers detected by the Kruskal Wallis test, his/her contribution is 17% while the average contribution is 8%. It is also important to note here that the observers 2 and 6 did not participate in the rating of the range Quantity. Nine observers presented at least one difficult case for the rating of Contrast, eleven for the Size, eight for the Quantity and seven for the Intensity. In the first trial, the descriptor Contrast was the one that was most difficult to understand (see Chapter 5, paragraph 5.4 and Table 5-8). The results obtained as part of the sensorial profiles elaboration for Contrast show the effectiveness of the training tool developed and the associated references based on real perceptive expert knowledge.

In the chart in Figure 6-25, the differences between the observers 1 to 6 and 7 to 12 can be seen. The first group represents the observers from France while the second one the observers from Germany. The two countries have light booths from different manufacturers.

This difference in equipment presumably leads to slight shifts in the ratings. Indeed, in the German light booth, it is easier to perceive the very fine particles as the pearlescent materials used for the range Color, than in the French one. However, it is important to put these differences into perspective. As previously mentioned, the outliers identified by the Kruskal Wallis test are mainly dependent on the IQR. Indeed, the height of the boxes in Figure 6-24 is connected to the strong or weak consensus between the observers. The outliers labelled by the Kruskal Wallis test for weak IQR are not necessarily so far from non-outlier values.

After the exclusion of outliers, the new values of the mean are then calculated to define the mean observer for each descriptor. The four mean observers are gathered in Table 6-5.

Table 6-5: Values of the mean observer for the four descriptors, determined after exclusion of outliers

Panel ID	Contrast	Size	Intensity	Quantity
S_1	3	1	1	4.8
S_2	4.04	2	1.72	4.78
S_3	5	3	2.79	3.91
S_4	5.44	3.75	3.14	3.3
C_8	4.36	2.09	2	3.95
C_7	1.25	0.37	1.11	2.48
C_6	3.63	1.69	2.58	3.3
C_5	3.38	1.66	2.25	3.57
C_1	4.17	2.27	1.46	5
C_2	4.33	2.26	1.43	4.58
C_3	4.23	1.94	2.64	4.25
C_4	3.69	1.2	2.8	2.73
K_1	1	0	0	1
K_2	2	1.08	2.3	3.63
K_3	3	1.78	2.54	3.45
K_4	4	2.27	2.7	4.25
K_5	5	3.32	2.85	3.91
K_6	6	4.49	4.19	2.68
I_1	2.93	1	1	5.44
I_2	4.39	2.27	2	4.2
I_3	5.21	3.62	3	2.55
I_4	4.79	2.89	4	1.5
Q_1	1	0	0	1
Q_2	5.42	3.67	3.32	2.03
Q_3	5.5	3.82	3.17	2.56
Q_4	5.22	3.72	2.88	3.28
Q_5	5	3	2.66	4
Q_6	4.54	2.73	2.27	4.83
Q_7	4.02	2.07	2.11	5.25
Q_8	3.29	1.58	1.93	6.02
Q_9	2.85	1.46	1.77	6
Q_10	3.04	1.63	1.7	6.37
Q_11	2.7	1.23	1.56	6.6
Q_12	2.25	1	1.23	7

6.4. Assessment on the elaboration of sensorial profiles

After the definition of the new texture descriptors in the previous chapter and the conception of the texture scales, the objective was to use the human eye as a metric to evaluate five descriptors: Contrast, Size, Intensity, Quantity and Color.

Twelve participants were involved in the visual assessment sessions. They are considered as expert observers. However, due to the multiple controls they had to perform when looking at panels (such as size, quantity, color differences or the color travel) they normally evaluate color based on dynamic evaluation by playing with the light angle. For this study, it was necessary to standardize the conditions of the tests. For example, the angle selected for the observations was close to specular angle to maximize the lighting level. Besides, the observations were performed either under diffuse or directional lighting system. This standardization allows to reduce the variations due to the surrounding and to evaluate more precisely the answers of each observer. It is then possible to compare the observers with each other.

The visual assessment sessions on the descriptor Color highlighted the non-adaptation of the range used for the visual determination of the apparent color of the particles. Indeed, some observers assumed a mix between particles of different colors. In that specific case, this was not possible because the formulations determined for the texture range creation were the simplest ones, containing only one type of effect pigment. However, the effect colors available on the market are made by mixing several effect pigments of different colors. The current evaluation is not applicable to a mix of effect pigments. Besides, the descriptor Color is based on hue evaluation and hue as presented in Chapter 3 paragraph 3.3, is not a system that behaves linearly, but rather on a circular scale. Indeed, only similar colors can be compared. This descriptor could be assessed on an angular scale inspired by the chromatic circle. Only the descriptors Contrast, Size, Intensity and Quantity were assessed by the twelve observers.

For the descriptors Contrast, Size and Intensity, the observations generally follow the same trend. However, some difficulties in the ratings of the panels of the range Color (C_1 to C_8) can be noticed, probably due to the low contrast and fine particles in the formula. The descriptor Quantity is the one which was the most complicated to assess due to the high number of standards but also due to a lack in understanding of this descriptor. The evaluation of the quantity is based on a visual segmentation of the observation by distinguishing the background from the particles followed by an estimation of the number of segmented objects (particles). When the quantity of effect particles in the formula is very important, it is likely a borderline situation. Indeed, the human visual system and the brain are not able anymore to distinguish the background from the particles, when the brain assimilates the information received as a whole rather than segmenting sparkling dots from a background. This is probably the reason behind the difficulties encountered by the observers for the evaluation of the descriptor Quantity.

To refine the obtained results, a statistical analysis was performed in order to remove outliers. According to the method selected, 66 ratings out of 1564 (i.e. 4%) were considered

as “absurd”. After removal of these values, the “corrected” mean values for each panel on each standard were calculated to determine the mean observer. This mean observer will be used in the next chapter to define the physical texture descriptors based on ground truth data.

Chapter 7. Definition of physical texture descriptors

Contents

Now, established ground truth data describing automotive coatings via real perceived criteria and without any consideration of the formulation is available, enabling the evaluation of the effectiveness and relevance of any measurement made from color or grey scale images.

The visual aspect of an effect coating is linked to its composition and the optical and physical properties inherent to the type of pigments in the formula but also to the viewing conditions such as the type of light or the angle of observation. Chapter 4 was devoted to the presentation of different effect pigments used in automotive coatings. The properties of each family of pigments were discussed in detail considering, for example, the impact of the type of aluminum particles (corn flakes or silver dollar) on the sparkling effect. Chapter 5 is based on the definition of new texture descriptors. Six of them were identified: Size, Color, Contrast, Intensity, Quantity and Face-Flop. However, since the descriptor Face-Flop revealed high complexity during visual assessment, this descriptor was not considered (Chapter 5). The five remaining descriptors and their associated texture scales were used in Chapter 6 to elaborate sensorial profiles on test panels. However, after the visual assessment performed on the descriptor Color, this descriptor was not considered anymore in the following visual evaluation due to the difficulties in the interpretation of the obtained results.

The definition of physical texture descriptors was based on experience and knowledge of experts. These ground truth data will in the following be used to better define physical texture descriptors which must represent the texture descriptors previously highlighted and defined. The physical texture descriptors should be as close as possible to the texture descriptors obtained by expert definition to better match the results from visual assessments. However, before defining the physical descriptors by picture analysis, the acquisition conditions had to be adapted to the observations conditions.

7.1. Picture acquisition

An image acquisition device captures light information before converting it into an analog electrical signal: the video signal. This video signal is sampled, quantized and stored in a digital image (Trémeau et al., 2004). To analyze and process a digital image without any problems, it is extremely important to master the acquisition phase. Indeed, this phase conditions and sets the limits of the use of digital images.

7.1.1. System of acquisition

Certain similarities exist between the human visual system and a digital single-lens reflex camera. Similarly to the human visual system (see Chapter 2, paragraph 2.3), the camera is composed of a lens which focuses light before it passes through a diaphragm, the shutter, which would correspond to the pupil in the human eye. The resulting virtual image is inverted and projected onto a sensor, which is equivalent to the human retina. Each optical system responds differently to light. It is therefore necessary to fully characterize the camera selected before using it.

For the picture acquisition, a digital single-lens reflex camera was used, the Nikon D800. It offers a high resolution (7,360 x 4,912 pixels), high sensitivity and a wide dynamic range. The camera is paired with a Nikon AF-S FX NIKKOR 50mm f/1.4G lens with auto focus. This lens is considered sufficiently effective to get enough details at a distance of about 70 cm from the undeformed panel. The lens aperture varies between f/1.4 and f/16. The samples photographed contain effect pigments with a considerable amount of small and sparkly particles. The sharpness of the picture is an important parameter to be able to consider the entire sparkle phenomenon. In addition, the brightness of the picture is also an important parameter. As detailed later, the pictures are taken in a black room, so a dark environment. The setting selected must be in accordance with the illumination of the scene. The acquisition of images is based on three pillars: ISO, lens aperture and the shutter time. The distance between the camera and the scene can also have an influence on the results but to simplify the acquisition system, it will be fixed at 70cm (see explanations in Chapter 7 paragraph 7.1.3).

ISO sensitivity is a setting which brightens or darkens a picture. By increasing the ISO value, the pictures tend to become lighter (see Figure 7-1). ISO sensitivity is based on a more or less strong amplification of the input signal. The stronger the amplification, the more noise the picture shows. Native ISO, meaning without amplification, is set at 160 for the Nikon D800.

Figure 7-1: Impact of the ISO value on the brightness of the picture from (Mansurov, 2010a)

The lens aperture allows the control of the amount of light entering into the camera. Depending on the opening size, a blurry background results from a large aperture whereas a sharp picture is the result of a small aperture in addition to the global brightness of the picture, see Figure 7-2. When the diaphragm is closed (small aperture), little light enters into the camera, leading to a deep depth of field in the resulting picture. Conversely, when the diaphragm is opened (large aperture), a large amount of light enters into the camera and the pictures present a shallow depth of field.

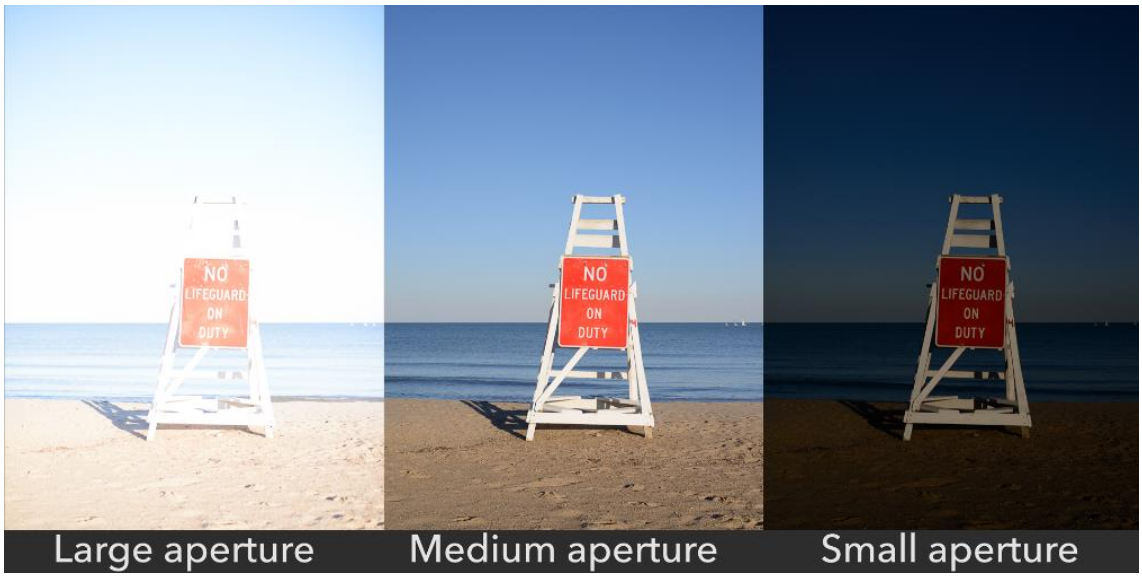

Figure 7-2: Impact of the lens aperture on the brightness and the blurry background of the picture adapted from (Mansurov, 2010c)

The shutter time is partly responsible for the global brightness of the picture. When the acquisition starts, the shutter opens to allow a full exposure of the sensor to the light passing through the lens for a predefined time. By setting up a long exposure time, the sensor accumulates a high quantity of light and the picture is bright. On the other hand, for a short exposure time, it is exposed to a low quantity of light and the picture is darker. This phenomenon is explained on Figure 7-3.

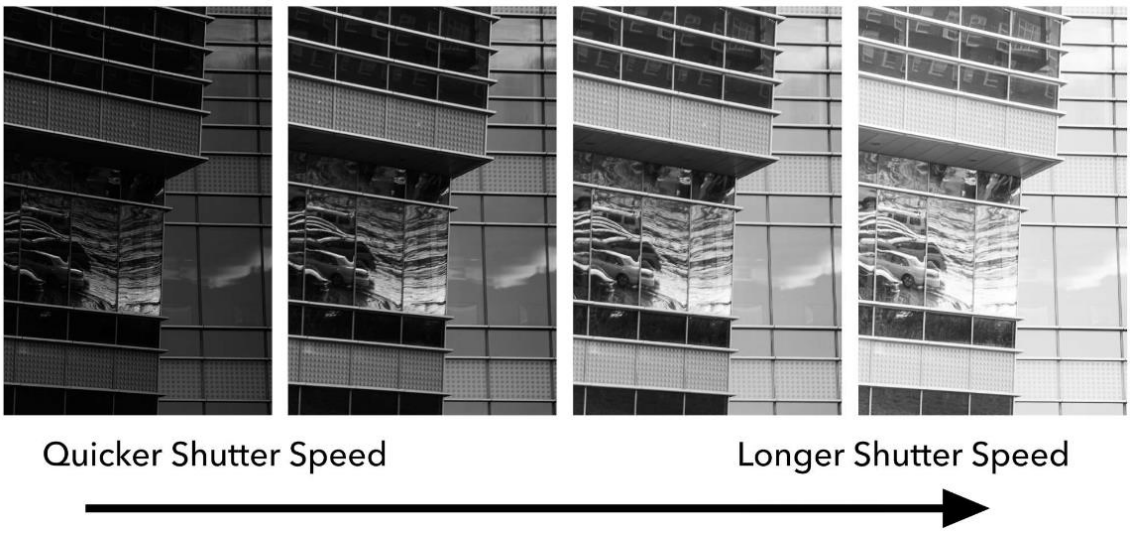

Figure 7-3: How image brightness changes with the exposure time from (Mansurov, 2010b)

To simplify the acquisition stage, two of these three parameters of the photography process were kept fixed: ISO 800 and f/6.3. In the present case, ISO 800 was preferred to maintain a balance between the amount of noise and the conservation of a high dynamic range without increasing the exposure time. Furthermore, as the photographic panel acquisition tends to be close to macro photography to catch the sparkles, the best overall sharpness and depth of field are obtained for f/6.3. This value corresponds to a physical aperture 6.3 times smaller than the focal length of the lens. In the present case, the samples photographed show the contrast of very bright areas (aluminum particles) on top of dark areas (background). The surface to be photographed thus presents a large dynamic range for the signal. Besides, the organization of the effect particles in the entire thickness of the coating film demands a deep depth of field. With a long exposure time, the bright areas are over-saturated and more details are obtained for the background. Inversely, for a shorter exposure time, the dark areas are under-saturated and the information coming from the bright pixels are better to interpret. The dynamic range of the digital single-lens reflex camera does not allow to acquire all the information. Table 7-1 summarizes the settings of the camera for the picture acquisition.

Table 7-1: Setting of the camera Nikon D800 for picture acquisition

Focal length	50 mm
ISO	800
Aperture	f/6.3
Time of exposure	To adapt

7.1.2. Calibration of the picture acquisition system

The definition of new physical texture descriptors is based on the applicability of these descriptors to match the texture effect perceived by the human eye; hence visual response is needed as input for their determination. As seen previously in Chapter 2, visual information is based on the retina sensitivity to light rays and subsequently radiometric signals. The aim here is to model the initial stage of the human visual response by using measurable parameters from images obtained with the Nikon D800. The acquisition system is therefore used as a color measuring device. It offers the same properties as the colorimetric expression of the optical signal considered as perceptively relevant. The main challenge consists in

giving the right weighting factor to each channel composing the image (Red, Green and Blue), so that the resulting picture contains colorimetric information that is representative to what is detected by the human eye. Color calibration is based on the matching of measured values (RGB) with the associated device-independent values (XYZ). By using a calibrated camera, it is furthermore possible to determine a map of the radiometric signals received by the sensor and to predict them with respect to the human visual system and its photoreceptors (Medina, 2016).

The RGB signals from the camera must be converted into XYZ representation. This transformation is known as camera characterization. It is important to recall here that RGB signals are generated for a specific camera with specific settings (ISO, aperture and time of exposure). The camera characterization must be performed for all sets of parameters used.

The camera characterization is not a linear transformation of RGB values into XYZ values and different methods exist such as the spectral characterization of camera sensors (Cheung et al., 2005, Laflaquiere et al., 1998) or the polynomial modeling (Hong et al., 2001). The polynomial modeling for the characterization of the Nikon D800 was chosen, which is expressed in equation (7-1).

$$\begin{pmatrix} X \\ Y \\ Z \end{pmatrix} = \begin{pmatrix} a_{11} & a_{12} & a_{13} \\ a_{21} & a_{22} & a_{23} \\ a_{31} & a_{32} & a_{33} \end{pmatrix} \times \begin{pmatrix} R \\ G \\ B \end{pmatrix} + \begin{pmatrix} v_1 \\ v_2 \\ v_3 \end{pmatrix} \Leftrightarrow \begin{pmatrix} X \\ Y \\ Z \end{pmatrix} = \begin{pmatrix} a_{11} & a_{12} & a_{13} & v_1 \\ a_{21} & a_{22} & a_{23} & v_2 \\ a_{31} & a_{32} & a_{33} & v_3 \end{pmatrix} \times \begin{pmatrix} R \\ G \\ B \\ 1 \end{pmatrix}$$

(7-1)

$$\begin{pmatrix} X \\ Y \\ Z \end{pmatrix} = C \times \begin{pmatrix} R \\ G \\ B \\ 1 \end{pmatrix}$$

With *XYZ, colorimetric representation*
RGB, signals recorded by the camera
a_{ij}, *coefficients of the color calibration matrix*
v_i, *contribution of the lighting conditions*
C, coefficient of the color calibration matrix

As explained by (Medina, 2016), the camera characterization is based on the determination of a linear relationship between RGB and XYZ values for a set of N colors. By considering H, a “N x 3” matrix corresponding to the XYZ values η_i of a color sample, and R, a “N x 3” matrix corresponding to the associated RGB values ρ_i, the equation (7-1) can be adapted as in (7-2).

$$\begin{pmatrix} X_1 & Y_1 & Z_1 \\ X_2 & Y_2 & Z_2 \\ X_3 & Y_3 & Z_3 \\ \dots & \dots & \dots \\ X_N & Y_N & Z_N \end{pmatrix} = \begin{pmatrix} R_1 & G_1 & B_1 & 1 \\ R_2 & G_2 & B_2 & 1 \\ R_3 & G_3 & B_3 & 1 \\ \dots & \dots & \dots & \dots \\ R_N & G_N & B_N & 1 \end{pmatrix} \times \begin{pmatrix} a_{11} & a_{12} & a_{13} & v_1 \\ a_{21} & a_{22} & a_{23} & v_2 \\ a_{31} & a_{32} & a_{33} & v_3 \end{pmatrix}^T$$

(7-2)

$$H = RC^T$$

With *C coefficient of the color calibration matrix*

The coefficient of the color calibration matrix, C, should be defined to minimize the color differences. As explained by (Hong et al., 2001), the XYZ space is not a uniform color space as the CIElab can be. The non-linearity of this color space can however be overcome by using the least-square fitting approach to define the color calibration matrix, C, see equation (7-3).

$$C = (R^T \times R)^{-1} \times R^T \times H \quad (7\text{-}3)$$

With R^T*, transpose matrix of R*
R^{-1}*, inverse matrix of R*

In order to simplify the camera characterization stage, an X-Rite ColorChecker® Classic was used. As can be seen in Figure 7-4, it is made of a 4 x 6 array of patches with the third row reserved for the additive and subtractive primaries and the fourth row dedicated to the grey scale. According to (McCamy et al., 1976), each patch is described by its colorimetric measurements CIE1931 xyY and its Munsell notation. One of the main features is that the patches are matte and thus display a Lambertian behavior.

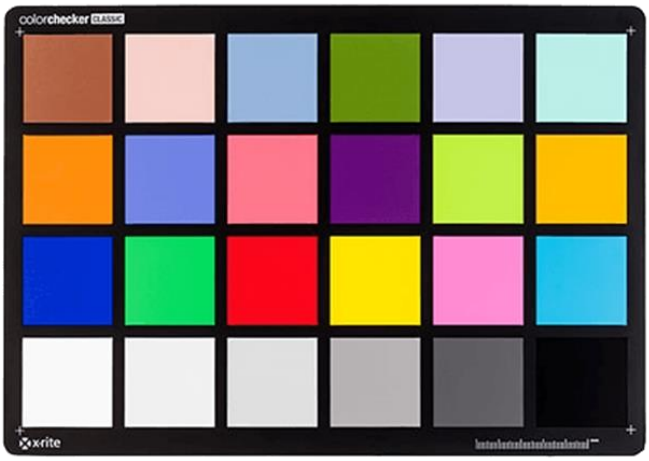

Figure 7-4: X-Rite ColorChecker® Classic from (X-Rite, 2018a)

The characterization process consists of two steps, colorimetric and radiometric, which are both performed with the same lighting system. For the colorimetric step, a raw picture of the X-Rite ColorChecker® is taken with the camera for a defined set of parameters (ISO sensitivity, aperture and exposure time). Once this step is done, the camera is replaced by a spectroradiometer (Konica-Minolta CS-2000) to measure the radiance received by the CCD sensor for each patch. By this process, a correspondence between RGB and XYZ values is established and the coefficients of the color calibration matrix are determined. The camera was characterized for ISO 800, f/6.3 and ten exposure times from 1/10s to 5s. ISO sensitivity, aperture and exposure time influence the amount of light transmitted to the sensor each time we shoot.

7.1.3. Presentation of the assembly and lighting systems used for picture acquisition

After the camera characterization had been performed for different settings, the picture acquisition phase was planned to get as close as possible to the conditions of the visual assessments. Indeed, as presented in Chapter 4, the lighting system is a critical point. For

example, by considering the descriptor Intensity, if the amount of light is not adequate, the relative intensity coming from the effect particles will not be sufficient and this can lead to a wrong characterization of the perceived effect. On the other hand, by using a high intensity for the lighting system, the evaluation of other descriptors such as size, will not be satisfactory due to the interferences linked to the reflective intensity coming from the particles.

To define physical texture descriptors, the considerations are based on ground truth data coming from visual assessments of texture by experts. To that end, the lighting conditions during visual assessments needed to be reproduced as accurately as possible for the taking of the images. As explained previously, a diffuse system and a directional lighting system needed to be used depending on the descriptor assessed.

For both geometries, the light system was provided by two direct Solux halogen bulbs. These lights are used to simulate solar daylight with incandescent lamps at 4 700K with a cone of illumination of 36 degrees. The spectral power distribution of the Solux bulbs is shown in Figure 7-5 and was measured with a Konica-Minolta CS-2000 spectroradiometer with a 1-degree angle.

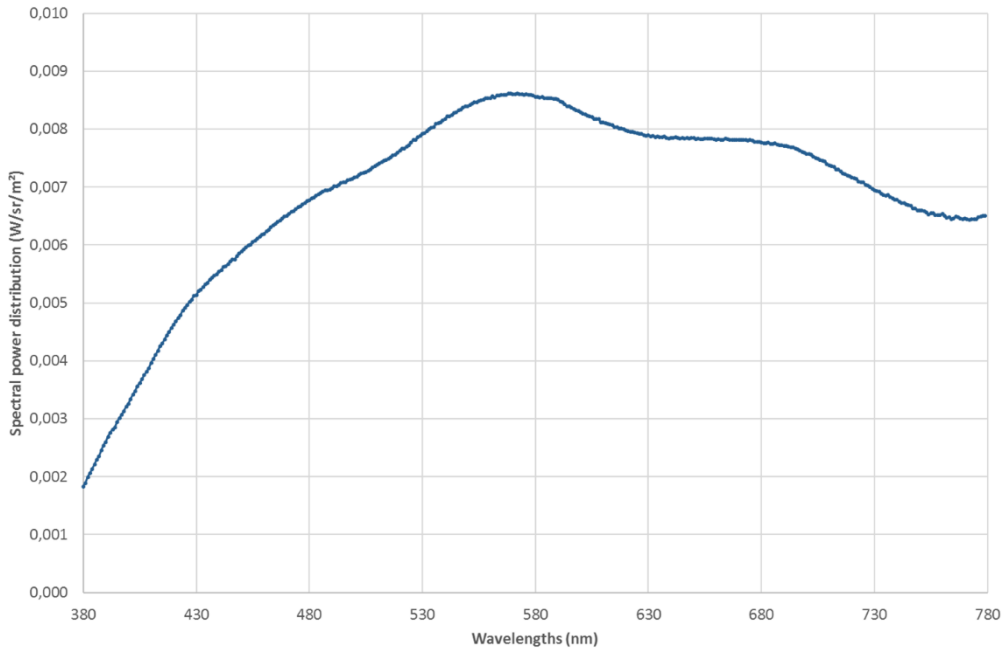

Figure 7-5: Spectral power distribution of one Solux incandescent lamp (36°, 12V, 50W, 4 700K) measured with a Konica-Minolta CS-2000 spectroradiometer with a 1-degree angle

The distance panel-camera was set at 70 cm. Indeed, the Nikon AF-S FX NIKKOR 50mm f/1.4G lens used is considered as sufficiently effective to get enough details without distorting the panel photographed. The panels on which all the formulations were sprayed measured 10 cm by 14.8 cm (width x height). The picture size is 7,360 x 4,912 pixels and the panel photographed is imaged with a total size of 2,400 x 1,600 pixels. With this equivalence cm-pixel, the size of one pixel is deduced to be 60 µm. In addition, at a distance of 70 cm, the angular resolution of an average human eye is approximately equal to 1 minute of angle so 1/60°. By using trigonometric relations detailed in Chapter 2 Figure 2-26, the minimum size of one element to be discernible at a distance of 70 cm is 200 µm, which is

roughly equivalent to three pixels. In this configuration, the elements smaller than 3 pixels in size cannot be seen by the human eye.

The diffuse lighting condition was ensured by two reflective umbrellas with Solux lamp oriented towards it. The purpose was to expand the light source and to reflect the incident light in different directions. As the power of the Solux bulbs is limited and to improve the global luminance of the scene and thereby to reduce the time of exposure during the acquisition phase, two umbrellas were set up. Many trials were needed to find the right inclination, orientation, height and distance of the umbrellas to the panels to obtain a homogeneous lighting and simultaneously avoiding the shadow of the camera. The final arrangement is shown in Figure 7-6. The camera is slightly shifted compared to the normal angle to avoid the shadow of the camera or its reflection in the glossy clearcoat of the painted panel. The two reflective umbrellas are located at -20° and 20°, respectively.

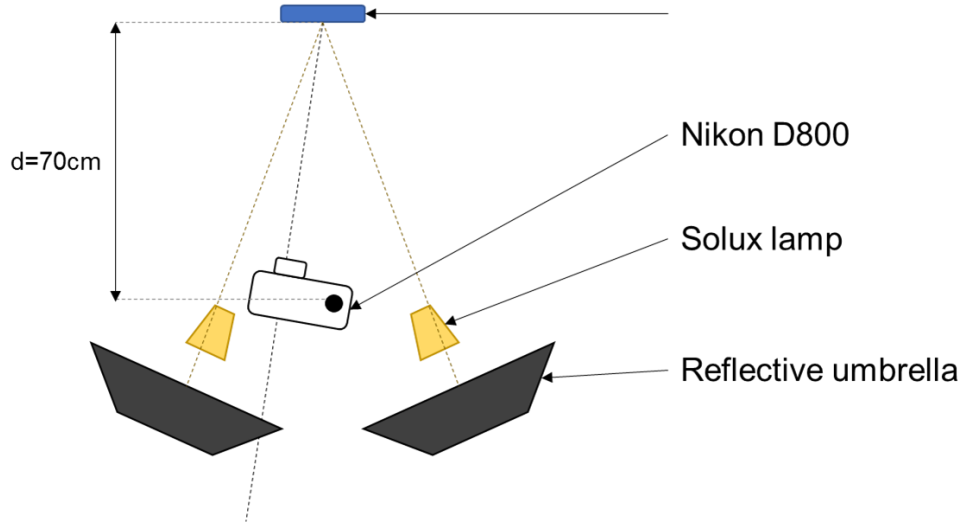

Figure 7-6: Schematic arrangement of the system used to create diffuse lighting conditions

Obtaining the ideal directional lighting conditions turned out to be more complicated than for the diffuse mode. The use of reflective umbrellas led to a loss of lighting intensity and the reflective intensity coming from the effect particles was almost inexistent. Besides, the panels, once photographed, showed oversaturated or undersaturated areas. To avoid this lack of information, a collimator was used to narrow the beam of waves and to convert the light rays coming from the bulb into parallel ones. The collimator was created by using a 1-meter black matte tube to ensure an almost perfectly collimated beam at its end. Besides, to facilitate this alignment, a honey-comb louver was fixed on the bulb to reduce stray light. The final set-up is shown in Figure 7-7. The Solux bulb and the collimator are placed in front of the panel to be photographed at 0° compared to the normal angle while the camera is located at 15° and at a distance of 70cm. The camera was slightly shifted from the normal angle to avoid the shadow of the camera on the panel.

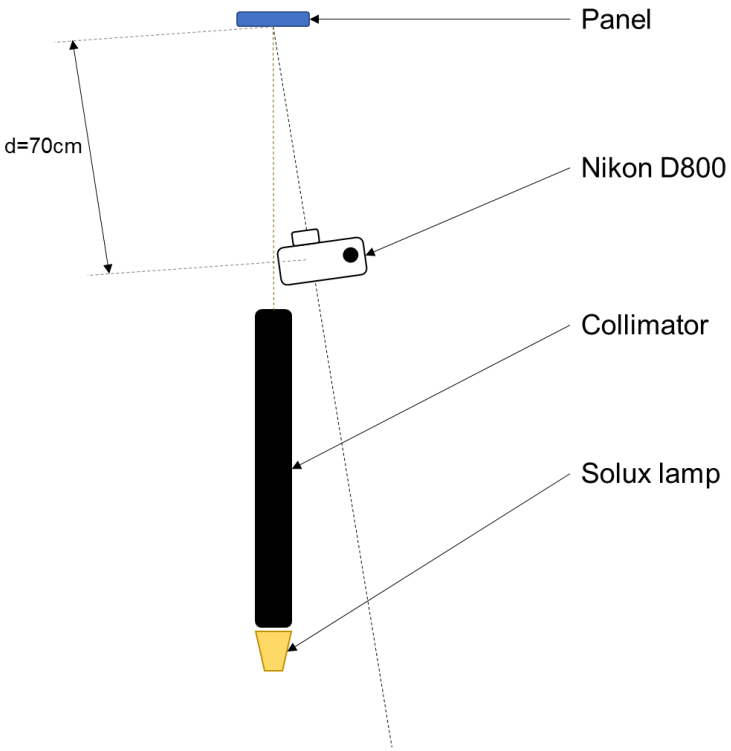

Figure 7-7: Schematic arrangement of the system used for direct lighting conditions

7.1.4. Picture acquisition

Once the assembly and the lighting systems were installed in the appropriate arrangement, the 34 standard panels used for the texture scale creation were photographed. As explained previously in the presentation of the system of acquisition and summarized in Table 7-1, two of the three parameters were fixed: ISO 800 and aperture f/6.3. The only variable is the time of exposure according to the global lightness of the panel and also to the percentage of effect particles in the formula. Indeed, the darker the panel is, the longer the exposure time will have to be to avoid under-exposed areas. The impact of effect particles is mainly visible for direct lighting conditions due to the light reflected by them. The standards exhibit strong contrasts combining dark areas (the background) and light areas (the effect particles which act like tiny mirrors). The technique of bracketing[1] was used by photographing the same surface several times, just changing the exposure time. By lengthening the exposure time, the lighter pixels are over-saturated while the background is well exposed. Inversely, for a shorter exposure time, the dark areas are under-saturated and the effect particles are well exposed. A subsequent brief picture analysis led to a good compromise between the data quality of the background and the effect particles in the selection of one picture by panel.

In order to establish a link between panel characteristics and the selection of the adequate exposure time, the panels were measured with a portable spectrophotometer, the MA-T6 developed by X-Rite (see Chapter 4 paragraph 4.2.4). Out of the six angles for color measurement, the 45° angle was preferred. Indeed, solid colors are measured at this angle.

[1] Bracketing: technique used in photography to take several pictures of the same scene by using different camera settings.

Using this angle also leads to the avoidance of a high contribution of reflected light of the effect particles which are mainly visible at low angles (-15°, 15° or 25°).

For diffuse lighting conditions, the evolution of the time of exposure depending on the lightness value, L*(45°), was studied and is plotted in Figure 7-8. Six exposure times were used: 5s (in grey), 4s (in red), 3s (in orange), 2s (in green), 1s (in blue) and 1/1.3s (in purple).

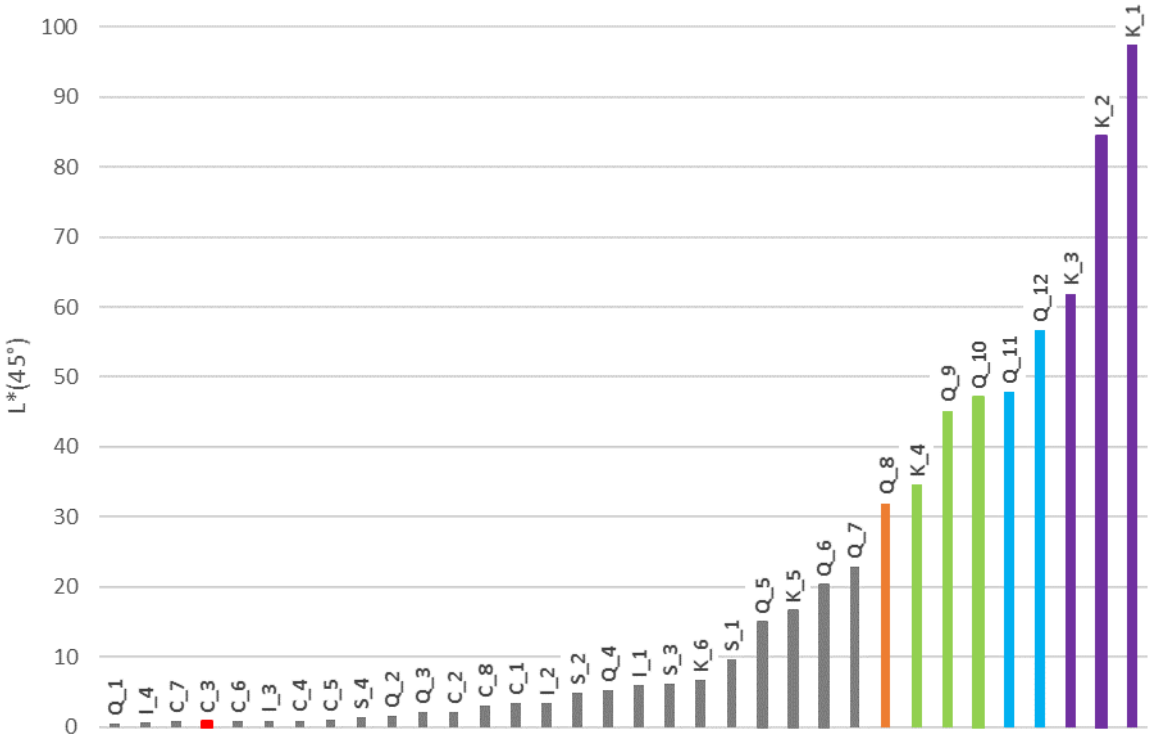

Figure 7-8: Evolution of the exposure time in dependence of the lightness value L(45°) for the 34 standard panels created for the texture scale*

According to the plot in Figure 7-8, an indication of the exposure time to select can be formulated as summarized in Table 7-2.

Table 7-2: Summary of the exposure time for picture acquisition with Nikon D800, ISO 800 and f/6.3 for diffuse lighting conditions

L*(45°)	Exposure time
< 25	4s or 5s
25 to 35	3s
35 to 45	2s
45 to 60	1s
> 60	1/1.3s

Direct lighting conditions were arranged in a way to obtain a high visible contribution of the effect particles. However, in contrary to what was decided for diffuse lighting conditions, it is not possible to identify a trend with either the quantity of effect particles in the formula or the lightness values. The bracketing method was used, changing the exposure time and a

brief subsequent picture analysis allowed for selection of the right exposure time and hence the right picture.

Once all panels had been photographed, the RGB images were converted into XYZ by using the calibration of the camera presented in Chapter 7 paragraph 7.1.2, for the corresponding exposure time. The XYZ cartographies are the ones used for picture analysis.

7.2. Basics of picture analysis

This paragraph is dedicated to a brief description of the image analysis concepts which are used for the determination of physical texture descriptors. The reader is referred to the cited sources for a better understanding of the filters and algorithms presented in the following.

A picture is a two-dimensional representation of a three-dimensional scene. From a mathematical point of view, it is a representation of the two-dimensional signal in a matrix NxM where N represents the width of the picture measured in numbers of pixels and M represents the height. Each pixel can have an intensity value between 0 (black) and 65 535 (white); the work is performed on 3x16 bit images with real values (X, Y and Z are real positive numbers). The first step carried out before starting the construction of the X, Y, Z cartographies is the thresholding of irrelevant values on the R, G and B channels. Indeed, to limit the impact of outliers, values below 2 000 and those above 60 000 were considered as irrelevant and only pixels of intensities between 2 000 and 60 000 were considered. Indeed, this range could be considered as the linear part of the digital single-lens reflex camera transfer function without noise (below 2 000) and over-saturated pixels (over 60,000). The resulting R, G and B images were then converted into X, Y and Z images according to the corresponding calibration. Finally, to avoid any falsely negative value generated by the calibration, a second thresholding is performed on the X, Y and Z images by applying a mask to return negative values to 0.

7.2.1. Filtering operations

Once the thresholding was performed, it was necessary to highlight the “useful” information contained in the picture and to reduce or eliminate the “useless” information. The “useless” information represents for example problems of inhomogeneity in the lighting conditions or noise during the acquisition. Before extracting objects from images, a preliminary step consists of performing a filtering operation on the picture. A large number of possible filters exists; they can be classified according to three categories: linear, morphological or adaptative (Coster and Chermant, 1989). Only low-pass and high-pass filtering are briefly explained in the following.

The low-pass filter is a linear system which does not modify the frequencies below a selected cutoff frequency. However, it attenuates or excludes the frequencies greater than the cutoff frequency, D_O. Abrupt changes in signal intensities linked to noise, dust or effect particles are attenuated or eliminated. However, this filtering operation leads to a picture

blurring, making it more difficult to extract the objects accordingly. The high-pass filter is the exact opposite of the low-pass filter; it attenuates low frequencies and enhances high frequencies. In a non-uniform picture with small dots of high frequencies, a pixel brighter than its neighbors is enhanced. However, high-pass filtering amplifies the noise.

7.2.2. Segmentation

Image segmentation is one of the most important operations in picture analysis. Image segmentation divides the image into “homogeneous” regions. Thus, the segmentation of an image makes it possible to find forms and areas sharing same properties (Dupas, 2009). The challenge is to define the so-called homogeneity criteria to achieve the targeted segmentation.

Many segmentation algorithms exist and they are subdivided into two categories: manual and automatic segmentation algorithms. For the manual method, the algorithm needs to have the number of classes to create as an input before performing the segmentation by determining the most appropriate threshold values. This determination can be based on for example the maximization of the interclass variance (Otsu, 1979). Automatic methods determine the number of classes and the associated threshold values (Jourlin et al., 2013).

A segmentation into two classes results in a binary image. To binarize a grey-scale image is equivalent to converting it to a black and white image. This two-class segmentation is performed with only one threshold value where all pixels of lower intensity than a determined threshold value are set to 0 while the others are set to 1. The two classes are called “background” for the pixels lower than the threshold value and the “foreground” for pixels greater than the threshold value. The difficulty of the segmentation lies in the determination of the threshold value to isolate the background on one side and the foreground on the other side. An example of two-class segmentation is presented in Figure 7-9.

Figure 7-9: Example of a two-class segmentation based on pixel intensity: (a) original picture; (b) binary picture with a threshold value of 150 from (Dupas, 2009)

In the case of color images, the thresholding leads to an issue if for example the blue sky in Figure 7-9 has to be isolated. First, the color criteria must be described, meaning the color subspace to be extracted, hoping that it corresponds to an identifiable subset in the representation mode used (ex. RGB).

7.2.3. Dilation, erosion, opening and closing

Mathematical morphology is the study of objects according to their shape, their size, the relations to their vicinity, their color or their level of greyscale. The transformations proposed are undertaken at different stages of image processing (filtering, segmentation, measurements or texture analysis) and thus provide tools for pattern recognition.

First, it is necessary to define, whether two pixels are part of the same object. Connectivity rules are used corresponding to the 4 or the 8-connectivity as shown in Figure 7-10. The 4-connected pixels rule considers the four nearest pixels while the 8-connected pixels rule includes also the four-corner-neighboring pixels. According to the connectivity rule selected, a different number of objects on a picture is defined.

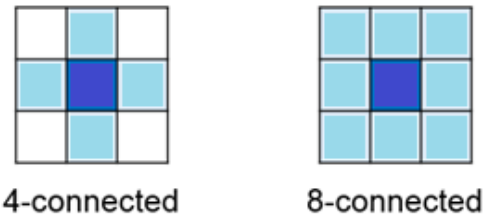

Figure 7-10: Example of vicinity pixels with the 4-connected and 8-connected pixels

The dilation δ(X) and the erosion ε(X) of a binary image X by a structuring element S are defined in equation (7-4).

$$\delta(X) = \{x + s | x \in X \wedge s \in S\} = X \oplus S$$
$$\varepsilon(X) = \{x | \forall s \in S,\ x + s \in X\} = X \ominus S \qquad (7\text{-}4)$$

With $\delta(X)$, *dilation*
$\varepsilon(X)$, *erosion*
X, binary image
S, structuring element

Dilation and erosion are based on a hit-or-miss approach (Maintz, 2005). For a dilation, any point of the image for which the structuring element intersects, the object is included in the foreground of the resulting image. For an erosion, only the points of the image for which the structuring element is totally included in the object are preserved in the foreground of the image. These two morphological operations are explained in Figure 7-11. The image (a) is the original binary picture where a 3x3-square structuring element is used for the dilation (b) and the erosion (c). The grey pixels correspond to the dilated or the eroded part. By dilation, the area of the foreground increases (white + grey) while it decreases by erosion (only white).

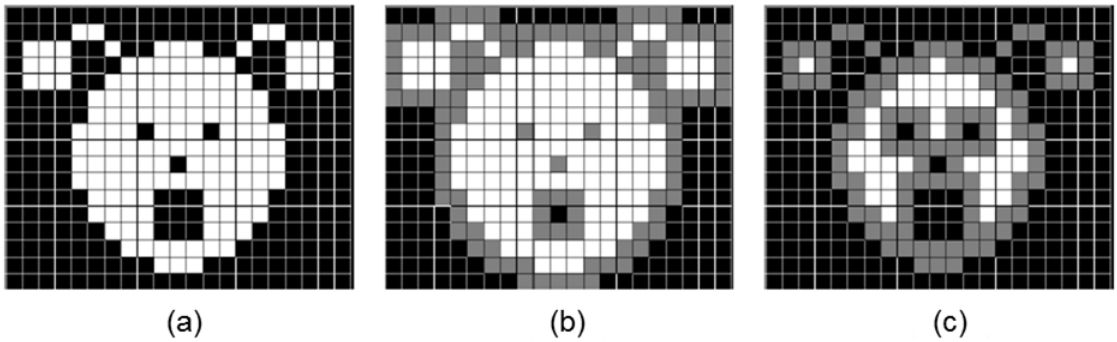

Figure 7-11: (a) Original image where the foreground is in white and the background in black; (b) dilated image where the grey pixels are the result of the dilation with a 3x3-square structuring element; (c) eroded image where the grey pixels are the result of the erosion with a 3x3-square structuring element from (Couka, 2015)

Applied on greyscale images, the erosion will consist in assigning the lowest values of its neighbors to a pixel while the dilation will consist in assigning the highest values of its neighbors to a pixel. The dilation widens the peaks while the erosion planes them.

After a dilation or an erosion, it is possible to perform morphological filtering operations, the opening, γ, and the closing, Φ. The opening corresponds to an erosion followed by a dilation while the closing is the exact opposite of the opening, so a dilation followed by an erosion, as detailed in equation (7-5).

$$\gamma(X) = \delta(X) \circ \varepsilon(X)$$
$$\phi(X) = \varepsilon(X) \circ \delta(X) \qquad (7\text{-}5)$$

With $\delta(X)$*, dilation*
$\varepsilon(X)$*, erosion*
$\gamma(X)$*, opening*
$\phi(X)$*, closing*

These two morphological filtering operations are explained in Figure 7-12. The image (a) is the original binary picture, same as in Figure 7-11, where a 3x3-squared structuring element is used for the opening (d) and the closing (e). The grey pixels correspond to the opened or the closed part. By opening, the area of the foreground decreases (only white) while it increases by closing (white + grey).

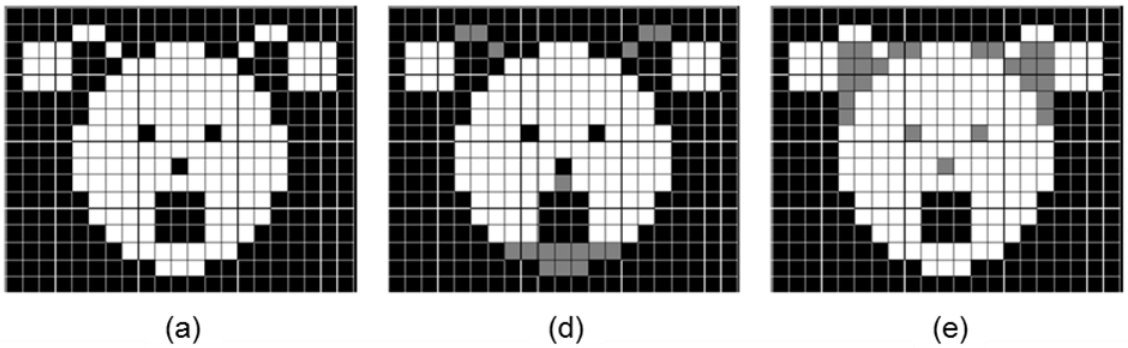

Figure 7-12: (a) Original image where the foreground is in white and the background in black; (b) opened image where the grey pixels are the result of the opening with a 3x3-square structuring element; (c) closed image where the grey pixels are the result of the closing with a 3x3-square structuring element from (Couka, 2015)

As the opening filtering operation tends to remove objects which are smaller in size than the structuring element, this operation could be considered for the size determination of segmented objects in an image. The procedure, known as granulometric analysis, is presented by (Maintz, 2005) and detailed in Figure 7-13.

1. Open the image with a structuring element of a certain size.
2. Do a size measurement on the current image, *e.g.*, the area of all object pixels, or the sum of all grey values.
3. Enlarge the structuring element.
4. Repeat from 1 until the opening removes the entire image.

Figure 7-13: Procedure for the size determination by successive openings from (Maintz, 2005)

7.2.4. Histogram analysis and statistical measurement

An image can be described using the statistical distribution of lightness. The number of pixels at each intensity level is then plotted as shown in Figure 7-14.

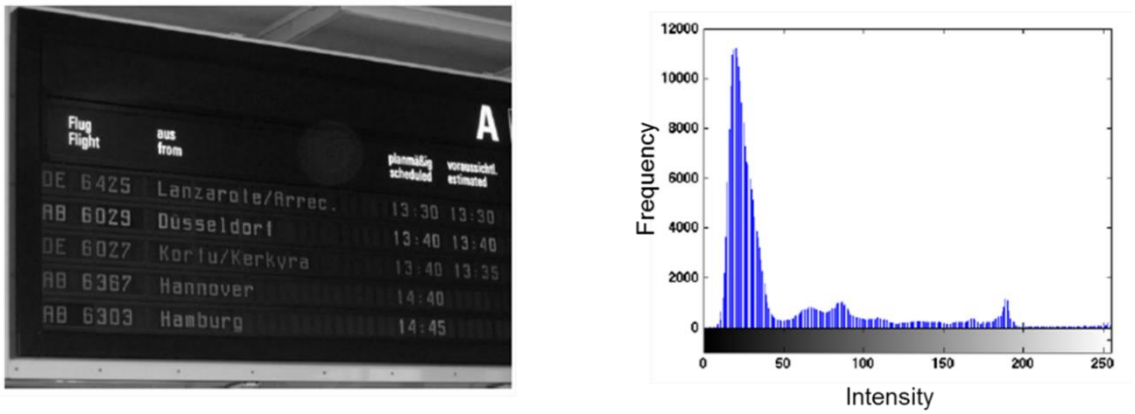

Figure 7-14: Flight display panel (left) and its associated histogram (right) from (Marques, 2011)

The histogram gives information on the lightness level of the image with the dominance of bright (close to 255) or dark (close to 0) pixels, hence the minimum or the maximum intensity values. For example, in Figure 7-14, the picture is mainly dark, the histogram is then shifted on the left side, so in the dark area. Moreover, the shape of the histogram holds information as to the existence of different classes of intensities by examining the local maxima.

In addition to the histogram, it is also possible to determine statistical parameters from the frequency of occurrence of each intensity value, the moments. There are four moments: mean, variance (and/or standard-deviation), skewness and kurtosis. Apart from these moments, the minimum and the maximum intensities are also determined as well as the quartiles or the mode values. The mode is the intensity value which presents the most occurrence. Median, or second quartile Q_2, can also be deducted. It corresponds to the intensity of the middle intensity value. Half of the pixel intensities are less than the median

intensity value and the other half greater. The first and the third quartiles, Q_1 and Q_3, represent respectively one fourth or three fourth of the pixels.

Mean is known as the first moment. It is one of the basics in statistics which represents the value that each pixel would have if the distribution was equitable. Mean is calculated according to equation (7-6).

$$\mu = \frac{\sum n_i X_i}{\sum n_i} \tag{7-6}$$

With *μ, mean value*
n_i, number of pixels for i
X_i, intensity values for i

The second moment is the variance. It measures the distribution around the mean of the pixels. From the variance value, the standard deviation can be deducted as its positive square root. A low standard deviation indicates a tendency for the pixels to approach the mean intensity value. A high standard deviation indicates a strong disparity of the pixel intensity values (Kumar and Gupta, 2012). The variance is calculated according to equation (7-7).

$$\sigma^2 = \frac{\sum (n_i X_i - \mu)^2}{\sum n_i} \tag{7-7}$$

With *σ², variance value*
μ, mean value
n_i, number of pixels for i
X_i, intensity values for i

The skewness is known as the third moment. It measures the asymmetry of the probability distribution of the pixels and can be positive, negative or null. Its calculation is given in equation (7-8).

$$\gamma = \frac{\sum (n_i X_i - \mu)^3}{\sum n_i} \tag{7-8}$$

With *γ, skewness value*
μ, mean value
n_i, number of pixels for i
X_i, intensity values for i

In a graphic representation, for a negative skewness value, the tail on the left side of the curve is longer than the one on the right side and the peak lies shifted to the right. Inversely, for a positive value, the tail on the right side of the curve is longer and the peak is shifted to the left side. If the skewness value tends to zero, the values are equally distributed on both sides of the maximum of the curve. All three cases are presented in Figure 7-15. It is also possible to estimate the sign of the skewness value according to the mean, median and mode values as detailed in Figure 7-15 and summarized in Table 7-3.

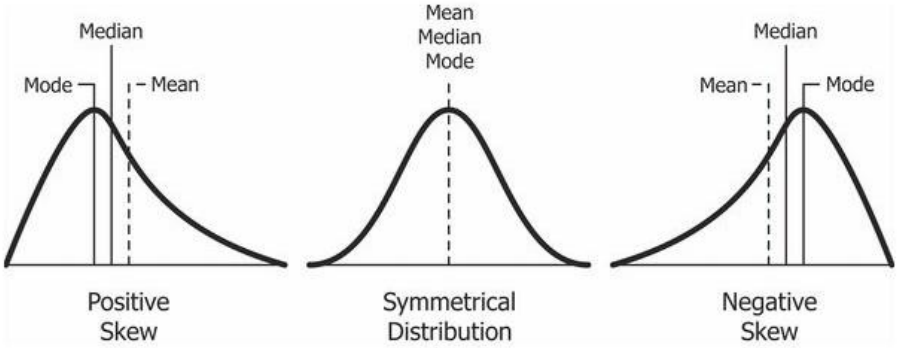

Figure 7-15: Example of the probability distribution according to the skewness value based on the mean, the median et the mode values from (Jain, 2018)

Table 7-3: Sign of the skewness value according to the mean, median and mode values

Mean = Median = Mode	γ = 0
Mean < Median < Mode	γ < 0
Mode > Median > Mean	γ > 0

The Karl Pearson's (KP) and the Bowley's (B) coefficients of skewness are also used to determine the skewness value with either mean, mode and standard deviation or quartiles values (Nagla, 2014). The formulas are given in equation (7-9).

$$KP = \frac{Mean - Mode}{Standard\ Deviation}$$
$$B = \frac{Q_3 + Q_1 - 2\,Q_2}{Q_3 - Q_1} \qquad (7\text{-}9)$$

The fourth moment is the kurtosis. It is used to estimate the flat or peaked shape of the histogram but also the outliers present in the distribution. The calculation is given in equation (7-10).

$$\kappa = \frac{\sum(n_i \times X_i - \mu)^4}{\sum n_i} \qquad (7\text{-}10)$$

With *κ, skewness value*
μ, mean value
n_i, number of pixels for i
X_i, intensity values for i

For a kurtosis value close to 3, the histogram follows a normal distribution (called mesokurtic). For a kurtosis value less than 3, the histogram displays a sharp peak with short tails (called platykurtic). For a kurtosis value greater than 3, the histogram presents a flatter top and wider tails with a high probability to encounter outliers (called leptokurtic). The three curve shapes are detailed in Figure 7-16.

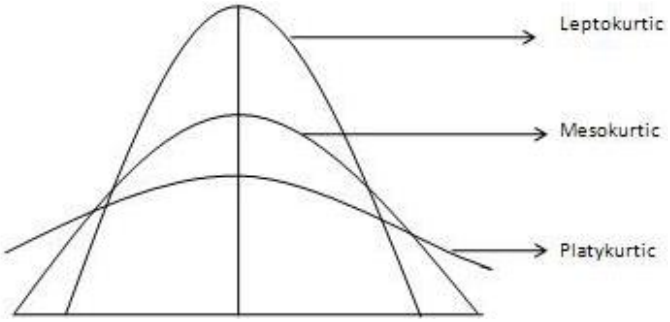

Figure 7-16: Example of the shape of the histogram according to the kurtosis value from (Jain, 2018)

In the following, three histograms corresponding to the associated pictures of three references of the descriptor Contrast (see Chapter 5, Table 5-12), K_2 / Very Low, K_4 / Intermediate and K_6 / Very Strong are considered, see Figure 7-17.

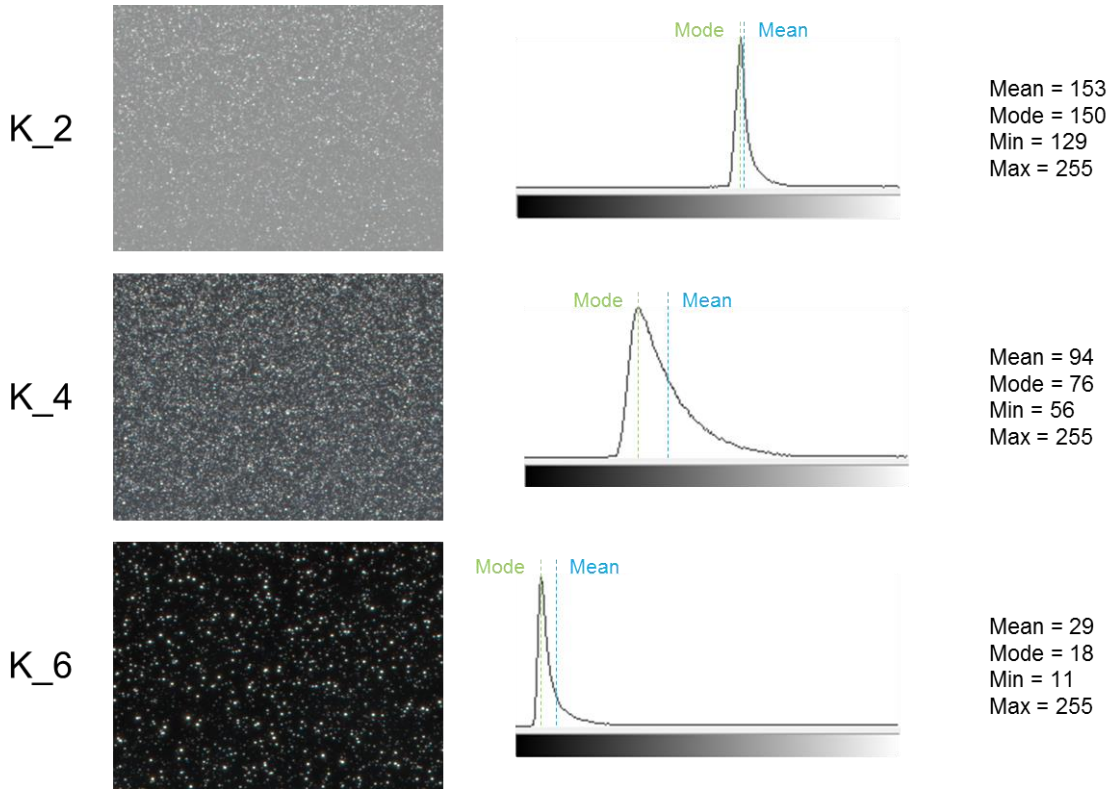

Figure 7-17: Histogram based pictures coming from MA-T6 measurements for three references from the range Contrast: K_2, K_4 and K_6

The histograms are based on pictures taken with the spectrophotometer MA-T6 under directional geometry. From these three histograms, we can assume a monomodal transformation. The quantity of sparkle points is negligible compared to the background and this population is not visible on the histogram. We can assume a positive skewness linked to the right tail of the curve.

7.3. Picture analysis for the determination of physical texture descriptors

The determination of physical texture descriptors is based on picture analysis. The objective is to match the results obtained by the elaboration of sensorial profiles on the visual descriptors to some physical texture descriptors. The results from the visual assessments are the basis of this determination.

As for the visual assessment, the determination of the physical texture descriptors is based on the 34 standards used to define the texture scale. All of them were photographed with the Nikon D800, ISO 800, f/6.3 at different exposure times. The best picture, meaning not too over or under-saturated, was then selected. The respective selected exposure times for each standard are gathered in Table 7-4 for both diffuse and directional lighting conditions.

Table 7-4: Exposure time selected for diffuse and directional lighting conditions for the 34 standards from texture scale

Panel Name	Diffuse	Direct	Panel Name	Diffuse	Direct
S_1	5s	1s	**K_6**	5s	1s
S_2	5s	1s	**I_1**	5s	1s
S_3	5s	1s	**I_2**	5s	1s
S_4	5s	1s	**I_3**	5s	1s
C_1	5s	2s	**I_4**	5s	4s
C_2	5s	2s	**Q_1**	5s	1s
C_3	4s	5s	**Q_2**	5s	1s
C_4	5s	5s	**Q_3**	5s	1s
C_5	5s	5s	**Q_4**	5s	1s
C_6	5s	5s	**Q_5**	5s	1/2s
C_7	5s	5s	**Q_6**	5s	1/4s
C_8	5s	1s	**Q_7**	5s	1/4s
K_1	1/1.3s	1/8s	**Q_8**	3s	1/6s
K_2	1/1.3s	1/4s	**Q_9**	2s	1/8s
K_3	1/1.3s	1/2s	**Q_10**	2s	1/8s
K_4	2s	1/2s	**Q_11**	1s	1/8s
K_5	5s	1/2s	**Q_12**	1s	1/10s

After the first trials on the visual descriptors, the viewing and lighting conditions were standardized (see Chapter 5, Table 5-9). In order to be as representative as possible of the visual assessment, the five physical texture descriptors were then determined with the same observation settings. Like this, the descriptors for Contrast, Size and Quantity should be defined from diffuse pictures while those for Intensity and Color come from directional pictures. However, Color was not studied due the non-evaluation during the visual assessment part.

7.3.1. Selection and pretreatment of the region of interest

The lighting systems used for picture acquisition were set up to represent the conditions used for the observations made by the experts. However, the lighting of the panels is not uniform. First, to reduce the total weight of the texture scales, the standards were sprayed

on cardboard sheets. With the humidity of the paint during the application process, they slightly crinkled in some places. Apart from that, as the position of the camera was slightly shifted to avoid its reflection or shadow in the glossy clearcoat of the panel, a non-uniformity at the acquisition stage is noticeable. For directional lighting, the size of the lighted circle on the panel is limited and does not cover the entire panel due to the collimator diameter. In Figure 7-18, an example of a raw picture in which a crinkle is visible on the left side of the panel (see green arrow) and the center of the lighted circle is located on the right side (see red cross) is shown. Also, the shadow of the camera is visible on the panel holder on the extreme right side of the picture (in white).

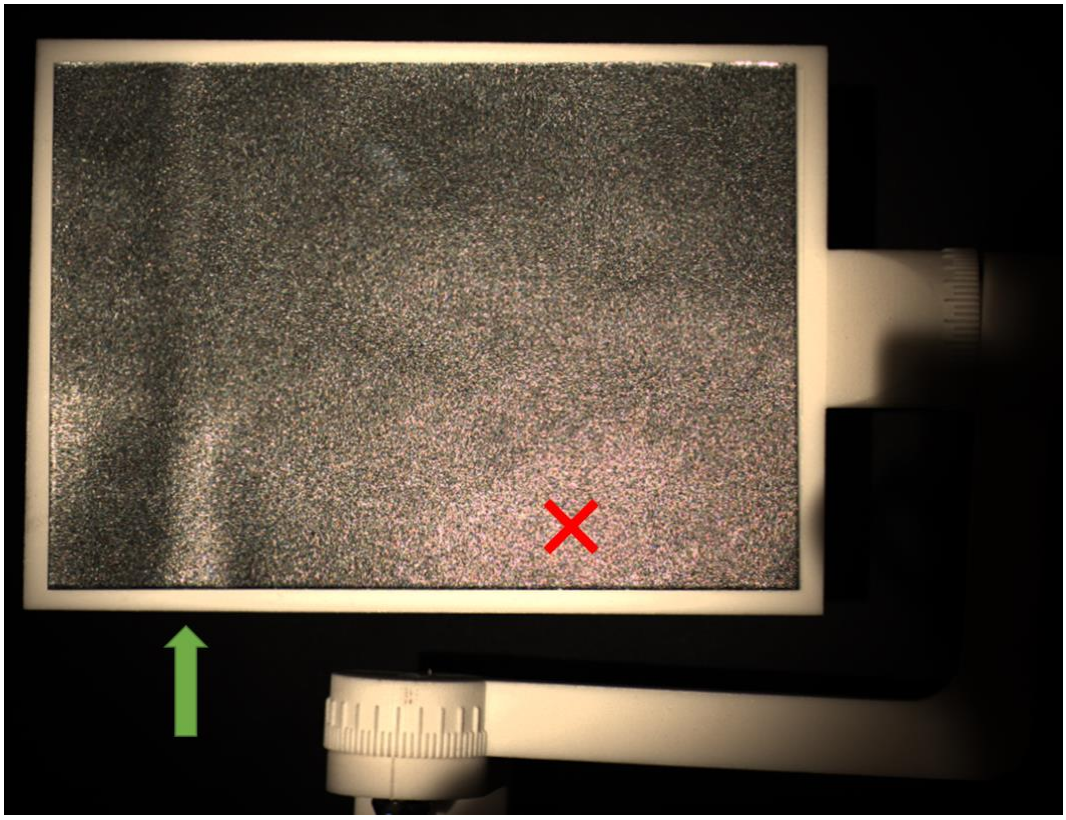

Figure 7-18: Non-uniformity of the lighting conditions explained by a photography of the panel K_5 taken with the Nikon D800, ISO 800, f/6.3 and an exposure time of 1/2s for directional lighting. The green arrow indicates the crinkle and the red cross the center of the lighted circle.

A panel holder was designed to guarantee the same position and the same angle for all panels photographed. From the raw picture, a region of interest (ROI) was extracted at the exact same place for all panels to obtain a picture large enough to be as representative as possible of the panel and to ensure a relative homogeneity and reproducibility in the lighting conditions. The ROI selected represents an area of 701 pixels in width and 301 pixels in height, accordingly 211 001 pixels in total.

Despite this careful approach, it was necessary to correct the lighting of the panel. Successive opening and closing filtering operations were applied to the ROI. The resulting image is a kind of luminance cartography at as small a scale as the sparkling effect. It is then subtracted from the original image, pixel by pixel. An example of this pretreatment stage is explained in Figure 7-19 with the ROI of panel K_5 under directional lighting. In Figure 7-19 (a), the brighter pixels represent the effect particles. One can distinguish a better illumination

slightly shifted to the right of the middle of the image. To improve lighting, the ROI is subject to an alternation of opening and closing filtering operations with a square of size 3. Twenty iterations are made to obtain the Figure 7-19 (b). It is easily noticeable that the lighting is non-uniform and stronger in the middle right (lighter area) than in the corner left (darker area). This image is then subtracted from the ROI before re-spreading the image to the same range as the initial ROI, Figure 7-19 (c). These mathematical operations carried out on the images remain coherent since only the Y cartographies (the luminance) were used.

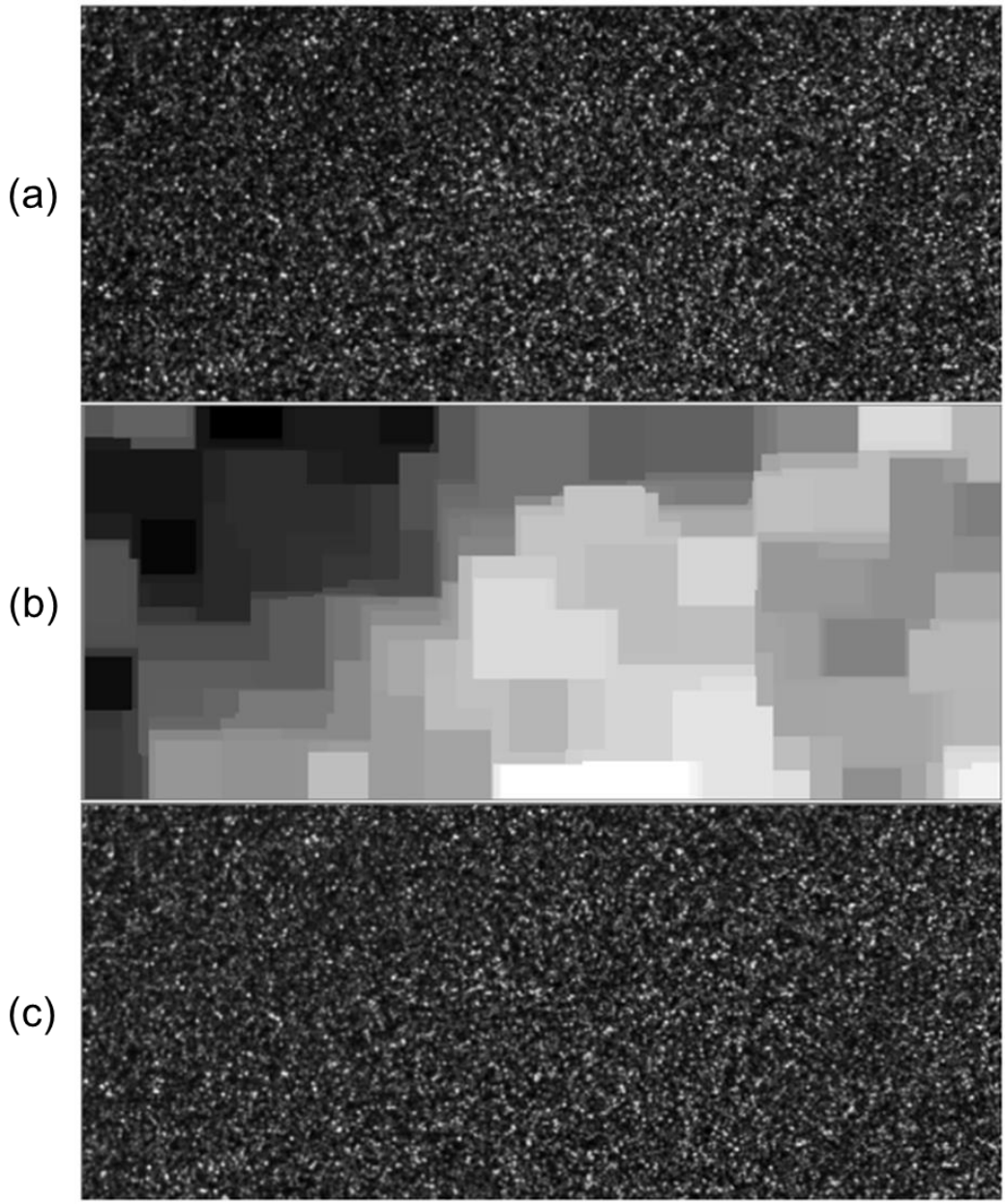

Figure 7-19: (a) initial ROI of K_5 under directional lighting (b) resulting ROI after alternate opening-closing filtering operations with a square of size 3 (c) resulting ROI after lighting correction

These two steps of selection of a ROI followed by the lighting correction as previously described were conducted for all panels under both types of lighting conditions. To simplify the determination of the four physical texture descriptors, the assumption selected is to consider only the lightness contribution of the effect particles. Therefore, only Y cartographies are used for their definitions.

7.3.2. Definition of Contrast by histogram analysis

The visual assessment of the descriptor Contrast was done under diffuse light conditions. For its determination by picture analysis, the picture obtained under diffuse light conditions was selected. Contrast can be explained as the difference in luminance between two objects which makes them discernible from one another. It is necessary to identify what is visible and what is not. In the coating film, the effect particles are located throughout the entire layer but when located at the bottom of the film are not visible due to the interactions of light with other particles.

As explained in Chapter 7 paragraph 7.1.3., elements smaller than 3 pixels in size cannot be seen by the human eye. On average and based on picture analysis, it is assumed that a single effect particle has at least an optical effect covering an area of 6 pixels, meaning 360 µm. By using trigonometric relations, an angle of 0.029° or 2' at a distance of 70 cm can be determined. Based on the contrast sensitivity function explained in Chapter 2 paragraph 2.3.6, visible contrast can be differentiated from the invisible contrast.

In this present case, the equivalent of the determined value in arc minutes is 2' so roughly 20 cpd[1]. By graphical resolution (see Figure 7-20), the contrast sensitivity is roughly equal to 20; this means that for a contrast value less than 0.2, the distinction of elements is not possible while it is possible for a contrast value greater than 0.2.

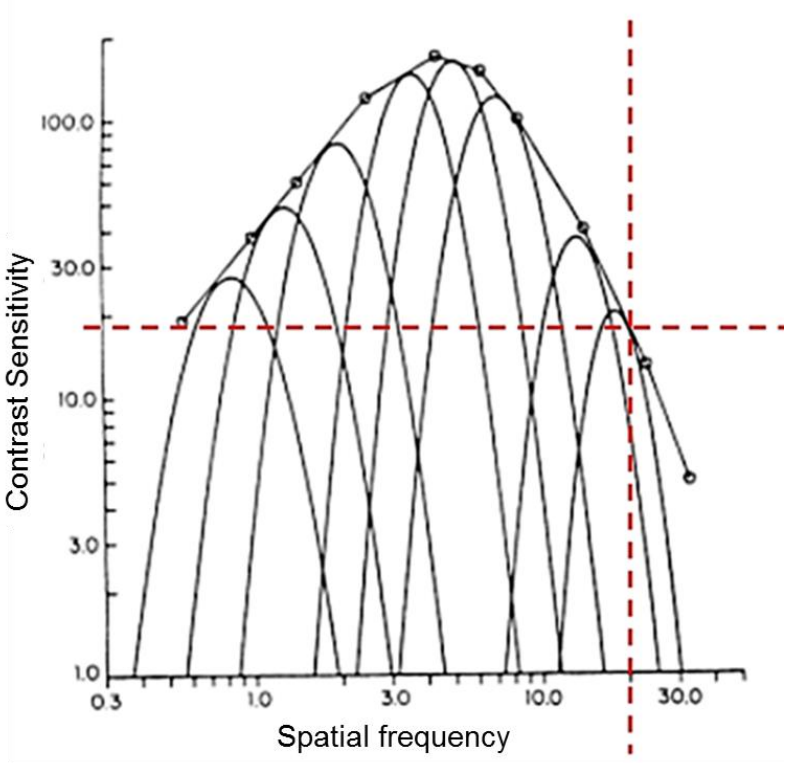

Figure 7-20: Determination of the contrast sensitivity of the visible effect particles in a panel photographed at a distance of 70 cm for an estimated optical behavior of one particle of 6 pixels or 20 in spatial frequency, picture adapted from (Yssaad-Fesselier, 2001)

[1] Cpd (cycle per degree): value in degrees of the visual angle that underlies both the retinal image and the object viewed

By considering the equation of the contrast of Michelson as previously explained in Chapter 2 paragraph 2.3.6, a relation between the maximum and minimum luminances can be determined as detailed in equation (7-11).

$$M = \frac{L_{max}-L_{min}}{L_{max}+L_{min}} > 0.2 \quad \Leftrightarrow \quad L_{max} - L_{min} > 0.2(L_{max} + L_{min})$$
$$\Leftrightarrow 0.8 \times L_{max} > 1.2 L_{min} \qquad (7\text{-}11)$$
$$\updownarrow$$
$$L_{max} > 1.5 L_{min}$$

After the pretreatment of the ROIs to smoothen the inhomogeneity of the panel lighting, the histogram of each panel was plotted. In order to have an estimation of the visible contrast, the number of pixels higher than 1.5 times the minimum value was calculated and plotted against the mean observer determined by visual assessment. The results are presented in Figure 7-21.

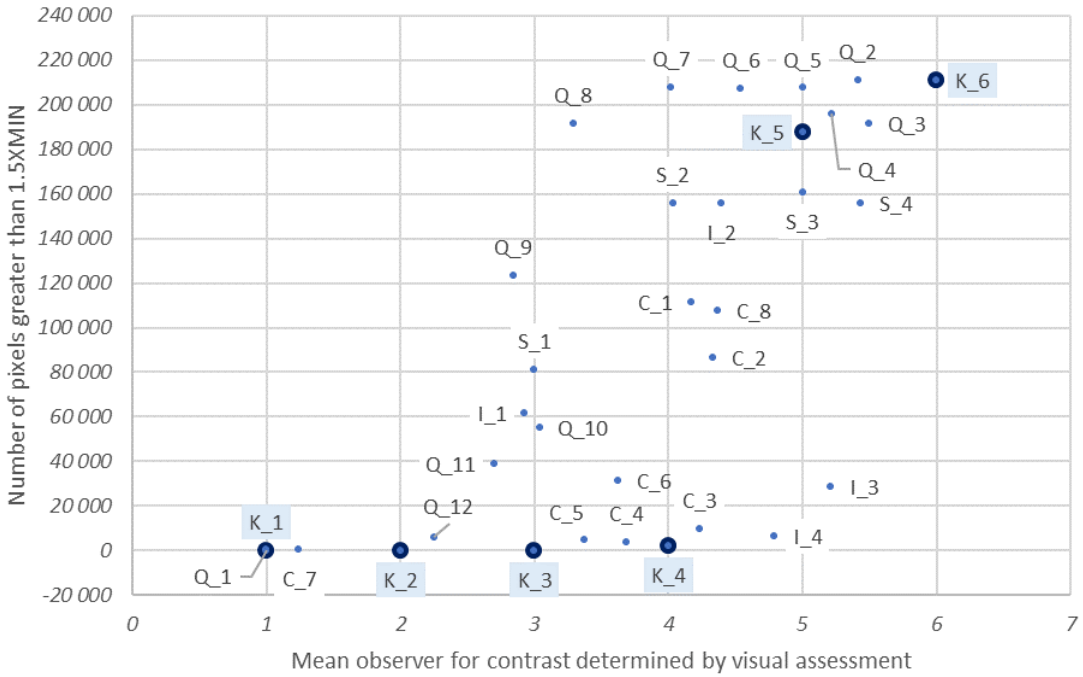

Figure 7-21: Number of pixels greater than 1.5 times the minimum value against the mean observer for Contrast where the 6 standards of this range are identified by a bigger circle

From this chart, it is easily noticeable that even if the observers were able to estimate a contrast for C_7, K_2, Q_12, K_3, C_5, C_4, K_4, C_3 and I_4 (positioned between 0 and 20,000 on the Y axis in Figure 7-21), the number of pixels greater than 1.5 times the minimum value is very low.

For panels C_7, C_5, C_4, C_3 and I_4, the observation can be explained by the inadequate selection of the exposure time. Indeed, these panels are very dark panels. The exposure time selected for them is equal to 5s except for C_3 for which it is 4s. This exposure time was probably too short to ensure a correct exposition of the effect particles with the selected lighting conditions. Besides, for panels K_2 and K_3, the exposure time selected is equal to 1/1.3s. These panels are lighter than the others but the exposure time was too long,

and the pictures are over-saturated. For the rest of the determinations, attention must be paid to these specific panels to avoid probable outliers which could hinder the identification of possible correlations.

There is no correlation to visual assessment observable. It seems that the minimum value selected with the contrast of Michelson equation is maybe too restrictive. Thus, instead of using the minimum value, the mode value is preferred. Indeed, by considering the mode value the average behavior of the background as it is entailed in the human visual system is selected. As explained in Chapter 7 paragraph 7.2.4, it represents the intensity value with the most occurrence.

Considering an example with the six references used for the range Contrast, where K_1 has no contrast and K_6 shows the highest contrast of the range, the histograms of the Y pictures acquired under diffuse conditions are plotted in Figure 7-22.

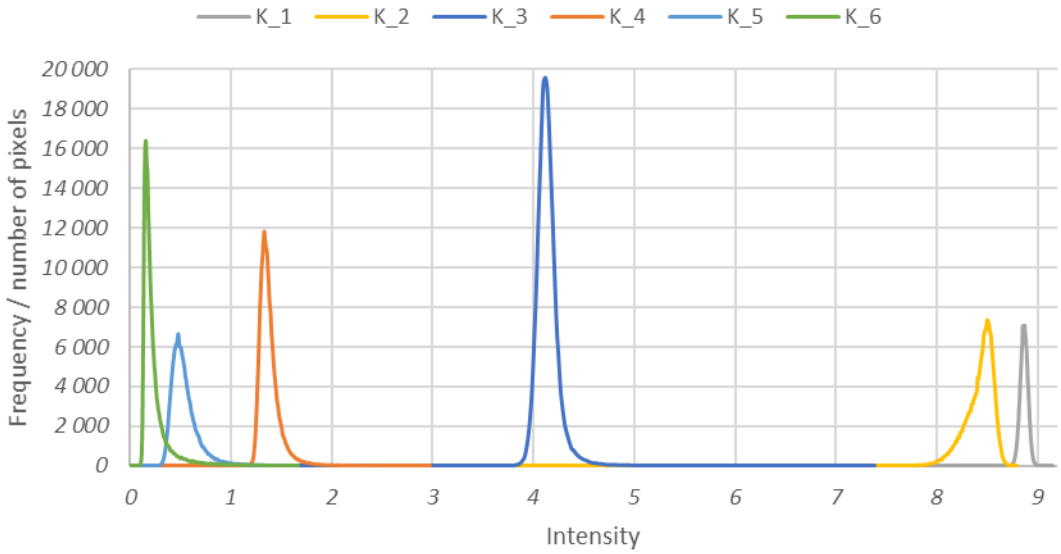

Figure 7-22: Histograms of the Y pictures under diffuse lighting conditions for the six references of the range Contrast

From the six histograms obtained, an interesting fact is noticeable. The organization of the peaks is inversely equivalent to the ranking obtained by visual assessment. The panel K_6 / Contrast _ Very Intense is the one having the highest contrast based on visual assessment but also the lowest mode value. Inversely, the panel K_1 / Contrast _ Inexistent has the highest mode value. By considering the mode value instead of the minimum value in the determination of the contrast coefficient, the thresholding background/foreground is simplified as the very dark pixels are not considered anymore.

Moreover, the coefficient of 1.5 was roughly determined by graphic readout. This value must be adapted and the best match is obtained for a factor of 1.29. For the ease of reading of the chart, the panel numbers are not added in Figure 7-23.

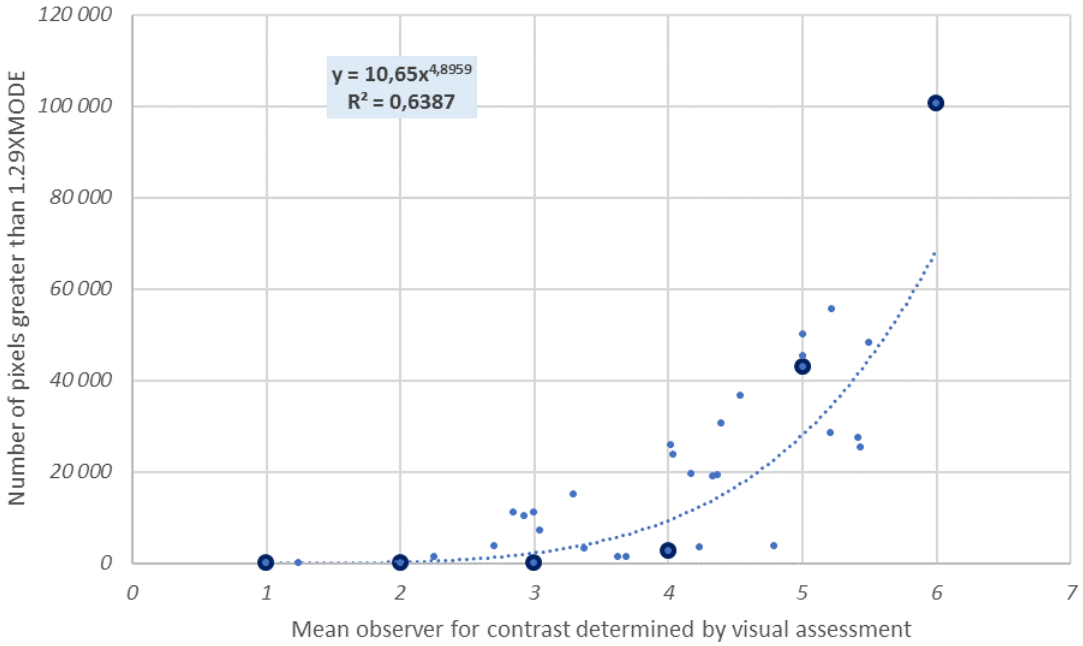

Figure 7-23: Number of pixels greater than 1.29 times the mode value against the mean observer for Contrast where the 6 standards of this range are identified by a bigger circle

Contrast can also be understood as the relative ratio in luminance between the background and the foreground. From the histogram distribution of each panel, other parameters were calculated:

- The weighted average of the background, meaning the global average of all pixels of intensity included between the minimum value and 1.29 times the mode value (note $Mean_{Back}$);
- The weighted average of the foreground, meaning the global average of all pixels of intensity included between 1.29 times the mode value and the maximum value (note $Mean_{Fore}$);
- The weighted sum of the headcount background (note WS_{Back});
- The weighted sum of the headcount foreground (note WS_{Fore}).

The weighted sums are obtained by multiplying each intensity value with the number of pixels having that intensity value and adding up the terms. Besides, the minimum (Min) and the maximum (Max) intensity values are also determined.

The best correlation to visual assessment is obtained by calculating for each panel the contrast coefficient, C, according to equation (7-12) as confirmed by the chart in Figure 7-24.

$$C = \frac{log\left(\frac{\frac{Mean_{Fore}}{Mean_{Back}}}{\left|\log\left(\frac{WS_{Fore}}{WS_{Back}}\right)\right|}\right)}{\sqrt{Max - Min}} \qquad (7\text{-}12)$$

With $Mean_{Fore}$, *average of pixel intensity in the range [1.29MODE;MAX]*
$Mean_{Back}$, *average of pixel intensity in the range [MIN;1.29MODE[*
WS_{Fore}, *weighted sum of the foreground*
WS_{Back}, *weighted sum of the background*
Max, maximum intensity value
Min, minimum intensity value

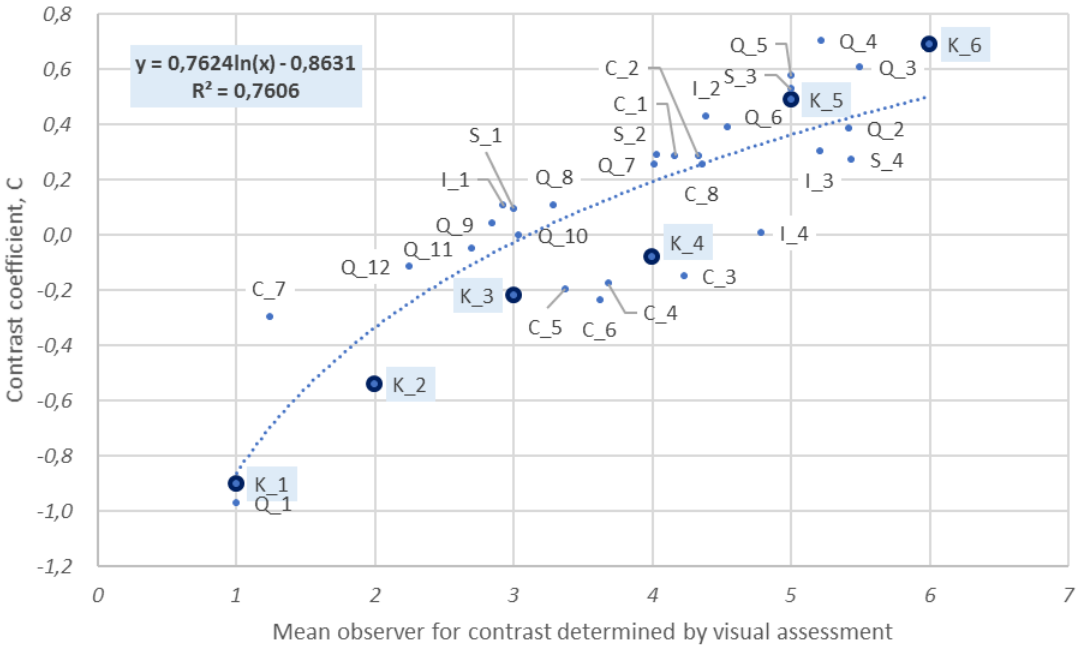

Figure 7-24: Contrast coefficient, C, against the mean observer for Contrast where the 6 standards of this range are identified by a bigger circle

The contrast coefficient, C, allows a good correlation to visual assessment with a coefficient of determination equal to 0.7606. Nevertheless, the correlation and the R-squared value can be improved by not considering the panels with incorrect exposure time leading to under-saturation (C_3, C_4, C_5, C_7 and I_4), see Figure 7-25. In that specific case, the coefficient of determination reaches a value of 0.8736.

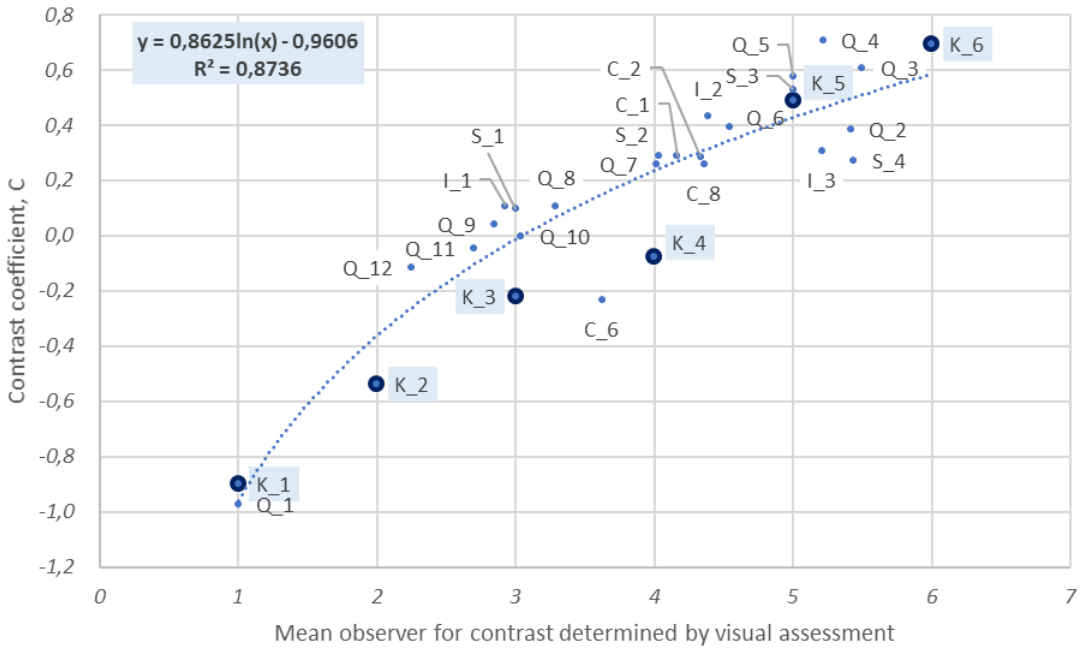

Figure 7-25: Contrast coefficient, C, against the mean observer for Contrast where the 6 standards of this range are identified by a bigger circle and with the withdrawal of C_3, C_4, C_5, C_7 and I_4 due to undersaturation

As presented before, the contrast is needed to distinguish the background from the foreground. The contrast coefficient determined here is quite efficient for this distinction and can be used for the other physical texture descriptors to focus only on the foreground where the visible effect particles are located.

However, the contrast coefficient in equation (7-12) is difficult to modulate according to the different perception parameters. Indeed, this formula does not have an immediate link to the human perception. This formula was tested on a simple and theoretical case where a picture is made of 100 pixels. The intensity of these pixels can either be equal to 50 or to 200 and located in the background or in the foreground, respectively. The number of pixels in the foreground is gradually increased from 0 to 100 to check the changing outcome of the contrast coefficient, see Figure 7-26.

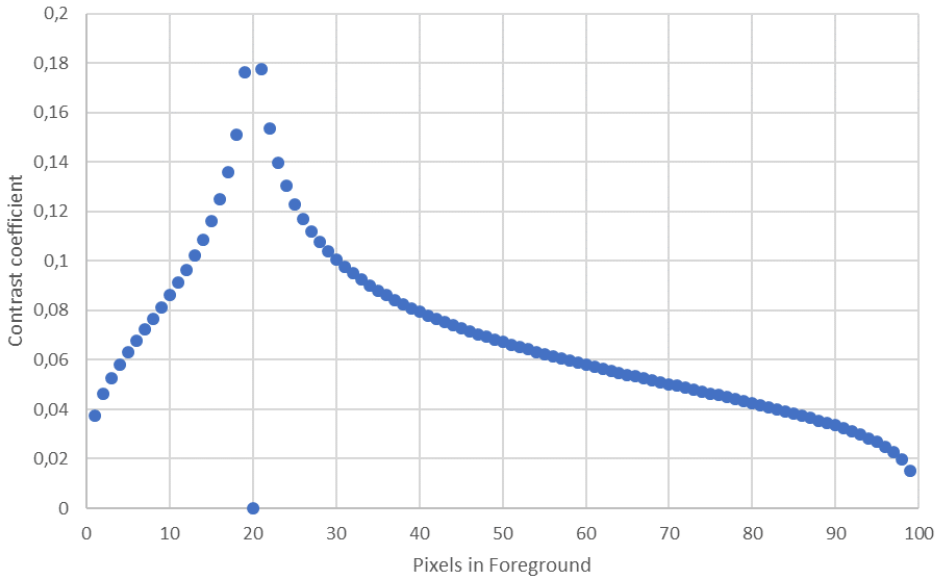

Figure 7-26: Evolution of the contrast coefficient, C, on a simple and theoretical case

The behavior of the curve is interesting. The contrast value increases in parallel to the number of pixels in the foreground until reaching a limit value at 20. After reaching this value, the contrast decreases. The contrast coefficient found seems to be applicable to the visual answer to contrast. When all is foreground, it is logical to have no contrast. However, this limit value leads to an abrupt change on the slope of the curve and the link to a similar change in visual assessment is clearly not proven.

In order to improve the coefficient and hence obtain a better correlation to visual assessment, its theoretical behavior was adapted to a gaussian-shaped function. The underlying hypothesis was to consider that at a content of 50 pixels in the foreground, the contrast decreases. This new coefficient is based on a modulation of the contrast linked to the number of pixels in each phase and not the associated weighted sum. This modulation is calculated according to the Michelson contrast (see equation (7-11)). The formula is given in equation (7-13).

$$C' = exp\left(0.5\frac{\left(\frac{N_{Fore}-N_{Back}}{N_{Fore}+N_{Back}}\right)^2}{\frac{Mean_{Back}-Mean_{Fore}}{Mean_{Back}+Mean_{Fore}}}\right) \quad (7\text{-}13)$$

With N_{Fore}*, number of pixels in the foreground*
N_{Back}*, number of pixels in the background*
$Mean_{Fore}$*, average of pixel intensity in the range [1.29MODE;MAX]*
$Mean_{Back}$*, average of pixel intensity in the range [MIN;1.29MODE[*

As previously undertaken for the contrast coefficient, C, this new version has been tested on the same simple and theoretical case where the pixel intensity is either equal to 50 or 200. The result of this new contrast coefficient, C', is plotted in Figure 7-27.

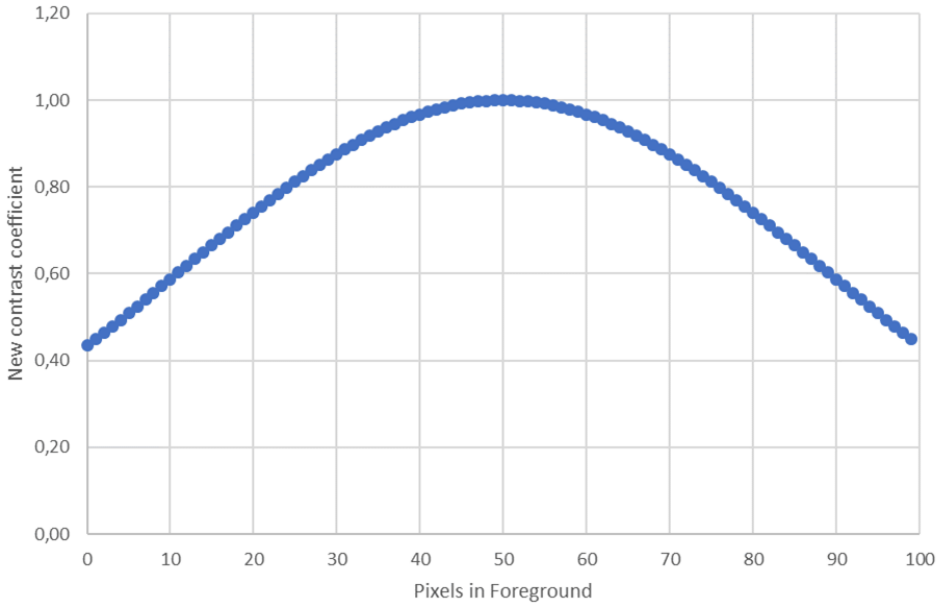

Figure 7-27: Evolution of the new contrast coefficient, C', on a simple and theoretical case

This new coefficient results in a smooth slope change at 50 pixels in the foreground. Furthermore, its determination is built on known visual parameters with the use of the Michelson contrast in the calculation of the numerator (based on the number of pixels in each phase) and of the denominator (based on the mean intensity of each phase). This coefficient uses the average contrast and the average quantity which both are linked to the visual appearance. This behavior of the theoretical data seems to correspond to the visual assessment since it does not lead to an abrupt change in the resulting curve.

However, the formula of the new contrast coefficient, C', needs to be adapted by the insertion of constants or adaptation coefficients. Indeed, at 0 pixel in the foreground or in the background, this formula should be equal to zero.

The new coefficient was then tested on a real data set by removing the panels with incorrect exposure time (C_3, C_4, C_5, C_7, K_2 and I_4) and the solid colors (K_1 and Q_1), see Figure 7-28 .

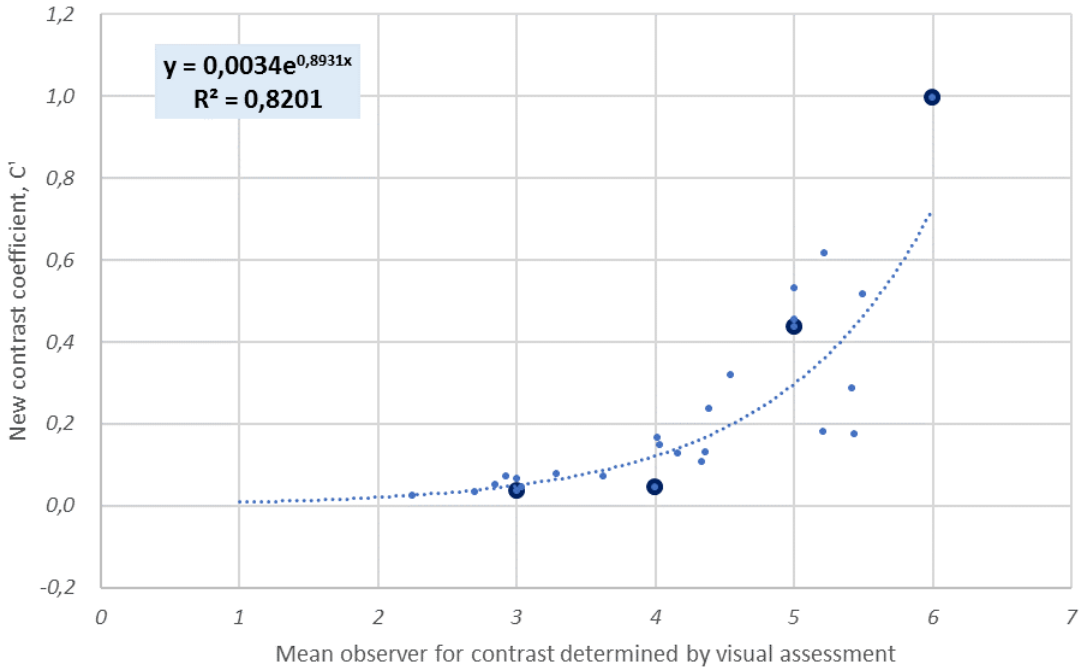

Figure 7-28: New contrast coefficient, C', against the mean observer for Contrast where the 6 standards of this range are identified by a bigger circle and with the exclusion of C_3, C_4, C_5, C_7, K_2, and I_4 due to incorrect exposure time and the two solid colors K_1 and Q_1

With this new contrast coefficient, a good correlation is obtained with a R-squared value of 0.8201. However, the assumption made here for its determination is based on a visible change in contrast when 50% of the pixels are in the foreground. There is no evidence that the 50% threshold is visually justified. This hypothesis should be adapted to a better correlation to the visual appearance.

7.3.3. Determination of Size based on opening operations

The visual assessment of the descriptor Size was performed under diffuse lighting conditions so for the determination of the physical descriptors, diffuse pictures were used. This descriptor can be explained as the apparent size depending on the optical behavior of a single effect particle under diffuse lighting.

For the determination of the size, only the foreground needs to be considered because it gathers the part visible and thus the particles visible to the human visual system. Only the pixels with a Y value greater than 1.29 times the mode value are kept, and the analysis is performed on the masked image. An example is given using panel K_5 under diffuse lighting (see Figure 7-29(a)) where a threshold value for Y of 0.61 is applied (1.29MODE). The masked image (see Figure 7-29(b)) represents in black the pixels lower than the threshold value and in red the pixels above the threshold value, hence, the background in black and the foreground in red. Also, in order to avoid inconsistencies, the groups of pixels at the boundaries of the ROI are removed from the masked image (see Figure 7-29 (c)). Indeed, it cannot be known if the grouping continues after the ROI or not.

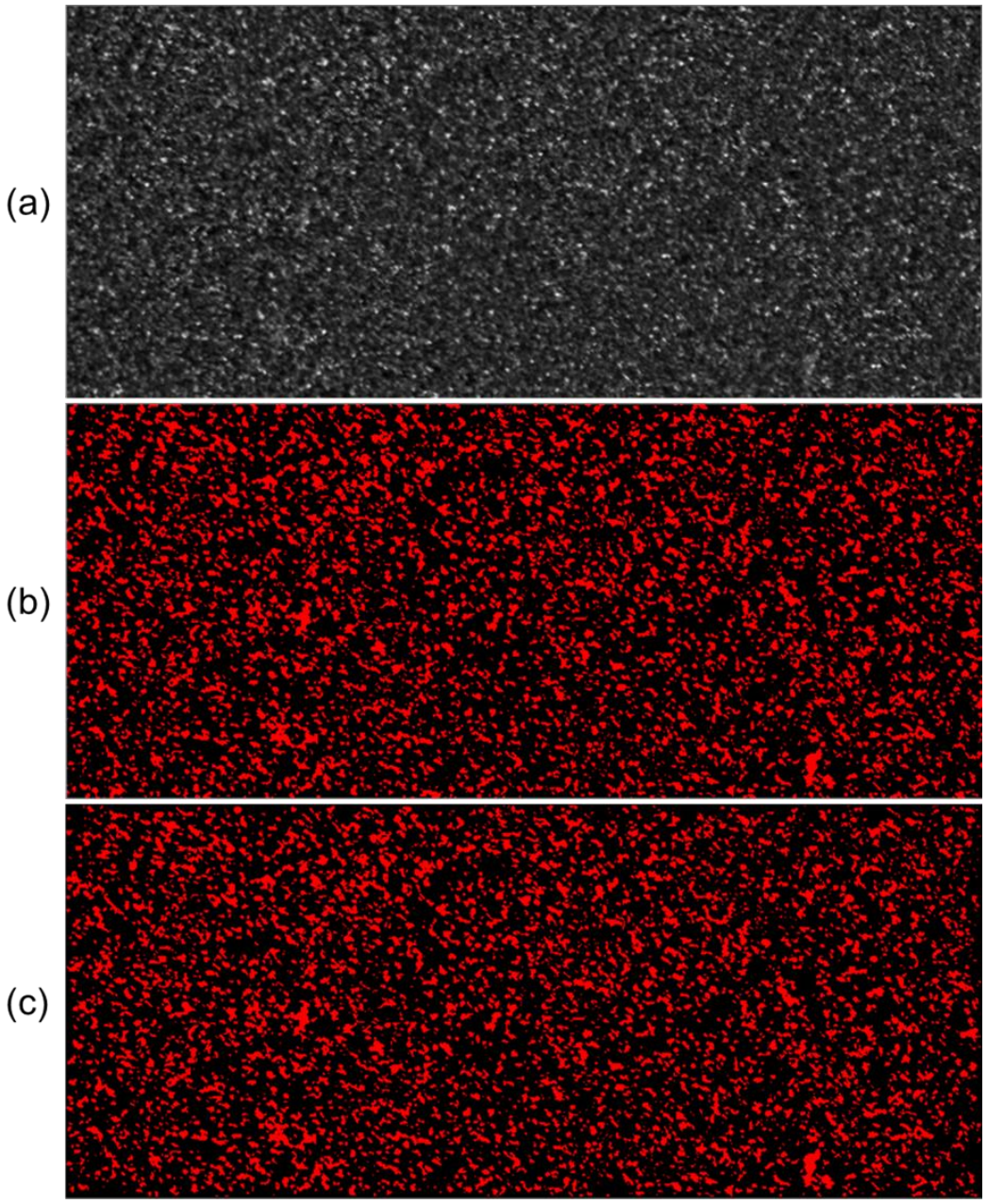

Figure 7-29: (a) Initial ROI of K_5 under diffuse lighting (b) Mask obtained after thresholding at 0.61 (1.29MODE) (c) Resulting masked image after removing the groups of pixels at the boundaries of the ROI

For size determination and as explained in Chapter 7 paragraph 7.2.3, the opening operations tend to remove objects which are smaller in size than the structuring elements. The opening operations act as a sieving method. The procedure for the size determination by successive openings detailed in Figure 7-13 was adapted to this case. The structuring element selected is a square to simplify the calculation. Indeed, choosing a circled structuring element does not make sense in this case because of the use of a square mesh to represent small size elements. The successive openings were performed by using a structuring element of size 2 to 10 in steps of 1 in size. After each opening operation, the remaining area of the red part was defined to calculate the relative loss in pixels compared to the initial masked image.

An example of the successive openings is given in Figure 7-30 where the resulting mask of the panel K_5 (see Figure 7-29 (c)) undergoes the different opening operations. For this example, only opening filtering operations with a squared structuring element from size 2 to 4 are presented in Figure 7-30.

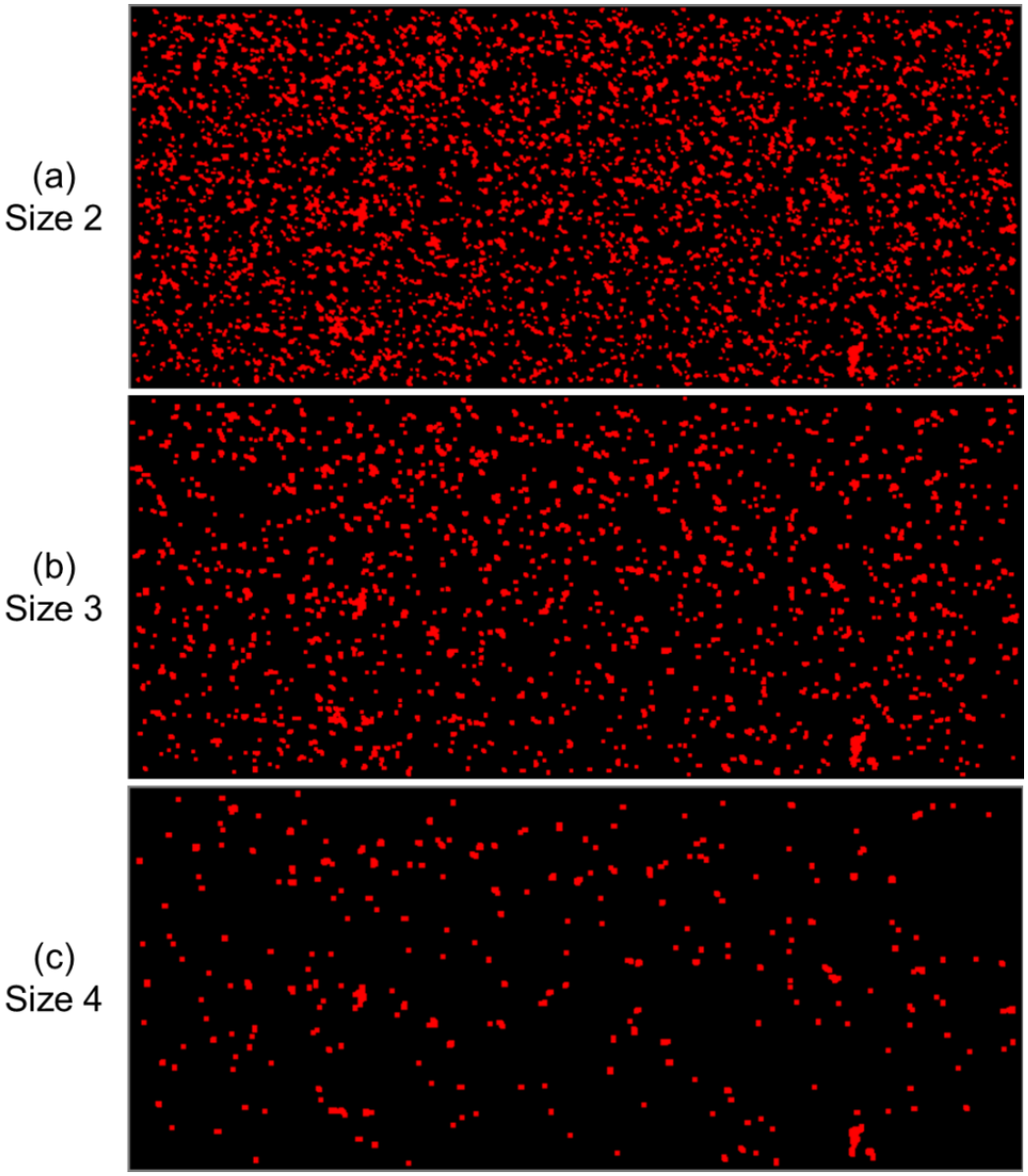

Figure 7-30: (a) Resulting mask after an opening of size 2 on K_5 (b) Resulting mask after an opening of size 3 on K_5 (c) Resulting mask after an opening of size 4 on K_5

The successive opening operations act like sieves after the application of which, only bigger groups of pixels are kept. It was not tried to separate convex objects from each other since it was not the intention to look for the size of the effect particles but for the size of the optical manifestations generated by effect particles. From the relative loss in pixels calculated for the remaining area after the opening filtering operations, it is possible to plot the granulometric curves for each panel (see Figure 7-31).

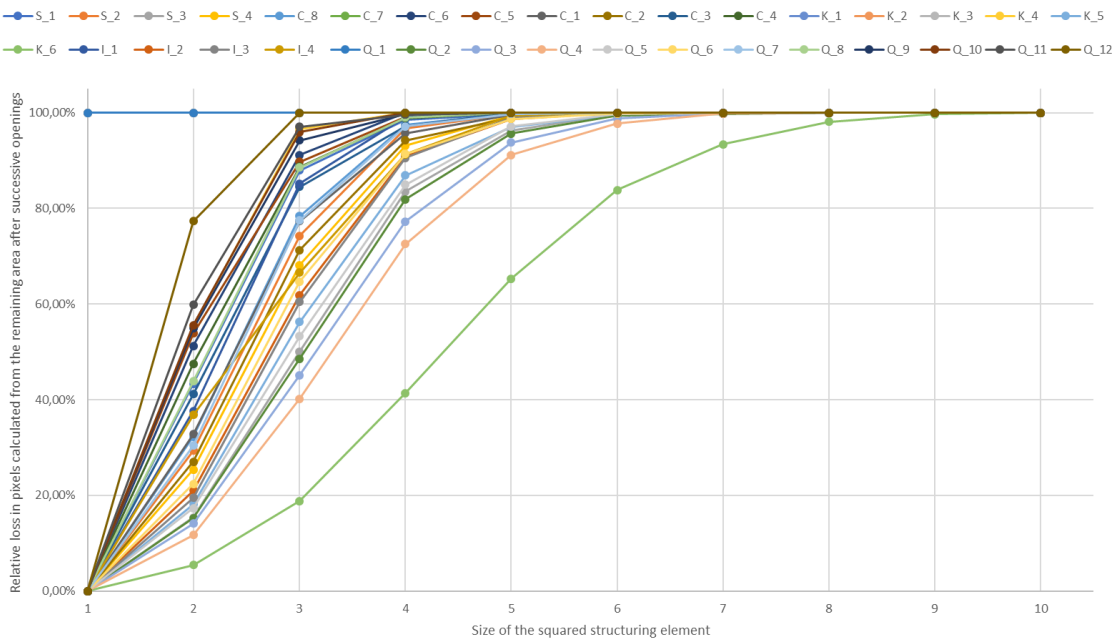

Figure 7-31: Granulometric curves obtained by successive opening filtering operations with a squared structuring element from size 2 to 10

From Figure 7-31, it can be easily seen, that there is no pixels left after thresholding with a relative loss in pixels equal to 100% before even starting the successive opening filtering operations. This is obviously the case for K_1 and Q_1 (solid colors without effect particles) for both the ranges of Contrast and of Quantity. These two panels are used to test the limits of the procedure. There is no effect on the algorithm developed and therefore no false detection results. Besides, for the panels with incorrect exposure time leading to oversaturation, K_2 and K_3, the number of pixels remaining after thresholding although containg effect pigment in the formulation, respectively 0 and 43 pixels, is absurd. Panels K_2 and K_3 cannot be considered for the determination of the size descriptor. There is a unclarity between background and foreground linked to wrong histogram shapes.

Based on the granulometric curves, the impact of the size of the squared structuring element on the relative loss in pixels is mainly noticeable for opening filtering operations of size 2 and 3. The slope of the curves is quite significant. In order to estimate which granulometric parameter could better represent the apparent size of particles in the panels, the slopes of each segment of the granulometric curves were defined according to equation (7-14).

$$Slope_i = \frac{\%Dis_i - \%Dis_{i-1}}{S_i - S_{i-1}} \qquad (7\text{-}14)$$

$$\%Dis_i = 1 - \frac{Number\ of\ pixels\ remaining\ after\ opening\ of\ size\ i}{Number\ of\ pixels\ after\ threshold + border\ kill}$$

With $Slope_i$, *slope value for an opening of size i*
$\%Dis_i$, *percentage of disappearance with an opening of size i*
$\%Dis_{i-1}$, *percentage of disappearance with an opening of size i-1*
S_i, *size of the structuring element for opening i*
S_{i-1}, *size of the structuring element for opening i-1*

The slope value is plotted against the mean observer defined by visual assessment. The size of the structuring element being the most correlated to the mean observer is size 2. This plot is presented in Figure 7-32.

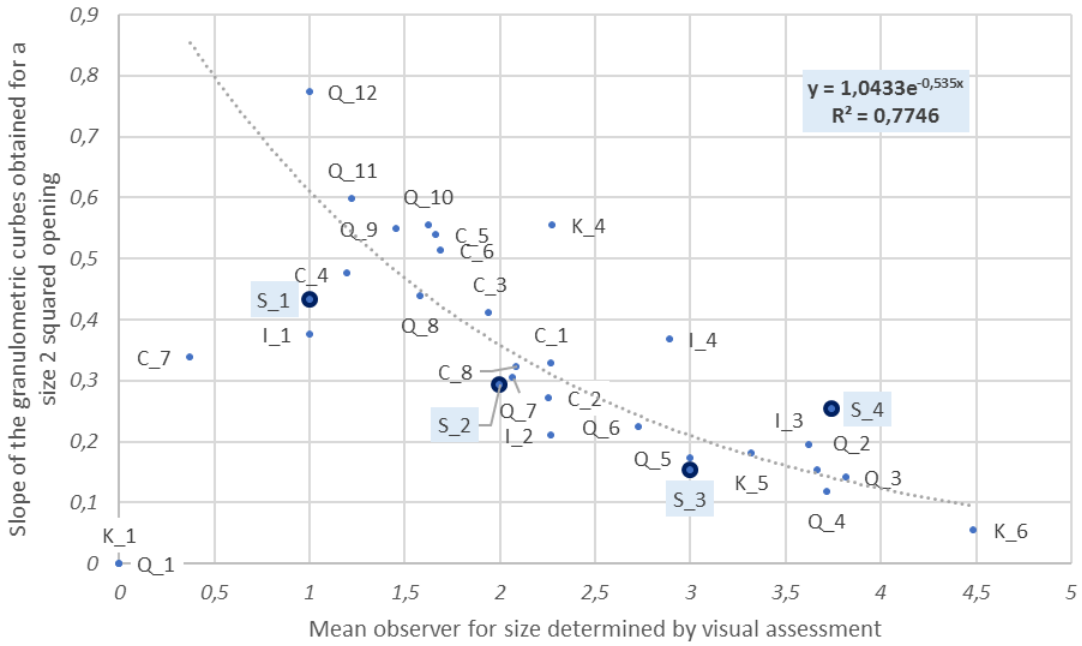

Figure 7-32: Slope of the granulometric curves obtained for a size 2 squared opening against the mean observer for the descriptor Size where the 4 standards of this range are identified by a bigger circle

This plot results in a trend, because, excepted for the two panels K_1 and Q_1 representing solid colors, all other panels follow more or less the same curve (in blue in Figure 7-32). Nevertheless, panel C_7 is shifted in its position, as was already the case for the Contrast determination.

From the trend resulting from Figure 7-32, the size coefficient, S, is defined as in equation (7-15) by considering the slope for an opening of size 2 and its correlation to visual assessment is confirmed in Figure 7-33.

$$S = ln\left(\frac{1}{Slope_2}\right) \qquad (7\text{-}15)$$

With $Slope_2$*, slope value for an opening of size 2*

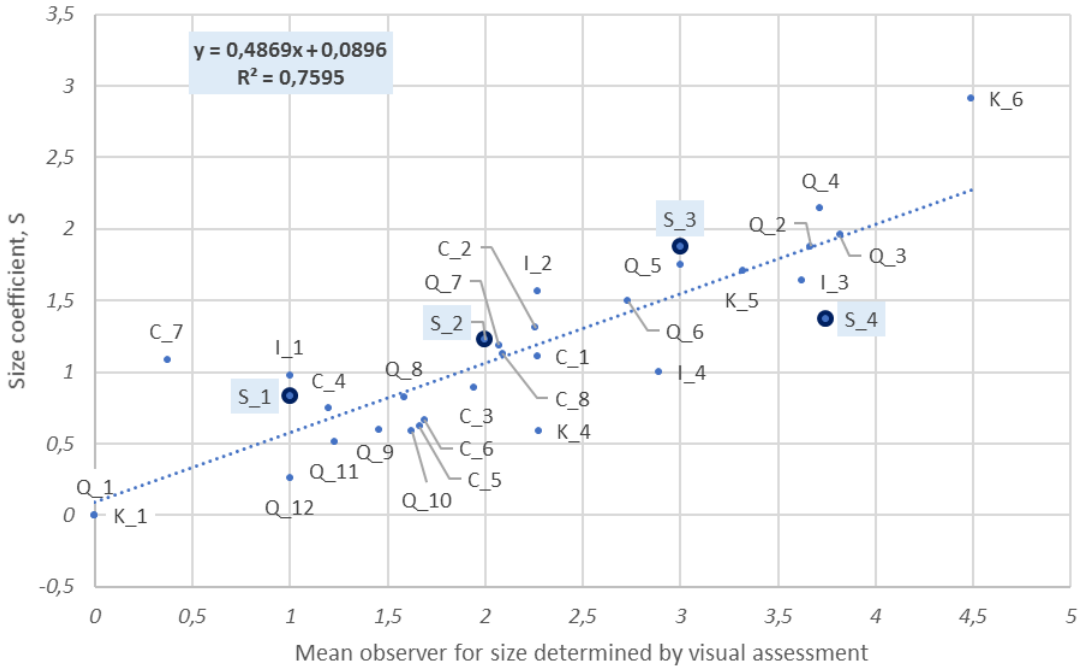

Figure 7-33: Size coefficient, S, against the mean observer for the descriptor Size where the 4 standards of this range are identified by a bigger circle

The size coefficient, S, allows for a sufficiently good correlation to visual assessment with a coefficient of determination equal to 0.7595. Nevertheless, the R-squared value can be improved by not considering the panels with incorrect exposure time and especially the panels C_7 and I_4 as presented in Figure 7-34.

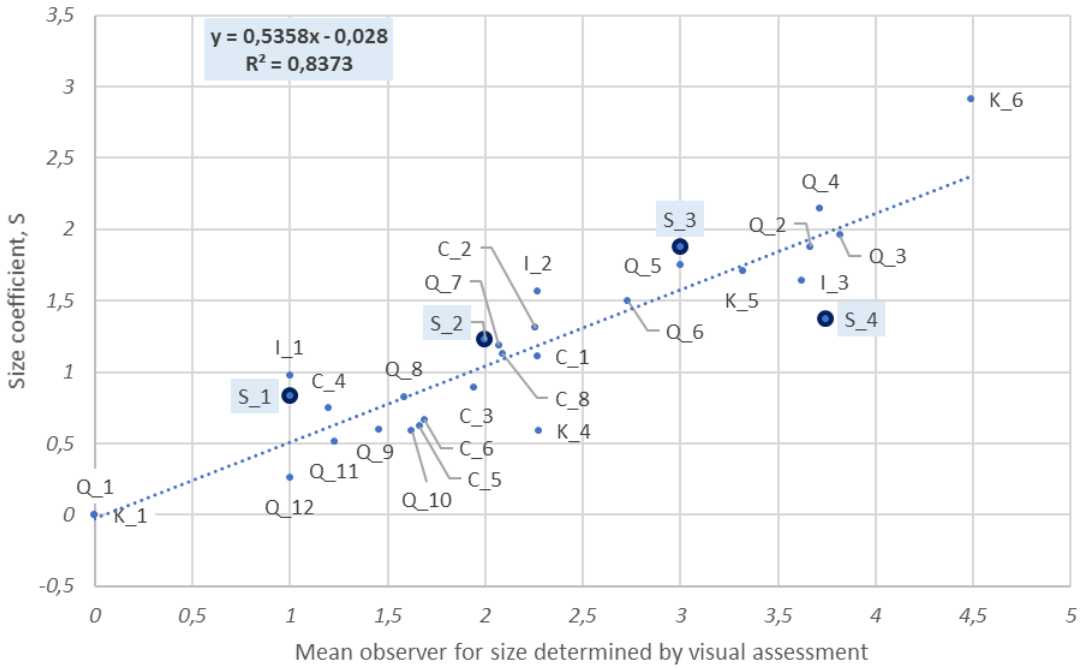

Figure 7-34: Size coefficient, S, against the mean observer for Size where the 4 standards of this range are identified by a bigger circle and with the withdrawal of 2 panels due to undersaturation C_7 and I_4

In that specific case, the coefficient of determination reaches a value of 0.8373. By using the same threshold value as the one needed for the contrast definition (ie. 1.29), characterization of the brighter pixels representing the foreground and the determination of the apparent size of the optical behavior of the particles is simplified.

7.3.4. Definition of Quantity by histogram analysis

The visual assessment of the descriptor Quantity was performed under diffuse illumination conditions so for its determination, pictures obtained under diffuse lighting were used. This descriptor can be defined as the number of visible particles under diffuse lighting or as the netting of the bright pixels, that is, tight when the concentration is high or loose for small amounts.

For the determination of the quantity, again, only the foreground of the images needs to be considered since the visible part, and thus the particles visible to the human visual system are gathered here. The threshold determined for the contrast definition is once again used because it allows a correct isolation of the pixels corresponding to the effect particles. By using this assumption, the quantity should correspond to the number of pixels greater than 1.29 times the mode value meaning the area occupied by effect particles. The number of pixels remaining after thresholding is plotted against the mean observer defined by visual assessment in Figure 7-35.

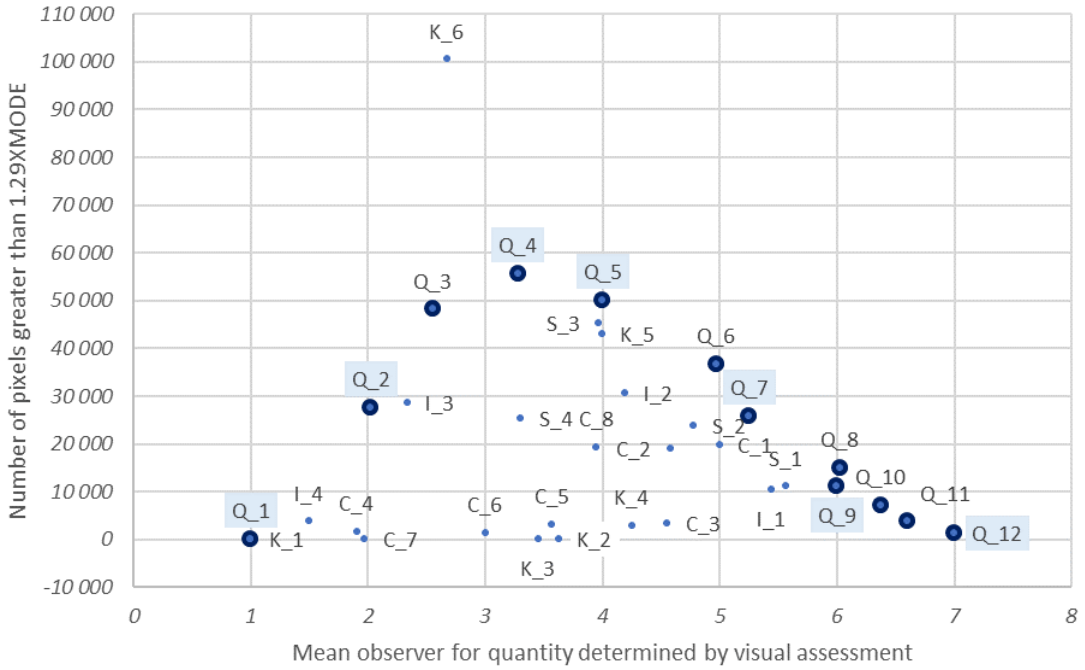

Figure 7-35: Number of pixels greater than 1.29 times the mode value against the mean observer for Quantity where the 12 panels created for this range are identified by a bigger circle

The arrangement of points in Figure 7-35 is quite interesting. The twelve panels created for the range Quantity, Q_1 to Q_12, form a limit beneath which all other panels are located with the exception of panel K_6. For panels C_7 and I_4, the effect particles in the formulation are very fine and estimating the number of particles is not trivial. Panels Q_8 to Q_12 contain

the same effect particles but in different concentrations. As the concentration of effect pigments in these panels is very high, everything appears to be particle to the human eye or everything is considered as background since there is almost no contrast for these panels. To estimate an apparent particle size is quite difficult and the values given by the observers are low, too. On the other hand, K_6 is the panel which shows most contrast and also contains the biggest particles. The panel in question is located far away from the other panels in Figure 7-35. The assumption made here is that the perceived apparent size of effect particles has a non-negligible effect on the visible quantity of effect particles – presumably considering a simple surface ratio is not sufficient for interpretation here, but the concept object/background need to be taken into account.

In addition, the mode value used for contrast and size determinations is maybe too strict and a change in the threshold of discernibility to contrast needs to be considered. As a result of several trials, the quantity coefficient, Q, is determined according to equation (7-16) by using the mean value instead of the mode, the square root of the threshold value and the size coefficient (see (7-15)).

$$Q = \frac{Number\ of\ pixels\ greater\ than\left\{\sqrt{1.29} \times Mean\right\}}{S} \qquad (7\text{-}16)$$

With *S, size coefficient*

As the size coefficient is used in the determination of the quantity coefficient, the panels K_2 and K_3 cannot be considered. Indeed, the number of pixels remaining after thresholding was absurd. The correlation of the quantity coefficient, Q, to visual assessment is confirmed in Figure 7-36.

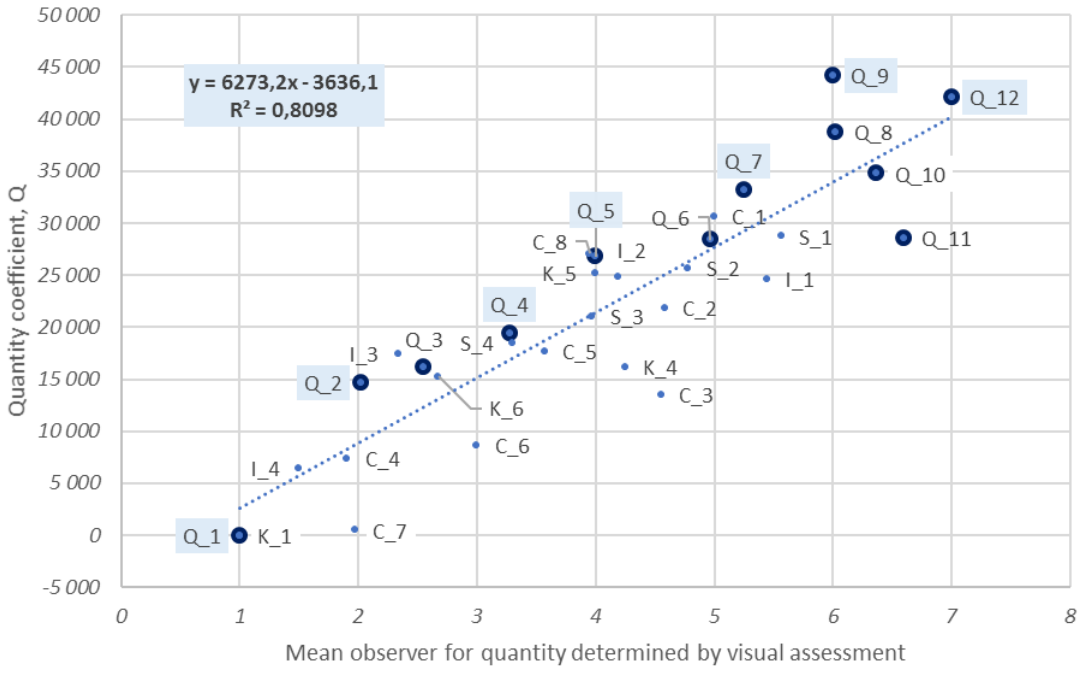

Figure 7-36: Quantity coefficient, Q, against the mean observer for the descriptor Quantity where the 12 standards of this range are identified by a bigger circle

The quantity coefficient determined herein allows for a good correlation to the mean observer. The coefficient of determination reaches a value of 0.8098.

7.3.5. Determination of Intensity based on histogram analysis

The last descriptor to be defined is Intensity. During visual assessment, this descriptor was assessed under directional lighting to maximize light reflected by the particles. The determination of this descriptor was performed on pictures obtained under directional illumination.

On pictures obtained under directional lighting, identification of the foreground was necessary to adapt the analysis only to the brighter pixels. Even if pictures obtained under directional illumination were preferred to find the intensity coefficient, the threshold determined on pictures obtained under diffuse illumination for the contrast definition and used for the size and quantity determinations was kept. As for the quantity determination, the mode value used is not adequate, so the mean value was preferred for the thresholding calculation. An example of this assumption is given with the four references of the range Intensity. The histograms of the Y pictures acquired under direct illumination conditions are plotted in Figure 7-37.

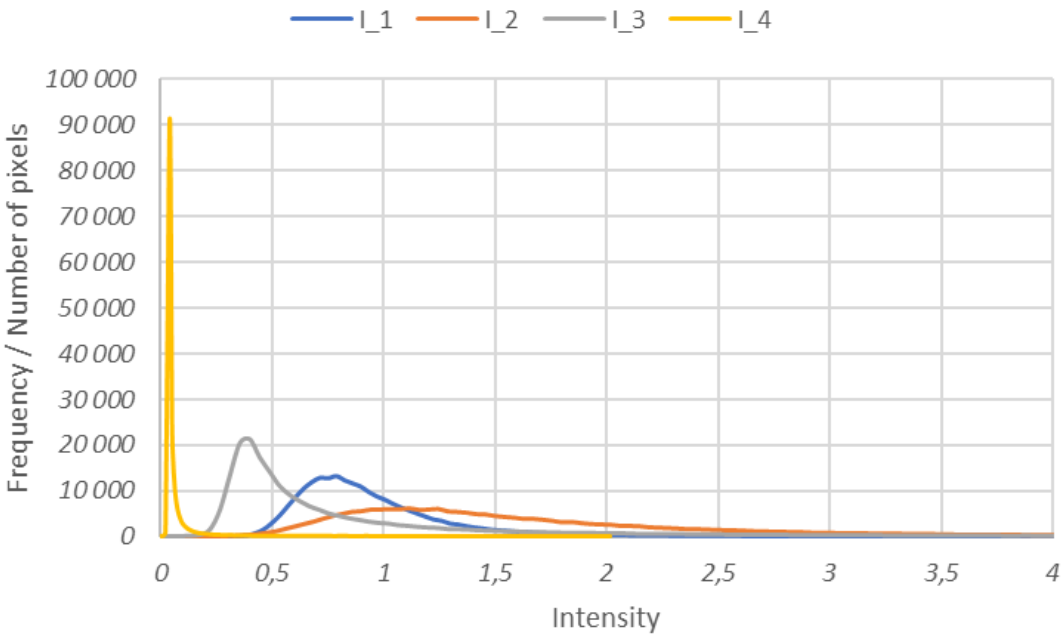

Figure 7-37: Histograms of the Y pictures under direct illumination conditions for the four references of the range Intensity

From the histograms, statistical characteristics inherent to each panel have been determined and are gathered in Table 7-5.

Table 7-5: Statistical characteristics inherent to the Y pictures of the panels of the range Intensity acquired under direct conditions

	I_1	I_2	I_3	I_4
Min value	0.21	0	0	0
Max value	7.44	8.53	8.82	2.01
Mode value	0.79	1.11	0.40	0.04
$\sqrt{1.29}$ MODE	0.89	1.27	0.45	0.05
Mean value	0.95	1.68	0.93	0.07
$\sqrt{1.29}$ MEAN	1.01	1.79	0.99	0.08
Number of Pixels [$\sqrt{1.29}$ MODE;Max]	100 419 48%	124 345 59%	147 450 70%	71 743 34%
Number of Pixels [$\sqrt{1.29}$ MODE;Max]	62 963 30%	69 755 33%	51 957 25%	30 228 14%

By changing the threshold value from the mode value to the mean value, the percentage of pixels in the foreground decreases. This change leads to a better determination of the visible effect particles and thus the determination of the intensity coefficient is improved by considering only the sparkle dots and not their surroundings.

Only the pixels greater than square root of the threshold value times the mean ($\sqrt{1.29}\,\mathrm{MEAN}$) are considered as the foreground. On the foreground, statistical measurements are performed to define the mean value, $Mean_{Fore}$. Besides, for the entire Y picture, the minimum, Min, the maximum, Max and the mean values, Mean, are calculated. However, as for the quantity determination, the relative perceived intensity seems to be linked to the apparent size of the particles. Even if the light reflection coming from the particles is very important, if they are small in size, the surface for reflection is limited. Indeed, the amount of light reflected reaching the human eye is less important than for coarser particles. The assumption made here is to consider the size coefficient, S, (equation (7-15)), in the calculation of the intensity coefficient. Also, as the size coefficient is considered in the intensity coefficient, panels K_2 and K_3 are not taken into account. The intensity coefficient, I, is then calculated according to equation (7-17) and plotted against the mean observer determined by visual assessment in Figure 7-38.

$$I = \sqrt{\frac{\sqrt{Max - Min}}{Mean} Mean_{Fore} S^{1.29}} \qquad (7\text{-}17)$$

With *Max, maximum intensity value of the entire Y picture*
Min, minimum intensity value of the entire Y picture
Mean, mean intensity value of the entire Y picture
$Mean_{Fore}$, average of pixels intensity in the range [$\sqrt{1.29}$MEAN;MAX]
S, size coefficient

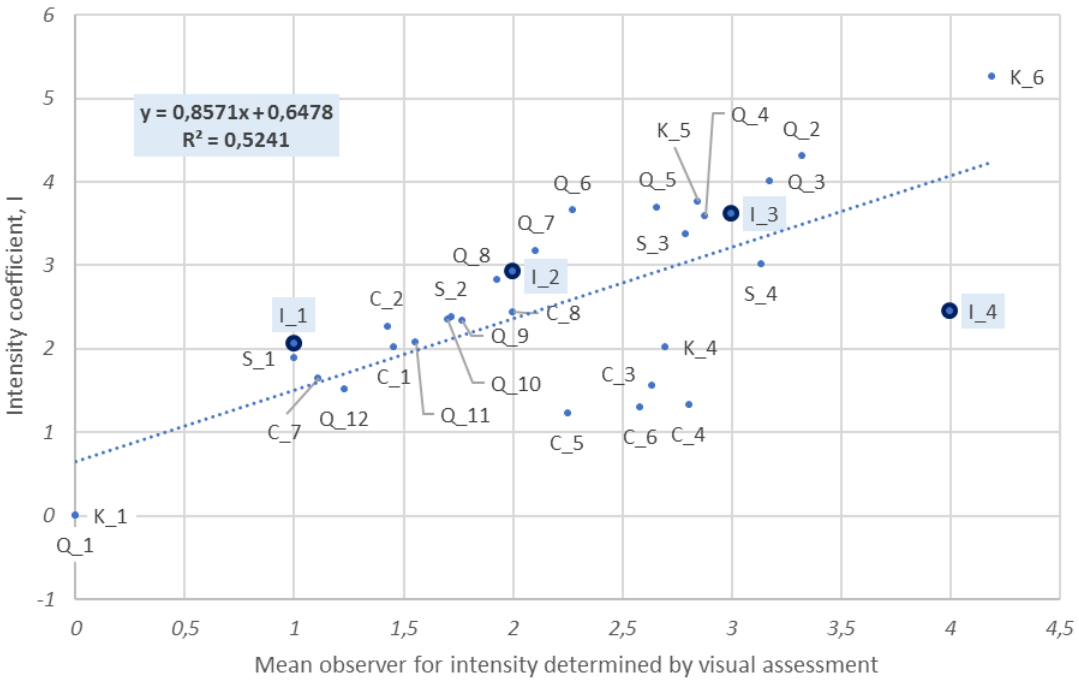

Figure 7-38: Intensity coefficient, I, against the mean observer for the descriptor Intensity where the 4 standards of this range are identified by a bigger circle

From the chart in Figure 7-38, a trend can be observed but it is also noticeable that even if the observers were able to estimate a moderate intensity for the panels C_3, C_4, C_5, C_6 and I_4, the results obtained by picture analysis are not in accordance with visual assessment. By analysis of the settings used for acquisition of these specific panels (see Table 7-4), the exposure time selected for directional lighting conditions is equal to 5s except for I_4 for which it is equal to 4s. As for the diffuse lighting conditions which were already detailed in Chapter 7 paragraph 7.3.2, they can be explained by the inadequate selection of the exposure time. Indeed, these panels are very dark panels. The exposure time selected was probably too short to ensure a correct exposition of the effect particles with the selected lighting conditions. By not considering these panels, the correlation is improved as detailed in Figure 7-39.

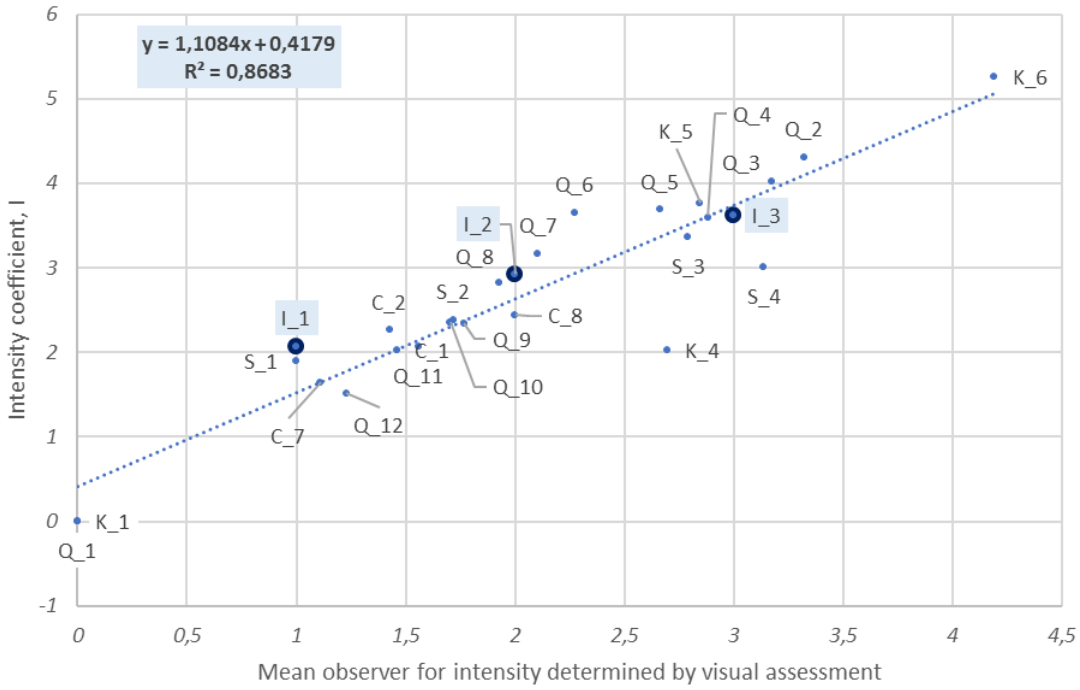

Figure 7-39: Intensity coefficient, I, against the mean observer for the descriptor Intensity where the 4 standards of this range are identified by a bigger circle and with the withdrawal of 5 panels due to undersaturation C_3, C_4, C_5, C_6 and I_4

In that specific case, the coefficient of determination reaches a value of 0.8683. By using the same threshold value as needed for the contrast definition (ie. 1.29), the characterization of the brighter pixels representing the foreground and the determination of the relative intensity coming from the effect particles is simplified.

7.4. Determination of panel similarities

According to the four correlations detailed previously in Chapter 7 paragraph 7.3, the results from picture analysis are in line with the mean observer determined by visual assessment in Chapter 6. However, it is interesting to determine panel similarities and potential clusters of panels sharing the same properties.

The Principal Component Analysis (PCA) can be used to improve the visualization of a data set containing individuals described by multiple quantitative variables, which are intercorrelated. In our case we have 4 variables (Contrast, Size, Intensity and Quantity) and 34 individuals (the 34 panels observed). The aim of this analysis is to find similarities in the data set. To clarify the interpretation in a plot, PCA transforms the data set into a new system in which it is better projected as PCA acts in a way of finding the best coordinates to spread the data out. The theoretical approach of PCA is not explained in detail here, we refer to (Abdi and Williams, 2010).

This non-parametric technique is mainly based on the determination of the first principal component which presents the largest inertia (or variance). The other components are

defined to be orthogonal to the first axis. PCA relies on matrix computation as detailed by (Abdi and Williams, 2010). The changes in graphic representation are illustrated in Figure 7-40.

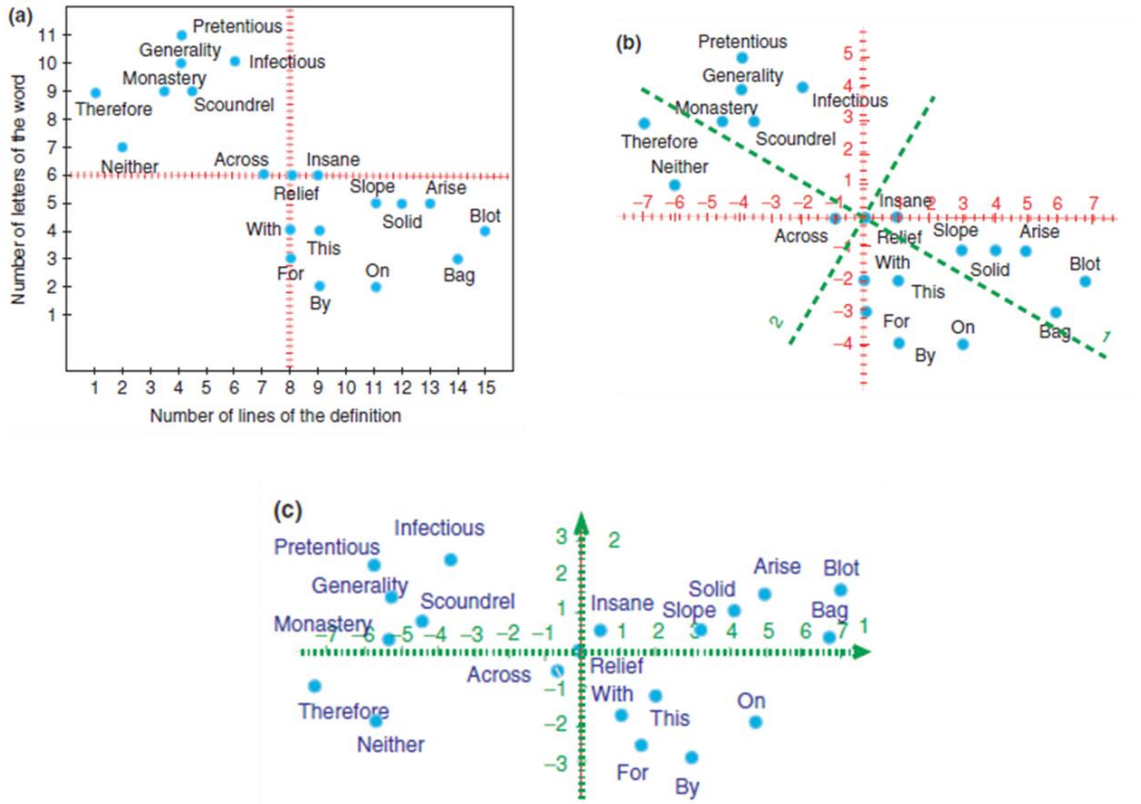

Figure 7-40: Illustrated geometric steps realized by PCA where the two axis of the initial plot (a) are changed for principal components (b) and then rotated (c) to better illustrate a link between the number of letters of the word and the number of lines of the definition from (Abdi and Williams, 2010)

In the example presented in Figure 7-40, a correlation between the number of letters of the word and the number of lines of the definition is looked for. Image (a) represents the initial plot without any transformation. In plot (b), the first two principal components are drawn. The first axis represents the maximum of variance while the second axis is orthogonal to the first one. The final representation (c) is obtained by simple rotation.

The data table to be analyzed is Table 6-5 (see Chapter 6, page 154) which gathers the mean observer values of the thirty-four panels for the four descriptors. The PCA was performed using R Studio and the library FactoMineR.

In a first step, it is important to determine how many components need to be considered. The eigenvalues are analyzed as they represent the proportion of information retained by each component. In Figure 7-41, the plot of the eigenvalues asserts that two dimensions are sufficient for an adequate spread out of the data set. With the first two components, 94% of the total variance is explained.

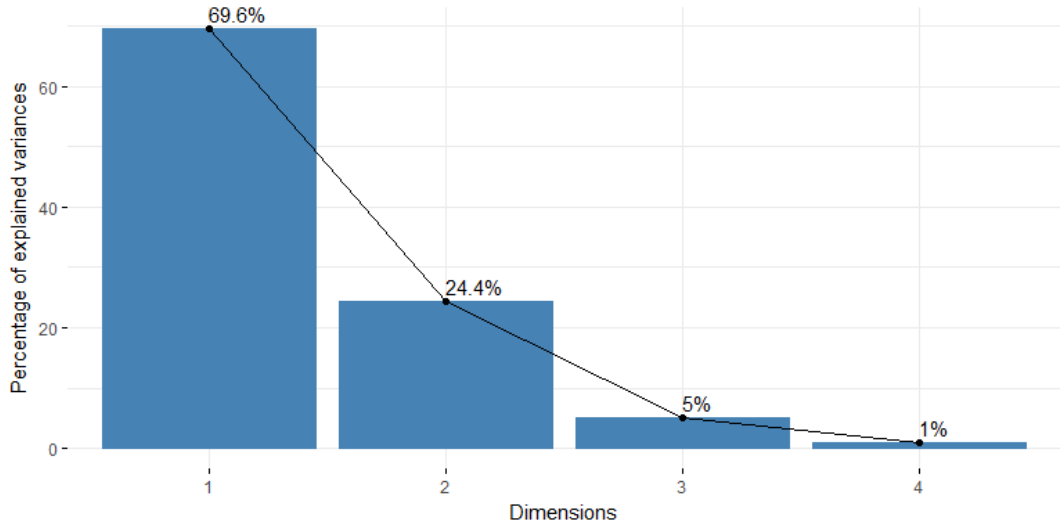

Figure 7-41: Plot of the eigenvalues for the PCA performed on the mean observer values

The biplot gathering the individuals and the variables factor maps is presented in Figure 7-42. The two dimensions selected correspond to the two axes of projection. One can notice the opposition between the descriptors Contrast, Size and Intensity described by dimension 1 (Dim1) and the descriptor Quantity describes by dimension 2 (Dim2). Their respective quality of projection on the two axes is summarized in Table 7-6. The squared cosines are important to interpret the observations according to the components. Based on the results in Table 7-6 and confirmed by the biplot in Figure 7-42, the descriptors Contrast, Size and Intensity are mainly described by the first component while the descriptor Quantity is described by the second component.

Table 7-6: Quality of projections of the descriptors on the two axes

	Cos²(dim1)	Cos²(dim2)
Contrast	0.919	0.029
Size	0.944	0.009
Intensity	0.860	0.000
Quantity	0.059	0.937

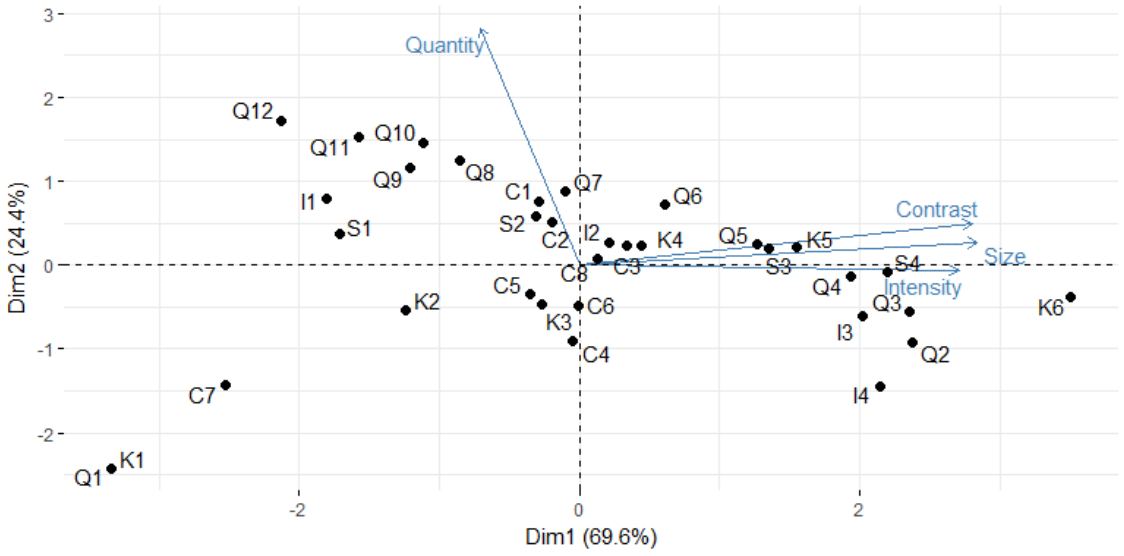

Figure 7-42: Biplot of individuals and variables obtained by PCA performed on the mean observer values

In the upper left corner, panels having a high quantity of effect pigments of low intensity, that are rather fine in size and with a low contrast are plotted. In the lower left corner, panels with small quantities of fine effect pigments with low or inexistent intensity and low contrast are gathered. On the right side, mainly panels with high contrast, high reflected intensity and coarse particles are displayed. In the upper part panels with a relatively high quantity of effect pigments are grouped and in the lower part, panels with a low quantity of effect pigments can be found.

After principal component analysis (PCA), a hierarchical clustering on principal components (HCPC) was performed to identify groups having similarities in the data set. The cluster dendrogram is shown in Figure 7-43. The thirty-four panels are subdivided into five groups.

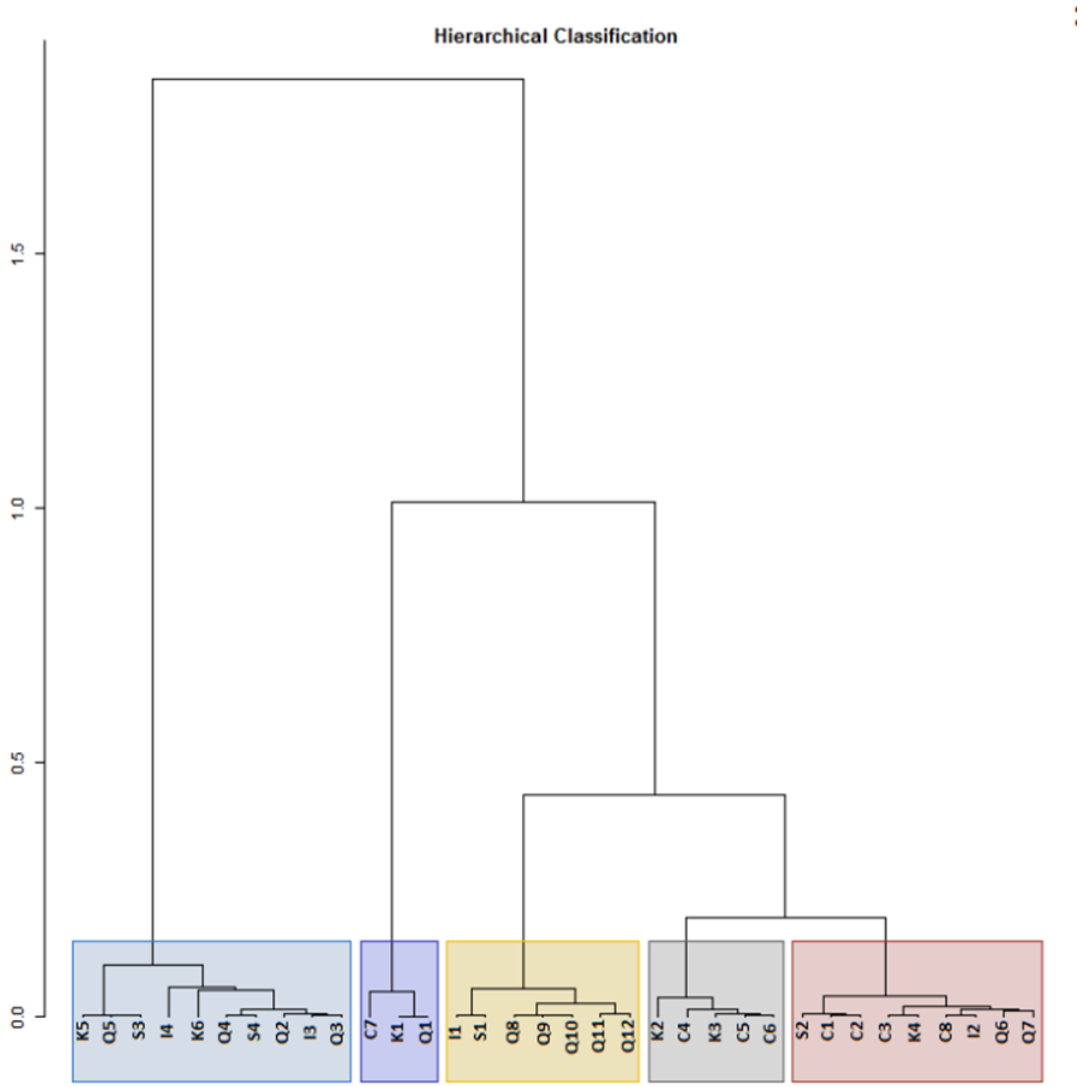

Figure 7-43: Cluster dendrogram obtained by HCPC defined by PCA on the mean observer values

These clusters are plotted into the chart of individuals in Figure 7-44.

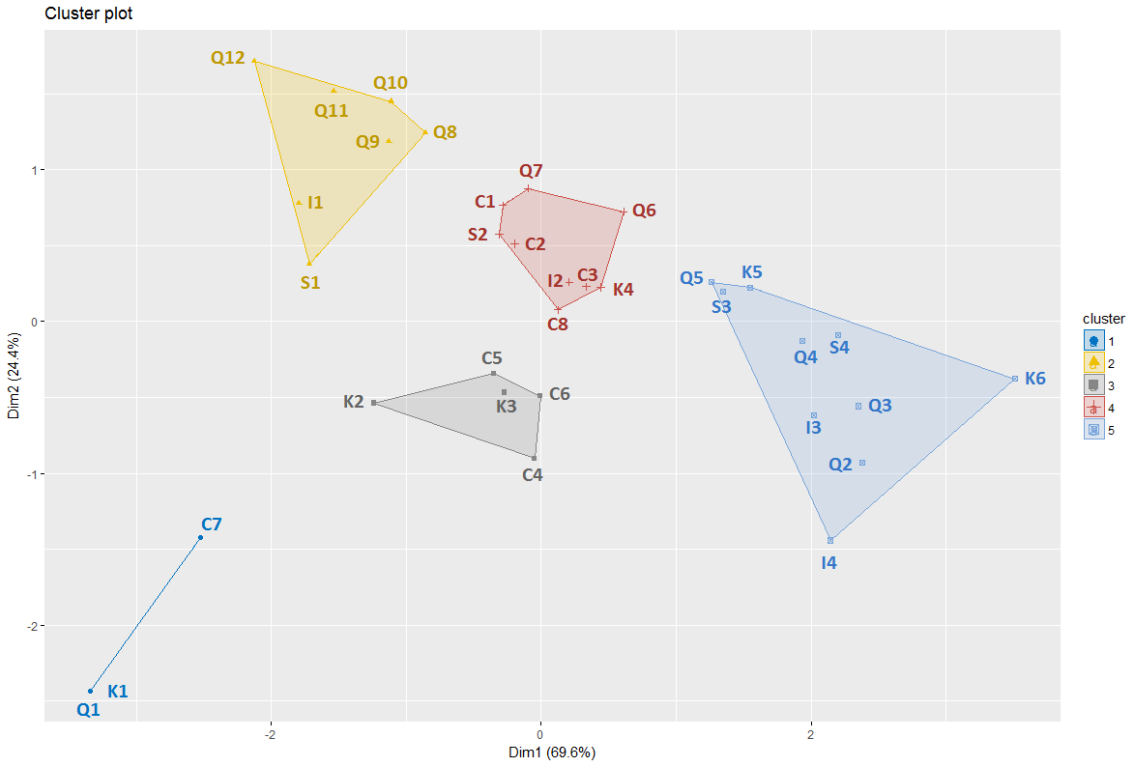

Figure 7-44: Cluster plot in five groups obtained by HCPC defined by PCA on mean observer values

From the chart in Figure 7-44, the similarities between individuals can be extrapolated. In each cluster, panels share the same characteristics. However, sample C7 seems to be on the verge of being isolated. According to the projection of the descriptors on the dimensions 1 and 2 (see Figure 7-42), the characteristics of each cluster are given in Table 7-7.

Table 7-7: Characteristics of each cluster according to the projection of the four descriptors after PCA based on mean observer values

Cluster	Panels	Quantity	Contrast	Size	Intensity
#1	C_7, K_1, Q_1	Low to inexistent	Low to inexistent	Fine to inexistent	Low to inexistent
#2	S_1, I_1, Q_8, Q_9, Q_10, Q_11, Q_12	Large	Low to moderate	Fine to medium	Low to moderate
#3	C_4, C_5, C_6, K_2, K_3	Low to moderate	Low to moderate	Fine to medium	Low to moderate
#4	C_1, C_2, C_3, C_8, I_2, K_4, S_2, Q_6, Q_7	Moderate	Moderate	Medium	Moderate
#5	S_3, S_4, K_5, K_6, I_3, I_4, Q_2, Q_3, Q_4, Q_5	Low to moderate	Moderate to high	Medium to coarse	Moderate to high

This clustering has thus been proven to be efficient for visual assessment. However, it is of interest to confirm the similarities in the results obtained by picture analysis with the determination of the four coefficients. They are gathered in Table 7-8.

Table 7-8: Values of the four coefficients (C, S, Q and I) obtained by picture analysis

Panel	Contrast coefficient C	Size coefficient S	Quantity coefficient Q	Intensity coefficient I	Cluster after HCPC and PCA
S_1	0.10	0.84	28 731.85	1.90	2
S_2	0.29	1.23	25 706.13	2.38	4
S_3	0.53	1.87	21 069.63	3.37	5
S_4	0.27	1.37	18 459.92	3.01	5
C_8	0.26	1.13	27 064.41	2.44	4
C_7	-0.30	1.09	477.18	1.65	1
C_6	-0.23	0.67	8 613.80	1.30	3
C_5	-0.19	0.62	17 665.01	1.23	3
C_1	0.29	1.11	30 686.87	2.02	4
C_2	0.29	1.31	21 790.90	2.26	4
C_3	-0.15	0.89	13 524.23	1.56	4
C_4	-0.17	0.74	7 416.91	1.32	3
K_1	-0.90	0.00	0.00	0.00	1
K_2	-0.54	N/A	N/A	N/A	3
K_3	-0.22	N/A	N/A	N/A	3
K_4	-0.08	0.59	16 200.52	2.02	4
K_5	0.49	1.71	25 223.19	3.77	5
K_6	0.69	2.91	15 293.80	5.26	5
I_1	0.11	0.98	24 593.54	2.07	2
I_2	0.43	1.56	24 824.24	2.93	4
I_3	0.31	1.64	17 473.94	3.62	5
I_4	0.01	1.00	6 390.88	2.46	5
Q_1	-0.97	0.00	0.00	0.00	1
Q_2	0.39	1.88	14 653.77	4.30	5
Q_3	0.61	1.96	16 118.86	4.01	5
Q_4	0.70	2.14	19 387.22	3.59	5
Q_5	0.58	1.75	26 808.36	3.69	5
Q_6	0.39	1.50	28 389.23	3.65	4
Q_7	0.26	1.19	33 196.68	3.17	4
Q_8	0.11	0.82	38 694.81	2.82	2
Q_9	0.04	0.60	44 131.73	2.34	2
Q_10	0.00	0.59	34 745.76	2.36	2
Q_11	-0.05	0.51	28 514.42	2.07	2
Q_12	-0.11	0.26	42 061.27	1.51	2

The values presented in Table 7-8 are normalized to improve the scale for the comparison. As explained before, panels K_2 and K_3 cannot be interpreted due to a maladjusted exposure time leading to overexposure. Panels of each cluster are plotted together in radar charts presented in Figure 7-45.

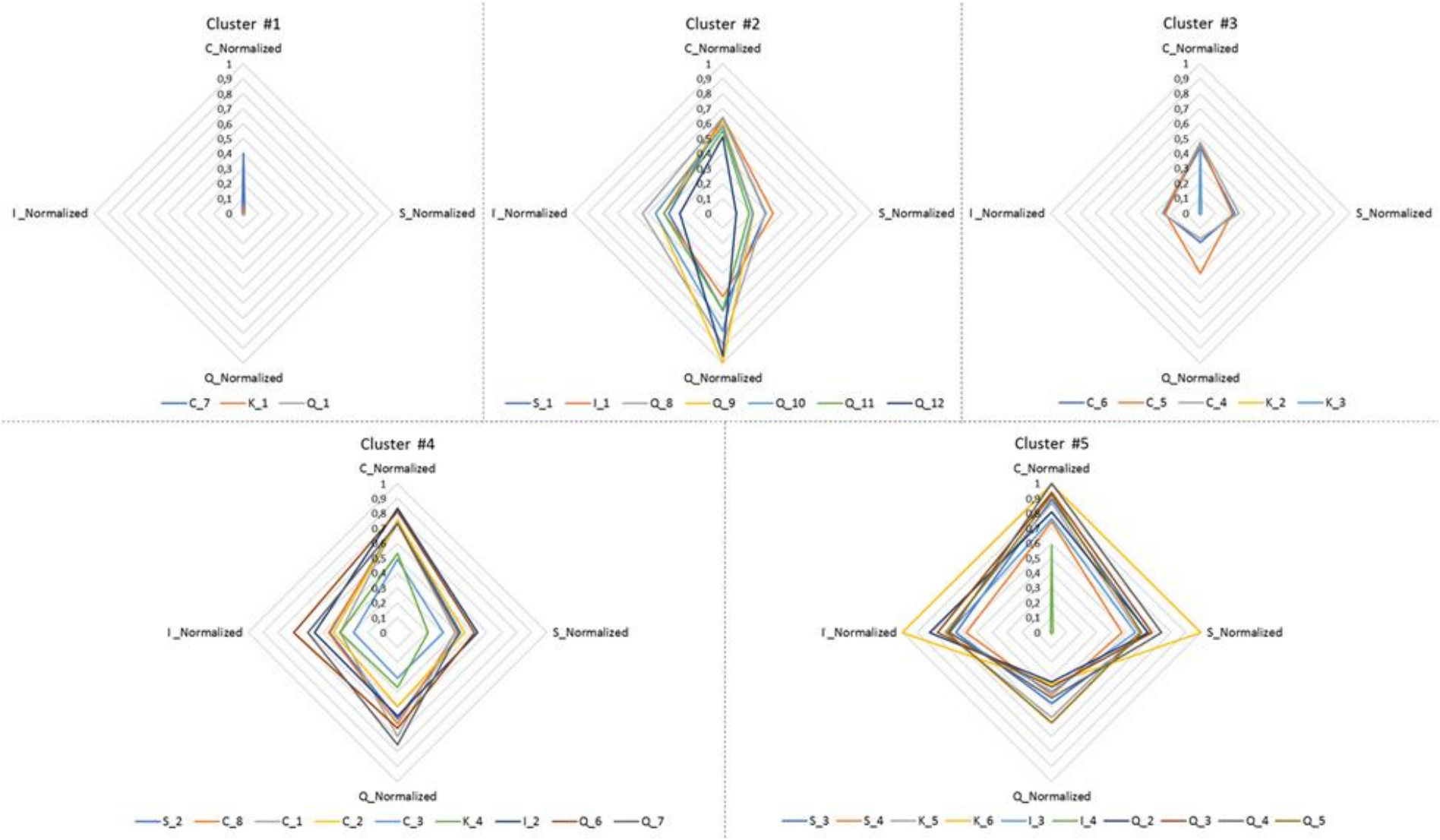

Figure 7-45: Radar charts of each cluster determined by PCA and HCPC based on the normalized values of the texture coefficients obtained by picture analysis

The clustering defined from visual assessment is in line with the texture coefficient values. The panels sharing similarities according to the human eye also share similarities based on picture analysis. The assumptions made from the biplot of individuals and variables in Figure 7-42 and from the cluster plot after HCPC in Figure 7-44 and gathered in Table 7-7 are consistent with the radar charts in Figure 7-45. However, it is important to note that the values obtained for the intensity coefficient, I, vary widely. By normalization, the values in the middle of the range, mainly for cluster #4, are attenuated by the higher ones (cluster #5). Cluster #3 brings together the panels with mid-range values for the four descriptors. Cluster #2 represents the panels with a high amount of effect particles in the formula while cluster #5 gathers the panels with the highest contrast, highest intensity and the coarsest pigments. Cluster #1 groups the solid colors or panels with very low contrast and particles, that are not easily discernible.

7.5. Assessment on the definition of physical texture descriptors

After the definition of the new texture descriptors presented in Chapter 5 and the determination of an average observer developed in Chapter 6, the last step was the adaptation of the ground truth data coming from expertise to the physical determination of the texture descriptors.

The different image acquisition methods have been presented with different parameters in terms of lighting conditions, angle of acquisition and settings of the camera. The camera used, a Nikon D800, was calibrated for each setting (ISO, aperture and exposure time). The standards created for the texture scale (see Chapter 5 paragraph 5.5) were all photographed under diffuse and directional lighting conditions. The RGB pictures thus obtained were converted into XYZ cartographies to establish the determination only on Y cartography. The objective of the determination of the physical texture descriptors was to make them as similar as possible to the sensorial profiles established by visual assessment.

The determination of the texture descriptors was based on the observations made during visual assessment. Based on the lighting conditions used, the descriptors Contrast, Size and Quantity were defined based on pictures taken under diffuse illumination conditions while the descriptor Intensity was derived from pictures obtained under directional lighting. The main difficulty arose from the delimitation of the effect particles from the background. An automatic thresholding would not have been efficient because histograms are rather different from one panel to another. The thresholding was based on the power of discernibility of the human eye and on its sensitivity to contrast to really isolate the brighter pixels (i.e. the particles) from the background. By adapting the threshold value to the human visual system, the correlation found for the four descriptors are in line with the response of the mean observer defined from 12 experienced observers.

It is also important to note the difference in lighting for the panels between the visual assessment and the picture acquisition. The average intensity level was much higher for the visual evaluation than it was for the acquisition of the images by camera. The use of

incandescent light bulbs, Solux, was favored over the use of LEDs because of the discontinuity of the light signal in the blue area for the latter - this would have been problematic for the definition of the particle color. The low lightness level leads to a loss of information because the effects of the optical phenomenon are no longer perceptible in the acquisition. The choice of the threshold value in contrast is then an approximation. The exposure times selected are at the limits of perceptibility of the camera. In the future, to improve the acquisition, the acquisition conditions should be adapted to identify when the phenomenon appears or the global lighting level during the acquisition phase should be increased.

However, the determination of physical texture descriptors was only performed on achromatic standards. By considering a panel with, for example, a red background color and red effect particles, the thresholding applied could lead to irrelevant information. As the background and the foreground are on the same chromaticity level, isolation of the particles would potentially lead to inconsistencies where some particles are visible for the human eye but not for the camera.

Chapter 8. Conclusion and Outlook

The experimental work for the present thesis was carried out in the field of automotive paints with a special focus on the refinish sector. In this sector, a repair must be invisible to be perfect, whatever the reason, why a car would need to be repaired. To reproduce an existing color is not always simple. Color formulations are a mix of different primary colors. In the case of effect coatings, effect particles such as metallic particles or pearlescent materials are added in the formulas to provide specific optical properties. As state of the art in actual color matching lab work, colorists need several trials to obtain a satisfying color, which is obtained based on his/her own experience; he/she is able to manually adjust the proposals for color correction given by an internal color matching software. The software used is developed based on statistical and physical optical models to minimize the theoretical color difference between a standard and the resulting formula. However, the software has some limitations due to the color descriptors currently used, meaning the reflectance curves and their associated CIELab coordinates. With increasing popularity of effect colors in the automotive market, it is essential to consider visual texture descriptors to better describe the color sensation produced in the eye of a human observer. The objective of present thesis was to qualify the perceived attributes and to associate some quantifiable parameters to them such as the apparent size of the particles or the sparkling effect. One of the main objectives was to correlate the visible to the measurable through the creation of new physical texture descriptors correlated with the perception of sparkling. These descriptors should correspond to the visual sensation of the phenomenon of optical signal texturing generated by effect particles in the specific case of automotive effect coatings.

First, expert knowledge and neophyte perception on the phenomena of optical signal texturing were utilized. The implementation of an unsupervised categorization test completed by a descriptive phase should have allowed for the generation of many criteria, specific to each observer. Conversely, this first test showed inconsistencies between the expert and the neophyte wordings. For example, the neophytes qualified colors with little sparkling as matte, while for the experts, this word means the use of a matte clearcoat instead of a glossy clearcoat layer. In addition, with the free sorting test, the number of potential descriptors was reduced as the observers established their categorization on a single criterion by nuancing its intensity.

Following the hypothesis that a single criterion was not sufficient to describe the entire optical behavior generated by effect particles, brainstorming sessions were organized to confront both types of wording and to generate many visible texture parameters. The use of common terms through the consensual explanation of their definitions by various brainstorming sessions allowed for the creation of a detailed lexicon. The vocabulary shared by all participants gives a valuable common reference that made possible the definition of six texture descriptors related to the optical manifestation of the present sparkling particles: Size, Quantity, Intensity, Contrast, Color and Face-Flop. These descriptors, based on visual appearance, are needed to better define the sparkling sensation on top of the existing color descriptors. The descriptor Size refers to the apparent particle size of the effect pigments

involved in the formulation (size of the bright spots). The descriptor Quantity is used to estimate the quantity or density of bright spots in the coating. The descriptor Intensity describes the quantity of light reflected by the particles or the sparkling. Contrast is needed to define the difference between particles and the masstone color or, in other words, to express the visibility of the effect particles in the film. Effect particles are colored, so the descriptor Color qualifies them (color of the bright spots). Last but not least, the descriptor Face-Flop is used to define the color travel at different viewing angles.

These new texture descriptors based on visually noticeable criteria were previously tested by three experienced observers to verify their understanding but also to standardize the conditions of observation, the type of lighting and the angle of inclination of the sample used. Standardization of the conditions of observation was mandatory to allow a better reproducibility of the tests between the observers and also the different locations. These tests made it possible to detect problems of understanding for some descriptors and especially the lack of references to assign ratings. Due to notable difficulties for its evaluation, the study of the descriptor Face-Flop was stopped after this first trial. As a matter of fact, to rate it, many parameters need to be considered. Finally, from the observations of the experienced observers, the descriptors Color and Intensity must be rated under directional lighting conditions to maximize the amount of light reaching the panel. On the other hand, to avoid being disturbed by the sparkling intensity of the effect particles, observers preferred diffuse lighting conditions to estimate the descriptors Size, Quantity and Contrast. Actually, if one observer assesses the apparent particle size under diffuse or direct light, the results will not be the same. In the latter case, his/her evaluation can be disturbed by the light intensity being reflected by the particles. In other cases, estimating the color particles without an intense light such as a spotlight does not make sense if the observer is not able to distinguish the particles from the masstone color. With a spotlight, the light intensity coming from the particles is more intense and may be more spread out.

The implementation of texture scales made it possible to describe each descriptor from references formulated according to perceived expert knowledge in order to explain the different levels expressed during the brainstorming sessions. The conception of these samples was made from purely perceptual specifications without seeking to emphasize any particular component in the mixture. Indeed, the standards were conceived according to really perceptible effects and not to effect particles. These different ranges of references allow the training of the observers to evaluate the criteria but also to gain a better understanding of the descriptors. These ranges have enabled the development of sensorial profiles for each descriptor. However, despite the introduction of references, the results are in some cases disparate, especially when evaluating panels with pearlescent materials in the formula due to the particle size (very fine). Thus, the definition of the mean observer required the use of statistical tests to label outliers. The mean observer was then used as ground truth data for the definition of the physical texture descriptors.

Before starting the image analysis, in a first step, the conditions of image acquisition were defined. To this end, the lighting as well as the camera settings were essential because the observation conditions had to be reproduced in order to be able to correlate the visual to the measurable. The whole challenge of this stage was based in particular on the visualization of three-dimensional phenomena such as sparkling, on two-dimensional

images. The diffuse and directional lighting were reproduced while ensuring the respect of the homogeneity of the lighting on the entire photographed panel. The possible problems of lighting (non-uniformity of the lighting system, shadow of the camera in the glossy clearcoat …) were corrected by morphological filtering (successive opening and closing operations) as pretreatment. In addition, in order to simplify the acquisition conditions, it was decided to vary only the exposure time depending on the luminance of the panel. Once the panels had been photographed, they were converted into colorimetric cartographies in the XYZ space (CIE 1931, 2° observer) by camera calibration, similar to what had been done with values obtained from the visual response before. Because the studied phenomena seem to be manifested mainly by luminance changes, all determinations of physical texture descriptors were based on the cartography Y which is close to the luminance.

The physical texture descriptors had to correspond to the texture descriptors and thus to the assessments of the experts. The definition of the edges of the optical impact of the particles allowed for the extraction of more precise information. Indeed, by distinguishing the specular spots from the background, it is more accurate to evaluate the occupied surface or the intensity. The objective was therefore to define the threshold from which the optical impact of the particle was discernible. For this task, all considerations were based on the functioning of the eye and especially its sensitivity to contrast and its power of discernibility in order to determine the threshold value for distinguishing the background from the foreground, which contains the effect particles. In other words, this choice was made possible by the use of unstandardized image data and effectively corresponded to the physical values specific to the luminous stimulus reemitted by the panels. From the definition of the critical threshold above which the particles are visible, it was thus possible to derive the four physical texture descriptors in accordance with the different observations.

The original aspect of present thesis is based on the use of sensory analysis in the field of the visible. With vision being a so-called subjective domain, the definition of sensory profiles enables the determination of physical texture descriptors from the collection of perceptible ground truth data. Even if the results obtained are promising, they only partially answer the initial problematic.

Indeed, the panels observed are only achromatic and simple formulas since only one type of effect particles is involved in the formulation. In a next step, the correlations found on simple chromatic colors could be confirmed using other panels where the black background would be replaced by colored backgrounds. The detection threshold of contrasts by the human eye does dependent on the chromatic component of the signals. This approach would make it possible to define whether the background color has an impact on the evaluation of the descriptors by the experts and also whether the correlations determined also work on colored image cartographies. Furthermore, it would also be necessary to consider more complex formulations including the mixing of different types of effect particles. In this specific case, in addition to the use of the previously defined threshold values, it would be probably necessary to define different phases of the foreground depending, for example, on the size of the optical manifestations or on the particles color to distinguish aluminum particles from pearls.

As discussed in Chapter 7, the lighting conditions of the panels during picture acquisition are not adapted and this has caused certain issues in the definition of physical texture descriptors. First of all, the overall lighting level of the visual observations made in light booths was much higher than the one available during the camera acquisition of images. The use of incandescent bulbs that guarantee a continuity of the lighting spectrum was favored at the expense of more powerful lighting provided by LEDs. LED lighting provides a discontinuous spectrum with a known weakness in the blue area. In order to characterize the color of the particles, incandescent bulbs have been preferred but the light intensity was too low, hence the sparkling was not strong enough to be perceptively realistic. Indeed, the level of illumination is relatively low and for particularly dark colors, the effects of optical phenomena are no longer perceptible during image acquisition by camera. Even though exposure times have been increased up to 5 seconds, the conditions chosen are at the limit of the perceptibility of the camera. To improve the overall illumination during the phase of picture acquisition, it would be necessary to use more incandescent bulbs in order to increase the level of lighting or to change the type of lighting altogether (a precise characterization of the light spectrum would be needed). Another aspect to be improved could be the definition of the level of illumination after which the phenomenon appears.

After defining the perceptual and physical texture descriptors, it should also be possible to correlate them to the formulation. For example, according to expert knowledge, it is known that the addition of white in formulas has an impact on the visibility of particles by limiting their reflectivity. At high concentration of white, they seem to be buried in the coating film and only the particles located on top of it are visible. Thus, the higher the concentration of white, the more the perceived contrast should decrease. This could especially be confirmed with scales at different concentrations of white. However, the perceived contrast is also closely related to particle size and the quantity of effect particles in the formula.

Finally, two perceptual texture descriptors have not been studied: Color and Face-Flop. For the first descriptor, XYZ cartographies should be considered to define the contributions of the particles on each cartography in order to draw a conclusion about their perceived color or to continue the transformation of the RGB images on the chromaticity diagram (xy) or CIELab color space. Again, in the case of mixing, one would have to be able to distinguish different types of particles to estimate their color. Moreover, in the case of interferential effect particles, picture acquisition at different angles would make it possible to distinguish these specific particles according to all observation angles. The descriptor Face-Flop should be based on the reflectance curves but also on the images. From the reflectance curves, the definition of a chroma index, like the already existing flop index, could allow for a better definition of the color travel. For example, considering the micro-milled white tinting base responsible for the frost effect, the yellowish-gold to bluish color travel peculiar to this type of pigment could be forecasted to the formulation expert. In addition to the reflectance curves, the use of images at different angles would make it possible to state, whether particles are still visible in flop view and therefore potentially to affirm the use of flop modifier in the formula.

Appendix A. Additional data on the elaboration of sensorial profiles

Contents

A.1. Ratings obtained on the descriptor Contrast by 12 observers

	Obs 1	Obs 2	Obs 3	Obs 4	Obs 5	Obs 6	Obs 7	Obs 8	Obs 9	Obs 10	Obs 11	Obs 12
S_1	4	3	3	3	4	3.75	3	3	2	1.8	3	3
S_2	5	3.5	4	4	5	4.5	4	4	2.75	3.2	5	3.5
S_3	5.5	4.5	5	5	5	5	5	5	4.75	4.5	5	5
S_4	5	4.5	5	6	6	4.75	6	5.5	5.5	5.5	6	5.5
C_1	4	4	5	4	5	5	5	4	4.5	2.5	3	4
C_2	4.5	4	5	5	5	5	4	4	3	3.5	5	4
C_3	5	4	4	4	5	4.75	5	4	3.5	2.5	4	5
C_4	3	2.5	3	2	2	3.75	5	3	5.5	5.5	6	3
C_5	2	3	4	3	4	4	5	3	3	2.5	3	4
C_6	2	3.5	3	3	3	3.5	5	5	3	2.5	6	4
C_7	1	1	1	1	1	1.5	3.5	2	2	1.2	1	1
C_8	4	4	5	5	5	4.5	4	4.5	4	2.5	4	4
K_1	1	1	1	1	1	1	1	1	1	1	1	1
K_2	2	2	2	2	2	2	2.5	2	2	2	2	2
K_3	3	3	3	3	3	3	3	3	3	2.5	3	3
K_4	4	4	4	4	4	4	4	3	4	3.8	4	3.8
K_5	5	5	5	5	5	5	5	5	5	4.5	5	5
K_6	6	6	6	6	6	6	6	6	6	6	6	6
I_1	3	3	3	3	4	4	4	2.5	2	1.5	3	3
I_2	5	4	5	4	5	5	5	4	3.5	4.2	3	5
I_3	5	4	5	5	6	4.5	6	4.5	5.5	5.5	6	5.5
I_4	6	3	3	3	6	4	6	3	6	5.5	6	6
Q_1	1	1	1	1	1	1	1	1	1	1	1	1
Q_2	6	5	5	6	6	4.5	5.5	5	5	5.5	6	5.5
Q_3	5.5	5	5	6	6	5.5	5.5	5	5.5	5.5	6	5.5
Q_4	5	5.3	5	5	6	5.5	5	5.5	5	4.8	5	5.5
Q_5	5	5	5	5	5	5	5	5	4.5	4.8	5	5
Q_6	4.5	5	5	5	5	4.5	4	4.5	4	4.5	4	4.5
Q_7	4	4	5	5	5	4.5	3	3.5	2.75	3.5	4	4
Q_8	4	3	4	4	4	3.5	2.5	4	1.5	2.5	3	3.5
Q_9	3	3	4	4	4	3.5	2	3.5	1.25	1.9	1	3
Q_10	4	3	4	4	4	3.5	2	3.5	1.5	2.5	1.5	3
Q_11	3.5	3	4	4	3	3.5	1.5	2.5	1.5	1.9	1	3
Q_12	2.5	2.5	3	4	2	3	1.5	2.5	1.5	1.5	1	2

A.2. Ratings obtained on the descriptor Size by 12 observers

	Obs 1	Obs 2	Obs 3	Obs 4	Obs 5	Obs 6	Obs 7	Obs 8	Obs 9	Obs 10	Obs 11	Obs 12
S_1	1	1	1	1	1	1	1	1	1	1	1	1
S_2	2	2	2	2	2	2	2	2	2	2	2	2
S_3	3	3	3	3	3	3	3	3	3	3	3	3
S_4	4	4	4	4	4	3.5	4	3	3.75	3.2	3.5	4
C_1	3	2.7	2	3	2	2	3	2	1.5	1.5	1.5	3
C_2	2.5	2.83	2	3	2	3	2	2	2.25	1.5	1	3
C_3	2	2.85	1	2	2	2	4	2	1.75	1.8	2	3.5
C_4	1	0.9	1	1	1	1	4	1.5	1	1.8	1	2
C_5	2	2.31	1	2	1.5	1.5	2	1.5	1	1.15	1	3
C_6	1	2.31	2	2	1.5	1.5	2.5	1.5	1.25	1.5	1.5	3
C_7	0.08	0.4	0	0	0.47	0	2	1	0.8	0.75	0.5	0.1
C_8	2.5	2.11	2	3	2	2	2	2	2	1.85	2	2.5
K_1	0	0	0	0	0	0	0	0	0	0	0	0
K_2	1	1	0.51	3	1	0.75	2.5	1.5	1.5	1.5	1.5	0.5
K_3	1	2	1	3	1	1	2.5	1.5	1.5	1.8	2	3
K_4	2	2.5	2	3	2	2	2	2	3	2.5	2	4
K_5	4	3.83	4	3	3	3	3	3	3	3.5	2.5	4
K_6	5	4.62	5	4.16	4.56	4.29	4	4.5	4.5	4.25	4.5	4.5
I_1	1	1	1	1	1	1	1	1	1	1.1	1	1
I_2	2.5	2	3	3	2	2	2	2	2.25	2	2	2.5
I_3	4	2.93	3	4	4	3	4	4	3.75	3.8	3	4
I_4	2.5	2.81	2	2.5	3	1	4	3	1.5	3.5	3	4
Q_1	0	0	0	0	0	0	0	0	0	0	0	0
Q_2	4.93	4.13	4	4	4	2.5	3.8	3.5	3.25	3.5	4	2.5
Q_3	4.48	4.31	4.51	4	4	3	4	3	3.5	4	3.5	3.5
Q_4	3.5	4.32	4.52	4	4	3	3	3.5	3.75	3.5	3.5	4
Q_5	3	3.1	3	4	3	3	3	2.5	2.75	3	2.5	3
Q_6	3	2.87	3	4	2	2.5	2	2	2.25	3.15	2	4
Q_7	2	2.89	2	2	2	2.5	2	2	2	2.2	2	3.5
Q_8	2	1	1	2	1	2	2	1	1	2.5	1.5	2
Q_9	1.5	1	1	1.5	1	2	1	2	1.5	1.5	1	2.5
Q_10	1	1.5	2	1	2	2.5	1	1.5	1.5	2.5	1	2
Q_11	0.49	1.5	1	1	1	1.5	1	1.5	1.5	2.8	1	2
Q_12	0.48	1	1	1	1	1	1	1	1	1.2	1	1

A.3. Ratings obtained on the descriptor Intensity by 12 observers

	Obs 1	Obs 2	Obs 3	Obs 4	Obs 5	Obs 6	Obs 7	Obs 8	Obs 9	Obs 10	Obs 11	Obs 12
S_1	1	1	1	1	1	0.63	1	1	1	1.15	1	1
S_2	2	1.72	2	2	2	1.5	1	2	1.25	2.15	1	2
S_3	2.5	2.76	2	3	2.5	2.5	3.69	3	3	2.8	3	2.75
S_4	3.25	3.98	3	3	3	3	3.5	3	3.25	3.5	3	3
C_1	1	1	2	2	1	1.25	2	3	1	1.5	0.75	1
C_2	1	2	3	2	1	0.79	0	2	1	2.75	0.6	1
C_3	2.5	2.17	3	3	2	2	2.5	3	2.79	3.2	2.5	3
C_4	3	3	3	2.5	3	2	2.94	2.5	3.5	2.5	4.35	2.9
C_5	2.5	2.5	1	2	2.5	2.25	2	3	2	2.5	1.5	2
C_6	3	3	3	1.5	3	2.5	2.5	2	3	2.5	3.5	1.5
C_7	0.18	1.33	0.48	1	0.55	1.25	2	2	0.75	1.8	1	1
C_8	2	2	2	2	2	2	2	2	1.77	1.5	1.75	2
K_1	0	0	0	0	0	0	0	0	0	0	0	0
K_2	1.5	3	2	3	3	1.5	1.5	1	4.58	1.5	3	2
K_3	2	2	2	2	3	2	3	2	3.5	2.5	4	2.5
K_4	3	2.21	2	3	3	2.9	2.25	2	4	2.5	2.5	3
K_5	3	3.5	2	3	3	2.5	3	2.5	3.5	3.15	2	3
K_6	5	4.7	5	4.46	3.5	3.73	4	3.5	5	3.5	4.4	3.5
I_1	1	1	1	1	1	1	1	1	0.78	1.2	1	1
I_2	2	2	2	2	2	2	2	2	2.5	2	1.5	2
I_3	3	3.5	3	3	3	3	3	3	3	3	4.35	3
I_4	4	4	4	4	4	4	4	4	4.55	4	4.5	4
Q_1	0	0	0	0	0	0	0	0	0	0	0	0
Q_2	3.5	4.19	3	3.17	3	2.25	3	3	4.53	2.8	4.4	3
Q_3	3.5	4	3	3	3	2.75	2.94	3	5	3.2	3.5	3
Q_4	2.5	3.23	3	2.5	3	2.83	2.94	2	4.56	2.8	3	3
Q_5	2.17	3.23	2	2	3	2	3	2	3.73	2.8	3	3
Q_6	2.17	3.05	2	2.5	3	1.5	2	1.5	3	1.8	2.5	2.25
Q_7	2.17	3	2	2.5	3	2.09	2	1	3	1.5	1	2
Q_8	2	2	2	1.5	2	2	2	1	3.25	1.85	0.55	2
Q_9	2	2.11	2	1.5	2	1.09	2.5	2	2.25	1.5	0.75	1.5
Q_10	1.5	3	2	1.5	2	1	2	2	1.88	1.85	1	2
Q_11	1.15	2.5	2	1.25	2.5	1.04	2	2	1.25	1.5	0.5	1
Q_12	1	2	1	1	1	0.76	2	1	1.5	1.5	1	1

A.4. Ratings obtained on the descriptor Quantity by 10 observers

	Obs 1	Obs 2	Obs 3	Obs 4	Obs 5	Obs 6	Obs 7	Obs 8	Obs 9	Obs 10
S_1	5.5	2	1.5	6	6	6	5.5	4.5	6	5
S_2	5	2	5	5	5	5	4	4.5	5	4.5
S_3	4	3	3.5	4	4	4	4	3.8	6	4
S_4	5	2	3	3	4	2.5	4	2.5	4	3
C_1	3	6	5	5	5	5	5	3.5	5	5
C_2	3	5	5	4	4	6	5	3.8	6	4
C_3	5	5	1.5	4	4	6	5	3.5	5	3.5
C_4	1	2	1.5	1.5	3	6.5	1.75	2.5	5.5	2
C_5	2	2	1.5	5	3	6	6	4.2	2	4
C_6	1.5	3	1.5	4	3	6	2.5	3.5	5	3
C_7	1	3	1	1.5	3	7	5	1.25	1	1
C_8	2.5	4	5	3	5	4	3.5	3.5	5	4
K_1	1	1	1	1	1	1	1	1	1	1
K_2	1.5	2	1.5	1.5	6	7	4	1.8	6	5
K_3	1	2	1.5	1.5	6	6	2	3.5	5	6
K_4	2	2	6	5	5	5	3	5.5	4	5
K_5	4	4	5	4	4	4	3.75	3.5	5	4
K_6	3	3	3	3	3	2	1.75	2.5	3	2.5
I_1	1.5	6	7	5	6	6	4.5	4.5	4	6
I_2	3	4	4	4	3.5	5	4.75	4.2	5	4.5
I_3	2	3	3	2	2	4.5	2	2.5	2.5	2
I_4	1	2	1.5	1.5	1.5	1.5	1.5	1.5	1.5	1.5
Q_1	1	1	1	1	1	1	1	1	1	1
Q_2	2	2	2	2	2	4	2	2.2	4	2
Q_3	2	2	2	2	3	3	2.75	2.8	3	3
Q_4	4	3	4	3	3.5	3	3	3	6	3
Q_5	4	4	4	4	4.5	4	4	4	4	4
Q_6	5	5	5	5	5	4	4.75	4.5	5	5
Q_7	5	5	5	5	5	5	6	5.5	6	5
Q_8	5.5	5	3.5	6	6	6	7	6.2	7	5.5
Q_9	6	6	6	6	6	6	6	5.5	6	6
Q_10	6	6	6	6	7	6.5	7	6.2	7	6
Q_11	6	6	7	6	7	7	6.5	6.5	7	7
Q_12	7	7	7	7	7	7	7	7	7	7

Appendix B. Additional data on picture analysis

Contents

B.1. Statistical measurements for the determination of the descriptor Contrast

	MIN	MAX	MEAN	MODE	1.29MODE
S_1	0.1951	0.7963	0.2887	0.2737	0.3530
S_2	0.1334	0.9354	0.2233	0.2059	0.2656
S_3	0.1195	1.4089	0.2179	0.1908	0.2461
S_4	0.0813	1.1984	0.1385	0.1262	0.1628
C_1	0.1023	0.6455	0.1583	0.1487	0.1919
C_2	0.0981	0.5492	0.1458	0.1366	0.1762
C_3	0.0723	0.3741	0.0934	0.0905	0.1168
C_4	0.0927	0.7194	0.1170	0.1148	0.1480
C_5	0.0854	0.3296	0.1068	0.1026	0.1323
C_6	0.0744	0.4488	0.1058	0.1045	0.1348
C_7	0.0883	0.6931	0.1041	0.1035	0.1335
C_8	0.1127	0.7895	0.1741	0.1637	0.2112
K_1	8.5227	9.1474	8.8624	8.8649	11.4357
K_2	7.0770	8.7971	8.4253	8.5033	10.9692
K_3	3.6679	7.3837	4.1367	4.1160	5.3096
K_4	1.1740	2.9748	1.3758	1.3278	1.7129
K_5	0.2713	1.6693	0.5358	0.4750	0.6128
K_6	0.0300	1.6677	0.2322	0.1535	0.1980
I_1	0.1494	0.6037	0.2139	0.2042	0.2634
I_2	0.1120	0.8214	0.1908	0.1762	0.2272
I_3	0.0854	1.1176	0.1131	0.1010	0.1303
I_4	0.0738	1.1161	0.0978	0.0947	0.1222
Q_1	0.0786	0.1863	0.0943	0.0943	0.1216
Q_2	0.0507	1.0820	0.1197	0.1077	0.1390
Q_3	0.0679	1.3101	0.1300	0.1116	0.1440
Q_4	0.0898	1.4563	0.1882	0.1585	0.2044
Q_5	0.1995	1.6502	0.4841	0.4255	0.5488
Q_6	0.3466	1.6825	0.7655	0.6957	0.8974
Q_7	0.4421	1.6514	0.9403	0.8736	1.1269
Q_8	0.7682	2.2435	1.3759	1.3020	1.6795
Q_9	1.6597	3.8237	2.5910	2.4535	3.1650
Q_10	1.1763	3.6156	1.6706	1.5931	2.0550
Q_11	2.3541	6.1263	3.3011	3.1692	4.0883
Q_12	3.5268	6.6846	4.5315	4.3996	5.6754

Panel	N Back[1]	N Fore[2]	WS Back[3]	WS Fore[4]	Mean Back[5]	Mean Fore[6]
S_1	199 951	11 050	56 699.3419	4 208.2452	0.2836	0.3808
S_2	187 134	23 867	40 090.3920	7 024.4888	0.2142	0.2943
S_3	165 751	45 250	32 491.1966	13 488.7303	0.1960	0.2981
S_4	185 711	25 290	24 543.4215	4 675.1152	0.1322	0.1849
C_1	191 343	19 658	29 247.2828	4 155.1367	0.1529	0.2114
C_2	191 995	19 006	27 120.2175	3 639.9471	0.1413	0.1915
C_3	207 569	3 432	19 272.3914	435.5764	0.0928	0.1269
C_4	209 484	1 517	24 434.3653	254.9795	0.1166	0.1681
C_5	207 855	3 146	22 072.9459	451.9688	0.1062	0.1437
C_6	209 645	1 356	22 115.8688	208.1949	0.1055	0.1535
C_7	210 829	172	21 926.8913	30.0918	0.1040	0.1750
C_8	191 799	19 202	32 248.4576	4 496.5798	0.1681	0.2342
K_1	211 000	1	1 869 970.7086	9.1474	8.8624	9.1474
K_2	211 000	1	1 777 730.9418	8.7971	8.4253	8.7971
K_3	210 959	42	872 603.1616	235.1259	4.1364	5.5982
K_4	208 154	2 847	285 010.8300	5 292.1087	1.3692	1.8588
K_5	167 910	43 091	81 110.3373	31 950.1899	0.4831	0.7415
K_6	110 511	100 490	17 350.2156	31 647.5804	0.1570	0.3149
I_1	200 692	10 309	42 177.0536	2 955.4864	0.2102	0.2867
I_2	180 412	30 589	32 442.3596	7 826.1185	0.1798	0.2558
I_3	182 393	28 608	19 653.9004	4 214.9064	0.1078	0.1473
I_4	207 264	3 737	20 057.5632	571.7026	0.0968	0.1530
Q_1	210 830	171	19 877.4203	22.7582	0.0943	0.1331
Q_2	183 450	27 551	20 475.9632	4 785.4917	0.1116	0.1737
Q_3	162 823	48 178	18 718.3771	8 719.6532	0.1150	0.1810
Q_4	155 385	55 616	25 214.9058	14 484.9338	0.1623	0.2604
Q_5	160 831	50 170	68 793.8379	33 345.1279	0.4277	0.6646
Q_6	174 236	36 765	123 586.9307	37 926.9702	0.7093	1.0316
Q_7	185 113	25 888	166 411.0655	31 984.4299	0.8990	1.2355
Q_8	195 932	15 069	263 291.2408	27 028.1244	1.3438	1.7936
Q_9	199 911	11 090	509 683.6696	37 009.6667	2.5496	3.3372
Q_10	203 861	7 140	336 826.0723	15 671.4436	1.6522	2.1949
Q_11	207 186	3 815	680 078.7661	16 446.7613	3.2825	4.3111
Q_12	209 677	1 324	948 342.3860	7 812.4879	4.5229	5.9007

[1] NBack: number of pixels in the background
[2] NFore: number of pixels in the foreground
[3] WS Back: weighted sum of the background
[4] WS Fore: weighted sum of the foreground
[5] Mean Back: weighted average of the background
[6] Mean Fore: weighted average of the foreground

B.2. Results of opening operations for the determination of the descriptor Size

	Init	BorderKill	2x2	3x3	4x4
S_1	11 644	11 448	6 486	1 384	170
S_2	29 091	28 160	19 900	7 250	946
S_3	54 530	51 954	43 972	25 961	8 549
S_4	32 920	31 766	23 694	10 136	2 207
C_1	21 776	21 197	14 241	4 804	915
C_2	25 394	24 632	17 976	7 081	1 425
C_3	7 644	7 431	4 375	1 152	206
C_4	3 610	3 535	1 856	400	40
C_5	3 886	3 772	1 741	387	36
C_6	1 966	1 933	942	171	-
C_7	228	228	151	91	32
C_8	19 959	19 414	13 145	4 207	485
K_1	-	-	-	-	-
K_2	-	-	-	-	-
K_3	43	43	-	-	-
K_4	2 942	2 889	1 289	99	-
K_5	44 543	43 073	35 270	18 835	5 653
K_6	105 484	81 030	76 617	65 817	47 508
I_1	11 761	11 567	7 217	1 715	112
I_2	36 682	35 355	27 949	13 489	3 247
I_3	32 108	31 029	24 993	12 287	2 936
I_4	3 975	3 889	2 457	1 301	339
Q_1	199	196	124	24	-
Q_2	40 902	39 490	33 465	20 325	7 152
Q_3	52 526	49 754	42 734	27 327	11 330
Q_4	63 417	59 325	52 360	35 499	16 280
Q_5	53 710	50 273	41 576	23 488	7 559
Q_6	37 906	36 424	28 256	12 853	3 136
Q_7	27 039	26 193	18 225	5 910	759
Q_8	15 676	15 196	8 530	1 747	152
Q_9	10 762	10 527	4 749	606	32
Q_10	7 390	7 285	3 238	296	-
Q_11	3 666	3 596	1 444	106	16
Q_12	1 262	1 249	283	-	-

	5x5	6x6	7x7	8x8	9x9	10x10
S_1	39	-	-	-	-	-
S_2	67	42	-	-	-	-
S_3	1 941	126	-	-	-	-
S_4	185	-	-	-	-	-
C_1	86	36	-	-	-	-
C_2	252	53	-	-	-	-
C_3	-	-	-	-	-	-
C_4	-	-	-	-	-	-
C_5	-	-	-	-	-	-
C_6	-	-	-	-	-	-
C_7	-	-	-	-	-	-
C_8	25	-	-	-	-	-
K_1	-	-	-	-	-	-
K_2	-	-	-	-	-	-
K_3	-	-	-	-	-	-
K_4	-	-	-	-	-	-
K_5	1 318	209	84	-	-	-
K_6	28 097	13 130	5 386	1 557	261	-
I_1	-	-	-	-	-	-
I_2	467	-	-	-	-	-
I_3	330	-	-	-	-	-
I_4	25	-	-	-	-	-
Q_1	-	-	-	-	-	-
Q_2	1 729	252	96	-	-	-
Q_3	3 095	602	56	-	-	-
Q_4	5 239	1 341	126	-	-	-
Q_5	1 439	120	-	-	-	-
Q_6	471	78	-	-	-	-
Q_7	60	-	-	-	-	-
Q_8	-	-	-	-	-	-
Q_9	-	-	-	-	-	-
Q_10	-	-	-	-	-	-
Q_11	-	-	-	-	-	-
Q_12	-	-	-	-	-	-

B.3. Statistical measurements for the determination of the descriptor Quantity

Panel	MEAN	SQRT(1.29)xMEAN	Number of pixels [SQRT(1.29)xMEAN;MAX]
S_1	0.2887	0.3279	26 768
S_2	0.2233	0.2536	36 268
S_3	0.2179	0.2475	45 250
S_4	0.1385	0.1573	33 763
C_1	0.1583	0.1798	39 052
C_2	0.1458	0.1656	32 531
C_3	0.0934	0.1061	15 167
C_4	0.1170	0.1329	8 650
C_5	0.1068	0.1212	13 044
C_6	0.1058	0.1202	7 615
C_7	0.1041	0.1182	927
C_8	0.1741	0.1978	35 585
K_1	8.8624	10.0658	1
K_2	8.4253	9.5693	1
K_3	4.1367	4.6983	718
K_4	1.3758	1.5627	10 429
K_5	0.5358	0.6086	45 730
K_6	0.2322	0.2637	47 973
I_1	0.2139	0.2429	26 775
I_2	0.1908	0.2168	43 594
I_3	0.1131	0.1285	39 491
I_4	0.0978	0.1110	12 431
Q_1	0.0943	0.1071	1 020
Q_2	0.1197	0.1360	34 892
Q_3	0.1300	0.1477	38 942
Q_4	0.1882	0.2137	47 974
Q_5	0.4841	0.5498	50 170
Q_6	0.7655	0.8694	44 572
Q_7	0.9403	1.0679	41 269
Q_8	1.3759	1.5627	33 427
Q_9	2.5910	2.9428	27 649
Q_10	1.6706	1.8974	22 304
Q_11	3.3011	3.7493	15 876
Q_12	4.5315	5.1468	11 514

B.4. Statistical measurements for the determination of the descriptor Intensity

	MIN	MAX	MEAN	MEAN FORE
S_1	0.3078	7.9878	1.4097	2.2395
S_2	0.3490	8.2921	2.2738	3.6272
S_3	0	8.7869	1.4048	2.6384
S_4	0	8.9077	1.4881	3.1545
C_1	0.0948	4.4224	0.5122	0.8909
C_2	0.0613	4.5437	0.4792	0.8530
C_3	0	1.8768	0.3008	0.6101
C_4	0.0040	2.0096	0.5501	0.9519
C_5	0	1.8333	0.2777	0.5336
C_6	0	1.6889	0.2413	0.4957
C_7	0	1.6103	0.1110	0.2158
C_8	0.0262	8.6990	1.4124	2.4849
K_1	8.4671	13.3257	9.5680	11.9629
K_2	6.5606	32.5835	10.8513	15.5218
K_3	4.2554	23.1806	9.7215	13.7802
K_4	0.9920	23.3224	7.0673	11.0807
K_5	0.6724	21.9680	4.9122	8.2170
K_6	0	8.5508	0.7851	2.2065
I_1	0.2056	7.4359	0.9473	1.5455
I_2	0	8.5292	1.6747	2.9567
I_3	0	8.8173	0.9315	2.3503
I_4	0	2.0148	0.0732	0.3117
Q_1	0	1.1951	0.0333	0.1209
Q_2	0	8.3753	0.2579	0.8052
Q_3	0	8.3201	0.5024	1.3079
Q_4	0	8.5751	1.6613	3.0847
Q_5	1.0243	23.3600	7.7003	11.6931
Q_6	1.7746	32.7684	9.1826	13.9527
Q_7	2.9510	35.3545	13.2918	19.2586
Q_8	5.6571	54.2663	19.4683	27.7544
Q_9	14.4771	67.6191	33.2787	44.7871
Q_10	13.2068	73.7994	42.3370	55.2887
Q_11	19.0502	67.9591	38.4733	50.2643
Q_12	19.4972	84.2114	41.6079	55.4923

References

ABBAS, W. 2014. *Contribution à l'étude et l'évaluation de la qualité et du confort au porter de produits confectionnés : Cas de la chemise homme.* Université de Haute Alsace - Mulhouse.

ABDI, H. & WILLIAMS, L. J. 2010. Principal component analysis. *In:* WILEY (ed.).

BALLESTER, J., PATRIS, B., SYMONEAUX, R. & VALENTIN, D. 2008. Conceptual vs. perceptual wine spaces: Does expertise matter? *Food quality and preference,* 19**,** 267-276.

BASF.COATINGS.GMBH. 2012. *Automotive OEM Coatings* [Online]. Available: http://www.basf-coatings.com/global/ecweb/en/content/products_industries/automotive-oem-coatings/index [Accessed November 21st 2018].

BEAUDOT, W. 1994. *Le traitement neuronal de l'information dans la rétine des vertébrés : un creuset d'idées pour la vision artificielle.* Institut polytechnique de Grenoble.

BECUE-BERTAUT, M. & LÊ, S. 2011. Analysis of multilingual labeled sorting tasks: application to a cross-cultural study in wine industry. *Journal of Sensory Studies,* 26**,** 299-310.

BEYMORE, P. M. & KRAWCIW, A. L. M. 2014. *Pigment identification of complex coating mixtures with sparkle color*

BLANCHER, G., LÊ, S., SIEFFERMANN, J.-M. & CHOLLET, S. 2008. Comparison of visual appearance and texture profiles of jellies in France and Vietnam and validation of attribute transfer between the two countries. *Food quality and preference,* 19**,** 185-196.

BOHREN, C. F. & HUFFMAN, D. R. 2007. Absorption and Scattering by an Arbitrary Particle. *Absorption and Scattering of Light by Small Particles.*

BOYNTON, R. M. 1986. A system of photometry and colorimetry based on cone excitations. *Color Research & Application,* 11**,** 244-252.

BUZHYNSKYY, N., SALESSE, C. & SCHEURING, S. 2011. Rhodopsin is spatially heterogenenously distributed in rod outer segment disk membranes. *Journal of molecular recognition,* 24**,** 483-489.

BYK.GARDNER.GMBH 2009. Complete color and effect measurement of metallics multi-angle color and sparkle graininess control.

CADORET, M. 2010. *Analyse factorielle de données de catégorisation - Application aux données sensorielles.* Université Européenne de Bretagne.

CARBON, C. C. 2014. Understanding human perception by human-made illusions. *Front Hum Neurosci,* 8**,** 566.

CARROSSERIE-GENEVE.CH. 2015. *Peinture avec différence de couleur en carrosserie* [Online]. Available: https://carrosserie-geneve.ch/blog/difference-couleur-peinture/ [Accessed September, 30th 2019].

CARTIER, R., RYTZ, A., LECOMTE, A., POBLETE, F., KRYSTLIK, J., BELIN, E. & MARTIN, N. 2006. Sorting procedure as an alternative to quantitative descriptive analysis to obtain a product sensory map. *Food quality and preference,* 17**,** 562-571.

CHEMISTRYLIBRETEXTS. 2018. *9.3: The Electromagnetic Spectrum* [Online]. Available: https://chem.libretexts.org/Bookshelves/Introductory_Chemistry/Map%3A_Introductory_Chemistry_(Tro)/09%3A_Electrons_in_Atoms_and_the_Periodic_Table/9.3%3A_The_Electromagnetic_Spectrum [Accessed February 8th 2019].

CHEUNG, V., LI, C., HARDEBERG, J., CONNAH, D. & WESTLAND, S. 2005. Characterization of trichromatic color cameras by using a new multispectral imaging technique. *Journal of the Optical Society of America A,* 22.

CHOLLET, S., LELIÈVRE, M., ABDI, H. & VALENTIN, D. 2011. Sort and beer: Everything you wanted to know about the sorting task but did not dare to ask. *Food quality and preference,* 22**,** 507-520.

CHOLLET, S. & VALENTIN, D. 2001. Impact of training on beer flavor perception and description: are trained and untrained subjects really different? *Journal of Sensory Studies,* 16**,** 601-618.

CHOLLET, S., VALENTIN, D. & ABDI, H. 2014. Free Sorting Task. *In:* PRESS, C. (ed.) *Novel Techniques in Sensory Characterization and Consumer Profiling.*

CHRISMENT, A., DURCHON, P., LANTHONY, P. & TAVERNIER, I. 1994. Mesurer les couleurs, la colorimétrie. *In:* 3CCONSEIL (ed.) *Communiquer par la couleur.*

CIE 1987. The 4th Edition of the International Lighting Vocabulary.

CIE 1998. Practical methods for the measurement of reflectance and transmittance.
COSTER, M. & CHERMANT, J.-L. 1989. Traitement des images en niveaux de gris. *In:* CNRS (ed.) *Précis d'analyse d'images.*
COUKA, E. 2015. *Modelisation des propriétés optiques de peintures par microstructures aléatoires et calculs numériques FFT.* Ecole Nationale Supérieure des Mines de Paris.
CROWELL, B. 2019. Light as a particle. *Light and Matter.*
CVRL. 2019. *Colour & Vision Research Laboratory* [Online]. Available: http://www.cvrl.org/ [Accessed].
DAUSER, T. 2012. *Color Management at Audi* [Online]. Available: https://detroitcc.org/wp-content/uploads/2018/07/Color-Management-at-AUDI-DCC-March-2012.pdf [Accessed November 20th 2019].
DE VALOIS, R. L., SMITH, C. J., KITAI, S. T. & KAROLY, A. J. 1958. Response of single cells in monkey lateral geniculate nucleus to monochromatic light. *Science,* 127**,** 238-9.
DELENGAIGNE, X., NEVEU, P. & VINCENZONI, C. 2016. De l'idée à l'action. *In:* DUNOD (ed.) *Managez avec le Mind Mapping.*
DIN 2001. Tolerances for automotive paints. *Goniochromatic paints.*
DUPAS, A. 2009. *Opérations et Algorithmes pour la Segmentation Topologique d'Images 3D.* Université de Poitiers.
DUPONT™ 2007. Polymers, light and the science of TiO_2.
EHBETS, P., FRICK, B., WEGMULLER, M., HUNKEMEIER, J. & NIEDERER, G. 2012. *Handheld measuring device for recording the visual appearance of an object to be measured*.
EIVAZI, S. 2010. *How to get changing patterns on a textile surface by using pearl luster and color travel pigments.* Master, University College of Boras.
ELSTER, A. D. 2018. *fMRI of visual system* [Online]. Available: http://mriquestions.com/visual.html [Accessed February 11th 2019].
FAIRCHILD, M. D. 2013a. Color appearance models. *Color appearance models.* 3rd ed.: John Wiley & Sons.
FAIRCHILD, M. D. 2013b. Colorimetry. *Color appearance models.* 3rd ed.: John Wiley & Sons.
FAIRCHILD, M. D. 2013c. Human color vision. *Color appearance models.* 3rd ed.: John Wiley & Sons.
FAYE, P., BREMAUD, D., DAUBIN, M. D., COURCOUX, P., GIBOREAU, A. & NICOD, H. 2004. Perceptive free sorting and verbalization tasks with naive subjects: an alternative to descriptive mappings. *Food quality and preference,* 15**,** 781-791.
FAYE, P., BRÉMAUD, D., TEILLET, E., COURCOUX, P., GIBOREAU, A. & NICOD, H. 2006. An alternative to external preference mapping based on consumer perceptive mapping. *Food quality and preference,* 17**,** 604-614.
FEISNER, E. A. 2006. What is color? *Colour.* 2 ed.
FOTIOS, S. & GOODMAN, T. 2012. Proposed UK guidance for lighting in residential roads. *Lighting Research & Technology,* 44**,** 69-83.
GENIET, F. 2013. *Introduction au transfert radiatif.* DEA.
GOTTENBOS, R. 2018. Review: X-Rite MA-T Multi-Angle Spectrophotometers.
GRANT, B. 2011. *Field Guide to Radiometry*, SPIE.
GRIFFITHS, D. J. 1999. Electrodynamics. *In:* PEARSON (ed.) *Introduction to electrodynamics.*
GRUBBS, F. E. 1969. Procedures for Detecting Outlying Observations in Samples. *Technometrics,* 11**,** 1-21.
HAMPEL, F. R. 1971. A general qualitative definition of robustness. *The Annals of Mathematical Statistics,* 42**,** 1887-1896.
HAWKINS, D. M. 1980. *Identification of Outliers*, Springer.
HOELSCHER, C. 2018. *Basic Color Theory - Why it's not that simple with paint* [Online]. Available: https://choelscherart.com/basic-color-theory-why-its-not-that-simple-with-paint/ [Accessed February 12th 2019].
HONG, G., LUO, M. R. & RHODES, P. A. 2001. A study of digital camera colorimetric characterization based on polynomial modeling. *Color Research & Application,* 26**,** 76-84.
HULIN, W. S. & KATZ, D. 1935. The Frois-Wittmann pictures of facial expression. *Journal of experimental psychology,* 18**,** 482-498.
IGLEWICZ, B. & HOAGLIN, D. 1991. *How to detect and handle outliers*.
IMBERT, M. 2006. *Traité du cerveau*.
IRISTECH. 2018. *Pain around the eye* [Online]. Available: https://iristech.co/pain-around-eye/ [Accessed February 8th 2019].

JAIN, D. 2018. *Skew and Kurtosis: 2 Important Statistics terms you need to know in Data Science* [Online]. Available: https://codeburst.io/2-important-statistics-terms-you-need-to-know-in-data-science-skewness-and-kurtosis-388fef94eeaa [Accessed September 25th 2019].
JARRIGE, R. 2013. *Détermination des propriétés optiques de matériaux granulaires.* Université Pierre et Marie Curie - Paris VI.
JOURLIN, M., BREUGNOT, J., ABDALLAH, B., CORVO, J., COUKA, E. & CARRÉ, M. 2013. Image Segmentation in the Field of the Logarithmic Image Processing Model.
KLEIN, G. 2010a. Light Sources, Types of Colorants, Observer. *In:* SPRINGER (ed.) *Industrial Color Physics.*
KLEIN, G. 2010b. Measuring Colors. *Industrial Color Physics.*
KLEIN, G. 2010c. Systems of Standardized Tristimulus Values, Color Qualities, Chroma of Effect Pigments. *In:* SPRINGER (ed.) *Industrial Color Physics.*
KONICAMINOLTA. 2019. *Multiangle spectrophotometer technology* [Online]. Available: https://www.konicaminolta.com/about/research/instruments/instrument_001.html [Accessed November 19th 2019].
KONO, M., GOLETZ, P. W. & CROUCH, R. K. 2008. 11-cis- and all-trans-retinols can activate rod opsin: rational design of the visual cycle. *Biochemistry,* 47**,** 7567-7571.
KUMAR, V. & GUPTA, P. 2012. Importance of statistical measures in digital image processing. *International Journal of Emerging Technology and Advanced Engineering,* 2**,** 56-62.
LAFLAQUIERE, P., LAFON, D., ETERRADOSSI, O. & SLANGEN, P. R. 1998. Characterization of color texture: CIEL*a*b* calibration of CCD device. *Electronic Imaging: Processing, Printing, and Publishing in Color.* Zurich (Switzerland).
LANDA, E. & FAIRCHILD, M. 2005. Charting Color from the Eye of the Beholder. *American Scientist,* 93.
LARBOULETTE, C. 2007. Celtic Knots Colorization based on Color Harmony Principles. *Computational Aesthetics.* Banff, Alberta, Canada.
LAWLESS, H. T. 1989. Exploration of fragrances categories and ambiguous odors using multidimensional scaling and cluster analysis. *Chemical Senses,* 14.
LAWLESS, H. T., SHENG, N. & KNOOPS, S. S. C. P. 1995. Multidimensional scaling of sorting data applied to cheese perception. *Food quality and preference,* 6.
LESKOV, I. B., KLENCHIN, V. A., HANDY, J. W., WHITLOCK, G. G., GOVARDOVSKII, V. I., BOWNDS, M. D., LAMB, T. D., PUGH, E. N. & ARSHAVSKY, V. Y. 2000. The Gain of Rod Phototransduction. *Neuron,* 27**,** 525-537.
LINDFIELD, D. & DAS-BHAUMIK, R. 2009. Emergency department management of penetrating eye injuries. *Int Emerg Nurs,* 17**,** 155-60.
LIU, Y., SHIGLEY, J., FRITSCH, E. & HEMPHILL, S. 1995. Abnormal Hue-Angle change of the gemstone tanzanite between CIE illuminants D65 and A in CIELab color space. *Color Research & Application,* 20**,** 245-250.
LUO, M. R. & LI, C. 2007. CIE Color Appearance Models and Associated Color Spaces. *Colorimetry - Understanding the CIE system.*
MAILE, F. J., PFAFF, G. & REYNDERS, P. 2005. Effect pigments—past, present and future. *Progress in Organic Coatings,* 54**,** 150-163.
MAINTZ, T. 2005. Mathematical morphology. *Digital and Medical Image Processing.*
MANSUROV, N. 2010a. *Complete Guide to ISO for Beginner Photographers* [Online]. Available: https://photographylife.com/what-is-iso-in-photography [Accessed August, 12th 2019].
MANSUROV, N. 2010b. *Introduction to Shutter Speed in Photography* [Online]. Available: https://photographylife.com/what-is-shutter-speed-in-photography [Accessed August, 12th 2019].
MANSUROV, N. 2010c. *Understanding Aperture in Photography* [Online]. Available: https://photographylife.com/what-is-aperture-in-photography [Accessed August, 12th 2019].
MARQUES, O. 2011. Histogram Processing. *Practical Image and Video Processing Using MATLAB®.*
MCCAMY, C. S., MARCUS, H. & DAVIDSON, J. G. 1976. A color-rendition chart. *Journal of Applied Photographic Engineering,* 2**,** 95-99.
MEDINA, V. 2016. *Visuo-perceptual validation methods for physically-based image synthesis.* MINES ParisTech.
MELGOSA, M., MARTINEZ-GARCIA, J., GOMEZ-ROBLEDO, L., PERALES, E., MARTINEZ-VERDU, F. M. & DAUSER, T. 2014. Measuring color differences in automotive samples

with lightness flop: a test of the AUDI2000 color-difference formula. *Optics Express,* 22**,** 3458-67.
MIE, G. 1908. Beiträge zur Optik trüber Medien, speziell kolloidaler Metallösungen. *Annalen der Physik,* 330**,** 377-445.
MINITAB. 2019. *Overview for Normality Test* [Online]. Available: https://support.minitab.com/en-us/minitab/18/help-and-how-to/statistics/basic-statistics/how-to/normality-test/before-you-start/overview/ [Accessed September 25th 2019].
MORNET, C. 2011. *Reconstruction couleur sous faible éclairement pour des capteurs d'images en technologie CMOS.* Université de Grenoble.
MOUW, T. 2017. *Colorimeter vs. Spectrophotometer* [Online]. X-Rite. Available: https://www.xrite.com/blog/colorimeter-vs-spectrophotometer [Accessed February 18th 2019].
MUNSELL.COLOR. 2019. *The Munsell Color Tree* [Online]. Available: https://munsell.com/color-blog/color-tree/ [Accessed June 3rd 2019].
NAGLA, J. R. 2014. Skewness and Kurtosis. *Statistics for Textile Engineers.*
NATIONAL.KERATOCONUS.FOUNDATION. *How the Human Eye Works* [Online]. Available: https://www.nkcf.org/about-keratoconus/how-the-human-eye-works/ [Accessed May 24th 2018].
NEWTON, I. 1671. A new theory about light and colors. *Philosophical Transactions of the Royal Society of London,* 6**,** 3075-3087.
NIH. 2019. *Color Blindness | National Eye Institute* [Online]. Available: https://www.nei.nih.gov/learn-about-eye-health/eye-conditions-and-diseases/color-blindness [Accessed November 19th 2019].
OLEWUEZI, N. P. 2011. Note on the comparison of some outlier labeling techniques. *Journal of Mathematics and Statistics,* 7**,** 353-355.
OTSU, N. 1979. A Threshold Selection Method from Gray-Level Histograms. *IEEE Transactions on Systems, Man, and Cybernetics,* 9**,** 62-66.
PAULI, H. 1976. Proposed extension of the CIE recommendation on "Uniform color spaces, color difference equations, and metric color terms. *Optical Society of America,* 66.
PELLI, D. G. & BEX, P. 2013. Measuring contrast sensitivity. *Vision Res,* 90**,** 10-4.
PEPPERBERG, D. R. & CROUCH, R. K. 2001. An illuminating new step in visual-pigment regeneration. *The Lancet,* 358**,** 2098-2099.
PERZ, M. 2010. *Flicker perception in the periphery.* Master, University of Eindhoven.
PFAFF, G. 2009. Special effect pigments. *In:* WILEY (ed.) *High Performance Pigments.*
POWELL, S. 2016. The Eye.
REMINGTON, L. A. 2012. Visual pathway. *Clinical anatomy and physiology of the visual system.* Elsevier.
RIGAUDIÈRE, F. 2013. III-1 : LA RETINE : ORGANISATION SCHEMATIQUE. *Oeil et physiologie de la vision* [Online]. Available: http://lodel.irevues.inist.fr/oeiletphysiologiedelavision/index.php?id=212.
ROBERSON, D., DAVIES, I. & DAVIDOFF, J. 2000. Color categories are not universal: replications and new evidence from a stone-age culture. *Journal of experimental psychology,* 129**,** 369-398.
RODIECK, R. W. 1998. *The First Steps in Seeing*, Sinauer.
SALESSE, C. 2017. Physiologie du signal visuel rétinien : de la phototransduction jusqu'au cycle visuel. *Journal français d'ophtalmologie,* 40**,** 239-250.
SCHANDA, J. 1997. Colorimetry. *In:* DECUSATIS, C. (ed.) *Handbook of Applied Photometry.*
SCHANDA, J. 2007. *Colorimetry - Understanding the CIE system*, Wiley-Interscience.
SPERLING, U. & SCHWARZ, P. 2011. *Apparatus and method of investigating coatings with effect pigments*.
STOYE, D. & FREITAG, W. 1998. Composition of paints. *In:* WILEY (ed.) *Paints, Coatings and Solvents.*
STRUTT, J. W. 2009. XXXVI. On the light from the sky, its polarization and colour. *The London, Edinburgh, and Dublin Philosophical Magazine and Journal of Science,* 41**,** 274-279.
SVAETICHIN, G. & MACNICHOL, E. F., JR. 1959. Retinal mechanisms for chromatic and achromatic vision. *Ann N Y Acad Sci,* 74**,** 385-404.
TANG, J. 2015. Unlocking Potentials of Microwaves for Food Safety and Quality. *Journal of Food Science,* 80**,** E1776-93.
THOMAS, A. 2016. *Analyse sensorielle temporelle descriptive et hédonique.* Université de Bourgogne.

TOVEE, M. J. 2008. The eye and forming the image. *An Introduction to the Visual System.*
TOVÉE, M. J. 2008. The organisation of the visual system. *An introduction to the visual system.* Cambridge University Press.
TRÉMEAU, A., FERNANDEZ-MALOIGNE, C. & BONTON, P. 2004. Les dispositifs d'acquisition d'images couleur et de gestion des couleurs. *In:* DUNOD (ed.) *Image numérique couleur : de l'acquisition au traitement.*
TUKEY, J. W. 1977. *Exploratory Data Analysis*.
TURBO. 2019. *M6 Turbo : Actualité et essais auto, dossiers et émission TV* [Online]. Available: https://www.turbo.fr/ [Accessed October 17 2019].
VIÉNOT, F. & LE ROHELLEC, J. 2013. Colorimetry and Physiology - The LMS Specification. *Digital Color.*
WALOWIT, E. 1985. *Spectrophotometric color formulation based on two-constant Kubelka-Munk theory.* Rochester Institute of Technology.
WASSLE, H. 2004. Parallel processing in the mammalian retina. *Nature reviews,* 5.
WEBSTER, M. A. & WILSON, J. A. 2000. Interactions between chromatic adaptation and contrast adaptation in color appearance. *Vision Research,* 40**,** 3801-3816.
WIESEL, T. N. & HUBEL, D. H. 1966. Spatial and chromatic interactions in the lateral geniculate body of the rhesus monkey. *J Neurophysiol,* 29**,** 1115-56.
WIKIPEDIA. 2019a. *Daltonisme* [Online]. Available: https://fr.wikipedia.org/wiki/Daltonisme [Accessed March 22nd 2019].
WIKIPEDIA. 2019b. *Purkinje effect* [Online]. Available: https://en.wikipedia.org/wiki/Purkinje_effect [Accessed July 9th 2019].
WYSZECKI, G. 1973. Current developments in colorimetry. *AIC Color,* 73**,** 21-51.
WYSZECKI, G. & STILES, W. S. 1982a. Colorimetry. *Color science : Concepts and methods, Quantitative Data and Formulae.*
WYSZECKI, G. & STILES, W. S. 1982b. The Eye. *Color science : Concepts and methods, Quantitative Data and Formulae.*
WYSZECKI, G. & STILES, W. S. 1982c. Photometry. *Color science : Concepts and methods, Quantitative Data and Formulae.*
WYSZECKI, G. & STILES, W. S. 1982d. Physical data. *Color science : Concepts and methods, Quantitative Data and Formulae.*
WYSZECKI, G. & STILES, W. S. 1982e. Visual threshold. *Color science : Concepts and methods, Quantitative Data and Formulae.*
X-RITE. 2018a. *ColorChecker Classic Product Support* [Online]. Available: https://www.xrite.com/service-support/product-support/calibration-solutions/colorchecker-classic [Accessed August 13th 2019].
X-RITE 2018b. MA-T _ The new way to characterize effect finishes.
X-RITE. 2018c. *Tolerancing Part 2 : The Role of Light* [Online]. Available: https://www.xrite.com/blog/tolerancing-part-2-the-role-of-light [Accessed August 13th 2019].
YSSAAD-FESSELIER, R. 2001. *Analyse psychophysique du champ visuel : détection, identification, effet de groupement et apprentissage perceptif* Lyon 2.
ZANLONGHI, X. 1991. Sensibilité au contraste. *Coup d'Oeil,* 7**,** 70-72.

Résumé

Aujourd'hui, le marché de la peinture automobile est gouverné par une demande pour des couleurs profondes et vives avec effets. Dans ce domaine, l'exigence est très haute car la couleur est associée à un signe de qualité. Dans une collision classique, différentes parties du véhicule peuvent être endommagées. La partie endommagée doit être réparée, poncée et préparée avant d'être repeinte. Pour réduire les coûts, le carrossier doit ensuite préparer une peinture avec un bon contretypage de teinte, et ce aussi vite que possible.

La formulation de la peinture de réparation consiste donc à reproduire les effets, aussi bien colorés que texturés, à partir de pigments absorbants ou à effets (particules d'aluminium, de nacre …) à partir d'une caractérisation de la peinture du véhicule concerné. Il est relativement simple de qualifier les effets colorés à partir des courbes de réflectance puis des coordonnées CIELab. Cependant, la description de la texturation engendrée par la distribution des particules à effets à l'échelle de la microstructure est assez complexe. L'approche métrologique des propriétés perceptives dont elle est la cause n'en est encore qu'à ses prémices. Les paramètres utilisés ne correspondent pas directement aux phénomènes réellement perçus par l'œil humain.

Dans le cadre de ce travail de thèse, la mobilisation de connaissances expertes à travers différentes sessions de tri libre et de brainstorming sur échantillons peints a permis la mise en évidence de descripteurs de texture réellement perceptifs. Ces descripteurs ont fait l'objet d'un travail d'évaluation "objective" par des évaluateurs expérimentés. Ces derniers ont ainsi permis d'associer à chaque descripteur une échelle d'évaluation quantitative. Cette étape du travail a permis d'établir une vérité terrain utilisable, matérialisée par un ensemble de gammes d'échantillons de référence représentant chacune différents états ordonnés d'un descripteur.

Ces vérités terrain ont ensuite été utilisées pour concevoir un ensemble de descripteurs physiques de texture mesurables et directement corrélés à des échelles perceptives construites dans l'étape précédente. Dans la procédure développée, l'œil humain a été remplacé par un appareil photo numérique agissant en qualité d'intégrateur tristimulaire d'informations radiométriques. La phase d'acquisition d'images a été une étape déterminante dans le processus : il a en effet fallu reproduire les conditions d'évaluation des propriétés perçues, reconnues et retenues lors des différentes étapes faisant appel aux observateurs humains experts. Il a été ensuite possible de caractériser les phénomènes de texture par analyse d'image et de les corréler aux valeurs de l'observateur moyen préalablement défini.

Mots clés

Peinture automobile, peintures à effet, texturation (ou texture), analyse sensorielle, perception visuelle humaine, descripteurs visuels, analyse d'image, observateur moyen

Abstract

Nowadays, the automotive coating market is governed by a demand for deep and vibrant colors with effects. In this field, the requirement is very high because the color is associated with a sign of quality. In a typical collision, different parts of the vehicle may be damaged. The damaged part must be repaired, sanded and prepared before being painted. To reduce costs, the body shop must then prepare a paint with a good color matching, and thus as fast as possible.

It is therefore necessary for the formulation of the repair coating to reproduce the effects, both colored and textured, from absorbent or effect pigments (aluminum particles, pearlescent materials …) from a characterization of the concerned vehicle coating. It is relatively simple to qualify the colored effects from the reflectance curves and then the CIELab coordinates. However, the description of the texturing effect generated by the distribution of effect particles at the microstructure scale is quite complex. The metrological approach of the perceptive properties is still at its beginnings. The parameters used do not necessarily correspond directly to the phenomena actually perceived by the human eye.

As part of this thesis work, the mobilization of expert knowledge through various sessions of free sorting and brainstorming on coated samples made it possible to highlight really perceptive texture descriptors. These descriptors have been the subject of "objective" evaluations by experienced observers. They thus made it possible to associate a quantitative evaluation scale with each descriptor. This stage of the present thesis work allowed the establishment of ground truth data materialized by a set of reference samples representing different ordered levels of a descriptor.

These ground truth data were then used to design a set of measurable physical texture descriptors that were directly correlated to perceptual scales constructed in the previous step. In the procedure developed, the human eye has been replaced by a digital camera acting as a tristimulus integrator of radiometric information. The image acquisition phase was a decisive step in the process: it was necessary to reproduce the conditions of evaluation of the properties perceived, recognized and retained during the various stages using expert human observers. It was then possible to characterize the texture phenomena by image analysis and to correlate them with the values of the previously defined mean observer.

Key words

Automotive coating, effect colors, texturing (or texture), sensory analysis, human visual perception, visual descriptors, image analysis, mean observer